UNIVERSITAT POLITÈCNICA
DE CATALUNYA
BARCELONATECH

Hybrid block and graft copolymers made from macrolactones and α-amino acids for applications as drug delivery nanosystems

Ernesto Tinajero Díaz

UNIVERSITAT POLITÈCNICA DE CATALUNYA
BARCELONA**TECH**

UPC

Escola Tècnica Superior d'Enginyeria Industrial de Barcelona

Hybrid block and graft copolymers made from macrolactones and α-amino acids for applications as drug delivery nanosystems

A thesis submitted by

Ernesto Tinajero Díaz

In fulfilment of the degree of

Doctor of Philosophy

Supervisor(s): Prof. Dr. Sebastián Muñoz Guerra

Dr. Antxon Martínez de Ilarduya

Barcelona, June 2019

Summary

Naturally produced peptides or proteins can be regarded as highly refined polymers. When synthetic polymers are married to proteins or peptides, the resulting bioconjugates can synergistically combine the properties of the individual components and overcome their separate limitations. The protein or peptide element can impart (bio)functional properties to the bioconjugate, whereas the polymer component can improve protein stability, solubility and biocompatibility. This Thesis is focused on the study of hybrid copolymers based on polypeptides and polymacrolactones. Block and graft copolymers have been synthesized by making use of the ring opening polymerization method (ROP) mainly and extensively characterized including both their chemical structure and their structure in the solid state. The self-assembly properties of the new copolymers have been preliminary examined regarding their potential application as nanocarriers for pharmaceutical compounds.

This Thesis initially reports the ROP of ω-pentadecalactone (PDL) using different amino-ended initiators and assisted by either organic or enzymatic catalysts. This method was then extended for the ROP of PDL using bisamino-ended poly(ethylene glycol) (PEG) for the preparation of poly(ω-pentadecalactone)-*b*-poly(ethylene glycol)-*b*-poly(ω-pentadecalactone) [PPDL$_x$-PEG-PPDL$_x$] triblock copolymers. These amphiphilic ABA-type copolymers were able to self-assemble in water to form nanoparticles with diameters between 100 and 200 nm.

Hybrid copolymers of poly(ester-peptide) or poly(ether-ester-peptide) type exhibiting different architectures (e.g. diblock, triblock, graft or triblock/grafted) respectively, were then synthesized using as building blocks: poly(ω-pentadecalactone), poly(globalide) (PGl), PEG as well as polypeptides derived from the L-glutamic acid (Glu), L-lysine (Lys), L-alanine (Ala) and L-phenylalanine (Phe) α-amino acids. The hybrid copolymers were synthesized through several stages depending on

the desired architecture. The first stage in the preparation of these copolymers was the synthesis of macroinitiators from PDL or PGI containing either an amino group at the end of the chain or multiple amine groups along their polymeric chain. In the second stage, such macroinitiators were used to trigger the polymerization of the α-amino acid *N*-carboxyanhyrides (NCA) with the COOH group of L-glutamic acid and NH_2 of L-lysine duly protected as γ-benzyl-L-glutamate (BLG) and $^\varepsilon$*N*-carbobenzoxy-L-lysine (ZLL) respectively. Some copolymers containing BLG or ZLL units were treated with acids to render copolymers bearing the amino acids residues with their COOH or NH_2 functionalities in the free form.

All of the synthesized copolymers were fully characterized through GPC and NMR spectroscopy. The thermal properties were studied by TGA and DSC techniques. The conformation adopted by the peptide-based copolymers in the solid-state was assessed by FTIR, and their crystalline structure was examined by X-ray diffraction using synchrotron radiation in most of cases. The conformation in aqueous solution of water-soluble copolymers containing Glu or Lys residues in the free form was explored by circular dichroism.

The self-assembly behavior in aqueous medium of all the amphiphilic copolymers was investigated with the purpose of obtaining nanoparticles with the appropriated diameters required for their application as biomedical nanocarriers. The nanoparticles were duly characterized by light scattering and SEM and TEM microscopies. Block and graft copolymers were able to load doxorubicin and release it under pH control. Copolymers containing L-lysine were shown to be able of condensing DNA. The potential of these copolymers as DDS of anticancer drugs and vectors for transfection have been evidenced.

Key words: peptides, synthetic polymers, ω-pentadecalactone, globalide, amino-ended initiator, amino acid, hybrid copolymers, self-assembly, nanostructures, doxorubicin, transfection.

Resumen

Los polipéptidos o proteínas obtenidos de manera natural son considerados como polímeros altamente refinados. Cuando los polímeros sintéticos se unen a proteínas o polipéptidos, los sistemas bioconjugados que se obtienen pueden sinérgicamente combinar las propiedades de sus componentes individuales y mejorar las propias limitaciones que tienen por separado. La proteína o el elemento polipeptídico puede impartir propiedades bifuncionales al bioconjugado, mientras que el polímero sintético puede mejorar la estabilidad proteica, la solubilidad y la biocompatibilidad. Esta tesis está enfocada en el estudio de copolímeros híbridos badados en polipéptidos y polimacrolactonas. Copolímeros tipo bloque e injerto fueron sintetizados utilizando principalmente la polimerización por apertura de anillo (ROP) y extensamente caractetizada tanto su estructura química, como su estructura en estado sólido. Las propiedades de auto-agregación de los nuevos copolímeros han sido anteriomente examinadas respecto a su potencial aplicación como nanotransportadores de compuestos farmacéuticos.

Esta Tesis inicialmente reporta la homopolimerización de ω-pentadecalactona (PDL) usando diferentes iniciadores amino-terminados mediante el uso de catalizadores tanto orgánicos como enzimáticos. Este se extiende a la ROP de PDL usando poli(etilén glicol) bisamino-terminado (PEG) para la preparar copolímeros tribloque poli(ω-pentadecalactona)-*b*-poli(etilén glicol)-*b*-poli(ω-pentadecalactona) [PPDL$_x$-PEG-PPDL$_x$]. Estos copolímeros de tipo ABA fueron capaces de auto-agregarse en agua para formar nanopartículas con diámetros entre 100 y 200 nm.

Por otra parte, sistemas híbridos de tipo poli(éster-péptido) o poli(éter-éster-péptido) que presentan distintas arquitecturas (por ejemplo dibloque, tribloque, injerto, o tribloque-injertado) respectivamente, se sintetizaron utilizando como bloques de construcción derivados de macrolactonas (ω-pentadecalactona), globalida) y α-amino

ácidos (ácido L-glutámico (Glu), L-lisina (Lys), L-alanina (Ala) y L-fenilalanina (Phe) así como poli(etien glicol) telequélico.

Los copolímeros híbridos fueron sintetizados en varias etapas dependiendo de cual fuese la arquitectura deseada. La primera etapa fue la preparación de los macroiniciadores a partir de PDL o PGl conteniendo en su estructura ya sea un grupo amino en el extremo de la cadena, o múltiples grupos aminos a lo largo de la cadena polimérica. En la segunda etapa, los macroiniciadores fueron utilizados en la polimerización de α-amino ácidos N-carboxianhídridos (NCA), con los grupos COOH del ácido L-glutámico y el grupo NH_2 de la L-lisina apropiadamente protegidos como γ-bencil-L-glutamato (BLG) y $^\varepsilon N$-carbobenzoxi-L-lisina (ZLL) respectivamente. Para los copolímeros que contienen bloques peptídicos de BLG o ZLL, las funcionalidades COOH o NH_2 fueron regeneradas bajo condiciones ácidas, para producir así los copolímeros conteniendo el amino ácido en su forma libre.

Todos los copolímeros sintetizados fueron completamente caracterizados mediante GPC y espectroscopia de RMN. Las propiedades térmicas fueron estudiadas por las técnicas de TGA y DSC. La conformación adoptada por los copolímeros en el estado sólido fue estudiada por FTIR, y su estructura cristalina fue analizada mediante difracción de rayos X usando radiación sincrotrón en la mayoría de los casos. La conformación en solución acuosa de los copolímeros solubles en agua, que contienen residuos de Glu o Lys, fue analizada por dicroísmo circular.

Se estudió el comportamiento de todos los copolímeros para auto-agregarse en agua obteniéndose partículas con diámetros del orden nanométrico, como se demostró por DLS así como también por SEM y TEM, las cuales son apropiadas para ser aplicadas en biomedicina. Las nanopartículas de copolímeros dibloque y de injerto conteniendo ácido L-glutámico fueron capaces de incorporar doxorubicina y efectuar su liberación bajo control por medio del pH. Por otro lado, los copolímeros dibloque y

de injerto con bloques conteniendo L-lisina mostraron la habilidad de condensar el ADN, demostrando así su potencial uso como vectores en transfección.

Palabras clave: péptidos, polímeros sintéticos, ω-pentadecalactona, globalida, iniciadores amino-terminados, amino ácido, copolímeros híbridos, auto-agregación, nanoestructuras, doxorubicina, transfección.

Index

Summary

Resumen

Acronyms

Acronyms

AA	Amino acid
AA-NCA	Amino acid *N*-carboxyanhidride
AIBN	2,2'-Azobis(2-methylpropionitrile)
AllA	Allylamine
AM	Activated monomer
AMM	Activated monomer mechanism
a-PSty	Atactic polystyrene
ATRP	Atom transfer radical polymerization
BAET	2-(Boc-amino)ethanethiol
BLG NCA	γ-benzyl-L-glutamate *N*-carboxyanhidride
Bn	Benzyl
CALB	Candida antarctica Lipase B
CD	Circular dichroism
CMC	Critical micelle concentration
DCM	Dichloromethane
DDS	Drug delivery systems
DLC	Drug-Loading Content
DLE	Drug-Loading Efficiency
DLS	Dynamic light scattering
DMF	Dimethyl formamide
DNA	Deoxyribonucleic acid
DOX	Doxorubicin
DOX·HCl	Doxorubicin hydrocloride
DSC	Differential scanning calorimetry
ED-ROP	Entropically-driven ring-opening polymerization
GI	Globalide
GPC	Gel permeation chromatography
HDPE	High density polyethylene
HexA	Hexylamine
HFIP	Hexafluoroisopropanol
IUPAQ	International Union of Pure and Applied Chemistry
LCST	Lower critical solution temperature
MLs	Macrolactones
NA	Normal amine
NCA	*N*-carboxyanhydride
NMP	Nitroxide mediated polymerization
NMR	Nuclear magnetic resonance
NPs	Nanoparticles
PAA	Poly(amino acid)
PBLG	Poly(γ-benzyl-L-glutamate)
PCL	Poly(ε-caprolactone)
PDL	ω-pentadecalactone
PEG	Poly(ethylene glycol)
PEO	Poly(ethylene oxide)
PGA	poly(glycolide)
PGI	Poly(globalide)

Phe NCA	L-Phenylalanine *N*-carboxyanhidride
PLA	Poly(lactide)
PLAla	Poly(L-alanine)
PLGA	Poly(L-gluamic acid)
PLL	Poly(L-lysine)
PLPhe	Poly(L-phenyalanine)
POM	Polarizing optical microscopy
PP	Polypeptide
PPDL	Poly(ω-pentadecalactone)
PSty	Poly(styrene)
PSty-PBLG	Polystyrene-*b*-poly(γ-benzyl-L-glutamate)
PSty-PZLL	Polystyrene-*b*-poly($^\varepsilon$*N*-benzyloxycarbonyl-L-lysine)
PVA	Poly(vinyl alcohol)
PZLL	Poly($^\varepsilon$*N*-carbobenzoxy-L-Lysine)
RAFT	Reversible addition-fragmentation chain transfer polymerization
RNH_2	Primary amines
ROH	Acohols
ROP	Ring opening metathesis polymerization
ROP	Ring opening polymerization
SAXS	Small angle X-ray scattering
SDDS	Smart drug delivery systems
SEM	Scanning electronic microscopy
stDNA	*salmon testes* DNA
TBD	1,5,7-Triazabiciclo[4.4.0]dec-5-ene
TEM	Transmission electronic microscopy
TGA	Thermogravimetric analysis
THF	Tetrahydrofuran
TMS	Tetramethylsilane
UCST	Upper critical solution temperature
UV-vis	Ultraviolet Visible Spectrophotometry
WAXS	Wide angle X-ray scattering
XRD	X-ray diffraction
Z	Benzyloxycarbonyl
ZLL NCA	$^\varepsilon$*N*-carbobenzoxy-L-Lysine *N*-carboxyanhidride

Chapter 1. Objectives and organization of the Thesis

1. Introduction

The conjugation of polypeptides and synthetic polymers to form hybrid copolymers is a useful strategy to overcome some of the limitations related with the use of the individual components. Polypeptides are ideal for building stimuli-sensitive structures because the flexibility of their ordered conformational arrangements. On the other side, synthetic polymers confer the amphiphilic character required for the formation of well-organized biphasic morphologies. Complex systems from the nanoscale upwards can be engineered from these copolymers taking benefit from molecular self-assembly strategies. After decades of research, the availability of efficient drug delivery systems for the treatment of diseases continues being still a significant challenge. The design amphiphilic hybrid copolymers based on polypeptides is envisaged as a promising approach to the achievement of nano-devices able to load therapeutic drugs with efficiency and to deliver them under control by effect of either external or internal stimuli.

1. 2 General objective

The main objective of this work is to design amphiphilic copolymers with different molecular architectures using easily available macrolactones (MLs), specifically ω-pentadecalactone and globalide, and α-amino acids (αAA) as bio-based monomers, and occasionally poly(ethylene glycol) (PEG) too. The prepared copolymers will be able to self-assemble in aqueous environment to generate nano-objects of potential utility as biomedical nanocarriers.

1.3 Specific objectives

➤ To study the ring-opening polymerization (ROP) of ω-pentadecalactone using different amino-ended initiators mediated by either organic or enzymatic catalysis.

➤ To synthesize amphiphilic triblock copolymers ABA-type from PEG and macrolactones and to explore their self-assembly behavior in aqueous medium.

➤ To synthesize hybrid copolymers with either block or graft microstructure using pentadecalactone, poly(globalide), and α-amino acids (L-glutamic acid, L-lysine, L-alanine and L-phenylalanine as starting comonomers.

➤ To study the crystalline structure and the self-assembly properties of the hybrid copolymers at the nanometric scale and to relate them with their chemical structure

➤ To assess the ability of the hybrid copolymers to form nano-objects (eg. nanoparticles, micelles, vesicles) by self-assembling in aqueous medium and to relate it with their chemical structure.

➤ To evaluate the capacity of the nano-objects based on the hybrid copolymers to be used as nanocarriers for anticancer drugs, specifically for doxorubicin, including aspects as the loading efficiency, the releasing controlled by external stimuli, and the packing of gene material through electrostatic interactions.

1.4 Outline

o **Chapter 1** contains a brief introduction to the Thesis, its objectives and its organization.

o **Chapter 2** provides an overview about the polyesters derived from macrolactones including their potential applications as drug delivery systems.

o **Chapter 3** describes the materials and methodology used for the synthesis of the polymers and copolymers as well as the techniques applied for their characterization. The methods used to prepare the nanoparticles from the

amphiphilic copolymers and to evaluate them as nanocarriers are also reported

- o **Chapter 4** is devoted to report the synthesis and characterization of poly(ω-pentadecalactone) (PPDL) using amino-ended initiators, as well as the synthesis of the triblock copolymers PPDL$_y$-PEG$_x$-PPDL$_y$ and their self-assembly in aqueous medium.

- o **Chapter 5** deals with the synthesis of poly(ω-pentadecalactone)-*b*-poly(α-amino acids) diblock copolymers (PPDL-*b*-pPAA) in which the amino acid are protected, their solid-state characterization and their self-assembly behavior in aqueous medium.

- o **Chapter 6** treats about the synthesis of poly(globalide)-*graft*-poly(α-amino acids) (PGl-*g*-PAA) copolymers. Their structure in the solid state is studied in detail and their suitability as nanocarriers for anticancer drugs or DNA vectors is brought into evidence.

- o **Chapter 7** reports on the chargeable PPDL-*b*-PAA diblock copolymers generated by removing the protecting groups from PPDL-*b*-pPAA copolymers which were described in Chapter 5. The capacity of these copolymers to form nanoparticles and to load and release cancer-therapy drugs (doxorubicin) or DNA is examined.

- o **Chapter 8** is an extension of Chapters 5 and 6, where the macroinitiators prepared there were successfully utilized for the ROP of the L-alanine *N*-carboxyanhydride to yield both diblock (PPDL$_x$-*b*-PAla$_y$) and graft (PGl$_x$-*g*-PAla$_y$) copolymers. A comparative study regarding structural and self-assembly aspects of the two types of copolymers is carried out.

- o **Chapter 9** reports on the copolymerization of globalide and ω-pentadecalactone and the utilization of such random copolymers to graft L-glutamic acid following the same procedures as in previous chapters. The influence of macrolactone copolymerization on the structure and properties of the graft terpolymers is examined.

- o **Chapter 10** reports the synthesis of amphiphilic copolymers made of poly(ethylene glycol), poly(globalide) and poly(L-phenylalanine) segments. The PEGylated nanoparticles prepared by self-assembly of these copolymers in aqueous medium are described.

The reader is encouraged to access to annexes to Chapters 4-10 containing supplementary graphical information for each one.

Chapter 2. Introduction

2.1 Amphiphilic copolymers with self-assembling properties

Self-assembly is a process by which the components of a system become arranged in ordered structures spontaneously. The type of structure adopted depends on the chemical nature of the components and the environment in which they are located. Self-assembly reflects the information coded (as shape, surface properties, charge, polarizability, magnetic dipole, mass, etc.) in the individual components since these characteristics determine the interactions among them [1]. Recent advances in the synthesis and design of amphiphilic copolymers have created a new surge of interest in the development of nano-assembled systems because many of their functions may be regulated by the shapes and dimensions of their counterparts. Self-assembly of amphiphilic copolymers constitutes today the most efficient and versatile strategy to create nano-systems suitable for a wide diversity of applications in drug delivery, sensor design, bio-imaging, nanoreaction, cosmetics and dispersant technologies [2].

2.1.1 Block copolymers

Advances in polymer chemistry have brought about many different strategies for producing amphiphilic-block copolymers from a given number of monomers (m) and a desired numbers of blocks (n) able to display different hydrophilic and hydrophobic characteristics. For example, synthesis using two chemically distinct monomers (m = 2) will lead to a diblock copolymer (n=2) or a symmetric triblock copolymer (n = 3), whereas synthesis of three different monomers (m = 3) will indefectibly result in asymmetric triblock copolymers (n = 3). In general, these block copolymers are defined as AB diblock copolymers or ABA and ABC triblock copolymers where A and C are chemically distinct hydrophilic blocks whereas B represents the hydrophobic block (Figure 1) [3].
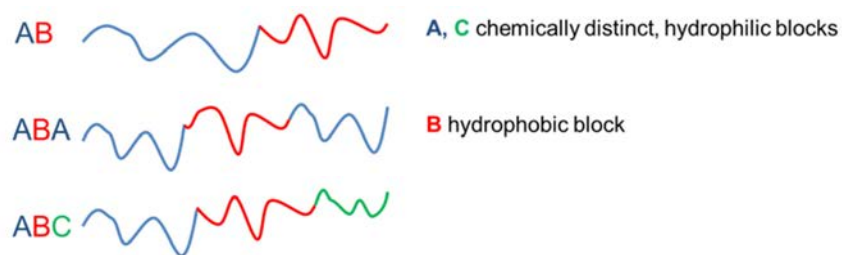
Figure 1. Illustration representing different types of block copolymers

By designing the nature and size of the blocks in such a way that they contain all necessary information to attain their self-assembly into functional materials, additional processing or modification steps could become superfluous. Three different representative classes of block copolymer are schematized in Figure 2.
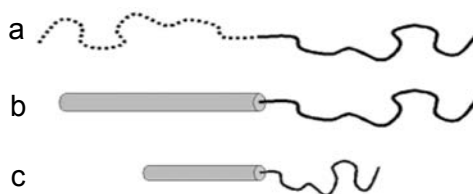
Figure 2. a) Coil-coil diblock copolymers, b) rod-coil diblock copolymers and c) rod-coil diblock oligomers [4].

Coil-coil diblock copolymers. Block copolymers comprised of two flexible incompatible blocks [e.g. poly(styrene)-*b*-poly(isoprene)] tend to be organized in separate nanophases with a variety of different morphologies.

Rod-coil diblock copolymers. Replacing one of the blocks of a coil-coil diblock copolymer by a stiff segment, a rod-coil type diblock copolymer will result. In this case, the self-assembly is no longer solely determined by phase-separation, but also by other factors related with the packing of the rigid phase.

Rod-coil diblock oligomers. These systems are of particular interest since they allow accessing to phase-separated morphologies with domain sizes that could not be attained with traditional coil-coil diblock copolymers.

The covalent coupling of two polymeric chains at their respective ends required to build a diblock copolymer can be accomplished using a variety of chemical means which can be expanded to the preparation of tri- and multiblock copolymer as well [5,6].

Controlled/living radical polymerization. Conventional radical polymerization can be carried out in bulk, in solution, and in dispersed media (suspension, emulsion, miniemulsion, microemulsion and inverse emulsion) to create block copolymers. Solvents should not contain easily abstractable atoms or groups, unless low MW polymers are desired [8].

Living anionic polymerization is frequently employed for the synthesis of block copolymers where two or more monomers are chain polymerized sequentially. These are polymerizations evolving through anionic growing species as active polymerization centers. Special precautions (i.e. dryness, inert atmosphere, solvent purity) are required to prevent unwanted side reactions and to control the process kinetics.

Ring opening polymerization (ROP). According to IUPAC there are two general methods of polymerization: chain polymerization and polycondensation. ROP belongs to chains polymerization, defined (according to IUPAQ): "A chain polymerization". Chain reaction which the growth of a polymer chain proceeds exclusively by reaction(s) between monomer(s) and *active site*(s) on the polymer chain with regeneration of the active site(s) at the end of each growth step. As any other chemical change, elementary reactions in ROP may be either driven by molecular features that are of enthalpic or entropic origin. The common feature of all the ROP is the presence of at least two elementary reactions that are necessary conditions of a macromolecule formation: initiation and chain growth. Chain transfer and termination could be avoided, but if present, then transfer (irreversible) and/or termination would lower the molar mass.

High molar mass aliphatic polyesters with low polydispersity indexes can be obtanined by ROP of lactones. The polymerization of lactones is generally carried out in bulk or in solution (THF, dioxane, toluene, etc.), emulsion, or dispersion. The temperature of the bulk polymerization is generally in the range of 100-150 ºC, whereas in solution polymerization, low temperatures haven been used (0-25 ºC) to minimize side reactions (inter- and intramolecular transesterification). A few lactones polymerize spontaneously on standing or on heating. Most do so in the presence of catalysts or initiators. Many organometallic compounds, such as oxides, carboxylates, and alkoxides are effective initiators for the controlled synthesis of polyesters using ROP of lactones. The mechanism of polymerization depends on the type of initiator [7].

Polycondensation. In order to perform polycondensation it is necessary for each monomer molecule to comprise at least two functional groups able to react during the process. Polycondensation involves reactions well-known from low molecular weight organic chemistry: amidation, esterification, and others, but they are realized many times and for this reason they are called polyamidation. Virtually, any homopolymer, or either polymerization of polycondensation type, may be used as the corresponding oligomer with terminal functional groups in polycondensation reactions leading to the formation of block copolymers. Block copolymers of the polycondensation type include block copolymers the last stage in the formation of which is a polycondesation reaction. Such copolymers can be linear, branched, grafted (graft block copolymers), and structured [9].

Amphiphilic-block copolymers have the ability to form various types of nanostructures the most representative being micelles, nanospheres and nanocapsules (see Figure 3). These materials when intended for use in drug delivery, are generally composed of biocompatible, biodegradable hydrophobic blocks such as polyesters that are covalently bonded to biocompatible hydrophilic blocks, such as PEG or polypeptides [10].
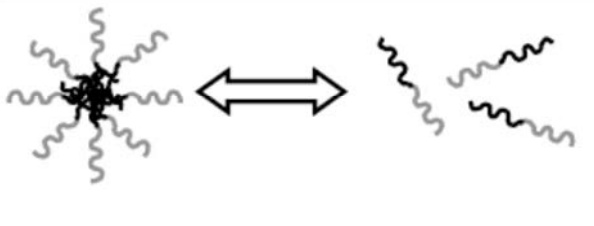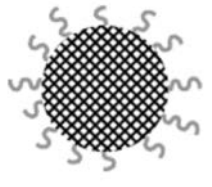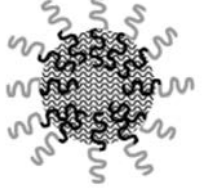
	Micelles Size: 10-100 nm Aggregated copolymers in dynamic equilibrium with copolymer unimers Mobile fluid-like core
	Nanospheres Size: 100-300 nm Copolymer unimers in a "frozen"state Phase-separated solid matrix core
	Polymersomes Size: 100-300 nm Copolymers unimers Or membrane surrounding A drug reservoir or Oily core

Figure 3. Nanoparticulate systems formed by amphiphilic block copolymers [10].

2.1.2 Graft copolymers

Graft copolymers belong to the general class segmented copolymers and generally consist of a linear backbone of one composition bearing randomly distributed branches of a different composition. Graft copolymers, having polymeric arms spaced regularly and densely along the backbone, are an interesting architecture of hiperbranched polymers with size, length of side chain and backbone, grafting density and composition being precisely controlled. In comparison with the linear block copolymers, graft copolymers have more freedom in tuning the self-assembled behaviors by changing the grafting densities and length of side chains. In some conditions, more stable uni-molecular micelles can be formed by amphiphilic graft copolymers, which have attracted considerable interest for using as drug and gen carries in chemotherapy [11]. Most usually the backbone of a graft copolymer is constituted by a hydrophobic polymer chain whereas the branches show a notable hydrophilic character. Water soluble polyethers like poly(ethylene oxide) (PEO),

poly(amino acids) or polysaccharides are frequent hydrophilic components of graft copolymers [12].

Graft copolymers can be synthesized by three different methods [13,14] (Figure. 4):

i) In the "*grafting onto*" method, the backbone and the arms are prepared separately and them jointed. The branching sites can be introduced onto the backbone either by post polymerization reactions or by copolymerization of the main backbone monomer with a suitable comonomer bearing the desired functional group (unprotected or in a protected form if this functional group interferes with the polymerization reaction). The branches are prepared with and reactive group able to react with the functionality provided by the backbone.

ii) In the *"grafting from"* method, the primary requirement is to have a preformed linear macromolecule with evenly distributed initiating-capacity functionality. The branches are formed by polymerization of the second monomer initiated by the active sites provided by the backbone.

iii) In the "*grafting through*" or macromonomer method, preformed long chain monomers are copolymerized with a conventional monomer.
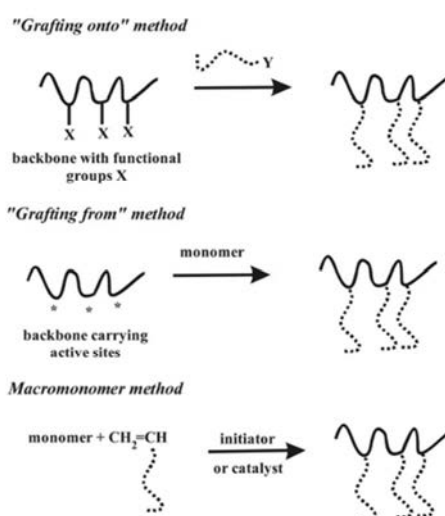
Figure 4. General synthetic methods for the synthesis of graft copolymers [14].

The hydrophobic/hydrophilic segment ratio of graft copolymers are tuned by appropriate selection of the comonomers. For biomedical applications, the self-aggregation characteristic of synthetic graft copolymer in aqueous media is of major interest. For copolymers containing a hydrophobic backbone and hydrophilic grafts, micellization becomes possible with either nonionic or ionic water-soluble side chains [15,16].

2.2 Amphiphilic copolymers containing polypeptide segments

The use of hybrid materials based on the combination of peptides with synthetic polymers takes advantage of providing well-controlled structures bearing multiple chemical functionalities. The chemical conjugation of peptides to polymers is feasible via certain specific types of chemical reaction, the so-called "click" reaction being the most common one. Apart from the conjugation of polymers and peptides, the insertion of peptide-based ion channels into polymer supramolecular structures represents another strategy to combine, in a functional manner, peptides and polymers. The exploitation of polymer-peptide self-assembly processes is opening new fascinating and promising routes in nanotechnology and nanomedicine [17].

2.2.1 Polypeptides

Synthetic polypeptides are polymers composed of α-amino acids. The investigation of polypeptides assemblies is a helpful approach for understanding the behavior of proteins systems. The polypeptide chain is known to adopt three typical conformations, random coil, α-helix, and β-sheet, which largely determine the rigidity of the polypeptide and in consequence its solubility. Both intrinsic factors as amino acid sequence and molecular weight and extrinsic factors as solvent nature, pH, and temperature, will influence the conformational and self-assembly properties of the polypeptides [18]. Peptide-based platforms for biomedical applications have been a subject of intense research and used in different areas including drug delivery, tissue engineering and biodiagnostic tools, among others [19].

2.2.1.1 α-Amino acids and polypeptides

α-Amino acids are the basic constituents of both polypeptides and proteins and they are indispensable compounds for life process. The chemistry of amino acids and peptides has been developed mainly addressed to the structural elucidation and synthesis of compounds of useful biological function [20]. Although there are only about 20 natural α-amino acids (Figure 5), the variety of their combinations results in an amazing diversity of materials differing in properties and functionalities [21].
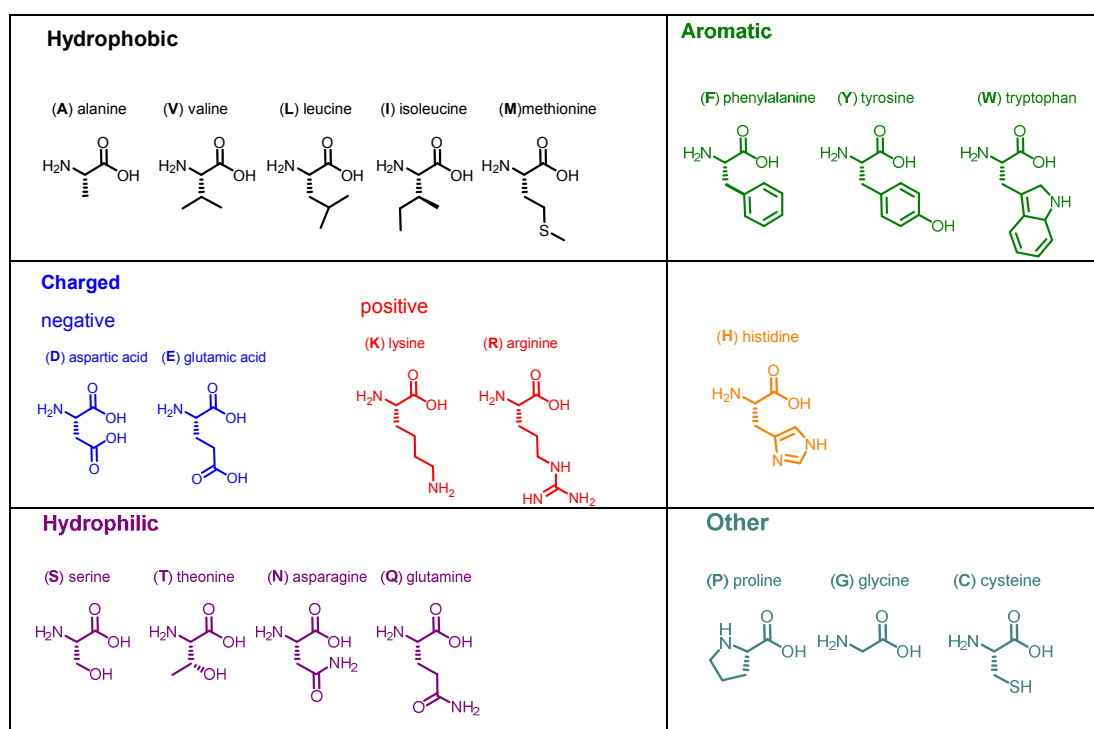
Figure 5. Twenty gene encoded α-amino acids shared by all life forms.

Proteins have fascinated scientists for long since their complex sequences and diversity of chemical functionality lead to structurally defined folded chains with highly specific biological activities. Synthetic polypeptides were attractive, and remain so today, since they possess the same backbone as proteins. Polypeptides may be degraded enzymatically within a safe profile and non-toxic metabolites, which are remarkable properties for biomedical applications requiring temporal use [33–35]. Their synthesis has been both extensively and intensively explored and today most of them

may be prepared chemically by the ring opening polymerization of α-amino acid *N*-carboxyanhidride (NCA ROP) monomers [26].

The polymerization of NCAs (Scheme 1) is a highly economical and expedient process for the synthesis of long polypeptide chains, especially if compared to the solid-phase synthesis. *N*-carboxyanhydrides are known to be polymerized by aliphatic primary amines in such a way that the initiator is attached to the growing chain and the propagation is living.
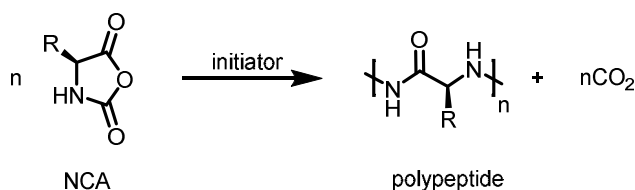
Scheme 1. Polymerization of *N*-carboxyanhidride (NCA) monomer.

Most authors agree that the most likely pathways for the ROP of NCAs are the "normal amine" (NA) and the "activated monomer" (AM) mechanisms (Scheme 2) [27].

i) *Normal amine mechanism (NAM)*. This mechanism is the generally one followed in the polymerization of NCAs initiated by non-ionic initiators having at least one mobile hydrogen atom (base-H), such as primary and secondary amines, alcohols and water.

ii) *Activated monomer mechanism (AMM)*. This mechanism was proposed to explain the ROP of DL-phenylalanine NCA, initiated by a tertiary amine. Later, the AMM was found to be also valid for the basic salt-initiated polymerization of *N*-unsubstituted NCAs. In the cases of tertiary and secondary amine, as well as the alkali halide-initiated polymerizations, it is believed that AMM and NAM coexist.

Path 1
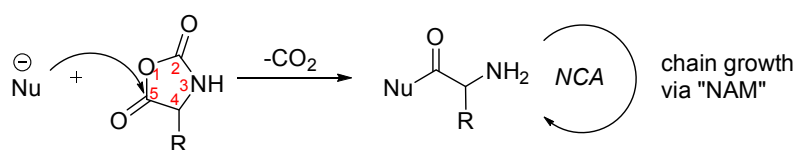
Path 2
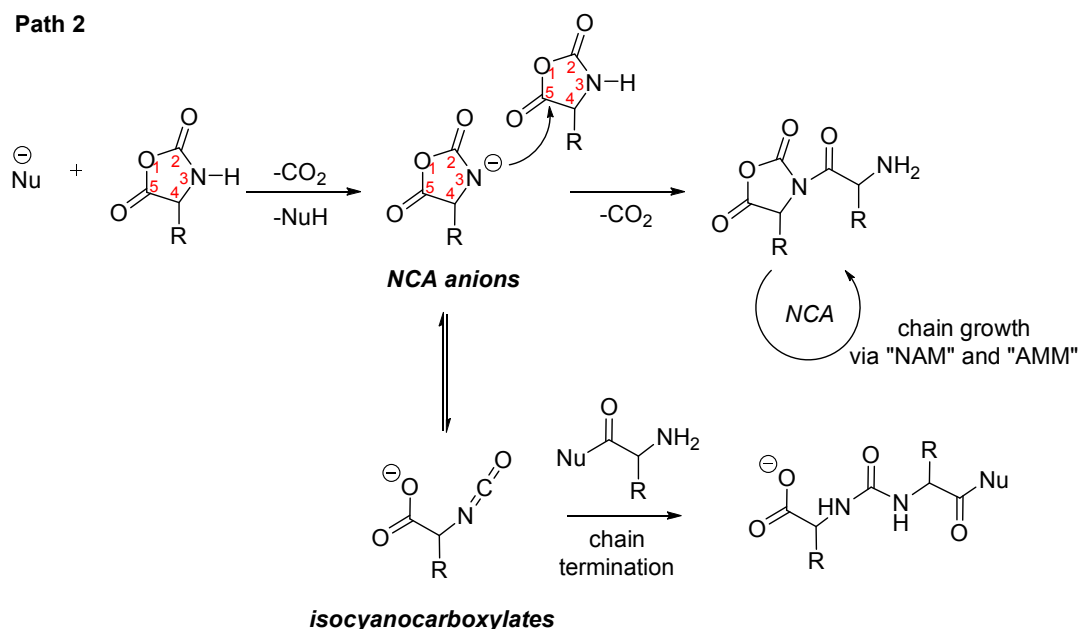
Scheme 2. Possible reactions in ROP of α-amino acids NCAs by nucleophilic initiators [27,28]

2.2.1.2 Structure and properties of polypeptides

Synthetic polypeptides can adopt ordered conformations such as α-helices or β-strands in addition to the disordered coil arrangement under specific environmental conditions. These secondary structures and their dynamic transitions play an important role in regulating the properties of polypeptides in self-assembly, catalysis, polymerizations, and biomedical applications [29,30].
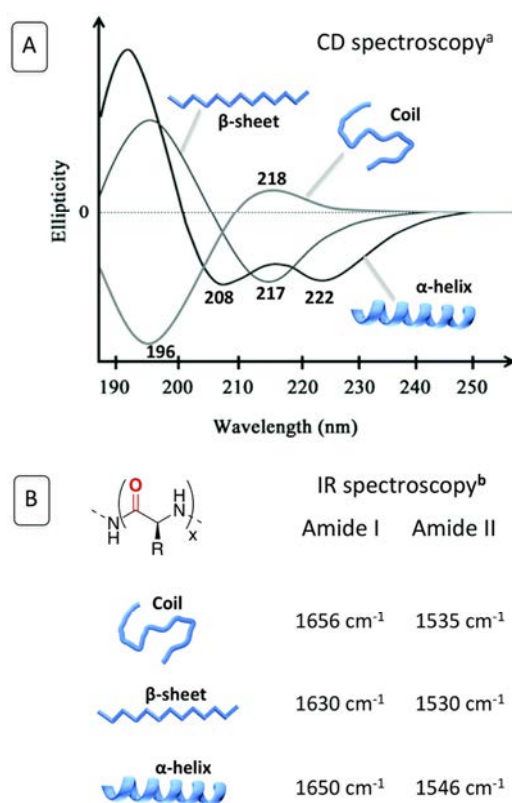
Figure 6. Circular dichroism (CD) and infrared spectroscopy (IR) as useful techniques in the secondary-structure elucidation of proteins and polypeptides.

Circular dichroism (CD) is an excellent method of determining the secondary structure of polypeptides since the different structural elements display characteristic CD spectra (Figure 6a). For example, α-helical polypeptides have negative bands at 222 nm and 208 nm and a positive band at 193 nm. Polypeptides with well-defined antiparallell β-pleated sheets (β-forms) present negative bands at 217 nm and positive bands at 196 nm while disordered chains exhibit very low ellipticity above 210 nm and negative bands at 196 nm [31]. Infrared spectroscopy is well suited for determining structural features of polypeptides. The major bands of interest are the amide I, II and III bands, which absorb in the 1600-1700, 1500-1600, and 1200-1350 cm^{-1} region, respectively. As each of the secondary structure motifs in peptides is associated with a characteristic hydrogen bonding pattern between the amide C=O and N-H groups, each type of secondary structure gives rise to characteristic amide I and amide II absorptions [32].

In this Thesis, four α-amino acids (L-glutamic acid, L-lysine, L-alanine and L-phenylalanine) have been used to build the polypeptide blocks needed for the synthesis of the copolymers.

Poly(L-glutamic acid) (PLGA). Poly(L-glutamic acid), which can be conveniently synthesized through the ROP of the γ-benzyl-L-glutamate *N*-carboxyanhidride (BLG-NCA), is a synthetic polypeptide that is biodegraded into L-glutamic acid, which is an essential amino acid for the human body. Every unit of poly(L-glutamic acid) bears a carboxyl group which is ionized at high pH forcing the polypeptide to adopt the random coil conformation due to the disturbing charge repulsion and to become therefore water soluble. When pH decreases, carboxyl groups are protonated and the polymer adopts then a helical conformation and becomes insoluble in water. PLGA is therefore responsive to external stimuli such as pH and ionic strength, and in addition, it provides functionality suitable for drug attachment. These features make PLGA an attractive candidate for the design of drug delivery systems [22].

Poly(L-lysine) (PLL). Poly(L-lysine) is a cell penetrating polypeptide capable of cell transfection and transportation of other molecules of interest into the cell. PLL is a cationic polypeptide since it is protonated on the side amino group at physiological pH, which confers it particular interest in the field of siRNA delivery. As a delivery agent, it has been shown to be very resilient, effective and capable of prolonging the therapeutic action. As a result, it has a great potential as a very flexible system for general drug delivery. The synthesis of PLL is rather problematic due to the negative interference of its long side chain length. Nevertheless, PLL can be synthesized by ROP of $^{\varepsilon}N$-carbobenzoxy-L-lysine *N*-carboxyanhidride (ZLL-NCA) and subsequently deprotection of the epsilon-amino groups [23].

Poly(L-alanine)(PLAla). L-Alanine is the simplest natural amino acid bearing a non-polar hydrophobic side group. Poly(L-alanine) has particular properties among polypeptides due to the presence of the methyl side group. PLAla displays good solubility in organic solvents that favors the possibility of obtaining nanoparticles useful as drug delivery

systems. Moreover, polymers based on L-alanine show better enzymatic degradation than those others based on glycine. PLAla may be readily synthesized by ROP of Al-NCA.

Poly(L-phenylalanine)(PLPhe). Although the interest for α-amino acids is high for hybrid copolymer preparation, little attention has been paid to L-phenylalanine so far. The stacking of aromatic rings plays a well-known role to facilitate self-assembling and formation of both chemical and biochemical supramolecular structures. The restricted geometry and attractive forces of the aromatic moieties provides order and directionality to the arrangements adopted by the polypeptide, as well as the energy needed for the formation of such well-ordered structures. PLPhe may obtained by Phe-NCA.[25].

2.2.2 Polypeptide-based copolymers

The capability of polypeptides to form ordered secondary structures through noncovalent interactions somewhat distinguishes them from many other synthetic polymers. Polypeptide based copolymers show considerable promise for building nano-systems regulated by controlling intra- and intermolecular interactions and the formation of secondary and tertiary structures.

Combining two different polypeptide blocks enables the formation of noteworthy block copolypeptides able to self-assemble into micelles, vesicles, and hydrogels depending on the nature of the polypeptide blocks selected and the physical interactions taking place between the two blocks. Specific polypeptide sequences can be generated synthetically by the solid-phase peptide synthesis but the fabrication of polypeptides containing more than 50 amino acid residues by this technique is often unfeasible. The introduction of controlled and living/controlled NCA ROP methods has resulted in extensive research that has culminated in the generation of a plethora of novel block copolypeptides. Self-assembly of these into systems that may be exploited

to create a whole host of three-dimensional architectures suitable for biomedical applications [37].

2.2.2.1 Polypeptide-PSty and polypeptide-PEG copolymers

While synthetic polymers present the random coil or well-stable crystal structures, peptide sequences can adopt interconvertible conformations such as the α-helix or β-strands. Hybrid materials based on the combination of peptides with synthetic polymers takes advantage of such polypeptide properties and provide nano-structures that may be controlled down to the molecular level and that may bear multiple chemical functionalities. Different polymerization techniques such as atom transfer radical polymerization (ATRP), reversible addition-fragmentation chain transfer polymerization (RAFT), nitroxide mediated polymerization (NMP), opening metathesis polymerization (ROMP), and ring opening polymerization (ROP) have facilitated the development of tailor-made polymers and copolymers with predictable molecular weight and narrow distributions. The properties of these polymers can then be further enhanced via conjugation of polypeptides to tune hierarchical assembly, stimuli response or desired targeting [36]. Some polypeptide-based hybrid copolymers of reference are those combining the polypeptide with highly hydrophobic or highly hydrophilic polymers. Selected examples of these two types are commented below.

Atactic polystyrene (*a*-PSty) is an amorphous hydrocarbon polymer that has been extensively used for the synthesis of the coil part of amphiphilic diblock-peptide-based copolymers with a rod-coil structure. Polystyrene-*b*-poly(ε-benzyloxycarbonyl-L-lysine) (PSty-PZLL) diblock copolymers were reported by Gallot et al. Wide and small angle X-rays scattering patterns indicated the presence in these copolymers of an hexagonal arrangement of the peptide helices [38]. Removal of the side-chain protecting groups resulted in non-water soluble polystyrene-*b*-poly(L-lysine) diblock copolymers that did not show evidence for any ordered arrangement of the peptides chains. Polystyrene-*b*-poly(γ-benzyl-L-glutamate) (PSty-PBLG) diblock copolymers with a hexagonal-in-

lamellar morphology have been also described [39]. Also the ABA-type triblock copolymers composed of a central polystyrene block flanked by two polypeptide segments made of PBLG or polysarcosine have been studied. Different block copolymers morphologies related to the different secondary structure of the peptide block were characterized with the PBLG blocks in the α-helical form and polysarcosine without adopting any regular structure.

Studies carried out on ABA triblock copolymers PBLG-PSty-PBLG with a variety of compositions [40] revealed that the molecular organization adopted in the solid-state was strongly affected by the PBLG/PSty ratio and the molecular weight of the copolymer. WAXS patterns revealed *d*-spacings corresponding to the distance between neighboring polypeptide α-helices in all cases but TEM micrographs indicated a lamellar morphology only for triblock copolymers with PBLG contents below 60%. Later studies were realized on series of PS-*b*-PBLG and PS-*b*-PZLL hybrid copolymers made of a short polystyrene block (PD~10) and a polypeptide block containing between 10 and 80 repeating units [41]. The structure of these copolymers was characterized by variable temperature infrared spectroscopy and X-ray diffraction, and it was found that below 200 ºC and for sufficiently long peptide blocks, the diblock copolymers adopted a hexagonal structure. On the contrary, the polypeptide was arranged in the β-sheet form for very short amino acid block lengths [42].

The chemistry and biological applications of poly(ethylene glycol) (PEG) have been the subject of intense both academic and industrial studies. PEG is a hydroxyl-capped water-soluble polyether with low-to-moderate molecular weight and good commercial availability. PEG has been used for long as an excellent co-partner in copolymerization reactions due mostly to its broad and worthy applications in drug delivery systems. Its mostly outstanding property is reducing the tendency of nanoparticles to aggregate by steric stabilization and producing thereby formulations

with increased stability during storage and application. Probably, PEG is the most commonly applied non-ionic hydrophilic polymer with stealth behavior.

Poly(ethylene glycol)-polypeptide block copolymers (PEG-*b*-PP), have attracted significant interest as drug and gene delivery systems by utilizing their most relevant feature, that is the formation of micelles with a distinguished core-shell architecture. The hydrophilic block in these systems is usually PEG with a molecular weight ranging from 1000 to 20,000 g·mol^{-1}. Micelles based on PEG-PP copolymers are unique among other micelle-forming block copolymers because the presence of a tailor-made non-polar core of PP compatible with water-insoluble drugs. A primary advantage of PEG-PP over other drug carriers is their capacity for loading drug, genes or intelligent vectors in the micellar core through the free functional groups (amino or carboxylic) of the polypeptide chain [43].

2.3 Polypeptide-polylactone copolymers

Peptides are attached to other polymeric inert materials as bioactive components with the main purpose of optimizing the interactions between the material and the surrounding proteins and cells. An additional point of interest derives from the stable amide backbone of peptides which makes them rather inert against hydrolysis and therefore more suitable for materials science applications compared to other bioorganic macromolecules such as oligonucleotides or oligosaccharides [44,45]. Aliphatic polyesters occupy a key position in the field of polymer science regarding their remarkable properties such as biodegradability and biocompatibility. Their hydrolytic and/or enzymatic chain cleavage yields hydroxyl carboxylic acids, which in most cases are ultimately metabolized.. These key properties can be optimized by copolymerization or blending of homo and/or copolymers [48], which opens up a wide range of applications as environmentally friendly thermoplastics and biomaterials.

The use of polyesters as counterpart of polypeptides to form hybrid copolymers is exceptionally appealing due to their relatively easy of synthesis, which is particularly applicable when lactones susceptible to ROP are used as monomers.

2.3.1 Lactones and ROP to polylactones

Polyesters of A-B type are usually prepared by two different approaches, i.e. polycondesation of hydroxy acids and ring opening polymerization (ROP) of lactones. A lactone is an organic compound containing an ester group that becomes part of a ring structure made of carbon atoms. In Scheme 3 the chemical structures of some representative lactones are shown.

acetolactone   propiolactone   butyrolactone

L-lactide   caprolactone   valerolactone
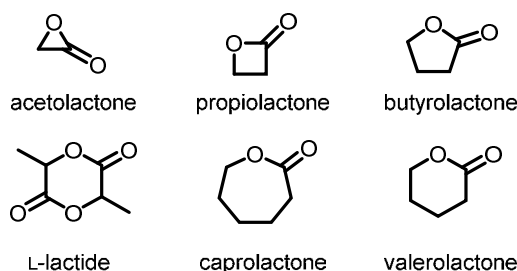
Scheme 3. Chemical structures of representative small to medium-size lactones.

In the ROP of lactones, polymers are formed when cyclic esters are initially opened by a nucleophile (initiator) and the opening reaction is continued at a good rate by assistance of a catalyst. The polymerization of lactones by ROP provides a facile route to the corresponding polyesters, commonly called polylactones [47]. Polylactones are important biodegradable and biocompatible environmentally friendly polyesters widely used for many applications.

The main mechanisms of polymerization of lactones by ROP can be roughly divided into five categories: anionic polymerization, coordination polymerization, cationic polymerization, organo-catalytic polymerization, and enzymatic polymerization [46]. As a rule, amines and alcohols are not nucleophilic enough to realize the continuous ring-opening involved in the polymerization at a satisfactory rate, and it is

mandatory to use catalysts to attain a successful reaction. Particularly interesting in this context are organo-catalytic and enzymatic polymerizations, since they were the methods used in this Thesis. As an example, 1,5,7-Triazabiciclo[4.4.0]dec-5-ene (TBD) is an efficient organo-catalyst commonly used for the ROP of lactones initiated by alcohols. The benefits of enzymes as catalyst in ROP of lactones are manifold: a) Enzymes are green catalysts obtained from renewable resources, b) Enzymes may be easily separated from the resulting polyesters, c) Enzymatic polymerizations proceed under mild conditions in terms of pH, temperature, and pressure and, d) Enzymes are very efficient catalysts for the polymerization of large-size strain-free lactones, which are particularly difficult to polymerize by the usual chemical methods.

Scheme 4 presents the two possible initiation-polymerization mechanisms followed in the ROP of a cyclic ester [46,48].

OH-ended polyester

COOH-ended polyester
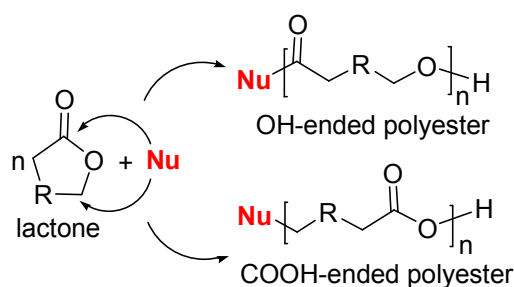
Scheme 4. Schematic representation of the initiation-polymerization ROP mechanisms of lactones. $R=(CH_2)_n$

Each macromolecule that is formed by ROP may contain chain ends functional groups that are provided by the initiator or generated in the termination reaction. By changing the catalyst or initiator and the termination reaction, the nature of the functional groups can be varied to fit the polyester in the application of the polymer. Functional groups accessible to post-polymerization reactions can be introduced into the polymer structure in this way.

Although alcohols (ROH) have been in most cases the initiators in the ROP of lactones, primary amines (RNH_2) can be also used for the purpose. In principle the system lactone/RNH_2 does not differ mechanistically from the lactone/ROH system

(Scheme 5), however the utilization of amines as nucleophiles in the ROP opens new possibilities such as the synthesis of polypeptide-polyester block and graft copolymers or star-shaped copolymers based on polyamino dendrimers [49–51].
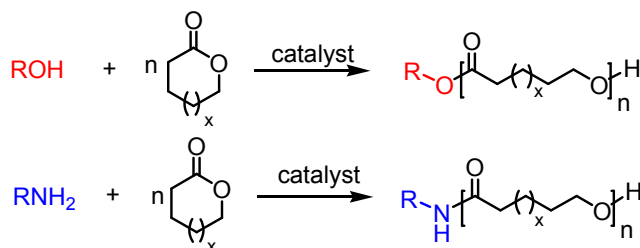
Scheme 5. Ring opening polymerization of lactones using alcohols or amines as initiators.

A number of architectures may be produced as a result of the great versatility of the ROP of cyclic esters: homopolymers, block copolymers, graft copolymers and star-shaped copolymers. Block copolymers are likely the most studied among these architectures. They may be readily prepared by sequential addition of monomers to systems polymerizing under living conditions. The order of monomer addition must be such that the macroinitiator generated by the preceding monomer is capable of rapidly initiating the ROP polymerization of the succeeding monomer. The preparation of prepolymers or macromers with functional end groups, so called telechelic polymers, is another approach to unconventional architectures. The functional end groups are introduced either by functional initiation or end-capping of living polymers, or by a combination of the two. In this way, monomers that are not able to copolymerize can be incorporated in a copolymer. Star-shaped polymers can be prepared by using a multifunctional initiator, e.g. pentaerythritol and a catalyst that initiates ROP of the selected monomer. A second approach is to use telechelic prepolymers that become linked together after polymerization.

2.3.2 Macrolactones and poly(macrolactones)

Macrolactones refer to lactones made of cyclic backbones made at least of 12 atoms. Some representative macrolactones are shown in Scheme 6. Compared to the

vast number of publications describing the ROP of small and medium ring-size cyclic esters (lactide, glycolide, caprolactone, etc), the ROP of macrolactones is underexposed and only few reports have been published to date [52]. The driving force behind the ROP of small-size lactones comes from the release of ring-strain during the polymerization process and it is therefore an enthalpy-driven process. On the contrary, when the ring size is large enough (usually ≥14 atoms), changes in enthalpy upon opening are minimal and polymerization becomes entropy-driven due to an increase of conformational freedom [53]. The interest for the macrolactones is rapidly increasing for the production of high hydrophobic polyesters, in particular of polyesters derived from fatty acids. Poly(macrolactone)s are highly hydrophobic and semicrystalline polymers with properties close to those of polyethylene, one of the highest volume and most versatile polymers.

Ambrettolide (am)   Globalide (Gl)   Hexadecalactone (HDL)

Nonadecalactone (NDL)   ω-Pentadecalactone (PDL)   Tricosalactone (TCL)
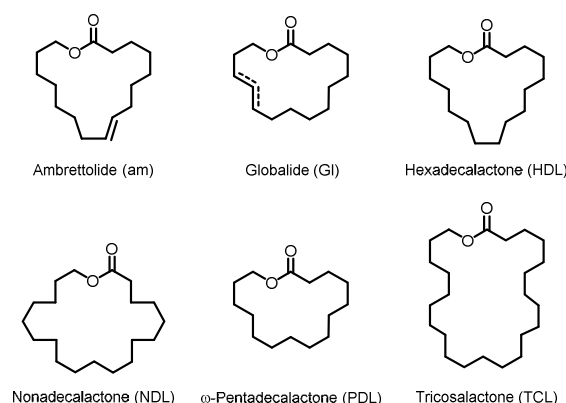
Scheme 6. Representative macrolactones. Only ω-pentadecalactone and globalide were used in this Thesis.

In this Thesis we did work on copolymers based on ω-pentadecalactone (PDL) (IUPAC name: Oxacyclohexadecan-2-one) and globalide (Gl) (IUPAC name: Oxacyclohexa-decen-2-one), both of them commercially available. PDL is a naturally-occurring macrolactone that is synthetically produced by expansion of the tetradecanone. Globalide is an unsaturated 16-membered lactone that contains one unsaturated double bond. It is also derived from hydroxy fatty acids and proven to be

non-toxic. It is actually a mixture of two different constitutional isomers with the double bond at the 11 or 12 positions. Such unsaturation provides it with a chemical handle for functionalization. Poly(ω-pentadecalactone) (PPDL) prepared from PDL is a semicrystalline polyester that display mechanical properties comparable to high density polyethylene (HDPE) [54]. PPDL owes its increased tensile properties to its long methylene sequences and its strength to its crystalline nature. Both its crystallinity and hydrophobicity are responsible for the low susceptibility to hydrolytic degradation exhibited by this polyester [55]. Polyglobalide (PGl) has a low melting point (~48 ºC), is highly crystalline, nontoxic and shows low hydrolytic or enzymatic degradability, being characterized by high hydrophobicity. Such properties make it a good candidate for biomaterials obtained from bioresources with low degradability [52].

2.3.3 Polypeptide-polylactone copolymers

Most of studies carried out on polypeptide-polylactone copolymers are based on a few synthetic polylactones, such as poly(ε-caprolactone) (PCL), poly(lactide) (PLA), and poly(glycolide) (PGA). All these polylactones are biocompatible and degradable by hydrolysis at different rates. Copolymerization of these lactones with amino acids to produce random, block, or graft copolymers has been carried out to produce materials with intermediate properties between those of the parent homopolymers. This approach has allowed permeability to be extensively controlled [56].

There are a number of papers on the studies of synthesis and characterization of poly(ester)-*co*-poly(α-amino acid) block or triblock copolymers. In most cases, poly(γ-benzyl-L-gutamate)(PBLG) or $^{\varepsilon}$*N*-carbobenzoxy-L-lysine (PZLL) has been copolymerized with ε-caprolactone [57–62] and L-lactide [63–66]. The subsequent removal of the protecting-amino acid group rendered the poly(ester-peptide) copolymers with the amino or acid group in its free form. Additionally, architectures like graft copolymers [67,68] based on the combination of peptides and polyesters have been also reported.

As far as we know, the marriage of macrolactones to polypeptides to form copolymers has not been reported to date. Neither block nor graft copolymers have been described, and the solely information available in literature dealing with this kind of poly(ester-peptide) copolymers is that emerging from the work presented in this Thesis.

Only few reports are known to deal with polypeptide-polyester copolymers displaying self-assembly behavior. Jérôme et al. performed DSC on a poly(ε-caprolactone)$_{50}$-b-poly(γ-benzyl-L-glutamate)$_{40}$ (PCL$_{50}$-PBLG$_{40}$) revealing two endotherms, one found at 60 ºC due to the melting of the PCL, and another one at 110 ºC that reflects the conformational transition of the PBLG helix from a 7/2 to a 18/5 helical structure. The observation of the two separate endotherms at temperatures identical to those found for the respective homopolymer transitions was a firm indication for the existence of a microphase-separated structure [70]. Similar results were later reported by other authors for PCL-PBLG and PLLA-PBLG diblock copolymers [69,71].

2.4. Hybrid polypeptide-based copolymers as drug delivery systems

The vast functionality of proteins and oligopeptides originate from a wide choice of α-amino acid monomers as well as the control of peptide sequences [72]. When synthetic polymers are married to proteins or peptides, the resulting bioconjugates can synergistically combine the properties of the individual components and overcome their separate limitations. The protein or peptide element can impart (bio)functional properties to the bioconjugate, whereas the polymer component can improve protein stability, solubility and biocompatibility. The synthetic polymer can also introduce new properties such as self –assembly and phase behavior, and even modulate protein activity [35]. The architecture of the bioconjugate has to be adjusted to the application for which it is developed. The most common architecture is the head-to-tail conjugate (Figure 7a)
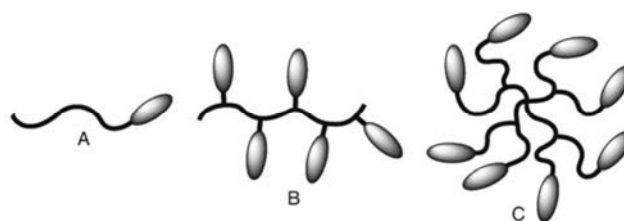
Figure. 7. Cartoon representation of the most common architectures of bioconjugates. The curved lines represent the synthetic polymer component and the ellipses the peptide or protein: (A) head-to-tail conjugate, (B) comb-shaped or grafted structure, (C) dendritic architecture [35].

Drug delivery is the method used for administration of a pharmaceutical compound in humans or animals in order to achieve a therapeutic effect [73]. Drug delivery at controlled rate and targeted are extremely important properties of the drug delivery systems that are vigorously pursued in the design of new formulations. The called "smart drug delivery systems" (SDDS) are able to deliver drugs to the targets sites with reduced dosage frequency and in a spatially controlled manner. Nanocarriers are the base of SDDSs. The eight most reported nanocarriers are presented in Figure 9 [78].
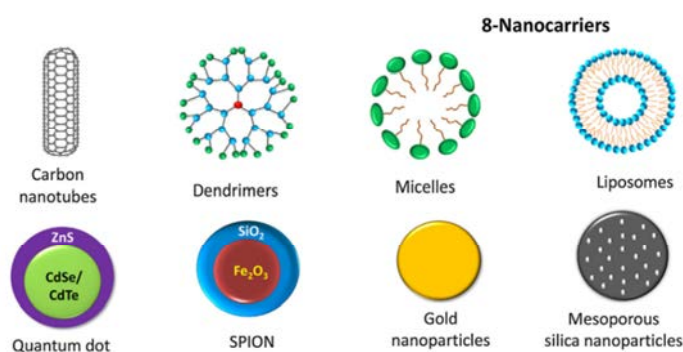
Figure 9. Schematic representation of the 8 nanocarriers used in smart drug delivery systems [78].

2.4.1. Polymeric nanoparticles

Polymeric nanoparticles (NPs) (Figure 8) are the nanocarriers mostly investigated as drug delivery systems (DDS). NPs are colloidal carriers that can have a natural or

synthetic origin and can vary from 1 to 1000 nm in size. They may be able to load drugs by different mechanism as chemical bonding, encapsulation, adsorption, or dispersion. The nano-size range of these systems allows them to be injected directly into the systemic circulation without the risk of blocking the blood vessels. It has been shown that the size of the nanoparticle is the major factor determining the in vivo fate of the particles. Synthetic NPs may be prepared from a wide diversity of polymeric materials such as poly(ethyleneimine), poly(ε-caprolactone), poly(lactic-co-glycolic acid), polypeptides, polyesters, and also from inorganic materials such as gold, silicon dioxide among others [43].
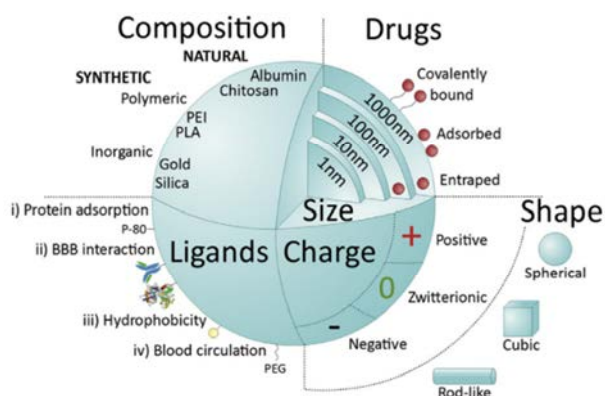
Figure 8. Main nanoparticle features influencing systemic delivery [43].

NPs can be conveniently prepared either from preformed polymers or by direct polymerization monomers using emulsion polymerization [73]. When dealing with preformed polymers, a rich assortment of preparation techniques such as solvent-evaporation, nanoprecipitation, or salting out among others, is available.

When amphiphilic copolymers are placed in an aqueous environment, the hydrophobic blocks constitute the core of the micelle while the hydrophilic blocks form the corona or outer shell. Within a specific and narrow concentration range of the amphiphile in solution, termed the critical micelle concentration (*cmc*), several amphiphile will self-assemble into colloidal-sized particles termed micelles. If the amphiphile concentration in solution remains above the *cmc*, micelles are

thermodynamically stabilized against disassembly. Upon dilution to a concentration below the *cmc*, micelles will disassembly at a rate largely depending on the structure of the amphiphiles and the interactions between the chains. The hydrophobic micelle core serves as a microenvironment for the incorporation of lipophilic drugs, while the corona shell serves as a stabilizing interface between the hydrophobic core and the external medium [74].

Polymer vesicles (or polymersomes) become increasingly attractive and experienced a blooming development in last decade. Typically, polymer vesicles are more complicated systems than polymer micelles and simple core-shell nanoparticles. They are nanoscale hollow spheres with a hydrophobic membrane and hydrophilic interior Polymersomes are highly expected to find promising applications in biomedical field, such as drug delivery, gene therapy, magnetic resonance imaging, cell mimicking, *etc*. [75]. There are six methods for the preparation of polymersomes using the self-assembly of polymers. Among them, only two are generally used. One is the 'solvent switch' method, where an organic solvent is used to dissolve the polymer before self-assembly. The second is an organic-solvent-free method, where only water is needed for the dissolution of the polymer for self-assembly. Other methods include polymerization-induced self-assembly, centrifugation induced self-assembly, microfluid, and nano-printing. A major drawback of the polymers vesicles is the lack of biofunctionality, which restricts their ability to either target or interact with cells and tissues. Incorporation of polypeptide segments into copolymers provides significant advantanges in controlling the function of bioinspired assemblies which are desirable for drug delivery applications [76].

2.4.2 Nanocarriers for drug delivery and transfection

Drug administration by means of NPs is in principle suitable for all kinds of therapy. However, particular attention has been and continues being paid to NPs addressed to the use in oncologic therapy. Cancer is a leading cause of morbidity and

mortality worldwide. It is estimated that there will be 13.1 million deaths due to the cancer in 2030 [81]. Doxorubicin is an anthracycline antibiotic derived from the actinobacteria *Streptomyces peucetius var. caesius*. Its chemical structure is shown in Figure 10. Doxorubicin is a cell cycle-nonspecific agent that acts by blocking topoisomerase II activity. The molecule becomes intercalated into the flat space between the bases of DNA double helix, where it can act further to disrupt DNA replication and transcription. Doxorubicin is indicated in the treatment of many human cancers, including breast, ovarian, lung, bladder, thyroid, liver, and gastric cancers [82]. Doxorubicin has been used in a plenty of investigations in drug delivery systems as a drug model [83]. This drug has been used in this Thesis for the preliminary evaluation of the DDS here investigated.
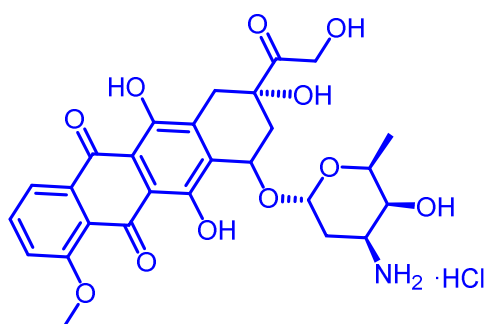
Figure 10. DOX·HCl is an amphiphilic drug, with a pronounce aromatic nature and containing a protonable amino group in the sugar moiety.

Gene therapy refers to the treatments that imply the transfer of genetic molecules into specific cells of a patient for the therapy of diseases. Condensing DNA into nanoparticles is critical in gene transfection, and electrostatic interactions of synthetic cationic liposomes or cationic polymers with DNA are generally used for condensing DNA [75]. Cationic polymer systems can load genes by forming polyplexes with negatively charged DNA, which can protect DNA from degradation and facilitate its cellular uptake and intracellular traffic into the nucleus. Up to now, more and more

studies have demonstrated that the interactions in DNA condensation can make a great contribution to enhance the efficacy of gene delivery [80].

For example, polyion complexes of a nucleotide with polycations are considered one of the promising systems for a gene vector. DNA has a polyanionic character and can be bound to polycations, e.g. poly(L-lysine), though electrostatic interaction (Fig. 11). It is well

known that polylysine strongly binds to DNA to induce compactation of the DNA molecule [84].
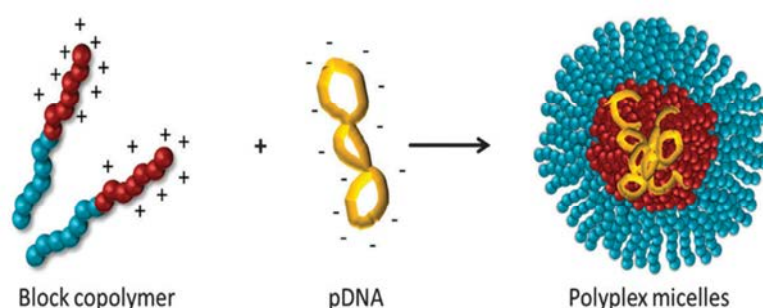
Figure 11. Polyplexes formed with preformed micelles and plasmid DNA. (+) Represents the cationic charges of the copolymers or the surfaces charges of the preformed micelles and (-) represents the negative charges of the pNDA [84].

2.4.3 Stimuli-responsive systems

The design of intelligent nanocarriers is undoubtedly a challenging issue, since the required drug delivery systems have to be both site-specific and time-release controlled. The controlled releasing of drugs can be triggered by various external or internal stimuli. pH, redox, and enzyme activity are envisaged as internal stimuli, whereas, light, magnetic fields, and ultrasounds are recognized as external stimuli. Temperature can be either an internal or external stimulus [85,86].

pH and temperatures are among the stimuli more extensively investigated. Many peptides can respond to switches in pH due to protonation or deprotonation from basic and acidic amino acids. The most well studied systems employing acidic and basic amino acids are those that consist of poly(L-glutamic acid) (PLGA) and poly(L-lysine) (PLLys). The linear PLGA homopolymer (pK$_a$ 4.32) dissolves in water in its anionic

form with the polymer in an extended random coil, but below 4.3 as it becomes neutral and changes to an α-helical conformation that precipitates from the solution. Likewise, PLLys whose pK_a is roughly 10.53 also displays helix-to-coil transitions as a function of pH [87,88].

Temperature has been investigated to control the release of drugs from DDS in both space and time. The hyperthermic nature of most inflamed pathological sites and tumors can act as internal stimulus. In fact, since there is a change in solubility with temperature. The most well-known temperature-sensitive materials are those able to switch their structure from a shrunken form to a swollen form (or *vice versa*) in response to a change in temperature. They are characterized by an upper critical solution temperature (UCST) or a lower critical solution temperature (LCST). By changing the temperature around the UCST or LCST, a phase transition leading to swelling or shrinking occurs. Drugs can be easily loaded into LCST polymers at room temperature, and then delivered to the target tissue where they are released by temperature effect [86,89].

2.5. References

[1]   G.M. Whitesides, Self-assembly at all scales, Science 295 (2002) 2418–2421.

[2]   H. Chi, M. Wang, Y. Xiao, F. Wang, J. K.S, Self-assembly and applications of amphiphilic hybrid POSS copolymers, Molecules 23 (2018) 2481

[3]   C.-A. Schoenenberger, W.P. Meier, M. Kyropoulou, S. Yorulmaz Avsar, S. Di Leone, C.G. Palivan, Biomolecules turn self-assembling amphiphilic block co-polymer platforms into biomimetic interfaces, Front. Chem. 6 (2019) 1–29.

[4]   H.-A. Klok, S. Lecommandoux, Supramolecular materials via block copolymer self-assembly, Adv. Mater. 13 (2001) 1217-1229.

[5]   M. Hillmyer, Block copolymer synthesis, Curr. Opin. Solid State Mater. Sci. 4 (1999) 559–564.

[6]   R. Faust, H. Schaald, Ionic polymerization, in: Appl. Polym. Sci. 21st Century,

Elsevier, 2000: pp. 999–1020.

[7] a) A.-C. Albertsson, I.K. Varma, Recent developments in ring opening polymerization of lactones for biomedical applications, Biomacromolecules 4 (2003) 1466–1486; b) Y. Yamashita, Ring-Opening Polymerization, Kobunshi. 29 (1980) 829-832,813; c) P. Lecomte, C. Jérôme, Recent Developments in Ring-Opening Polymerization of Lactones, in: Adv. Comput. Simul. Approaches Soft Matter Sci. I, 2011: pp. 173–217.

[8] W.A. Braunecker, K. Matyjaszewski, Controlled/living radical polymerization: features, developments, and perspectives, Prog. Polym. Sci. 32 (2007) 93–146.

[9] a) S. Fakirov, Polycondensation (condensation polymerization), in: Fundam. Polym. Sci. Eng., Wiley-VCH Verlag GmbH & Co. KGaA, Weinheim, Germany, 2017: pp. 221–240; b) P.M. Valetskii, I.P. Storozhuk, Block copolymers of the polycondensation type, Russ. Chem. Rev. 48 (1979) 42–61.

[10] K. Letchford, H. Burt, A review of the formation and classification of amphiphilic block copolymer nanoparticulate structures: micelles, nanospheres, nanocapsules and polymersomes, Eur. J. Pharm. Biopharm. 65 (2007) 259–269.

[11] C. Feng, Y. Li, D. Yang, J. Hu, X. Zhang, X. Huang, Well-defined graft copolymers: from controlled synthesis to multipurpose applications, Chem. Soc. Rev. 40 (2011) 1282–1295.

[12] H. Freichels, D. Alaimo, R. Auzély-Velty, C. Jérôme, α-Acetal, ω-alkyne Poly(ethylene oxide) as a versatile building block for the synthesis of glycoconjugated graft-copolymers suited for targeted drug delivery, Bioconjug. Chem. 23 (2012) 1740–1752.

[13] D. Margerison, G.C. East, Ionic polymerization, in: An Introd. to Polym. Chem., Elsevier, 1967: pp. 238–283.

[14] M. Pitsikalis, Ionic polymerization, in: Ref. Modul. Chem. Mol. Sci. Chem. Eng., Elsevier, 2013: pp. 1–19.

[15] C. Cai, L. Wang, J. Lin, Self-assembly of polypeptide-based copolymers into

diverse aggregates, Chem. Commun. 47 (2011) 11189–11203.

[16] L.I. Atanase, J. Desbrieres, G. Riess, Micellization of synthetic and polysaccharides-based graft copolymers in aqueous media, Prog. Polym. Sci. 73 (2017) 32–60.

[17] V. Mikhalevich, I. Craciun, M. Kyropoulou, C.G. Palivan, W. Meier, Amphiphilic peptide self-assembly: expansion to hybrid materials, Biomacromolecules 18 (2017) 3471–3480.

[18] J. Wang, K. Liu, R. Xing, X. Yan, Peptide self-assembly: thermodynamics and kinetics, Chem. Soc. Rev. 45 (2016) 5589–5604.

[19] S. Wong, M.S. Shim, Y.J. Kwon, Synthetically designed peptide-based biomaterials with stimuli-responsive and membrane-active properties for biomedical applications, J. Mater. Chem. B. 2 (2014) 595–615.

[20] F. Sanda, T. Endo, Syntheses and functions of polymers based on amino acids, Macromol. Chem. Phys. 200 (1999) 2651–2661.

[21] S. Fleming, R. V. Ulijn, Design of nanostructures based on aromatic peptide amphiphiles, Chem. Soc. Rev. 43 (2014) 8150–8177.

[22] J. Wang, H. Lu, R. Kamat, S. V. Pingali, V.S. Urban, J. Cheng, Y. Lin, Supramolecular polymerization from polypeptide-grafted comb polymers, J. Am. Chem. Soc. 133 (2011) 12906–12909.

[23] W.N.E. Van Dijk-Wolthuis, L. Van De Water, P. Van De Wetering, M.J. Van Steenbergen, J.J. Kettenes-van Den Bosch, W.J.W. Schuyl, W.E. Hennink, Synthesis and characterization of poly-L-lysine with controlled low molecular weight, Macromol. Chem. Phys. 198 (1997) 3893–3906.

[24] G. Zhang, Jianbiao, Y. Li, Y. Wang, Synthesis and characterization of poly(L-alanine)-*block*-poly(ethylene glycol) monomethyl ether as amphiphilic biodegradable co-polymers, J. Biomater. Sci. Polym. Ed. 14 (2003) 1389–1400.

[25] M. Planellas, J. Puiggalí, Synthesis and Properties of Poly(L-lactide)-*b*-poly(L-phenylalanine) hybrid copolymers, Int. J. Mol. Sci. 15 (2014) 13247–13266.

[26]   T.J. Deming, Synthesis of side-chain modified polypeptides, Chem. Rev. 116 (2016) 786–808.

[27]   N. Hadjichristidis, H. Iatrou, M. Pitsikalis, G. Sakellariou, Synthesis of well-defined polypeptide-based materials via the ring-opening polymerization of α-amino acid N-carboxyanhydrides, Chem. Rev. 109 (2009) 5528–5578.

[28]   W. Zhao, Y. Gnanou, N. Hadjichristidis, Organocatalysis by hydrogen-bonding: a new approach to controlled/living polymerization of α-amino acid N-carboxyanhydrides, Polym. Chem. 6 (2015) 6193–6201.

[29]   Z. Song, H. Fu, R. Wang, L.A. Pacheco, X. Wang, Y. Lin, J. Cheng, Secondary structures in synthetic polypeptides from N-carboxyanhydrides: design, modulation, association, and material applications, Chem. Soc. Rev. 47 (2018) 7401–7425.

[30]   A. Carlsen, S. Lecommandoux, Current opinion in colloid & interface science self-assembly of polypeptide-based block copolymer amphiphiles, Curr. Opin. Colloid Interface Sci. 14 (2009) 329–339.

[31]   N.J. Greenfield, Using circular dichroism spectra to estimate protein secondary structure, Nat. Protoc. 1 (2006) 2876–2890.

[32]   S. Seshadri, R. Khurana, A.L. Fink, Fourier transform infrared spectroscopy in analysis of protein deposits, in: Methods Enzymol., 1999: pp. 559–576.

[33]   Z. Song, H. Fu, R. Wang, L.A. Pacheco, X. Wang, Y. Lin, J. Cheng, Secondary structures in synthetic polypeptides from N-carboxyanhydrides: design, modulation, association, and material applications, Chem. Soc. Rev. 47 (2018) 7401–7425.

[34]   C. He, X. Zhuang, Z. Tang, H. Tian, X. Chen, Stimuli-sensitive synthetic polypeptide-based materials for drug and gene delivery, Adv. Healthc. Mater. 1 (2012) 48–78.

[35]   L.A. Canalle, D.W.P.M. Löwik, J.C.M. van Hest, Polypeptide–polymer bioconjugates, Chem. Soc. Rev. 39 (2010) 329–353.

[36] B.A. Paik, S.R. Mane, X. Jia, K.L. Kiick, Responsive hybrid (poly)peptide–polymer conjugates, J. Mater. Chem. B. 5 (2017) 8274–8288.

[37] G.J.M. Habraken, A. Heise, P.D. Thornton, Block copolypeptides prepared by *N*-carboxyanhydride ring-opening polymerization, Macromol. Rapid Commun. 33 (2012) 272–286.

[38] J. Billot, A. Douy, B. Gallot, Preparation, fractionation, and structure of block copolymers polystyrene-poly(carbobenzoxy-L-lysine) and polybutadiene-poly(carbobenzoxy-L-lysine), Die Makromol. Chemie. 178 (1977) 1641–1650.

[39] A. Douy, B. Gallot, Block copolymers with a polyvinyl and a polypeptide block: factors governing the folding of the polypeptide chains, Polymer (Guildf). 23 (1982) 1039–1044.

[40] K. Janssen, M. van Beylen, C. Samyn, R. Scherrenberg, H. Reynaers, Morphology of ABA triblock copolymers consisting of poly(γ-benzyl-L-glutamate) as the A component and polystyrene as the B component, Die Makromol. Chemie. 191 (1990) 2777–2785.

[41] H.A. Klok, J.F. Langenwalter, S. Locommandoux, Self-assembly of peptide-based diblock oligomers, Macromolecules 33 (2000) 7819–7826.

[42] H.-A. Klok, S. Lecommandoux, Solid-state structure, organizationand properties of peptide—synthetic hybrid block copolymers, in: Pept. Hybrid Polym., Springer-Verlag, Berlin/Heidelberg, 2006: pp. 75–111.

[43] K. Kataoka, K. Osada, Drug and gene delivery based on supramolecular assembly of PEG-Polypeptide hybrid block copolymers, Adv. Polym. Sci. 202 (2006) 113–153.

[44] M. Morell, J. Puiggalí, Hybrid block copolymers constituted by peptides and synthetic polymers: an overview of synthetic approaches, supramolecular behavior and potential applications, Polymers (Basel). 5 (2013) 188–224.

[45] H. Schlaad, M. Antonietti, Block copolymers with amino acid sequences: Molecular chimeras of polypeptides and synthetic polymers, Eur. Phys. J. E. 10

(2003) 17–23.

[46] P. Lecomte, C. Jérôme, Recent developments in ring-opening polymerization of lactones, in: Adv. Polym. Sci., 2011: pp. 173–217.

[47] S. Clarke, Families of compounds that occur in essential oils, in: Essent. Chem. Aromather., Elsevier, 2008: pp. 41–77.

[48] K.M. Stridsberg, M. Ryner, A. Albertsson, Controlled ring-opening polymerization: polymers with designed macromolecular architecture, in: Degrad. Aliphatic Polyesters, Springer Berlin Heidelberg, Berlin, Heidelberg, 2002: pp. 41–65.

[49] P.H. Dubois, P.H. Degée, R. Jérôme, P.H. Teyssié, Macromolecular engineering of polylactones and polylactides. 8. ring-opening polymerization of ε-caprolactone initiated by primary amines and trialkylaluminum, Macromolecules 25 (1992) 2614–2618.

[50] A. Kowalski, J. Libiszowski, T. Biela, M. Cypryk, A. Duda, S. Penczek, Kinetics and mechanism of cyclic esters polymerization initiated with tin(II) octoate. Polymerization of ε-caprolactone and L,L-Lactide co-initiated with primary amines, Macromolecules 38 (2005) 8170–8176.

[51] M. Marzorati, C. Navarra, R. Mendichi, S. Riva, B. Danieli, Incorporation of primary amines into a poly(1,5-dioxepan-2-one) via lipase-catalyzed ring-opening polymerization, J. Mol. Catal. B Enzym. 52–53 (2008) 158–161.

[52] a) J.A. Wilson, Z. Ates, R.L. Pflughaupt, A.P. Dove, A. Heise, Polymers from macrolactones: from pheromones to functional materials, Prog. Polym. Sci. 91 (2019) 29–50; b) I. van der Meulen, M. de Geus, H. Antheunis, R. Deumens, E.A.J. Joosten, C.E. Koning, A. Heise, Polymers from functional macrolactones as potential biomaterials: enzymatic ring opening polymerization, biodegradation, and biocompatibility, Biomacromolecules 9 (2008) 3404–3410.

[53] S. Strandman, J.E. Gautrot, X.X. Zhu, Recent advances in entropy-driven ring-opening polymerizations, Polym. Chem. 2 (2011) 791–799.

[54] M. Gazzano, V. Malta, M.L. Focarete, M. Scandola, R. A. Gross, Crystal structure of poly(ω-pentadecalactone), J. Polym. Sci. Part B Polym. Phys. 41 (2003) 1009–1013.

[55] R. Todd, S. Tempelaar, G. Lo Re, S. Spinella, S.A. McCallum, R.A. Gross, J.-M. Raquez, P. Dubois, Poly(ω-pentadecalactone)-b-poly(L-lactide) block copolymers via organic-catalyzed ring opening polymerization and potential applications, ACS Macro Lett. 4 (2015) 408–411.

[56] P. Vanhoorne, P. Dubois, R. Jerome, P. Teyssie, Macromolecular engineering of polylactones and polylactides. 7. Structural analysis of copolyesters of ε-caprolactone and L- or D,L-lactide initiated by triisopropoxyaluminum, Macromolecules 25 (1992) 37–44.

[57] Š. Gradišar, E. Žagar, D. Pahovnik, Hybrid block copolymers of polyesters/polycarbonates and polypeptides synthesized via one-pot sequential ring-opening polymerization, Polym. Chem. 9 (2018) 4764–4771.

[58] G. Rong, M. Deng, C. Deng, Z. Tang, L. Piao, X. Chen, X. Jing, Synthesis of poly(ε-caprolactone)-*b*-poly(γ-benzyl-L-glutamic acid) block copolymer using amino organic calcium catalyst, Biomacromolecules 4 (2003) 1800–1804.

[59] H.R. Kricheldorf, K. Hauser, Polylactones . 55 . A - B - A triblock copolymers of various polypeptides. Syntheses involving 4-aminobenzoyl-terminated poly (ε-caprolactone) as b block, (2001) 1110–1115.

[60] C. Tsai, Z. Gan, T. Chen, S. Kuo, Competitive hydrogen bonding interactions influence the secondary and hierarchical self-assembled structures of polypeptide-based triblock copolymers, Macromolecules 51 (2018) 3017–3029.

[61] Q. Wu, L. Zhou, D. Zhang, X. Song, G. Zhang, Synthesis and characterization of biodegradable poly(ε-caprolactone)/poly(γ-benzyl-L-glutamate) block copolymer, Polym. Bull. 67 (2011) 1227–1236.

[62] S. Motala-Timol, D. Jhurry, J. Zhou, A. Bhaw-Luximon, G. Mohun, H. Ritter,

Amphiphilic poly(L-lysine-*b*-caprolactone) block copolymers: Synthesis, characterization and solution properties, Macromolecules 41 (2008) 5571–5576.

[63] M. Gotsche, Amino-termined poly(L-Lactide)s as initiators for the polymerization of *N*-carboxyanhydrides: synthesis of poly(L-lactide)-*block*-poly(α-amino acid)s, Macromol. Chem. Phys. 196 (1995) 3891–3903.

[64] E. Mayans, S.K. Murase, M.M. Pérez-Madrigal, C. Cativiela, C. Alemán, J. Puiggalí, Hybrid polypeptide/polylactide copolymers with short phenylalanine Blocks, Macromol. Chem. Phys. 219 (2018) 1800168.

[65] J. Sun, C. Deng, X. Chen, H. Yu, H. Tian, J. Sun, X. Jing, Self-assembly of polypeptide-containing ABC-type triblock copolymers in aqueous solution and its pH dependence, Biomacromolecules 8 (2007) 1013–1017.

[66] Y.F. Fan, G. Chen, J. Tanaka, T. Tateishi, L-Phe end-capped poly(L-lactide) as macroinitiator for the synthesis of poly(L-lactide)-*b*-poly(L-lysine) block copolymer, Biomacromolecules 6 (2005) 3051–3056.

[67] N. Xu, F. Du, Z. Li, Synthesis of Poly(L-lysine)-*graft*-polyesters through Michael Addition and their self-assemblies in aqueous solutions, J. Polym. Sci. Part A Polym. Chem. 45 (2007) 1889–1898.

[68] B. Nottelet, A. El Ghzaoui, J. Coudane, M. Vert, Novel amphiphilic poly(ε-caprolactone)-*g*-poly(L-lysine) degradable copolymers, Biomacromolecules 8 (2007) 2594–2601.

[69] S. Caillol, S. Lecommandoux, A.-F. Mingotaud, M. Schappacher, A. Soum, N. Bryson, R. Meyrueix, Synthesis and self-assembly properties of peptide-polylactide block copolymers, Macromolecules 36 (2003) 1118–1124

[70] T. Degée, Ph, Dubois, Ph. Jérôme, R., Synthesis and characterization of biocompatible and biodegradable poly(ε-caprolactone-*b*-γ-benzyl glutamate) diblock copolymers, J. Polym. Sci. Part A Polym. Chem. 31 (1993) 275–278.

[71] G. Rong, M. Deng, C. Deng, Z. Tang, L. Piao, X. Chen, X. Jing, Synthesis of

poly(ε-caprolactone)-*b*-poly(γ-benzyl-L-glutamic acid) block copolymer using amino organic calcium catalyst, (2003) 1800–1804.

[72] C. Deng, J. Wu, R. Cheng, F. Meng, H. Klok, Functional polypeptide and hybrid materials: precision synthesis via α-amino acid *N*-carboxyanhydride polymerization and emerging biomedical applications, Prog. Polym. Sci. 39 (2014) 330–364.

[73] J.P. Rao, K.E. Geckeler, Progress in polymer science polymer nanoparticles: preparation techniques and size-control parameters, Prog. Polym. Sci. 36 (2011) 887–913.

[74] C. Allen, D. Maysinger, A. Eisenberg, Nano-engineering block copolymer aggregates for drug delivery, Colloids Surfaces B Biointerfaces. 16 (1999) 3–27.

[75] Y. Zhu, B. Yang, S. Chen, J. Du, Progress in polymer science polymer vesicles: mechanism, preparation, application, and responsive behavior, Prog. Polym. Sci. 64 (2017) 1–22.

[76] L. Zhao, N. Li, K. Wang, C. Shi, L. Zhang, Y. Luan, A review of polypeptide-based polymersomes, Biomaterials 35 (2014) 1284–1301.

[77] S. Bannerjee, B. Sriwastawa, P. Pandey, S. Pandey, R. Tiwari, G. Tiwari, L. Bhati, Drug delivery systems: an updated review, Int. J. Pharm. Investig. 2 (2012) 2.

[78] M.K. Hossain, S. Hossen, M.J. Uddin, M.T. Rahman, M.N.H. Mia, M.K. Basher, Smart nanocarrier-based drug delivery systems for cancer therapy and toxicity studies: A review, J. Adv. Res. 15 (2018) 1–18.

[79] X. Nie, Z. Zhang, C.H. Wang, Y.S. Fan, Q.Y. Meng, Y.Z. You, Interactions in DNA condensation: an important factor for improving the efficacy of gene transfection, Bioconjug. Chem. 30 (2018) 284–292.

[80] X. Chen, P. Sun, Z. Guo, C. Xu, L. Lin, H. Tian, J. Wu, J. Chen, H. Fang, Molecular strings significantly improved the gene transfection efficiency of polycations, J. Am. Chem. Soc. 140 (2018) 11992–12000.

[81] S. Rivankar, An overview of doxorubicin formulations in cancer therapy, J. Cancer Res. Ther. 10 (2014) 853.

[82] R. Thirumaran, G.C. Prendergast, P.B. Gilman, Cytotoxic chemotherapy in clinical treatment of cancer, in: Cancer Immunother., Elsevier, 2007: pp. 101–116.

[83] N. Zhao, M. C Woodle, A.J. Mixson, Advances in delivery systems for doxorubicin, J. Nanomed. Nanotechnol. 09 (2018) 1–9.

[84] A.C. Rinkenauer, S. Schubert, A. Traeger, U.S. Schubert, The influence of polymer architecture on in vitro pDNA transfection, J. Mater. Chem. B. 3 (2015) 7477–7493.

[85] M. Karimi, A. Ghasemi, P. Sahandi Zangabad, R. Rahighi, S.M. Moosavi Basri, H. Mirshekari, M. Amiri, Z. Shafaei Pishabad, A. Aslani, M. Bozorgomid, D. Ghosh, A. Beyzavi, A. Vaseghi, A.R. Aref, L. Haghani, S. Bahrami, M.R. Hamblin, Smart micro/nanoparticles in stimulus-responsive drug/gene delivery systems, Chem. Soc. Rev. 45 (2016) 1457–1501.

[86] Y. Shen, X. Fu, Z. Li, Biodegradable stimuli-responsive polypeptide materials materials prepared by ring opening polymerization, Chem. Soc. Rev. 44 (2015) 612–622.

[87] Z. Wang, X. Deng, J. Ding, W. Zhou, X. Zheng, G. Tang, Mechanisms of drug release in pH-sensitive micelles for tumour targeted drug delivery system: A review, Int. J. Pharm. 535 (2018) 253–260.

[88] J. Rodríguez-Hernández, S. Lecommandoux, Reversible Inside−Out Micellization of pH-responsive and Water-Soluble Vesicles Based on Polypeptide Diblock Copolymers, J. Am. Chem. Soc. 127 (2005) 2026–2027.

[89] D. Schmaljohann, Thermo- and pH-responsive polymers in drug delivery, Adv. Drug Deliv. Rev. 58 (2006) 1655–1670.

Chapter 3. Materials and Methods

3.1 Introduction

Polymerization is the tool universally used for building new polymers. The synthesis of a new polymer is preceded by the synthesis of the monomers needed for polymerization. There are a good number of polymerization procedures that may be applied to provide the desired polymer chemical structure. The synthesis possibilities increase for building copolymers since polymer modification approaches are then feasible. To verify that the polymer chain synthesized is what was expected, or in order to relate the polymer properties to the structure of the material, polymer characterization tools and properties evaluation tests are required. Characterization in its wider scope will include the analysis of the structure and the evaluation of the basic properties. The structure of a polymer comprises both its chemical and physical features and the basic properties include thermal and mechanical properties. However the structural analysis may be focused in certain features according to the function expected for the new polymer. Similarly, the properties evaluated may include the specific behavior of the polymer according to the applications to which it is addressed.

3.2 Materials

All chemicals, except otherwise stated, were purchased from Aldrich Chemical Co. Hexylamine (HexA), *c* (A-DEG-A)*,* allyamine (AllA), 1,5,7-triazabicyclo[4.4.0]dec-5-ene (TBD) was dried in a desiccator with P_2O_5 for 16 h at 50 ^{0}C and bisamino-ended poly(ethylene glycol) (PEG) with M_n ≈ 2,600 was used as received. ω-Pentadecalactone was freshly distilled in vacuum and stored under nitrogen. Globalide was provided by Grupo Indukern, Barcelona. Novozym 435 (supported *Candida antarctica* Lipase B, CALB), a gift of Novozymes, Denmark. Poly(vinyl alcohol) (PVA, M_W ≈ 3000, 88%

hydrolyzed) was obtained from Scientific Polymer Products, Inc. Triphosgene, α-pinene, γ-benzyl L-glutamate (BLG) and $^\varepsilon$N-carbobenzoxy-L-lysine (ZLL), L-alanine (Ala) were purchased from Bachem. 2-(Boc-amino)ethanethiol (BAET). 2,2'-Azobis(2-methylpropionitrile) (AIBN). Doxorubicin (DOX·HCl) was purchased from AK Scientific, Inc. (USA), DNA (~2000 bp) (from salmon testes).

Solvents used for isolation and purification were of high-purity grade and used as received. Toluene was freshly distilled and kept on 3 Å molecular sieves. Trifluoroacetic acid (TFA) and HBr/acetic acid, anhydrous dimethyl formamide (DMF), tetrahydrofuran (THF), ethyl acetate and heptane were used directly from the bottle under an inert atmosphere. Hexafluoroisopropanol (HFIP) from Apollo Scientic, UK.

3.3 Measurements

NMR spectroscopy. ^{1}H and ^{13}C NMR spectra were recorded on a Bruker AMX-300 spectrometer at 25 ^{o}C operating at 300.1 and 75.5 MHz, respectively. Compounds were dissolved in deuterated chloroform (CDCl$_3$) or a mixture of trifluoroacetic acid (TFA) and CDCl$_3$, and spectra were internally referenced to tetramethylsilane (TMS). About 10 and 50 mg of sample in 1 mL of solvent were used for ^{1}H and ^{13}C NMR, respectively. Sixty-four scans were recorded for ^{1}H, and between 1000 and 10,000 scans for ^{13}C NMR.

TGA and DSC. Thermogravimetric analysis (TGA) was performed on a Mettler-Toledo TGA/DSC 1 Star System under a nitrogen flow of 20 mL min^{-1} at a heating rate of 10 °C min^{-1} and within a temperature range of 30-600 °C. The thermal transitions were examined by differential scanning calorimetry (DSC) using a Perkin-Elmer Pyris apparatus. Thermograms were registered from 4-6 mg samples at heating and cooling rates of 10 °C min^{-1} under a nitrogen flow of 20 mL min^{-1}. Indium and zinc were used as standards for temperature and enthalpy calibration.

FT-IR spectroscopy. FTIR measurements were made on a Perkin-Elmer FT-IR spectrophotometer Frontier. Spectra were obtained from powder samples using a Universal ATR sampling accessory in the 4000-450 cm^{-1} region from 8 scans with a resolution of 4 cm^{-1}. For the spectra recorded a variable temperature, solutions of 5 mg of polymer dissolved in 1 mL HFIP were prepared. Then, these solutions were deposited over a NaCl plate, and a film was formed after HFIP evaporation. The plate was set on Variable Temperature FTIR CELL.

Gel permeation chromatography (GPC). Molecular weight analysis was performed by GPC on a Waters equipment provided with RI and UV detectors using hexafluoro-2-propanol (HFIP) as eluent. 100 µL of 0.1% (w/v) sample solution were injected and chromatographed with a flow of 0.4 $mL·min^{-1}$. HR5E and HR2 Waters linear Styragel columns (7.8 mm x 300 mm, pore size 10^3-10^4 Å) packed with crosslinked polystyrene and protected with a pre-column were used. Molar mass averages and their distributions were calculated against PMMA standards.

X-ray diffraction (XRD). Real time X-ray diffraction (XRD) studies were carried out using synchrotron radiation at the BL11 beamline for non-crystalline diffraction (NCD), at ALBA (Cerdanyola del Vallès, Barcelona, Spain). WAXS and SAXS spectra were recorded simultaneously from powder samples subjected to heating–cooling cycles at a rate of 10 ^{o}C min^{-1}. The energy employed corresponded to a 0.10 nm wavelength, and spectra were calibrated with silver behenate (AgBh) and Cr_2O_3.

Circular dichroism (CD). Measurements were performed using a Jasco spectropolarimeter J-815) (Centres Científics i Tecnològics, Universitat de Barcelona). Briefly, PPDL-*b*-PAA copolymer solutions were prepared at a concentration of 50 $µg·mL^{-1}$ in deionized water previously adjusted at the desired pH (2.0 or 10.0). Triplicate CD spectra were recorded using a 10 mm quartz cell at a scanning speed of

10 nm·s^{-1} in the 190-250 nm range either at constant temperature of 25 °C or at variable temperature in the 10-80 °C range.

Dynamic light scattering (DLS). Dynamic light scattering studies were performed using a Zetasizer Nano ZS series Malvern instrument equipped with a 4 mW He-Ne laser operated at a wavelength of 633 nm. Samples were placed in disposable cuvettes thermostated at 25 °C. The non-invasive back-scatter optical arrangement was used to collect the light scattered by the particles at an angle of 173°.

Ultraviolet Visible Spectrophotometry (UV-vis). UV-vis was used to quantify the amount of doxorubicin either entrapped or released in the nanoparticles. Samples were withdrawn and directly measured using a 10 mm quartz cuvette at 480 nm in a Cecil Aurius Series CE 2021 spectrophotometer.

Scanning electronic microscopy (SEM) and Transmission electronic microscopy (TEM). SEM images were taken with a field-emission JOEL JSM-7001F instrument (JEOL, Japan) from platinum/palladium coated samples. TEM images were recorded on a Hitachi 7650 microscope working at 120 kV. Samples were prepared by spraying a 1 g·L^{-1} solution of the copolymer onto a copper grid (200 mesh, carbon coated), dripping the water excess, and applying negative staining with 1% uranyl acetate aqueous solution.

Polarizing optical microscopy (POM). Micrographs were recorded using an Olimpus BX51 polarizing optical microscopy with a Linkam THMS 600 stage attached. For observation, 10 mg of sample were dissolved in 1 mL of chloroform and 0.2 mL aliquots of these solutions were slowly evaporated on a glass slide.

3.4 Syntheses

3.4.1 ROP of PDL using amino-ended compounds

Synthesis of PPDL. ROP of PDL was performed with the concourse of either enzymes or organic compounds as catalysts. For enzymatic polymerization, the amount of CALB was 20% (w/w) with respect to monomer in all cases, and for chemo-catalyzed polymerization, different amounts of TBD were tested in order to reach high conversions of PDL. The general procedure was as follows: CALB or TBD was introduced in an open round-bottom flask provided with a magnetic stirrer which was placed in a desiccator at 50 ºC for 16 h. For CALB mediated polymerization, the amine used as initiator was dissolved in dry toluene and the solution poured into the reaction flask, which was then transferred to an oil-bath at 100 ºC, and the calculated amount of PDL immediately added. When TBD was used, the required amounts of amine and PDL were added simultaneously to the catalyst, the flask was sealed, and the mixture was magnetically stirred at 100 ºC for the scheduled period of time. In both cases, aliquots were withdrawn at scheduled times and dissolved in CDCl$_3$ to be subjected to ^{1}H NMR analysis in order to follow the reaction progress. As soon as conversion remained unchanged, the reaction was stopped by cooling. For removing the enzyme, the toluene was evaporated, the residue dispersed in chloroform, and CALB filtered off. The polymer was then precipitated by pouring the filtrate in cold methanol. For polymerizations catalyzed by TBD, the crude reaction mass was dissolved in chloroform and precipitated in cold methanol. Irrespective of the catalyst used, the polymer was recovered by filtration and dried at room temperature under vacuum before characterization.

3.4.2 Synthesis of PPDL$_y$-PEG$_{56}$-PPDL$_y$ triblock copolymers.

Synthesis of PPDL-PEG-PPDL triblock copolymers. For the reactions carried out by enzymatic catalysis, the amount of CALB used was 20% (w/w) respect to monomer. For polymerizations catalyzed by TBD, the amount of catalyst added was previously optimized to attain the highest conversion of PDL. The general procedure was as follows: CALB or TBD was introduced in a round-bottom flask provided with a magnetic

stirrer which was then placed in a desiccator at 50 ºC for 16 h. When CALB was used, a solution of PEG ($M_n \approx 2{,}600$) in dry toluene was added to the flask, which was transferred to an oil-bath at 100 ºC. Then, PDL was added and the solution magnetically stirred for at least 4 h. When TBD was the catalyst of choice, the required amounts of PEG and PDL were added into the flask, which was then sealed and heated at 100 ^{0}C under magnetic stirring for 12 h. In all cases aliquots of the reaction mixture were withdrawn and analyzed by ^{1}H NMR in order to assess the advance of the polymerization reaction. For removing CALB, the toluene was evaporated under vacuum, the residue was re-dissolved in an excess of chloroform, and the enzyme was removed by filtration. The filtrate was then concentrated and precipitated in an excess of cold methanol. For polymerizations using TBD, the crude reaction mass was dissolved in chloroform and the solution precipitated in an excess of methanol. Regardless of the catalyst chosen, the copolymer was collected by filtration and dried in vacuum before characterization.

3.4.3 Synthesis of the poly[(ω-pentadecalactone)-*b*-(α-amino acid)] copolymers (PPDL$_x$-*b*-pPAA$_y$).

3.4.4 Synthesis of α-amino acids *N*-carboxyanhydrides (NCA)

Amino acids *N*-carboxyanhydrides (BLG-NCA, ZLL-NCA, Ala-NCA and Phe-NCA). γ-Benzyl L-glutamate and $^\varepsilon$*N*-carbobenzoxy L-lysine *N*-carboxyanhydrides. L-alanine and L-phenylalanine were prepared using the usual procedures described in literature [1, 2].

γ-Benzyl L-glutamate NCA. Yield: 90%. ^{1}H NMR (300 Mhz, CDCl$_3$, δ, ppm): 7.33 (m, 5H, ArH), 6.28 (broad, 1H, NH), 5.07 (s, 2H, CH$_2$), 4.30 (t, 1H, CH), 2.54 (t, 2H, CH$_2$), 2.22 (m, 1H, CH$_2$), 2.06 (m, 1H, CH$_2$).

ε*N*-carbobenzoxy L-lysine NCA. Yield: 80%. ^{1}H-NMR (300 Mhz, d_6-DMSO, δ, ppm): 9.10 (s, 1H, NH), 7.39-7.27 (m, 6H, -C_6H_5), 5.00 (s, 2H, -$OCCH_2$-C_6H_5), 4.42 (t, 1H, -CO-CH-CH_2), 2.98 (q, 2H, -CH_2-NH), 1.77-1.21 (m, 6H, -CH_2-CH_2-CH_2-NH).

L-Alanine NCA. Yield: 70%. ^{1}H-NMR (300 Mhz, d_6-DMSO, δ, ppm): 8.96 (s, 1H, NH), 4.46 (q, 1H, CH), 1.31 (d, 3H, CH_3).

L-Phenylalanine NCA. Yield: 80%. ^{1}H-NMR (400 Mhz, d_6-DMSO, δ, ppm): 9.10 (broad, 1H, NH), 7.26 (m, 5H, ArH), 4.79 (t, 1H, CH), 3.03 (d, 2H, CH_2).

3.4.5 Synthesis of the PPDL-NH$_2$ macroinitiator

Allyl-ended poly(ω-pentadecalactone) (PPDL-All). An exact amount (82 mg) of dried Novozym 435 was weighed into a Schlenk tube provided with a magnetic stirrer and added with 2 mL of dried toluene and then with 67 µL of a 1.33 M solution of allyl amine in toluene by means of a syringe through a rubber septum. The tube was immersed in an oil bath at 100 ºC and the reaction started upon injection of a solution of PDL (414 mg, 1.66 mmol) in toluene (1.5 mL). After 4 hours of reaction under stirring, the mixture was allowed cooling down and toluene was fully removed using a rotary evaporator. The solid residue was re-dissolved in chloroform and the enzyme removed by filtration. The filtered clean solution was then poured into cold methanol to render PPDL$_x$-All as a precipitate that was recovered by filtration and dried overnight under vacuum. Yield: 90%.

PPDL$_x$-NH$_2$. PPDL$_x$-All (474 mg, 1.595 mmol) and 2-(Boc-amino)ethanethiol (BAET) (1.49 g, 8.41 mmol) were added into a Schlenk tube containing azo-*bis*-isobutyronitrile (AIBN) (138 mg, 0.841 mmol) and provided with magnetic stirring. The mixture was then dissolved in 1 mL of chlorobenzene and the reaction tube was purged with nitrogen gas. The reaction was started by immersing the tube into an oil bath at 80 ºC and it was left to proceed for 4 h. For isolation and purification of the 2-(Boc-

amino)ethanethiol-ended poly(ω-pentadecalactone) (PPDL$_x$-BAET), the reaction mass was poured into cold methanol, the precipitate recovered by centrifugation, and the operation repeated for two times. Yield: 87%.

For unblocking the amino group in PPDL$_x$-BAET, 245 mg of this compound were dissolved in TFA (2.5 mL) and the solution stirred at room temperature for 3 min. The solution was then poured into a large excess of diethyl ether to precipitate the free amino-ended poly(ω-pentadecalactone) (PPDL$_x$-NH$_2$) as a white powder that was recovered by centrifugation, repeatedly washed with fresh solvent, and finally with 0.5 M NaHCO$_3$ aqueous solution. Yield: 82%.

Poly[(ω-pentadecalactone)-*b*-(γ-benzyl-L-glutamate)] copolymers (PPDL$_X$-*b*-PBLG$_y$). In a Schlenk tube, BLG-NCA (308.1 mg, 1.170 mmol) was dissolved in dried CHCl$_3$ (6 mL) and immersed in a 0 ºC water bath. Then a solution of PPDL$_x$-NH$_2$ (72.1 mg, 0.023 mmol) in dried CHCl$_3$ (3 mL) was injected into the Schlenk tube through a septum with a syringe under nitrogen atmosphere. The reaction was left under stirring until the BLG-NCA was completely consumed as monitored by FTIR spectroscopy. Then the copolymer was precipitated into an excess of diethyl ether, recovered by centrifugation and dried under vacuum. Yield: 90%.

Poly(ω-pentadecalactone)-*b*-($^{\varepsilon}N$-carbobenzoxy-L-lysine)] copolymers (PPDL$_X$-*b*-PZLL$_y$). The synthesis of these copolymers was carried out using the same procedure as for PPDL$_X$-*b*-PLGA$_y$ with a yield of 80%.

3.4.6 Deprotection of benzyl (Bn) and benzyloxycarbonyl (Z) groups from the (PPDL$_x$-*b*-pPAA$_y$) diblock copolymers

Poly[(ω-pentadecalactone)-*b*-(L-glutamic acid)] diblock copolymers (PPDL$_x$-*b*-PLGA$_y$). The benzyl carboxylate group of the polypeptide block of PPDL$_x$-*b*-PBLG$_y$ copolymers was split by treatment with hydrobromic acid. 220 mg of the esterified copolymer were dissolved in TFA (2 mL) and then 1 mL of 33% (w/w) HBr in acetic

acid was added slowly to this solution at 0 °C. After 3 h of reaction, the mixture was poured into an excess of diethyl ether and the precipitate was recovered by centrifugation. The carboxylic-free $PPDL_X$-b-$PLGA_y$ was washed twice with fresh diethyl ether and then dissolved in a 0.5 M $NaHCO_3$ aqueous solution. Other sodium salts generated in the reaction were removed by dialysis against distilled water for 72 h at room temperature using MW-CO 2.0 kDa membranes. The deprotected copolymer $PPDL_x$-b-$PLGA_y$ in the sodium salt form was recovered as a white powder after removing the water by rotaevaporation. Yield: 60-74%.

Poly[(ω-pentadecalactone)-b-(L-lysine)] ($PPDL_X$-b-PLL_y). Deprotection of $PPDL_X$-b-$PZLL_y$ copolymers by applying the same procedure described above for $PPDL_X$-b-$PBLG_y$ led to the amino-free copolymers $PPDL_X$-b-PLL_y. Yield: 65-72%

3.4.7 Synthesis of poly[GI_{20}-$graft$-$(AA)_z$] copolymers

3.4.8 Poly[GI_8-co-$(GINH_2)_{12}$] macroinitiator

Synthesis of polyglobalide (PGI). Novozyme 435 (0.44 g) was dried in a Schlenk flask over molecular sieves at 40 °C in a desiccator overnight. Globalide (2.1 g) and dried toluene (4.0 mL) were then added to the reaction flask which was purged with nitrogen gas and heated in an oil bath at 60 °C for four hours. Dichloromethane (DCM) was then added to dissolve the reaction product and inhibit the enzyme activity. The polyester was isolated from the filtered solution by precipitation into ice-cold methanol and dried overnight. Yield: 97%.

Synthesis of poly[GI_8-co-$(GI$-$AET)_{12}$]. Polyglobalide (0.2 g) and 2-(Boc-amino)ethanethiol (1.11 g) were weighed into a Schlenk tube together with AIBN (50 mg). 1 mL of THF was then added and the mixture purged with nitrogen gas. The reaction was commenced by immersing it into an oil bath at 80 °C under agitation provided by a magnetic stirrer. The reaction was allowed to run for 24 h and was terminated by addition of DCM to the reaction mixture immersed in an ice bath. The mixture was precipitated in cold methanol and the copolymer recovered by

centrifugation. The obtained poly[globalide-*co*-2-(Boc-amino)ethyl-thio globalide)] was dissolved in DCM and reprecipitated. Yield: 90%.

Removal of Boc from the 2-(Boc-amino)ethylthio side groups was made by treatment with TFA. A solution of the protected copolyester (100 mg) in 2 mL of TFA was stirred at room temperature for 3 h. Then, the solution was added to 30 mL of diethyl ether and the amino-free poly[Gl_8-*co*-($GlNH_2$)$_{12}$] copolymer was separated by centrifugation, washed twice with saturated 0.5 M aqueous $NaHCO_3$, and finally dried under vacuum at RT. Yield: 90%.

Poly[globalide-*graft*-(γ-benzyl-L-glutamate)$_z$] (Poly[Gl_{20}-*graft*-(BLG)$_z$]). In a Schlenk tube, BLG-NCA (124 mg, 0.468 mmol or 200 mg, 0.760 mmol) was dissolved in 6 mL anhydrous DMF and placed in a water-NaCl bath. A solution of poly[Gl_8-*co*-($GlNH_2$)$_{12}$] (36 mg, 0.0063 mmol or 25 mg, 0.0043 mmol) in 2 mL anhydrous DMF was injected through a rubber septum with a syringe. The reaction was left under stirring for 5 days and then it was precipitated into an excess of cold diethyl ether, recovered by centrifugation and dried under vacuum. Yield: 80%.

Poly[globalide-*graft*-(N^ε-carbobenzoxy-L-lysine)$_z$]   (Poly[Gl_{20}-*graft*-(ZLL)$_z$]) was synthesized in a similar fashion as poly[Gl_{20}-*graft*-(BLG)$_z$] with a yield of 80%.

For removal the benzyl group from poly[Gl_{20}-*graft*-(BLG)$_z$], 150 mg of copolymer were dissolved in 1 mL of TFA. Then a solution of HBr in glacial acetic acid (2.5 or 5 times excess with respect to polypeptide) was added slowly to the copolymer solution at 0 °C and after standing 3 h the solution was poured into an excess of diethyl ether. The precipitate was recovered by centrifugation, washed twice with diethyl ether, and dissolved in a 0.5 M $NaHCO_3$ aqueous solution to have the polymer in the sodium salt form. The basic solution was dialyzed against distilled water (MWCO 2.0 kDa) for 12 h at room temperature and dried under vacuum to render poly[Gl_{20}-*graft*-(LGA)$_z$] as a white solid. Yield: 80%.

Poly[Gl_{20}-*graft*-(LL)$_z$] was obtained by applying the same procedure to poly[Gl-*graft*-(ZLL)$_z$]. Yield: 75%.

3.4.9 Synthesis of the poly(macrolactone)-poly(alanine) copolymers

Poly(ω-pentadecalactone)-*block*-poly(L-alanine) P(PDL$_{10}$-*b*-PAla$_y$). By varying the Ala-NCA/PPDL$_{10}$NH$_2$ feed ratios, (30/1, 60/1 and 200/1), diblock copolymers with different polypeptide chain lengths were obtained. As an example for the synthesis of PPDL$_{10}$-*b*-PAla$_{60}$, Ala-NCA (100 mg, 0.87 mmol) was dissolved in dried CHCl$_3$ (6 mL) in a Schlenk tube and placed in a 0 $^\circ$C water-NaCl bath. A solution of PPDL$_{10}$-NH$_2$ (42 mg, 0.014 mmol) dissolved in dried CHCl$_3$ (3 mL) under nitrogen atmosphere was injected into the Ala-NCA solution through a rubber septum with a syringe. The reaction was left under stirring until the Ala-NCA had been completely consumed as monitored by FTIR spectroscopy. After full monomer conversion the polymer was precipitated into an excess of diethyl ether, recovered by centrifugation and dried under vacuum. Yield: 80%. ^{1}H and ^{13}C NMR spectra of a selection of these copolymers are provided in Figure S5 of the SI file.

Poly[globalide$_{20}$-*graft*-(L-alanine)$_z$] P[Gl$_{20}$-*g*-(Ala)$_z$]. Two copolymers were prepared by using Ala-NCA/P[Gl$_8$-*co*-(Gl-NH$_2$)$_{12}$] feed ratios of 1/5 and 1/25. Ala-NCA [(60 mg, 0.52 mmol) or (360 mg, 3.13 mmol)] was dissolved in 6 mL of anhydrous DMF in a Schlenk tube and placed in a 0 ºC water-NaCl bath. Solutions of P[Gl$_8$-*co*-(Gl-NH$_2$)$_{12}$] in 2 mL of anhydrous DMF [(30 mg, 0.095 mmol) or (40 mg, 0.126 mmol) per repeating unit] were injected into the solution through a rubber septum with a syringe. The reactions were left under stirring for 5 days under vacuum, and then the polymer was precipitated into an excess of cold diethyl ether, recovered by centrifugation and dried under vacuum. Yield: 80%. The ^{1}H NMR spectra of P[Gl$_{20}$-*g*-(Ala)$_{20}$] graft copolymer is provided in Figure S6 of the SI file.

3.4.10 Synthesis of P[(Gl$_x$-*r*-PDL$_y$)-*g*-BLG$_y$] graft copolymers

Synthesis of P(Gl$_x$-*r*-PDL$_y$) copolyesters by eROP. An exact amount of CALB (400 mg, 20 % w/w with respect to monomers) was added into a round bottom flask, which was then placed in a desiccator with P$_2$O$_5$ for 16 h at 50 ºC. Dry toluene (7 mL) was added and mixtures of ω-pentadecalactone (1 g, 4.60 mmol) and globalide (1 g, 4.19

mmol) at different composition molar ratios (Gl/PDL: 0/100, 10/90, 30/70, 50/50, 70/30, 90/10 and 100/0) were placed into the round bottom flask and immediately immersed in an oil bath at 70°C under nitrogen atmosphere and magnetic stirring. The reaction mixtures were lead to proceed for 24 h. Then, the mixtures were cooled down and the toluene removed by rota-evaporation. The obtained residue was dispersed in chloroform and the enzyme was filtered out. The polymer was precipitated in cold methanol, recovered by filtration and dried before characterization. Yield: 80-90%.

Functionalization of the P(Gl$_x$-r-PDL$_y$) copolyesters *via* thiol-ene click reaction

The P(Gl$_{13\%}$-r-PDL$_{87\%}$) or P(Gl$_{48\%}$-r-PDL$_{52\%}$) copolyesters were chosen as sources for the synthesis of the grafted copolymers. Briefly, the corresponding copolyester (0.2 g) and 2-(Boc-amino)ethanethiol (1.11 g) and AIBN (50 mg) were weighed in a Schlenk tube. Then, 1 mL of THF was added and the reaction tube was purged with nitrogen gas. The reaction commenced by immersing the tube into an oil bath at 80 ^{0}C and agitation was provided by magnetic stirring for 24 h. The reaction was terminated by the addition of dichloromethane (DCM) to the reaction mixture immersed in an ice bath. Afterward, the product was precipitated in cold methanol and recovered by centrifugation. This process was performed twice to render either the BAET modified copolymers P[(Gl-BAET)$_{13}$-r-PDL$_{87}$] or P[(Gl$_{24}$-r-(Gl-BAET)$_{24}$-r-PDL$_{52}$], respectively. Yield: 90%.

Removal of Boc-amino protecting groups. Solutions of copolyesters, P[(Gl-BAE)$_{13}$-r-PDL$_{87}$] and P[Gl$_{24}$-r-(Gl-BAET)$_{24}$-r-PDL$_{52}$], (100 mg) in trifluoroacetic acid (2 mL), were stirred at room temperature for 10 min. Then, the solutions were added to an excess of diethyl ether and the polymers recovered by centrifugation. The precipitates were washed twice with saturated aq NaHCO$_3$ (0.5 M). Finally, the products were dried in vacuum at room temperature before used to produce P[(Gl-NH$_2$)$_{13}$-r-PDL$_{87}$] and P[Gl$_{24}$-r-(Gl-NH$_2$)$_{24}$-r-PDL$_{52}$]. Yield: 90%.

Synthesis of the P[(Gl$_x$-r-PDL$_y$)-g-BLG$_y$] graft copolymers. Two graft copolymers were prepared using P[(Gl-NH$_2$)$_{13}$-r-PDL$_{87}$] and P[Gl$_{24}$-r-(Gl-NH$_2$)$_{24}$-r-PDL$_{52}$] as

macroinitiators, respectively, for the ROP of BLG-NCA. To prepare P[(Gl$_{13}$-r-PDL$_{87}$)-g-BLG$_2$], the P[(Gl-NH$_2$)$_{13}$-r-PDL$_{87}$] copolymer in a Schlenk tube was added with BLG-NCA [(290 mg, 1.10 mmol) dissolved in 6 mL of dry CHCl$_3$, and the tube placed in a NaCl-water bath. A solution of P[(Gl-NH$_2$)$_{13}$-r-PDL$_{87}$] [(5.2 mg, 0.016 mmol) in 2 mL of dried CHCl$_3$ was injected to the flask through a rubber septum with a syringe. The reaction was left to stir for 48 h and then precipitated into an excess of diethyl ether, recovered by centrifugation and dried under vacuum. The same methodology was used to prepare P[(Gl$_{48}$-r-PDL$_{52}$)-g-BLG$_{10}$] copolymer from P[Gl$_{24}$-r-(Gl-NH$_2$)$_{24}$-r-PDL$_{52}$] [(6.02 mg, 0.019 mmol) and BLG-NCA (100 mg, 0.382 mmol) but using DMF instead of CHCl$_3$ as solvent. Yield: 80-90%.

Graft copolymer deprotection. A general procedure was used for the deprotection of the PBLG pendant groups. Briefly, 2 mL of TFA was added to 170 mg of P[(Gl$_{13}$-r-PDL$_{87}$)-g-BLG$_2$] to dissolve the copolymer. A solution HBr in glacial acetic acid (2.5 or 5 times excess with respect to polypeptide) was added slowly to the copolymer solution at 0 ^{0}C. After 2 h, the solution was poured into an excess of diethyl ether. The precipitate was centrifuged and washed twice with diethyl ether. The obtained polymer was dissolved in 0.5 M Na$_2$HCO$_3$ aqueous solution and then dialyzed (MWCO 2000) against distilled water to yield P[(Gl$_{13}$-r-PDL$_{87}$)-g-LGA$_2$] in the salt form. The P[(Gl$_{48}$-r-PDL$_{52}$)-g-BLG$_{10}$] was treated in a similar trend to yield P[(Gl$_{48}$-r-PDL$_{52}$)-g-LGA$_{10}$] in 70% yield.

3.4.11 Synthesis of poly(globalide-g-L-phenylalanine)-b-poly(ethylene glycol)-b-poly(globalide-g-L-phenylalanine) P(Gl$_x$-g-Phe$_y$)-b-PEG$_{56}$-b-P(Gl$_x$-g-Phe$_y$)

Synthesis of PGl$_x$-PEG$_{56}$-PGl$_x$ triblock copolymers. Two copolymers were prepared varying the PEG/Gl feed ratio (1/40, 1/150). The amount of CALB used was 20% (w/w) respect to monomer in every case. For the synthesis of (PGl$_{15}$)-b-PEG$_{56}$-b-(PGl$_{15}$) CALB (146 mg) was introduced in a round-bottom flask provided with a magnetic stirrer which was then placed in a desiccator at 50 ^{0}C for 16 h. A solution of PEG (200 mg,

0.077 mmol) in dry toluene was added to the flask, which was transferred to an oil-bath at 100 ^{0}C. Then, GI (732 mg, 3.07 mmol) was added through a septum using a syringe and the solution magnetically stirred for at least 4 h. For removing CALB, the toluene was evaporated under vacuum and the residue re-dissolved in an excess of chloroform. The enzyme was removed by filtration. The filtrate was then concentrated and precipitated in an excess of cold methanol. The copolymer was collected by filtration and dried in vacuum prior to characterization. Yield: 90%. For the synthesis of **(PGI$_{70}$)**-*b*-PEG$_{56}$-*b*-**(PGI$_{70}$)**, CALB (120 mg), PEG (43 mg, 0.016 mmol) and GI (600 mg, 2.52 mmol) were used, and further steps were carried out as in **(PGI$_{15}$)**-*b*-PEG$_{56}$-*b*-**(PGI$_{15}$)**. Yield: 89%.

Insertion of Boc-amino protected groups onto GI units (Thiol-ene click reaction). (PGI$_{15}$)-*b*-PEG$_{56}$-*b*-(PGI$_{15}$) (190 mg) in the presence of AIBN (50 mg) were weighed and added into a Schlenk tube. Then 2-(Boc-amino)ethanethiol (1.13 g) was added with a syringe. To enhance mixture miscibility, 1 mL of THF was added and the reaction flask was purged with nitrogen gas. The reaction commenced by immersing the Schlenk tube into an oil bath at 80 $^{\circ}$C; solution agitation was provided by magnetic stirring. The reaction was terminated by addition of DCM to the reaction mixture immersed in an ice bath. The polymer was precipitated in ice-cold methanol and recovered by centrifugation. The final product P(GI$_{15}$-BAE)-*b*-PEG$_{56}$-*b*-P(GI$_{15}$-BAE) was dried overnight under vacuum at room temperature prior to further analysis. Yield: 86%. The post-functionalization of **(PGI$_{70}$)**-*b*-PEG$_{56}$-*b*-**(PGI$_{70}$)** was carried out in a similar trend using BAET (1.13 g), a 50 mg (AIBN) and THF (1 mL) to render P(GI$_{70}$-BAE)-*b*-PEG$_{56}$-*b*-P(GI$_{70}$-BAE). Yield: 85%.

Boc-amino deprotection. A solution **of** P(GI$_{15}$-BAE)-*b*-PEG$_{56}$-*b*-P(GI$_{15}$-BAE) copolymer (60 mg) in trifluoroacetic acid (TFA, 1.5 mL) was stirred at room temperature for 3 h. Then, the solution was added to 30 mL of diethyl ether and the polymer recovered by centrifugation. The precipitated was washed twice with saturated aq Na$_2$HCO$_3$ (0.5 M). Finally, the product P(GI$_{15}$-NH$_2$)-*b*-PEG$_{56}$-*b*-P(GI$_{15}$-NH$_2$) was dried in

vacuum at RT before used. Yield: 80%. The P(Gl$_{70}$-BAE)-*b*-PEG$_{56}$-*b*-P(Gl$_{70}$-BAE) copolymer was treated similarly to obtain P(Gl$_{70}$-NH$_2$)-*b*-PEG$_{56}$-*b*-P(Gl$_{70}$-NH$_2$). Yield: 80%.

Synthesis of poly(globalide-*g*-L-phenylalanine)-*b*-(poly(ethylene glycol)-*b*-poly(globalide-*g*-L-phenylalanine) P(Gl$_x$-*g*-Phe$_y$)-*b*-PEG$_{56}$-*b*-P(Gl$_x$-*g*-Phe$_y$). Three copolymers were prepared by varying the P(Gl$_x$-NH$_2$)-*b*-PEG$_{56}$-*b*-P(Gl$_x$-NH$_2$)/Phe-NCA feed ratio. For preparing the P(Gl$_{15}$-*g*-Phe$_y$)-PEG$_{56}$-P(Gl$_{15}$-*g*-Phe$_y$) copolymer, in a Schlenk tube, Phe-NCA (170 mg, 0.9 mmol, or 322 mg, 1.68 mmol) was dissolved in 6 mL anhydrous DMF and placed in a water-NaCl bath. A solution of P(Gl$_{15}$-NH$_2$)-PEG$_{56}$-P(Gl$_{15}$-NH$_2$) (56 mg, 0.18 mmol, or 76 mg, 0.24 mmol) in 2 mL anhydrous DMF was injected through a rubber septum with a syringe. The reaction was left to stir under vacuum until the Phe-NCA had been completely consumed as monitored by FTIR spectroscopy. After full monomer conversion, the copolymer was precipitated into an excess of cold diethyl ether, recovered by centrifugation and dried under vacuum. Yield: 70-80%. For preparing the P(Gl$_{70}$-*g*-Phe$_y$)-*b*-PEG$_{56}$-*b*-P(Gl$_{70}$-*g*-Phe$_y$) copolymer, Phe-NCA (220 mg, 1.14 mmol) and P(Gl$_{70}$-NH$_2$)-PEG$_{56}$-P(Gl$_{70}$-NH$_2$) (40 mg, 0.126 mmol) were used and further steps performed as in P(Gl$_{15}$-*g*-Phe$_y$)-PEG$_{56}$-P(Gl$_{15}$-*g*-Phe$_y$). Yield: 84%

3.5 Preparation of nanoparticles

3.5.1 Emulsion-solvent evaporation method

Nanoparticles were prepared by the oil-in-water single emulsion technique with minor modifications [3]. Specifically, 10 mg of PPDL$_x$PEG$_{56}$PPDL$_x$ copolymer were dissolved in 2 mL of methylene chloride and the solution added to 10 mL of 5% (w/w) PVA (M_w=2000 g·mol^{-1}) aqueous solution. The mixture was sonicated for 15 s three times to yield a homogeneous oil-in-water emulsion. This emulsion was immediately poured into 10 mL of the 0.3% PVA solution, and the mixture was magnetically stirred in an open beaker at room temperature for 3 h. Nanoparticles were formed along with

the gradual evaporation of methylene chloride. The nanoparticles were collected by centrifugation at 11,000 g for 15 min and washed three times with distilled water.

NPs from the $PPDL_x$-b-$PBLG_y$ and $P[(Gl_x$-r-$PDL_y)$-g-$BLG_z]$ copolymers were obtained in a similar fashion. For the $PPDL_x$-b-$PZLL_y$, $PPDL_{10}$-b-$PAla_y$ and $(PGl_x$-g-$Phe_y)$-b-PEG_{56}-b-$(PGl_x$-g-$Phe_y)$ copolymers, a mixture of CHCl$_3$/TFA (95:5), in order to get the copolymer completely solubilized in the organic phase, was used to obtain the NPs.

3.5.2 Nanoprecipitation method

The nanoprecipitation method was applied to prepare NPs from poly[Gl$_{20}$-*graft*-(BLG)$_z$], poly[Gl$_{20}$-*graft*-(ZLL)$_z$] and $(PGl_x$-g-$Phe_y)$-b-PEG_{56}-b-$(PGl_x$-g-$Phe_y)$ copolymers [4, 5]. Briefly, 5 mg of copolymer were dissolved in 1.5 mL of DMF (for the poly[Gl$_{20}$-*graft*-(BLG)$_z$], poly[Gl$_{20}$-*graft*-(ZLL)$_z$]) or DMSO (for the $(PGl_x$-g-$Phe_y)$-b-PEG_{56}-b-$(PGl_x$-g-$Phe_y)$ copolymers) at room temperature. Then, 3 mL of deionized water were added dropwise into the solution under vigorous magnetic stirring (300 rpm). To remove the solvent, the solution was transferred to a dialysis tube (MWCO 2.0 kDa) and dialyzed against 0.5 L of deionized water for 24 h with replacement of the dialyzing medium every 5 h.

3.5.2 Ionotropic gelation method

The ionotropic gelation method was used to form polyplexes derived from stoichiometric mixtures of poly[Gl$_{20}$-*graft*-(LGA)$_z$] and poly[Gl$_{20}$-*graft*-(LL)$_z$] copolymers [6]. Complexes NPs were prepared by adding drop-wise the poly[Gl-*graft*-(LL)$_z$] solution (1.5 mg·mL^{-1}) to that containing poly[Gl-*graft*-(LGA)$_z$] (5 mg·mL^{-1}) under magnetic stirring.

In the all three methods, the NPs aqueous suspension finally obtained was used for DLS measurements and TEM or SEM observations.

3.6 Drug loading

Drug loading in PPDL$_{15}$-*b*-PLGA$_y$ and poly[Gl$_{20}$-*g*-(LGA)$_z$) copolymers was performed applying the following procedure: 5 mg of the copolymer were placed in deionized water (4 mL) and stirred for 10 min until complete dissolution. Solutions of DOX·HCl in deionized water at different concentrations (1 to 5 mg·mL^{-1}) were prepared and added dropwise with a syringe to the copolymer solution and the mixture left under stirring overnight. Excess of drug was removed by dialysis (MWCO 2000) against distilled water for 24 h (the dialysis medium was replaced intermittently). Afterwards, the mixtures were lyophilized. Loaded NPs were characterized by DLS and SEM/TEM. Drug-Loading Efficiency (DLE) and Drug-Loading Content (DLC) of the resulting Dox-NPs were estimated by using the following equations:

$$\mathrm{DLE\%} = \frac{\text{Mass of the drug in NPs}}{\text{Mass of the drug in feed}}100 \qquad \mathrm{DLC\%} = \frac{Mass\ of\ drug\ in\ NPs}{Mass\ of\ NPs}100$$

3.7 *In vitro* drug releasing

Drug releasing from the DOX·poly[Gl$_{20}$-*graft*-(LGA)$_z$] and DOX·PPDL$_{15}$-*b*-PLGA$_{80}$ NPs. Drug releasing was studied at two pHs (PBS; pH 7.4 and citrate-phosphate; pH 4.2). DOX·poly[Gl$_{20}$-*graft*-(LGA)$_z$] or DOX·PPDL$_{15}$-*b*-PLGA$_{80}$ NPs suspension in each buffer (2.5 mL) was placed in a dialysis tube (MWCO 6-8 kDa, Spectrum Labs) and placed in 25 mL of the same buffer under mild stirring at 37 ºC. At scheduled time intervals, 1.5 mL aliquots of the release medium was taken out and replenished with an equal volume of fresh medium. The amount of released DOX was determined by measuring the absorbance of the withdrawn aliquots at 480 nm by UV-vis spectrophotometry.

3.8 References

[1]   G.J.M. Habraken, M. Peeters, C.H.J.T. Dietz, C.E. Koning, A. Heise, How controlled and versatile is *N*-carboxyanhydride (NCA) polymerization at 0 ºC? Effect of temperature on homo-, block- and graft (co)polymerization. Polym. Chem. 1 (2010) 514–524.

[2]   W.H. Daly, D. Poché, The preparation of *N*-carboxyanhydrides of α-amino acids using bis(trichloromethyl)carbonate, Tetrahedron Lett. 29 (1988) 5859-5862.

[3]   C. Chen, C.H. Yu, Y.C. Cheng, P.H.F. Yu, M.K. Cheung, Biodegradable nanoparticles of amphiphilic triblock copolymers based on poly(3-hydroxybutyrate) and poly(ethylene glycol) as drug carriers, Biomaterials 27 (2006) 4804–4814.

[4]   S. Hornig, T. Heinze, C.R. Becer, U.S. Schubert, Synthetic polymeric nanoparticles by nanoprecipitation, J. Mater. Chem. 19 (2009) 3838–3840.

[5]   J. Huang, C. Bonduelle, J. Thévenot, S. Lecommandoux, A. Heise, Biologically active polymersomes from amphiphilic glycopeptides, J. Am. Chem. Soc. 134 (2012) 119–122.

[6]   T.M. Aminabhavi, S.P. Dharupaneedi, U.A. More, The role of nanotechnology and chitosan-based biomaterials for tissue engineering and therapeutic delivery, in: Chitosan   Based   Biomater.   Vol.   2,   Elsevier,   2017:   pp.   1–29.

Chapter 4. Metal-free catalyzed ring-opening polymerization and block copolymerization of ω-pentadecalactone using amino-ended initiators

Abstract

Metal-free catalysis was successfully applied to polymerize ω-pentadecalactone (PDL) by ring-opening polymerization (ROP) using several amino-ended initiators, namely hexylamine, allylamine and O,O′-bis(3-aminopropyl)diethylene glycol. This polymerization method was suitable to prepare telechelic polyesters carrying functional-end groups. The technique was then extended to the synthesis of block copolymers by ROP of PDL using bisamino-ended poly(ethylene glycol) (M_n=2600) as macroinitiator. PPDL$_x$-PEG$_{56}$-PPDL$_x$ triblock copolymers with M_n ranging between ~4000 and ~90,000 g·mol^{-1} were synthesized and extensively characterized by NMR, DSC, TGA and XRD. The amphiphilic copolymers thus produced were demonstrated to be able to self-assemble in nanoparticles with average diameters of ~100-200 nm and morphologies highly depending on blocks lengths. The described synthetic route distinguishes in providing "clean" amphiphilic copolymers, which are attractive candidates for biomedical applications.
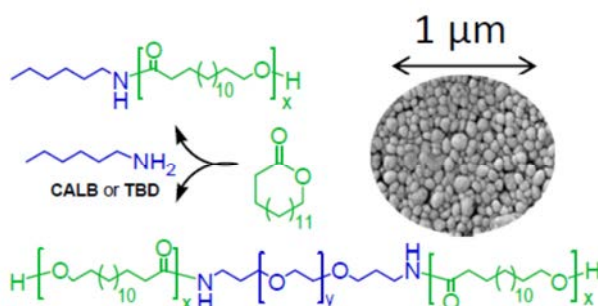
Publication derived from this work:

Supporting information to this chapter in Annex A

4.1 Introduction

Aliphatic polyesters are biodegradable polymers with a great potential as materials to be used in temporary applications, particularly in biomedicine [1]. Macrolactones are easily accessible compounds that may be exploited for the production of polyesters by entropically-driven ring-opening polymerization (ED-ROP) [2]. Polyesters from macrolactones are distinguished by displaying thermal and mechanical properties close to polyethylene while maintaining certain degree of biodegradability [3]. The interest for macrolactones-based polyesters has largely increased in these last decades, not only because their singular properties but also due to the sustainability of newly appearing macrolactones that are synthesized from renewable resources [4].

The increasing demand for polymers free of metal-contaminants to be used as biomaterials has motivated that organic catalysts including enzymes are receiving great attention nowadays in the synthesis of polyesters [5]. In this regards, supported *Candida antarctica* Lipase B immobilized on Lewatit VP OC (CALB), commercialized as Novozyme 435, has been used with great efficiency for the ROP of macrolactones, in particular for ω-pentadecalactone (PDL) [3,6] providing a synthetic route greener than the traditional ones based on the use of organometallic catalyst [7,8]. In addition, higher efficient processes of synthesis based on low-cost enzymes have been recently reported [9]. On the other hand, the use of organo-catalysts is another interesting approach that is gaining recognition in the synthesis of polyesters [10,11]. Thus (1,5,7-triazabicyclo[4.4.0]dec-5-ene), known as TBD, is a powerful nucleophile able to efficiently catalyze esterification reactions and that is widely recognized as an extremely active catalyst for the ROP of macrolactones [11,12].

Nucleophiles are the common species initiating the ROP of lactones, and a good number of both medium- and large-size lactones have been successfully polymerized by this method using alcohols as initiators [13–16]. By contrast, the ROP of lactones

initiated by amines has been scarcely explored in spite that their greater electron-releasing capability makes them particularly effective for such purpose. In fact, the information presently available for the ROP of lactones initiated by amino-ended compounds is scarce and limited almost exclusively to medium-size rings [17–21]. As far as we know, no papers reporting the homopolymerization or copolymerization of macrolactones initiated by amines, either primary or secondary, amino acids, peptides or amino-terminated oligomers, are found in the accessible literature. Nevertheless, polymerization of either strained lactones (ε-caprolactone or lactides) or strainless lactones (large-ring size >9) initiated by primary amines could not differ appreciably from that initiated by alcohols. The use of amines as initiators will be then well justified when amino-ended compounds are desired to be jointed to the final polyesters, as it is for example the case of block copolymers made of polypeptides.

Telechelic polymers bearing end groups able to take part in polymerization reactions are interesting building blocks for the preparation of polymers with relatively complex chemical structures such as block copolymers and network polymers [22,23]. Poly(ethylene glycol) (PEG) and its derivatives are well-known hydrophilic polymers with a great presence in both chemical and biological fields. Amphiphilic copolymers based on telechelic PEG are on the focus of numerous investigations addressed to the development of copolymer designs spontaneously generated by self-assembly and suitable for applications as drug delivery systems (DDS) [24,25]. PEG copolymers exhibiting amphiphilic behavior are common and a good number of them are based on the ROP of medium-size lactones initiated by the hydroxyl-end groups of PEG [26–29]. On the contrary, only a few reports on the copolymerization of PEG with PDL have been published so far, and none dealing with amine-initiated ROP reactions. Recently Hadjichristidis et al.,[16] have described PEG-*b*-PPDL diblock copolymers obtained by ROP of PDL initiated by PEG and catalyzed by phosphazene superbases but the properties of these copolymers were not examined.

In this work, we exploit the advantages of organo-catalysts and enzymes to prepare telechelic polyesters using amino-ended compounds as initiators for the ED-ROP of PDL. On the basis of these exploratory results, commercial bisamino-ended poly(ethylene glycol) (NH_2-PEG_{56}-NH_2) was then used as a bisfunctional macroinitiator for the polymerization of PDL to render amphiphilic $PPDL_x$-PEG_{56}-$PPDL_x$ triblock copolymers avoiding the concourse of metallic compounds. These novel copolymers have been extensively characterized, their thermal properties evaluated, and their ability to form nanoparticles has been brought into evidence.

4.2 Results and discussion

4.2.1 ROP of ω-pentadecalactone

The route used for the synthesis of PPDL and $PPDL_xPEG_{56}PPDL_x$ using CALB or TBD catalysts is depicted in Scheme 4.1, and results obtained in the homopolymerization of PDL under different conditions are compared In Table 4.1.
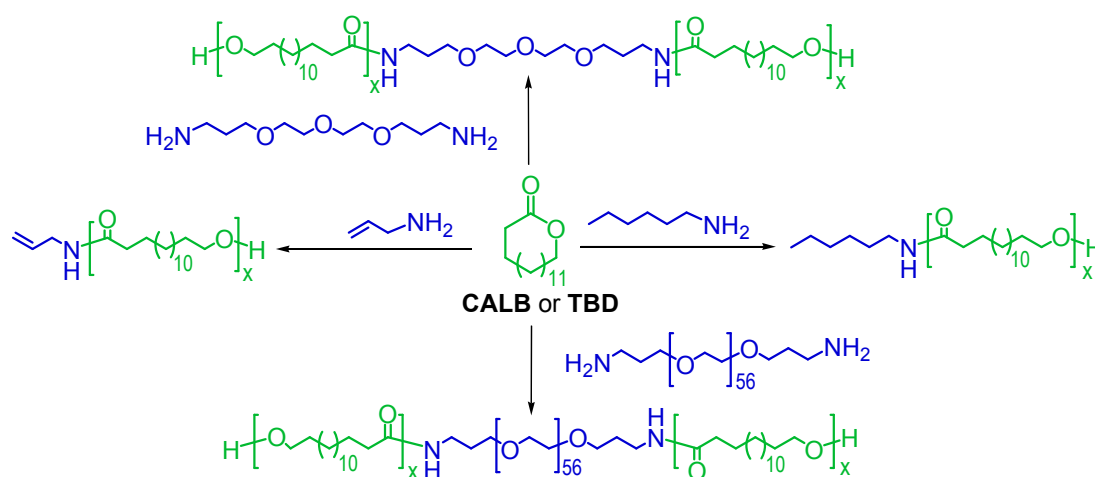
Scheme 4.1. ROP of ω-pentadecalactone with either CALB or TBD as catalyst and amino-ended compounds as initiators.

Table 4.1. ROP of ω-pentadecalactone (PDL) initiated by amines and catalyzed by either TBD or CALB.

Entry	Initiator[a]	$[PDL]_0/[Cat]_0/[Ini]_0$ [b]	Time (h)	Conversion[c] (%)	Yield (%)	Mn [d] (g·mol^{-1})
TBD						
1	-	100/5/0	12	-	-	-
2	HexA	100/1/1	96	40	24	5,300
3	HexA	100/10/10	96	64	37	2,100
4	A-DEG-A	100/1/1	72	40	22	9,000
5	A-DEG-A	100/5/1	12	99	87	19,700
CALB						
6	HexA	100/5	3	99	97	5,500
7	A-DEG-A	100/10	3	99	95	5,300
8	AllA	100/5	3	99	93	5,000
9	AllA	100/10	3	96	83	3,400

[a]HexA: hexylamine; A-DEG-A: *O,O'*-bis(3-aminopropyl)diethylene glycol; AllA: allylamine.
[b]Molar ratio in the feed. For enzymatic reactions the amount of CALB was 20% (w/w) respect to PDL.
[c]Conversion of PDL at the indicated reaction time as determined by ^{1}H NMR.
[d]Number-average molecular weight of the resulting PPDL determined by ^{1}H NMR.

The ^{1}H NMR spectra of the PPDL obtained by ROP catalyzed by CALB and initiated by the three amino-ended nucleophiles under study (entries 6-8) are shown in Fig. 4.1. These amines acted as initiators in the polymerization of PDL and remained therefore incorporated in the growing polymer chain [30]. In every case a signal appeared at 2.15 ppm which is indicative of the presence of the amide group generated by the nucleophilic attack of the amine to the carboxylate group of PDL with subsequent ring opening and polymerization initiation. Additional signals could be detected at 3.37 ppm and 3.25 ppm when HexA and A-DEG-A were used as initiators (signal A in spectra a and b, respectively). Such quadruplet signals arise from the α-methylene protons of the amide group and their presence confirmed the incorporation of the amino-compounds into the polymer chain. Conversely, this signal appeared at 3.9 ppm in the spectrum of the PDDL initiated by AllA (signal A in spectrum c) as a consequence of the deshielding effect provoked by the presence of the adjacent double bond. On the other hand, characteristic signals arising from the polyester are shared by PPDL regardless the nucleophile used. Triplets at 3.64 ppm and 4.05 ppm corresponding to protons of ended-chain C$\underline{H}_2$OH and COOC$\underline{H}_2$, respectively, were

present in all spectra. A quantification of the areas of these signals allowed estimating the number-average molecular weights of the resulting PPDL, which oscillated between ~2,000 and ~20,000 g·mol^{-1} showing a large dependence on the reaction conditions used. A comparison of the conversion, yield and M_n values given in Table 4.1 led to conclude the following: (a) ROP of PDL was not feasible in the absence of initiator (entry 1), (b) the influence of initiator on results was small as far as CALB was used as catalyst (entries 6-9), and c) the best results were attained in the ROP initiated by 1 mol-% DEG and catalyzed by 5 mol-% TBD relative to the amount of used monomer (entry 5).

It should be remarked that ROP of the macrolactone took place almost exclusively by amine initiation ROP of PDL as it is demonstrated by measuring the CH_2OH and CH_2NCO signals areas of the formed polyesters. ^1H NMR spectra of AllA-PPDL before and after purification (Table 4.1, entry 8) with these signals enlarge for a reliable comparison are shown in Fig. A1 of the Annex A. On the other hand, it can be stated that the low yields attained for entries 2, 3 and 4 are due to the lack of reactivity of the macrolactone under the conditions used in such cases. The ^1H NMR spectrum of the reaction product of the polymerization initiated by hexylamine before purification (Table 4.1, entry 2) is shown in Fig. A2 of the annex A.
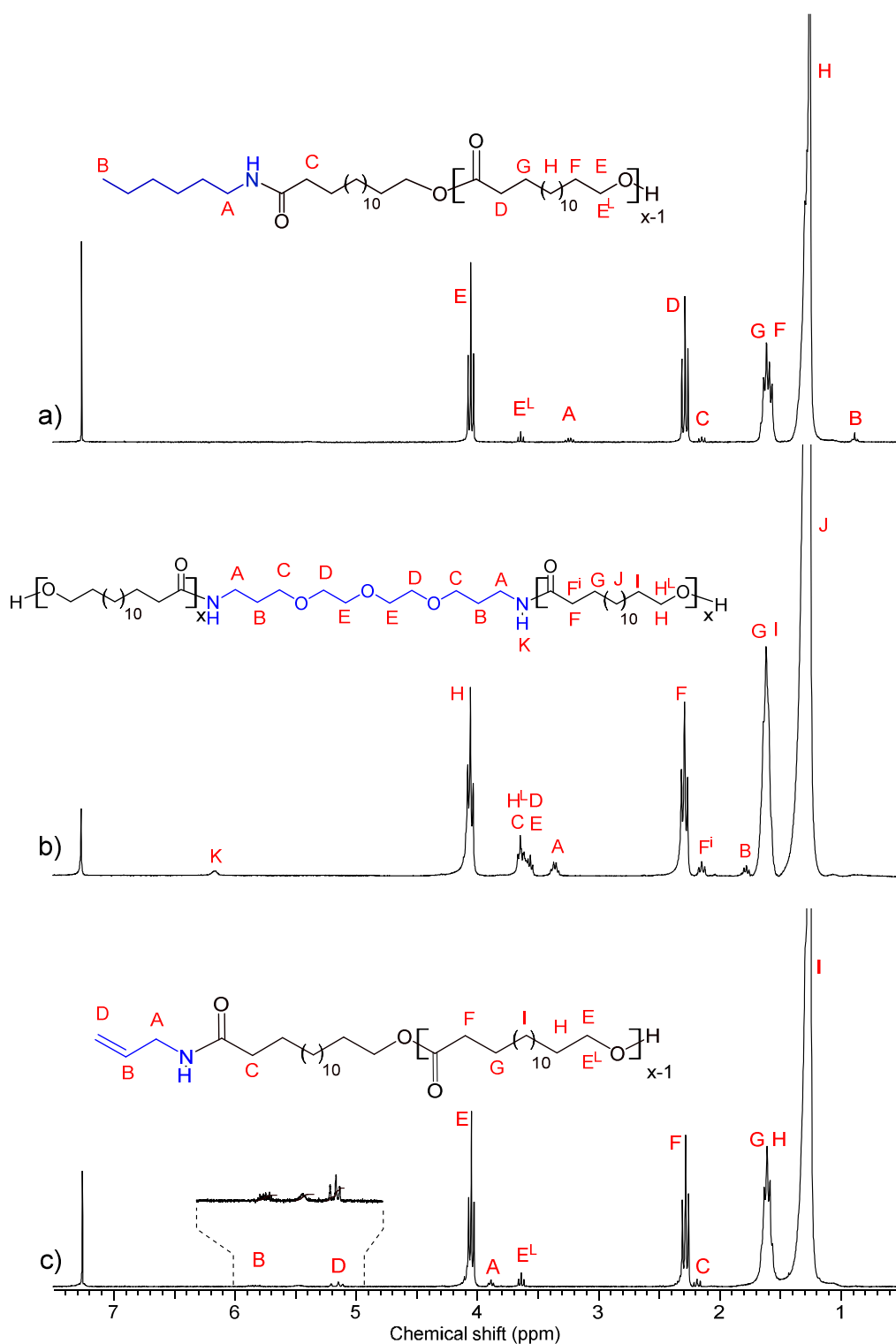
Fig. 4.1. ^{1}H NMR (CDCl$_3$) spectra of PPDL prepared by ROP initiated by a) HexA, b) A-DEG-A, and c) AllA. Superscripts I and L refer to signals arising from the first and last repeating units of the polyester chain, respectively.

A preliminary thermal characterization of PPDLs obtained by amine-initiated ROP was carried out by TGA and DSC. TGA thermograms of PPDLs synthesized using

each different nucleophile are compared in Fig. 4.2a. The thermal decomposition process started above 300 ºC and happened in one step with the maximum decomposition rate at ~425 ºC regardless the initiator used. Essentially the same behavior was observed for the three cases with small differences being within the limits of experimental errors. Fig. 4.2b displays the DSC traces of the amino-initiated PPDLs. The thermograms recorded at both cooling and heating are extremely similar showing in the three case sharp crystallization and melting peaks at temperatures around 75 ºC and 90 ºC, respectively.
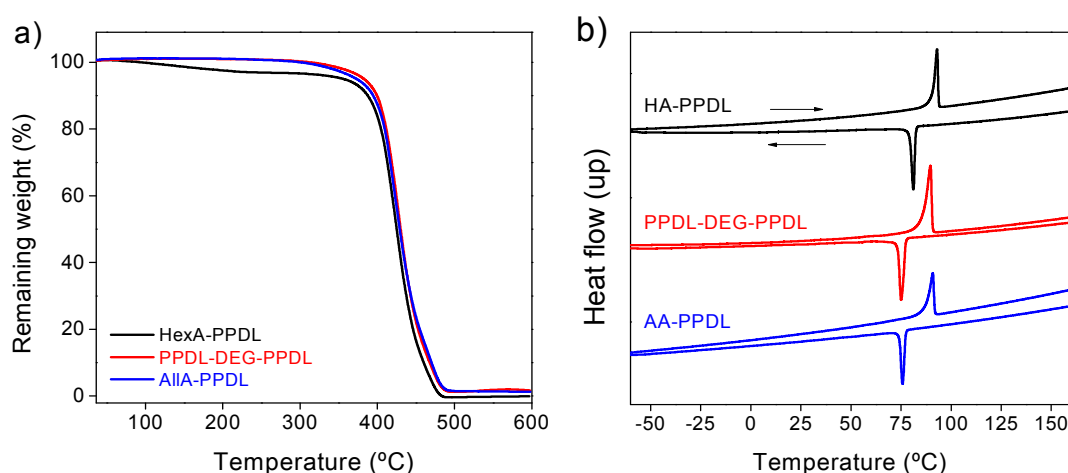
Fig. 4.2. Thermal analysis of amine-initiated PPDLs. a) TGA traces recorded under an inert atmosphere. b) DSC traces registered at cooling and reheating from samples previously heated at 200 ºC.

4.2.2 Synthesis PPDL$_x$PEG$_y$PPDL$_x$ triblock copolymers

The promising results obtained in the ROP of PDL initiated by amino compounds encouraged us to carry out the synthesis of amphiphilic triblock copolymers by using diamine-ended PEG as double initiator for generating the PPDL blocks from PDL (Scheme 4.1). The PEG of choice was a sample with number-average polymerization degree of 56 (corresponding to a M_n of approximately 2,700 g·mol^{-1}) and both organo-chemical (TBD) and enzymatic (CALB) catalysts were used. All reactions were conducted in bulk at a temperature of 100 ºC. Copolymerizations with PEG:PDL molar ratios in the feed ranging between 1:25 and 1:420, which correspond to EG:PDL ratios of 2 to 0.13, were performed. Reaction conditions and results obtained for every case

are collected in Table 2. Acceptable yield values were attained in all cases (>70%) and according to the copolymer compositions, loses of product are due to incomplete reaction of PDL. Such a defect in the reactivity of the macrolactone was more pronounced when the polymerization was catalyzed by TBD.

Table 4.2. Reaction conditions and results of the synthesis of $PPDL_xPEG_{56}PPDL_x$ triblock copolymers.[a]

| Entry | Copolymer[b] | Time (h) | Yield (%) | [PEG]/[PDL][c] | | M_n[d] (g·mol^{-1}) |
				Feed	Copolymer	
Organic catalysis (TBD)[e]						
1	$PPDL_{12}PEG_{56}PPDL_{12}$	3	87	1/25	1/23	8,300
2	$PPDL_{34}PEG_{56}PPDL_{34}$	3	71	1/100	1/68	18,700
3	$PPDL_{65}PEG_{56}PPDL_{65}$	12	70	1/200	1/131	33,600
Enzymatic catalysis (CALB)[f]						
4	$PPDL_{16}PEG_{56}PPDL_{16}$	3	92	1/35	1/32	10,650
5	$PPDL_{47}PEG_{56}PPDL_{47}$	12	94	1/100	1/94	25,600
6	$PPDL_{191}PEG_{56}PPDL_{191}$	12	85	1/420	1/392	94,600

[a]All reactions performed at 100 ºC in bulk.
[b]Obtained copolymers with the indicated block lengths as determined from their compositions.
[c]Molar PEG:PDL ratio in the feed and in the copolymer as determined by ^{1}H NMR analysis.
[d]Number-average molecular weight determined by ^{1}H NMR analysis of end-groups.
[e]Reactions catalyzed by 5 %-mol of TBD.
[f]Reactions catalyzed by 20% (w/w) of CALB.

The chemical constitution and block composition of the copolymers were ascertained by NMR. ^{1}H and ^{13}C NMR spectra of $PPDL_{46}PEG_{56}PPDL_{46}$ (entry 5 of Table 4.2) are depicted in Fig. 4.3. ^{1}H NMR spectra of the all other copolymers are given in Fig. A3 of the Annex A. Insets containing enlarged regions have been inserted to show details difficult to observe in the straight representations. Signals arising from methylenes of the first and last pentadecanoate units as well as those due to the protons contained in the 3-oxyaminopropylene units of the central PEG block are made visible in the insets and used to determine the molecular weight of the copolymers. The M_n values obtained by this analysis are given in Table 4.2 and found to be consistent with the block lengths calculated by area quantification of signals specifically arising from PEG and PPDL blocks.
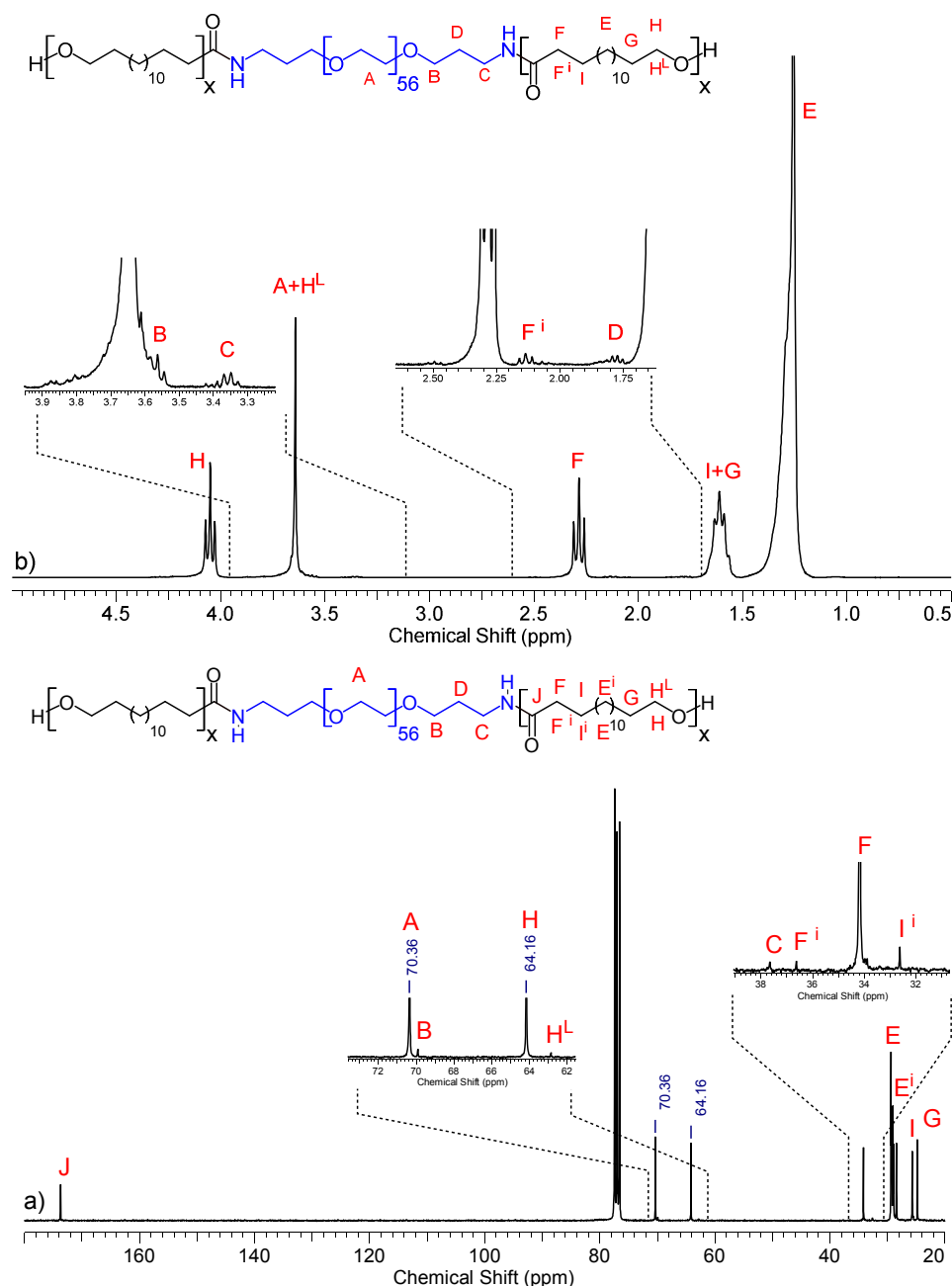
Fig. 4.3. ^{13}C-NMR (a) and ^{1}H-NMR (b) spectra of PPDL$_{46}$PEG$_{56}$PPDL$_{46}$ (entry 5, Table 4.2). Superscripts I and L refer to signals arising from the first and last repeating units of the polyester chain, respectively.

It should be noticed that no signals arising from the aminopropyl groups of the bisamino-ended PEG used as macroinitiator were detected in the ^{1}H NMR spectra of the reaction product before purification, which is taken as indicative that all amine groups were active at initiating ROP of PDL (Fig. A4). On the other hand, the absence of homopolyester PPDL was ascertained by comparing ^{1}H NMR signals arising from end C$\underline{H}_2$OH, HNCOC$\underline{H}_2$ and C$\underline{H}_2$O, which gave the same number of protons for the all

three (Fig. A5). Similar results were obtained for the analysis of PPDL prepared by short amine initiation (Fig.A6).

4.2.3 Thermal properties of PPDL$_x$PEG$_{56}$PPDL$_x$ triblock copolymers

The triblock copolymers synthesized by the two procedures were comparatively examined by TGA and DSC with the purpose of assessing their thermal behavior as a function of both the length of the PPDL blocks and the method used for their synthesis. The thermal parameters obtained from these assays are collected in Table 4.3. The TGA traces recorded from the copolymers and the two homopolymers as well as their derivative curves are shown in Fig. 4.4.

Table 4.3. Thermal properties and crystallizability of PPDL$_x$PEG$_{56}$PPDL$_x$ triblock copolymers.

Copolymer	TGA[a]			DSC[b] Heating				Cooling		Crystallization kinetics[c]		
	${}^oT_d$ °C	${}^{max}T_d$ °C	R_w %	${}^1T_m$ °C	${}^1\Delta H_m$ J·g^{-1}	${}^2T_m$ °C	${}^2\Delta H_m$ J·g^{-1}	T_c °C	ΔH_c J·g^{-1}	n	$\ln K$	$t_{1/2}$ s
Organic catalysis (TBD)												
PPDL$_{12}$PEG$_{56}$PPDL$_{12}$	385	427,470	2	90	121	77	121	77	-110	2.1	-1.4	1.7
PPDL$_{33}$PEG$_{56}$PPDL$_{33}$	381	424,470	2	95	135	89	138	81	-117	2.0	-1.4	1.7
PPDL$_{65}$PEG$_{56}$PPDL$_{65}$	399	424,472	4	95	143	90	150	81	-123	1.9	-1.1	1.5
Enzymatic catalysis (CALB)												
PPDL$_{16}$PEG$_{56}$PPDL$_{16}$	394	423,472	1	92	122	84	102	77	-111	1.7	-2.2	2.7
PPDL$_{46}$PEG$_{56}$PPDL$_{46}$	394	422,472	1	94	132	88	110	79	-115	1.9	-2.3	2.7
PPDL$_{191}$PEG$_{56}$PPDL$_{191}$	383	421,472	6	95	180	90	160	81	-162	2.1	-2.5	2.8
PEG	373	406,472	2	59	169	56	148	20	-136			
PPDL	399	423,470	2	93	150	91	143	75	-119	1.4	-4.3	9.6

[a] Onset for 10% weight loss (${}^oT_d$) and maximum rate (${}^{max}T_d$) thermal decomposition temperatures measured in the TGA analysis performed under inert atmosphere. R_w: weight (%) remaining after heating at 600 ºC.
[b] Melting (T_m and ΔH_m) and crystallization (T_c and ΔH_c) temperatures and enthalpies measured by DSC. 1 and 2 superscripts refer to the first and second heating runs.
[c] Avrami parameters for the isothermal crystallization taking place at 84 ºC.
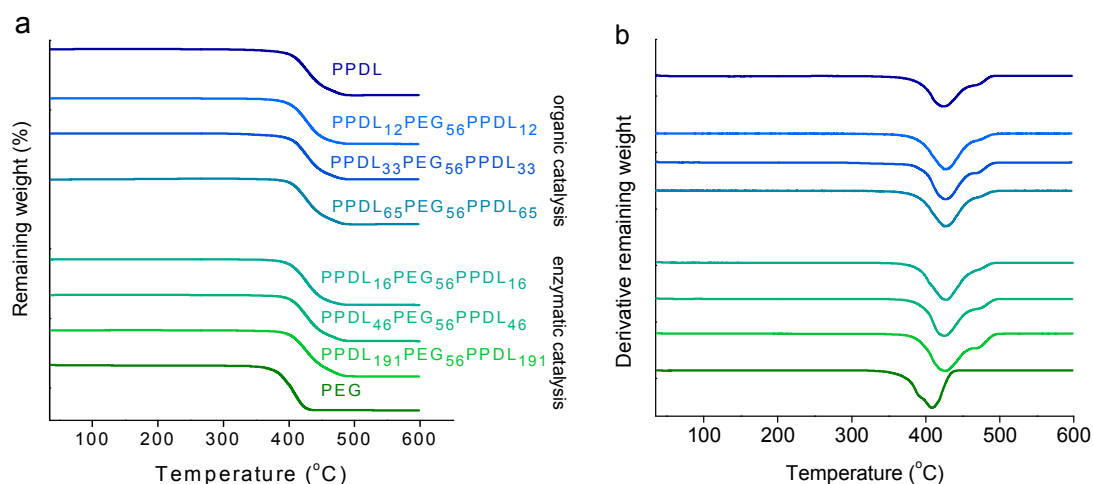
Fig. 4.4. a) TGA traces registered under inert atmosphere of PPDL$_x$PEG$_{56}$PPDL$_x$ copolymers and and b) their derivative curves.

The high thermal stability of PEG and PPDL homopolymers is a well-known fact [3,31]. Both compounds start to undergone perceivable decomposition well above 350 ºC and their decomposition in bulk happens in two stages at temperatures between 400 ºC and 500 ºC leaving insignificant amounts of remaining weight. As it is shown in Table 4.3 the thermal stability of the PPDL$_x$PEG$_{56}$PPDL$_x$ triblock copolymers is fully consistent with the behavior observed for the homopolymers. ^oT_d of copolymers are in the 380-400 ºC range and their $^{max}T_d$ are about 420-425 ºC and 470-472 ºC for the first and second decomposition steps, respectively. Although differences in the decomposition temperatures of the copolymers are small and practically negligible when the two series are compared, it is noticed that onset temperatures are slightly higher for the copolymers prepared by enzymatic ROP, and that in general all decomposition temperatures are closer to those of PPDL. The first observation is rather reasonable since the catalyst remaining in the copolyesters is expected to enhance the starting decomposition of the polymer. On the contrary, the stronger influence of the PDL blocks on the thermal stability of the copolymers compare to the EG blocks is not readily explainable and a more detailed study of the decomposition mechanism is needed to account for such difference.

The DSC study carried out on the $PPDL_xPEG_{56}PPDL_x$ copolymers included the analysis of the melting-crystallization process taking place at heating, cooling and reheating. Traces registered for the two copolymers series are compared in Fig. 4.5 and the T_m and T_c values observed for each one of them together with their associated enthalpies are listed in Table 4.3. Apparently, the PDL's block is crystallized in all copolymers whichever is the composition. "As synthesized" samples melted in the 90-95 ºC with values showing no significant differences between the two series but slightly increasing in each of them with the length of the polyester block. Also the melting enthalpies measured for the copolymers increased monotonically with the content in PDL as expected, but it was striking to observe that values are greater than those for the PPDL homopolyester when they are referred to the weight fraction of PDL in the copolymer. It seems therefore that the PEG segment operates as a crystallization hastener probably due to the self-assembling effect that is exerted on the whole copolymer in concomitance with phase separation. Additionally a plasticizing effect of PEG could be invoked to explain the high crystallinity found in the copolymers. Crystallization upon cooling from the melt was found to take place in all cases at supercoolings below 10 ºC which are values significantly lower than that required for the recrystallization of the homopolyester (16 ºC).
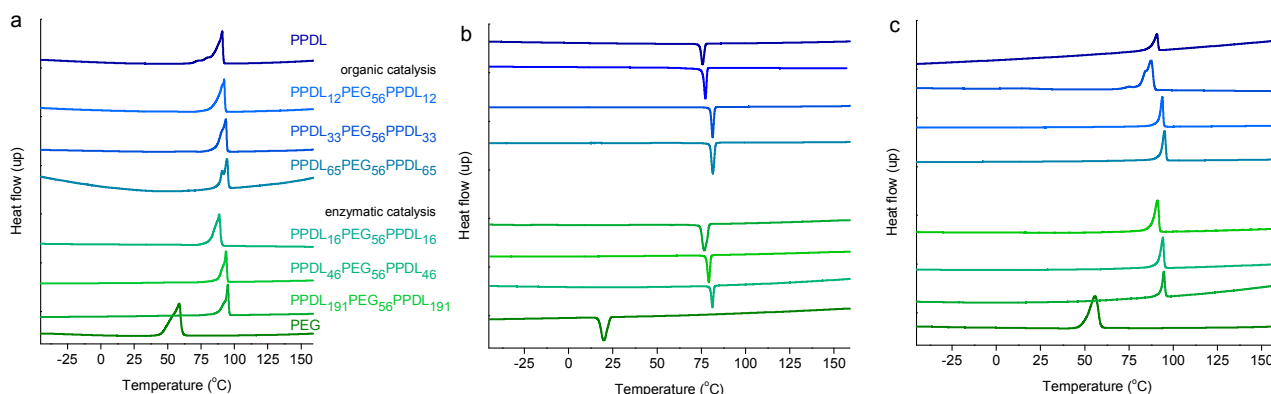

Fig. 4.5. DSC traces of $PPDL_xPEG_{56}PPDL_x$ copolymers. a) First heating, b) cooling, c) second heating.

The crystallizability of the copolymers as a function of their composition was assessed by isothermal crystallization. For this purpose PPDL and copolymers samples were heated in the DSC up to 200 ºC, then rapidly cooled down to 84 ºC, and finally left to crystallize at this temperature. The advance of the crystallization process was followed by measuring the increasing in the enthalpy along time. The curves resulting from the representation of the relative crystallinity against crystallization time are compared in Fig. 4.6 for the two series and the kinetic parameters determined by applying the Avrami approach for each copolymer and PPDL are listed in Table 4.3. It is apparent that the PPDL segments crystallized faster when they were dangling from the PEG, and that such effect is even more pronounced in the copolymers synthesized in the presence of the organic catalyst than in those obtained with CALB. The POM micrographs obtained from films of copolyesters crystallized under the same conditions that were used for the kinetic analysis (insets of Fig. 4.6) revealed an axialite-like texture in both cases but with bigger size and less profusion of individual entities in the former case.
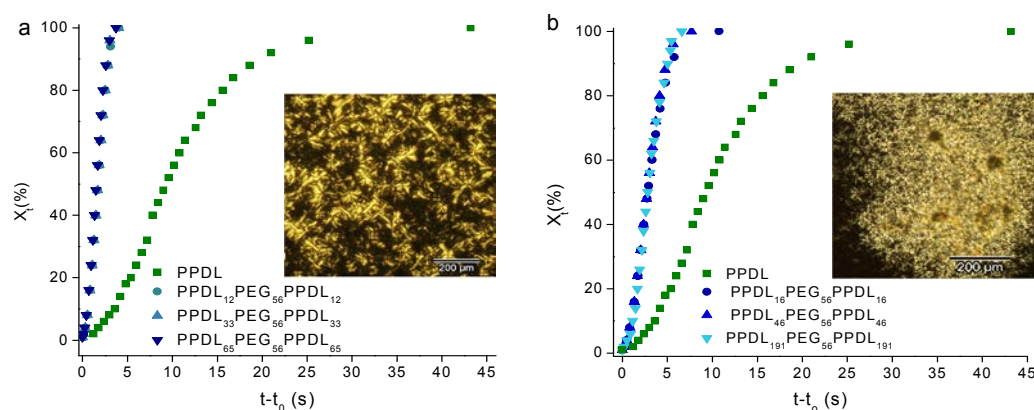
Fig. 4.6. Evolution of the relative crystallinity as a function of time in the isothermal crystallization at 84 ºC of $PPDL_xPEG_{56}PPDL_x$ copolymers. Insets: POM micrographs recorded from crystallized $PPDL_{33}PEG_{56}PPD_{33}$ (a) and $PPDL_{46}PEG_{56}PPDL_{46}$ (b).

These findings are in line with the differences detected in the melting-crystallization and corroborated the occurrence of heterogeneous crystallization in the TBD synthesized copolymer. Avrami parameters are in partial agreement with such

observations. Half crystallization times are in fact much lower for the organo-catalyzed copolymers whereas no significant differences in *n* between the two series where noticed.

The crystalline structure generated upon crystallization of $PPDL_xPEG_{56}PPDL_x$ was investigated by XRD at variable temperature by using synchrotron radiation. All the copolymers showed at room temperature a couple of well-resolved sharp peaks in the WAXS region corresponding to 0.41 and 0.37 nm Bragg spacings (Fig. 4.7).These are identified as the interplanar spacings characteristic of the PPDL rhombic lattice, [3,32–34] and their presence brings into evidence that the PPDL segments are similarly crystallized in the copolyesters whichever is their composition. As expected, both peaks vanished when the copolymers were heated at their melting temperature to reappear upon cooling to reproduce almost exactly the initial pattern. According to the results obtained by DSC, the amount of PEG that is crystallized must be small. In fact no peak arising from PEG was detectable in the XRD profiles of the copolymers except in those containing the shortest PPDL blocks. In these cases a weak peak became detectable at 0.46 nm that disappeared at temperatures around 50-60 ºC and that was unable to recover upon cooling (Fig. 4.7c).

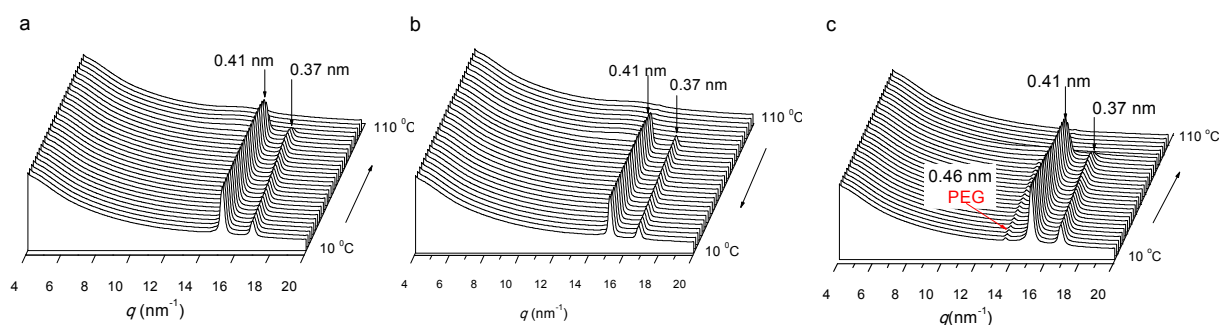**Fig. 4.7.** Evolution of WAXS recorded from $PPDL_{46}PEG_{56}PPDL_{46}$ at heating (a) and cooling (b) over the 10-110 °C range. c) WAXS profiles recorded from $PPDL_{16}PEG_{56}PPDL_{16}$ showing the PEG peak. Additional heating and cooling profile collections obtained for $PPDL_{191}PEG_{56}PPDL_{191}$ are given in Fig. A2 of the ESI file.

4.2.4 Nanoparticles formation and characterization

The $PPDL_xPEG_{56}PPDL_x$ triblock copolymers are amphiphilic chains consisting of an inner hydrophilic segment of around 20 nm in length and two outer hydrophobic segments of variable length ranging from about 25 nm for x = 12 up to about 400 nm for x = 191. Since in the solid state the PEG segment is likely to be in non-regular conformation, and that PPDL must be crystallized in folded lamellae with a more or less defined thickness (presumably in the 5-30 nm range), the copolymers are expected to be arranged in an amphiphilic nanostructure with the PEG (amorphous and hydrophilic) and PPDL (crystalline and hydrophobic) phases sharply segregated one from the other. Since no peak was detected in the SAXS region of the XRD profiles of these copolymers it is interpreted that such structure is made of globular PEG amorphous aggregates surrounded by a continuous phase made of PPDL lamellae. Nevertheless, the size and mutual distribution of the two phases will be determined by the x value.

A different behavior could be however expected for the copolymers when they are compelled to form small particles in an aqueous environment given the strong affinity of PEG for water. The preparation of nanoparticles (NPs) from the $PPDL_xPEG_{56}PPDL_x$ copolyesters was carried out by the solvent evaporation method with dichloromethane as organic solvent. The copolymer series made by enzymatic copolymerization was the material of choice because a greener synthesis route was used in this case. The size and ζ-potential measured for the resulting NPs for the three copolymers under study are given in Table 4.4, and a selected assortment of TEM micrographs are shown in Fig. 4.8.

Table 4.4. Triblock nanoparticles characteristics.

| Copolymer | Particle size[a] | | ζ-potential (mV) |
	Diameter (nm)	Dispersity(D)	
PPDL$_{16}$PEG$_{56}$PPDL$_{16}$	125	0.12	-3.33
PPDL$_{46}$PEG$_{56}$PPDL$_{46}$	165	0.19	-3.90
PPDL$_{191}$PEG$_{56}$PPDL$_{191}$	161	0.13	-2.96

[a] Measured by DLS in water. Size distribution plots are accessible in the ESI file (Fig. S8).

The DLS results gave particle sizes between 125 and 160 nm with the value clearly increasing when the length of the PPDL block came from x=16 up to x=46 but keeping essentially unchanged for further x increasing to 191. Negative weak values were found for the ζ-potential, as it should be expected for particles with the surface enriched in ethylene oxide groups. Differences among ζ-potential values are not relevant although it is rather remarkable that PPDL$_{46}$PEG$_{56}$PPDL$_{46}$ displays the top value despite that PPDL$_{16}$PEG$_{56}$PPDL$_{16}$ is the copolyester containing the highest proportion of ether groups. The entities examined by SEM display sizes and shapes in agreement with the data afforded by DLS. Although more or less rounded particles with diameters in the 100-200 nm range are invariably observed for the three copolymers, their appearance varies largely from one to the other. NP's made of PPDL$_{16}$PEG$_{56}$PPDL$_{16}$ are very prone to collapse and aggregate so that patches integrated by large numbers of attached NP are frequently seen (Fig. 4.8a). On the contrary, NP's made of PPDL$_{191}$PEG$_{56}$PPDL$_{191}$ appear very disperse maintaining their individual entity and displaying somewhat elongate shapes (Fig. 4.8c). An intermediate situation was found for NP's made of PPDL$_{46}$PEG$_{56}$PPDL$_{46}$ where rounded particles appear densely packed without losing their individuality. Additional SEM micrographs providing larger views of the PPD$_x$PEG$_{56}$PPDL$_x$ NP's may be inspected in Fig. A9 of the Annex A.
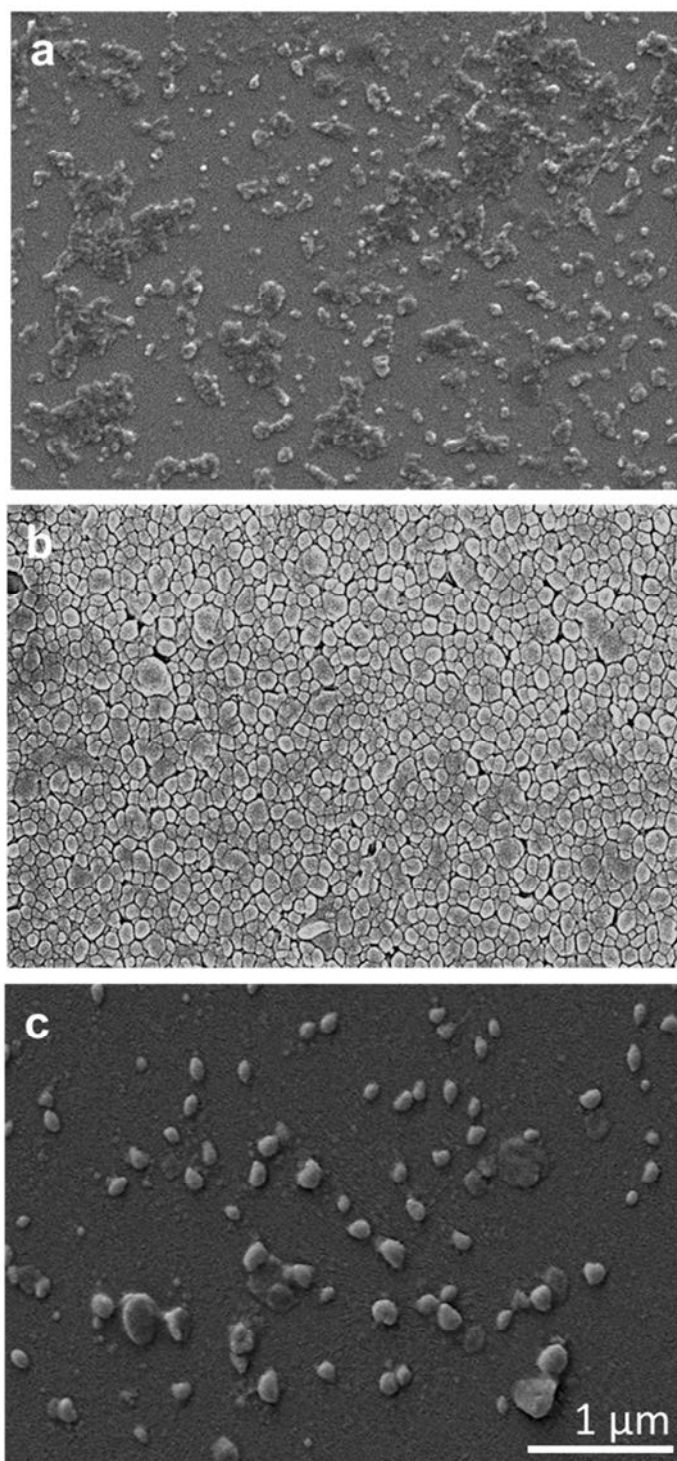
Fig. 4.8. SEM images of nanoparticles made from PPDL$_{16}$PEG$_{56}$PPDL$_{16}$ (a), PPDL$_{46}$PEG$_{56}$PPDL$_{46}$ (b) and PPDL$_{191}$PEG$_{56}$PPDL$_{191}$(c) triblock copolymers.

The DSC analysis of the NP's demonstrated that the polyester blocks are crystallized in these entities in a similar manner as it happens in the bulk but the crystallinity attained is much lower depending on copolymer composition (see Fig. A10 and Table A1 of the Annex A). On the other hand, no sign of crystallinity associated to

the PEG blocks is perceived at any case. It is remarkable that the amount of crystalline PPDL in the NPs made of PPDL$_{46}$PEG$_{56}$PPDL$_{46}$ is about 80% of that present in the copolymer in bulk whereas it becomes less than 7% in NPs made of PPDL$_{16}$PEG$_{56}$PPDL$_{16}$. The situation is intermediate for PPDL$_{191}$PEG$_{56}$PPDL$_{191}$ NPs where PPDL crystallized in about 25% relative to the amount that is crystallized in the powder.

It is tempting to try relating the differences in shape and behavior exhibited by the NP's in aqueous suspension with the block composition of the copolymers given the influence of the block length on crystallinity and the low T_g values displayed by both PEG and PPDL. The soft behavior and consequent shape definition and tendency to form unspecific aggregates that is displayed by PPDL$_{16}$PEG$_{56}$PPDL$_{16}$ NPs is thought to be due to the rubbery nature of these particles in which the molar fraction of EG units is almost twofold that of PDL and crystallinity is almost negligible. Conversely the good dispersion and almond-like shape exhibited by PPDL$_{191}$PEG$_{56}$PPDL$_{191}$ NPs is consistent with the presence of a considerable crystallinity and the small content in PEG, which will be segregated out from polyester core, as expected, but that is insufficient to cover the whole surface of the nanoparticle. NPs made of PPDL$_{46}$PEG$_{56}$PPDL$_{46}$, despite showing a good mutual affinity, they keep inalterable their identity and display a satisfactory rounded shape. In this case, PPDL is extensively crystallized in the inner part of the NP so that PEG is segregated out to create a water-like surface. Nevertheless, the amorphous polymer fraction in these NP must be still considerable as it inferred from the polygonal contour exhibited when they are closely packed to each other.

4.3 Conclusions

In this paper it is reported for the first time the synthesis of polymacrolactones by ROP using amino-initiators and avoiding the concourse of organo-metallic catalysts. This approach is very suitable to prepare telechelic PE-like polyesters bearing diverse

functional-end groups which can be then used for further extensive reaction. In this work, the methodology has been applied to the preparation of amphiphilic triblock copolyesters (PPDL-PEG-PPDL) made of a central block of PEG and two dangling blocks of PPDL. Copolymerization was performed by ROP of PDL initiated by amino-ended PEG and using either TBD or CALB catalysis with similar synthesis results. The length of the polyester blocks could be precisely controlled by adjusting the PEG/PDL ratio. Thermal properties and crystalline structure of the copolymers were found to be depending on the PEG/PDL ratio but differences between the two copolymer series were not significant. Strikingly the crystallizability of the PPDL in the copolymers was enhanced compared to that of the homopolyester and this effect was more pronounced for the copolymer series prepared with TBD as catalyst. Nanoparticles with 100-200 nm diameter could be prepared from the enzymatically-synthesized copolyesters bringing into evidence their self-assembling capacity. The green route followed for the preparation of the PPDL-PEG-PPDL triblock copolyesters, their largely expected biodegradability and good cytocompatibility, and their capacity to form structured nanoparticles make these copolyesters materials of exceptional interest for the design of drug delivery systems.

4.4 References

[1]   K.M. Zia, A. Noreen, M. Zuber, S. Tabasum, M. Mujahid, Recent developments and future prospects on bio-based polyesters derived from renewable resources: A review, Int. J. Biol. Macromol. 82 (2016) 1028–1040.

[2]   P. Hodge, Entropically driven ring-opening polymerization of strainless organic macrocycles, Chem. Rev. 114 (2014) 2278–2312.

[3]   M.L. Focarete, M. Scandola, A. Kumar, R. a Gross, Physical characterization of poly(pentadecalactone) synthesized by lipase-catalyzed ring-opening polymerization, J. Polym. Sci. Part B Polym. Phys. 39 (2001) 1721–1729.

[4]   Y. Li, X. Yin, M. Dai, Catalytic macrolactonizations for natural product synthesis,

Nat. Prod. Rep. 34 (2017) 1185–1192.

[5]   C. Thomas, B. Bibal, Hydrogen-bonding organocatalysts for ring-opening polymerization, Green Chem. 16 (2014) 1687–1699.

[6]   M. Takwa, N. Simpson, E. Mcilmsiтröm, K. Hult, M. Martinelle, One-pot difunctionalization of poly(ω-pentadecalactone) with thiol-thiol or thiol-acrylate groups, catalyzed by candida antarctica lipase Ba, Macromol. Rapid Commun. 27 (2006) 1932–1936.

[7]   M. Bouyahyi, M.P.F. Pepels, A. Heise, R. Duchateau, ω-Pentandecalactone polymerization and ω-pentadecalactone/ε-caprolactone copolymerization reactions using organic catalysts, Macromolecules 45 (2012) 3356–3366.

[8]   T. Fuoco, D. Pappalardo, Aluminum alkyl complexes bearing salicylaldiminato ligands: versatile initiators in the ring-opening polymerization of cyclic esters, Catalysts 7 (2017) 64.

[9]   A.E. Polloni, V. Chiaradia, E.M. Figura, J.P. de Paoli, D. de Oliveira, J.V. de Oliveira, P.H.H. de Araujo, C. Sayer, Polyesters from macrolactones using commercial Lipase NS 88011 and Novozym 435 as biocatalysts, Appl. Biochem. Biotechnol. (2017) 1–14.

[10]   L. Mezzasalma, A.P. Dove, O. Coulembier, Organocatalytic ring-opening polymerization of L-lactide in bulk: a long standing challenge, Eur. Polym. J. 95 (2017) 628–634.

[11]   L. Simón, J.M. Goodman, The mechanism of TBD-catalyzed ring-opening polymerization of cyclic esters, J. Org. Chem. 72 (2007) 9656–9662.

[12]   R.C. Pratt, B.G.G. Lohmeijer, D.A. Long, R.M. Waymouth, J.L. Hedrick, Triazabicyclodecene : a simple bifunctional organocatalyst for acyl transfer and ring-opening polymerization of cyclic esters triazabicyclodecene : a simple bifunctional organocatalyst for acyl transfer and ring-opening polymerization of cyclic esters, J. Am. Chem. Soc. 128 (2006) 4556–4557.

[13] A. Duda, A. Kowalski, S. Penczek, H. Uyama, S. Kobayashi, Kinetics of the ring-opening polymerization of 6-, 7-, 9-, 12-, 13-, 16-, and 17-membered lactones. comparison of chemical and enzymatic polymerizations, Macromolecules 35 (2002) 4266–4270.

[14] J.C. Chen, J.Z. Li, J.H. Liu, L.Q. Xu, Amphiphilic poly(ethylene glycol)-*b*-poly(ethylene brassylate) copolymers: one-pot synthesis, self-assembly, and controlled drug release, Chinese Chem. Lett. 26 (2015) 1319–1321.

[15] C.-M. Dong, K.-Y. Qiu, Z.-W. Gu, X.-D. Feng, Synthesis of star-shaped poly(ε-caprolactone)-*b*-poly(DL-lactic acid-*alt*-glycolic acid) with multifunctional initiator and stannous octoate catalyst, Macromolecules 34 (2001) 4691–4696.

[16] V. Ladelta, P. Bilalis, Y. Gnanou, N. Hadjichristidis, Ring-opening polymerization of ⅂-pentadecalactone catalyzed by phosphazene superbases, Polym. Chem. 8 (2017) 511–515.

[17] M. Yuan, Y. Wang, X. Li, C. Xiong, X. Deng, Polymerization of lactides and lactones. 10. Synthesis, characterization, and application of amino-terminated poly(ethylene glycol)-*co*-poly(ε-caprolactone) block copolymer, Macromolecules 33 (2000) 1613–1617.

[18] M. Marzorati, K. Hult, S. Riva, B. Danieli, Incorporation of primary amines into a polyester chain by a combination of chemical and lipase-catalyzed ε-caprolactone ring-opening processes, Adv. Synth. Catal. 349 (2007) 1963–1968.

[19] M. Bednarek, M. Basko, T. Biedron, E. Wojtczak, A. Michalski, Polymerization of lactide initiated by primary amines and catalyzed by a protic acid, Eur. Polym. J. 71 (2015) 380–388.

[20] T. Biela, A. Kowalski, J.A.N. Libiszowski, Amines as (co) initiators of cyclic esters polymerization, Polimery 7-8 (2005) 501–504.

[21] J. Liu, L. Liu, Ring-opening polymerization of ε-caprolactone initiated by natural amino acids, Macromolecules 37 (2004) 2674–2676.

[22] Y. Tsukahara, K. Adachi, Telechelic Polymer: preparation and application, in: S. Kobayashi, K. Müllen (Eds.), Encycl. Polym. Nanomater., Springer Berlin Heidelberg, Berlin, Heidelberg, 2014: pp. 1–8.

[23] M. de Geus, R. Peters, C.E. Koning, A. Heise, Insights into the initiation process of enzymatic ring-opening polymerization from monofunctional alcohols using liquid chromatography under critical conditions, Biomacromolecules 9 (2008) 752–757

[24] X.W. Wei, C.Y. Gong, M.L. Gou, S.Z. Fu, Q.F. Guo, S. Shi, F. Luo, G. Guo, L.Y. Qiu, Z.Y. Qian, Biodegradable poly(ε-caprolactone)-poly(ethylene glycol) copolymers as drug delivery system, Int. J. Pharm. 381 (2009) 1–18.

[25] L.S. Nair, C.T. Laurencin, Biodegradable polymers as biomaterials, Prog. Polym. Sci. 32 (2007) 762–798.

[26] M. Sobczak, Enzyme-catalyzed ring-opening polymerization of cyclic esters in the presence of poly(ethylene glycol), J. Appl. Polym. Sci. 125 (2012) 3602–3609.

[27] H. Ge, Y. Hu, X. Jiang, D. Cheng, Y. Yuan, H. Bi, C. Yang, Preparation, characterization, and drug release behaviors of drug nimodipine-loaded poly(ε-caprolactone)-poly(ethylene oxide)-poly(ε-caprolactone) amphiphilic triblock copolymer micelles., J. Pharm. Sci. 91 (2002) 1463–1473.

[28] C. Chen, C.H. Yu, Y.C. Cheng, P.H.F. Yu, M.K. Cheung, Biodegradable nanoparticles of amphiphilic triblock copolymers based on poly(3-hydroxybutyrate) and poly(ethylene glycol) as drug carriers, Biomaterials 27 (2006) 4804–4814.

[29] J. Lee, E.C. Cho, K. Cho, Incorporation and release behavior of hydrophobic drug in functionalized poly(D,L-lactide)-*block*-poly(ethylene oxide) micelles, J. Control. Release. 94 (2004) 323–335.

[30] O. Nuyken, S.D. Pask, Ring-opening polymerization-An introductory review,

Polymers 5 (2013) 361–403.

[31]   E. Calahorra, M. Cortazar, G.M. Guzman, Thermal decomposition of poly(ethylene oxide), poly(methyl methacrylate), and their mixtures by thermogravimetric method., J. Polym. Sci. Polym. Lett. Ed. 23 (1985) 257–260.

[32]   L. Mazzocchetti, M. Scandola, Z. Jiang, Copolymers of ethyl glycolate and ω-pentadecalactone: enzymatic synthesis and solid-state characterization, Eur. Polym. J. 47 (2011) 942–948.

[33]   J. Fernández, A. Etxeberria, J.-R. Sarasua, Synthesis and properties of ω-pentadecalactone-*co*-δ-hexalactone copolymers: a biodegradable thermoplastic elastomer as an alternative to poly(ε-caprolactone), RSC Adv. 6 (2016) 3137–3149.

[34]   Z. Jiang, H. Azim, R.A. Gross, M.L. Focarete, M. Scandola, Lipase-catalyzed copolymerization of ω-pentadecalactone with *p*-dioxanone and characterization of copolymer thermal and crystalline properties, Biomacromolecules 8 (2007) 2262–2269.

Chapter 5. Synthesis and properties of diblock copolymers of ω-pentadecalactone and α-amino acids

Abstract

Diblock copolymers (PPDLx-*b*-pPAAy) were prepared from ω-pentadecalactone and L-glutamic acid or L-lysine amino acids by ring opening polymerization initiated by amino groups. Telechelic amino-ended poly(ω-pentadecalactone) with a length of 15-20 repeating units was firstly synthesized by enzymatic polymerization by means of CALB and then used as macroinitiator for the polymerization of the *N*-carboxyanhydrides of the two α-amino acids conveniently protected as benzyl and $^{\varepsilon}N$-carbobenzoxy derivatives, respectively. The molecular weight of the polypeptide block was accurately controlled by adjusting the amino acid/macroinitiator ratio used in the feed. Copolymers with M_n ranging between ~5000 and ~40,000 g·mol^{-1} and varying ester/peptide ratio were obtained and characterized in detail by GPC and NMR spectroscopy. The thermal properties of these copolymers were evaluated by TGA and DSC, and their structure in the solid-state including their response to heating, were examined by FTIR and XRD at variable temperature. It was shown that the polypentadecalactone segment was crystallized for all compositions and that the polypeptide counterpart adopted a two-dimensional hexagonal packing of α-helices at temperatures above melting of the polyester block. SAXS revealed the presence of a biphasic nanostructure with a repeating distance of 27 nm for the case of glutamic-based copolymers. It was demonstrated that both glutamic and lysine-based PPDL$_x$-*b*-pPAA$_y$ copolymers could self-assemble in well-shaped nanospheres with a diameter in the ~200-400 nm range and a negative zeta-potential.
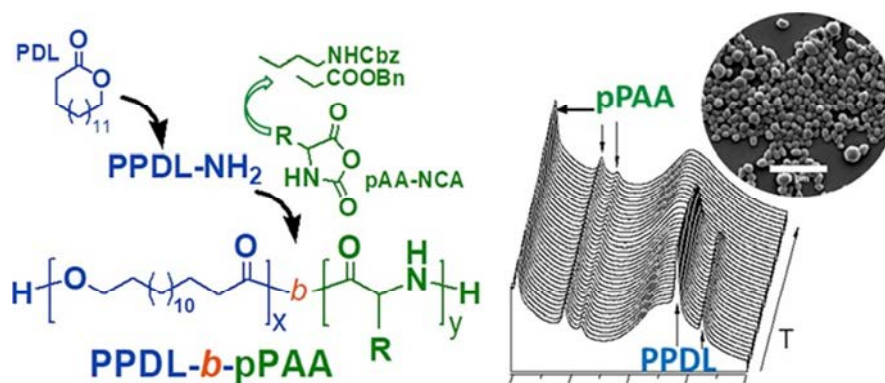
Publication derived from this work:

E. Tinajero-Díaz, A. Martínez de Ilarduya, S. Muñoz-Guerra, Synthesis and properties of diblock copolymers of ω-pentadecalactone and α-amino acids, Eur. Polym. J. 116 (**2019**) 169–179.

Supporting information to this chapter in Annex B

5.1 Introduction

Block copolymers containing at least one polypeptide block provide advantages over conventional synthetic polymers due to their ability to hierarchically self-assemble into stable ordered arrangements [1,2]. The polypeptide moiety in these copolymers is usually arranged in the familiar α-helix or β-sheet structure depending on the side chain of the constituent amino acid. The stiff polypeptide conformation is known to exert a decisive influence on the copolymer structure adopted in the solid state and its self-assembling properties [3,4]. In fact structures at several length-scales with uncommon properties have been observed in the solid state for these copolymers, in which one of the blocks is a rod-like polypeptide and the other one is a flexible polymer [5,6]. Formation of micelles [7], vesicles, and bilayer aggregates [8] is also known to take place in these copolymers in aqueous medium according to their composition and environment conditions. Polypeptide-based copolymers are therefore outstanding building compounds for biomaterials due to their tunable chemical architecture, biocompatibility, biodegradability, and ability to take up responsive secondary structures [9].

Among the diversity of peptide-based block copolymers today available [10,11], those derived from lactones become distinguished by both their feasible synthesis through ring opening polymerization (ROP) and their distinguishing properties. It is well known that amino acid *N*-carboxyanhydrides (NCA) are prone to undergo ROP initiated by aliphatic primary amines with the initiator remaining attached to the growing chain [9]. This approach has been applied to the synthesis of a number of polyester-*b*-polypeptide copolymers. In most of cases the polyester is generated from medium-size lactones (ε-caprolactone, L-lactide, etc), and the synthesis strategy consisted of preparing first the macroinitiator with an ending free-amino group to initiate then the ROP of the NCA's. Thus Caillol *et al.* synthesized a poly(L-lactide) amino-ended macroinitiator, which was then used for the ROP of γ-benzyl L-glutamate *N*-carboxyanhydride (BLG-NCA). These PLLA-*b*-PBLG copolymers were organized in

separated domains containing crystalline PLLA and liquid-crystal columnar hexagonal PBLG [6]. Likewise others amino acids (L-Ala, L-Phe, L-Leu, etc.) have been used in the preparation of a diversity of poly(ester-peptide)s with the hydrophobic block made from L-lactide or ε-caprolactone [12-16].

A critical factor for the successful synthesis of telechelic polymers is the end-group fidelity, which is achieved by a good control of the functionalizing reaction [17]. Ritter prepared a library of poly(L-lysine-*b*-caprolactone) block copolymers using amino-ended poly(^{ε}N-carbobenzoxy L-lysine) (PZLL$_x$-NH$_2$) to effectively initiated the ROP of ε-caprolactone [18]. After removal of the *Z*-protecting group, water-soluble copolymers were obtained which were able to spontaneously self-organize into nanometer size aggregates (core-shell particles or vesicles). In our research, we initially tried this approach using well-defined PBLG$_x$-NH$_2$ or PZLL$_x$-NH$_2$ for the ROP of ω-pentadecalactone (PDL) mediated by 1,5,7-triazabicyclo[4.4.0]dec-5-ene (TBD) or *Candida antarctica* lipase B (CALB) as catalysts. According to what has been reported [19,20] the use of TBD promoted transesterification reactions over the –COOBn group with release of benzyl alcohol as a by-product, and when CALB was used, the steric hindrance of the macroinitiator precluded its attack to the enzyme activated PDL so that copolymerization did not proceed. Recently we reported on the synthesis of well-defined allyl-ended telechelic poly(ω-pentadecalactone)s (PPDL) intended to be used as initiator of ROP after appropriate functionalization [21]. Deliberately, an adequate functionalized alkene was used as initiator to insert an unsaturation into the PPDL end-chain. The amine functionality was then introduced into the double-bond ended polyester via thiol-ene coupling with 2-(Boc-amino)-ethanethiol (BAET) followed by Boc removal. Such amine-functionalized polyester was claimed to be suitable for initiating ROP of either NCAs or other lactones, and this is in fact the approach we have adopted for the synthesis of the copolymers studied in this work.

In biomedical applications, and more specifically in the design of polymeric drug carriers, polymer amphiphilicity plays a crucial role. Drug carriers with significant lipophilic character have been found to be particularly effective in the stabilization of certain drugs and enlarging its circulatory retention in the blood stream. Macrolactones (MLs) have recently emerged as a family of building blocks for novel polymer biomaterials displaying properties close to those typical of long aliphatic chains but being potentially biodegradables [22]. The polyesters generated in the ROP of MLs have a hydrophobic character comparable to paraffins and display a strong tendency to crystallize producing well-developed crystallites of high thermal and chemical stability. Such features have motivated their use in the building of different block copolymers intended for drug delivery applications [23-25]. ω-Pentadecalactone is an easily accessible macrolactone that has been largely studied as ROP monomer for producing hydrophobic polyesters (PPDLs). Despite the exceptional potential of PPDL as biomaterial component, to our knowledge its marriage to polypeptides has never been reported, which prompted us to investigate the family of block copolymers made of PDL and L-glutamic or L-lysine (PPDL-*b*-pPAA). The work reported in this paper constitutes a first step in this investigation which is focused on neutral copolymers with the amino acids bearing their carboxylic or amino side groups conveniently protected. The PPDL-*b*-pPAA copolymers are exempted of organometallic catalysts and are of interest, not only by themselves due to their capacity to form stable nano-aggregates, but also as precursors of ionic copolymers potentially exploitable in highly sophisticated biomedical applications. In fact the -COOH and -NH_2 side groups of the glutamic and lysine residues are readily recoverable by acid treatment to render negatively and positively charged copolymers, respectively. These copolymers will display strong affinity for proteins and will be able to combine ionically with drugs and DNA's to form stable nanoconjugates [26,27].

5.2 Results and discussion

5.2.1 Synthesis of the PPDL-NH$_2$ macroinitiator

The three-step pathway followed for the preparation of the PPDL$_x$-NH$_2$ macroinitiator is depicted in Scheme 1. Partial yields were between 80 and 90% and the ^{1}H NMR spectra of the three intermediate compounds respectively isolated in each step are depicted in Figure 5.1. The NMR analysis proved that the synthesis of the amino-ended macroinitiator was successfully achieved.
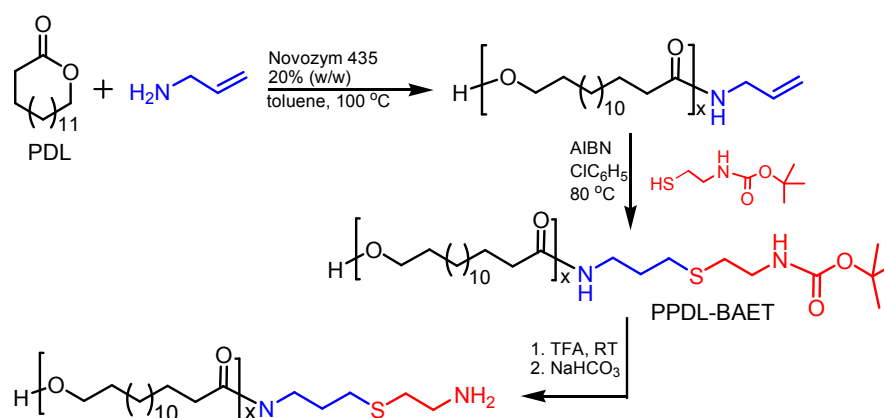
Scheme 5.1. Synthetic pathway leading to the PPDL-NH$_2$ macroinitiator.

The triplet b appearing at 2.2 ppm is the only signal arising from methylene neighboring to the carbonyl group apart from that due to the repeating CH$_2$COO unit of the polyester chain. This is taken as indicative that all polyester chains have been amino-initiated in the ROP process. The b signal is shared by the three spectra and its area is consistent with that of the f$^\perp$ signal at 3.65 ppm arising from the methylene protons of the end CH$_2$OH. It can be hence inferred that both thiol-ene click and Boc-deprotection reactions occurred as expected, and that therefore the PPDL-NH$_2$ sample is practically exempted of not amino-ended chains. The ratio of the areas of the b and f signals measured in the ^{1}H NMR spectra of this compound was used to determine the number-average length of the PPDL-NH$_2$ which resulted to be in the range of 15 or 20 units depending on the batch
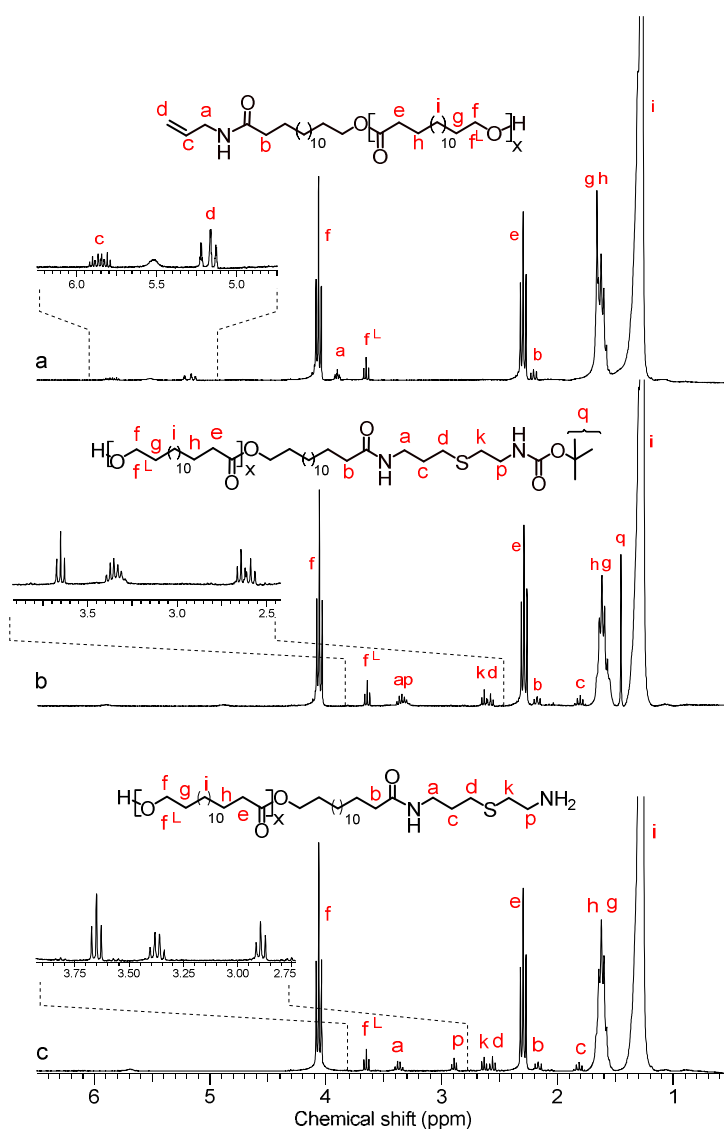
Figure 5.1. ^{1}H NMR (CDCl$_3$) spectra of a) PPDL-All, b) PPDL-BAE and c) PPDL-NH$_2$. f^L notation refers to the last repeating unit.

5.2.2 Synthesis of the PPDL$_x$-*b*-pPAA$_y$ copolymers

Two series of PPDL$_x$-*b*-pPAA$_y$ diblock copolymers with the poly(amino acid) block (pPAA$_y$) duly protected were prepared by ROP of the NCA of γ-benzyl L-glutamate and $^\varepsilon N$-carbobenzoxy L-lysine, respectively, initiated by PPDL-NH$_2$, as it is depicted in Scheme 5.2. Yields, compositions and molecular weights of the resulting copolymers are given in Table 5.1.
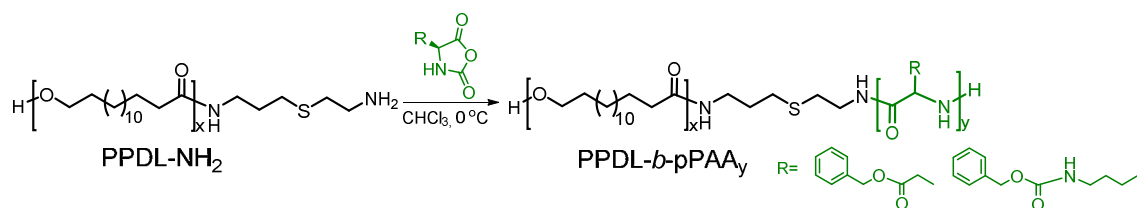
Scheme 5.2. ROP of AA-NCA initiated by PPDL-NH$_2$.

Table 5.1. Yields, compositions and molecular weights of PPDL$_x$-*b*-pPAA$_y$ copolyesters.

Copolymer[a]	Yield (%)	Feed [Init]/[NCA]	Copolymer[a,b] [PDL]/[AA]	M_n[c] (g·mol^{-1})	L_{PPDL}/L_{PAA}[d] (nm)/(nm)
PPDL$_{15}$-*b*-PBLG$_{30}$	81	1/30	15/33	10,500	29/12
PPDL$_{15}$-*b*-PBLG$_{60}$	73	1/60	15/56	15,500	29/20
PPDL$_{15}$-*b*-PBLG$_{80}$	79	1/80	15/84	21,600	29/30
PPDL$_{15}$-*b*-PBLG$_{180}$	80	1/180	15/187	44,200	29/67
PPDL$_{20}$-*b*-PZLL$_{30}$	94	1/30	20/32	12,800	38/11
PPDL$_{20}$-*b*-PZLL$_{70}$	81	1/70	20/68	22,300	38/28
PPDL$_{20}$-*b*-PZLL$_{100}$	80	1/100	20/98	30,000	38/35
PPDL$_{20}$-*b*-PZLL$_{190}$	88	1/200	20/190	54,300	38/68

[a]Subscripts indicate the degrees of polymerization of the two blocks corresponding to the PPDL-NH$_2$ initiator to NCA molar ratio used in the feed as indicated in column 3 after having been rounded to ten.
[b]Copolymers composition expressed as the number of units of each block as determined by ^{1}H NMR.
[c]Number-average molecular weight of copolymers determined by ^{1}H NMR.
[d]PDL and AA-block average lengths calculated from the compositions given in column 4 for an extended chain and assuming an average projected bond length of 0.120 nm.

Copolymerization yields were in the 70-90% range with significantly higher values attained for copolymers made of Lys. The ^{1}H and ^{13}C NMR spectra of the PPDL$_x$-*b*-PBLG$_y$ and PPDL$_x$-*b*-PZLL$_y$ ascertained their constitution and no signals other than those assignable to the monomeric repeating units present in these copolymers were therein detected. The PPDL$_{15}$-*b*-PBLG$_{30}$ and PPDL$_{20}$-*b*-PZLL$_{30}$ ^{1}H NMR spectra are shown in Figure 5.2 as representative for their respective series. Some illustrative ^{13}C NMR spectra are shown in Figure B1 of the Annex B. Compositions as well as number-average molecular weights were determined by ^{1}H NMR using the areas of signals specifically arising from each block and from both amino and hydroxyl end groups (see details in Figure B2 of the Annex B. The compositions of the resulting copolymers were very close to those expected from the initiator to amino acid ratios set for their respective feeds with deviations being lower than 10%. M_n oscillated between ~10,000

and ~55,000 g·mol^{-1} which correspond to copolymer chain lengths between 40 and 100 nm and block lengths ratios ranging from 0.4 to 3.5 with values close to 1 in the cases of PPDL$_{15}$-*b*-PBLG$_{80}$ and PPDL$_{20}$-*b*-PZLL$_{100}$.
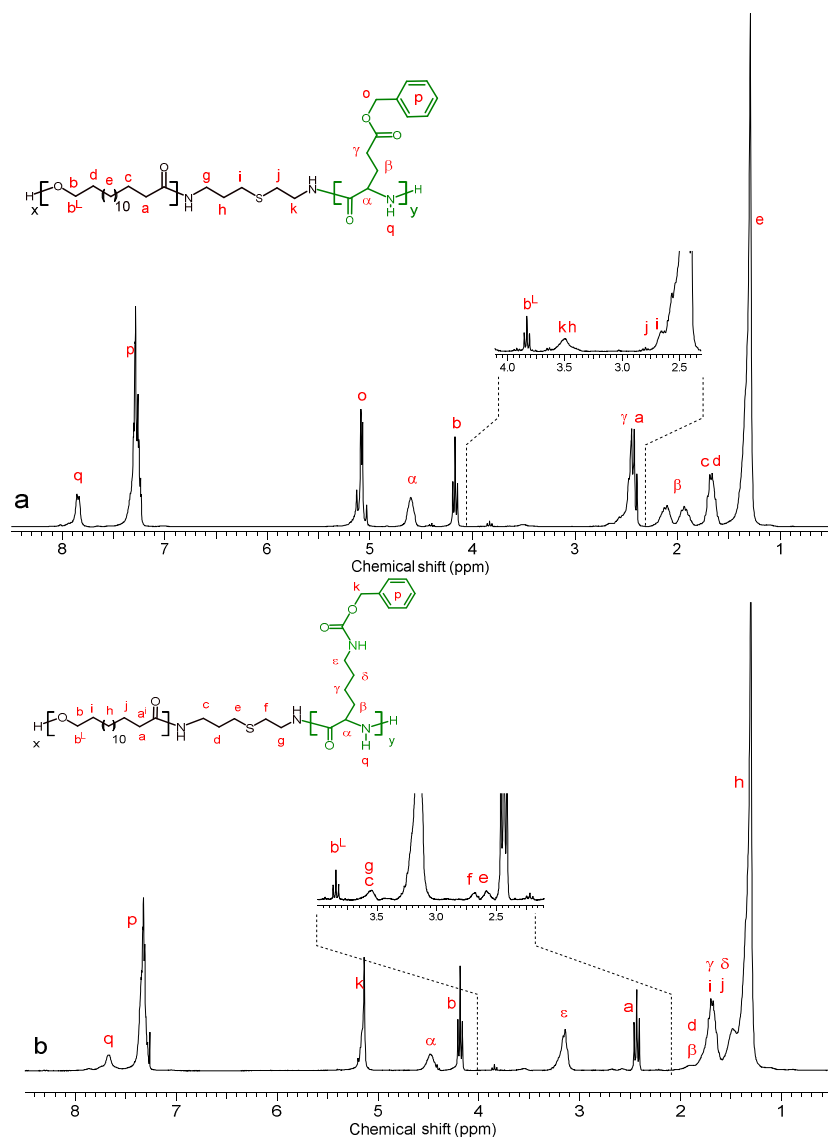

Figure 5.2. ^{1}H-NMR spectra (CDCl$_3$/TFA) of the PPDL$_{15}$-*b*-PBLG$_{30}$ (a) and PPDL$_{20}$-*b*-PZLL$_{30}$ (b) diblock copolymers. (b^L corresponds to the end repeating unit).

On the other hand, the chromatograms recorded in the GPC analysis displayed monomodal distributions (peaks appearing a longer elution times do arise from salts, Annex B, Figure B3) with molar dispersities within the 1.2-2.2 range. However molecular weight values given by this technique were found to be much lower than those determined by NMR. As it has been reported for polypeptides carrying aromatic groups [16,31], it can be assumed that exceptional interactions taking place between

the benzyl groups of the polypeptides and the aromatic matrix of the column could be responsible for the delay observed in the elution times.

Contamination of the copolymers with some minor amounts of homo-oligopeptides that might be generated by non-amino initiated ROP of the NCA cannot be discarded. Although dried $CHCl_3$ was the solvent used, the presence of small quantities of water may initiate NCA polymerization. Unfortunately the detection and quantification of these oligopeptides is not easy. Nevertheless, their amount must be small since GPC results do not provide indication on their existence. Their elution together with the salts is highly unlikely because their molecular weights would be much greater and expected therefore to come out at noticeable shorter times. It should be noticed anyhow that the presence of minor oligopeptide impurity in the PPDL$_x$-*b*-pPAA$_y$ copolymers would not invalidate the structural and property study carried out on them.

5.2.3 Thermal properties of the PPDL$_x$-*b*-pPAA$_y$ copolymers

The thermal stability of the PPDL$_x$-*b*-pPAA$_y$ copolymers was examined by TGA under an inert atmosphere. The thermogravimetry traces recorded in the 25-600 ºC range for the two whole series including the parent homopolymers, as well as their derivative curves, are given in Figure B4 in the Annex B, and decomposition parameters are listed in Table 5.2. The onset temperatures of copolymers vary unsteadily from 237 to 230 ºC whereas the two homopolypeptides started to decompose above 285 ºC and 260 ºC, respectively. Decomposition of PPDL took place through one main step at a $^{max}T_d$ of 430 ºC with a weight loss of about 90% followed by a second minor step at a $^{max}T_d$ of 475 ºC. These two steps have been made to correspond to decarboxylation and polymethylene disintegration reactions, respectively.

On the other hand the polypeptides displayed a thermal decomposition behavior consisting basically in two well-separated stages centered about 290 and 320 ºC for

PBLG, and 320 and 430 ºC for PZLL. At difference with the homopolymers, the response of the copolymers to heating was complex and rather aleatory without showing apparent correlation between decomposition temperatures and composition. All derivative curves display several peaks corresponding to partial $^{max}T_d$ located within the interval delimited by the parents homopolymers and with values approaching to the one or the other limit according to composition.

The existence of thermal transitions in the PPDL$_x$-b-pPAA$_y$ diblock copolymers was investigated by DSC. The traces recorded at both heating and cooling for the two whole series including the parent homopolymers are depicted in Figure 5.3 and the characteristic parameters measured in this analysis are listed in Table 5.2. As expected from what is reported from literature PPDL behaved as a semicrystalline polyester with T_m around 90 ºC and being able to crystallize upon cooling from the melt with high recovery of the original crystallinity [32].

Table 5.2. Thermal properties of the PPDL$_x$-b-pPAA$_y$ diblock copolymers.

Copolymers	TGA[a]			DCS[b]								
				first heating					cooling		second heating	
	^oT_d ^oC	$^{max}T_d$ ^oC	R_w %	T_g ^oC	T_m ^oC	ΔH J·g^{-1}	$T_{LC}{}^c$ ^oC	ΔH J·g^{-1}	T_c ^oC	ΔH J·g^{-1}	T_m ^oC	ΔH J·g^{-1}
PPDL$_{15}$	285	430, 470	1	-	90	151	-	-	75	-119	90	123
PPDL$_{15}$-b-PBLG$_{30}$	237	230-470	1	21	90	49	109	2	73	-45	89	44
PPDL$_{15}$-b-PBLG$_{60}$	230	235-470	16	21	88	26	109	2	68	-24	86	27
PPDL$_{15}$-b-PBLG$_{80}$	230	240-470	15	21	88	13	119	2	67	-10	85	12
PPDL$_{15}$-b-PBLG$_{180}$	230	260-430	14	20	88	9	120	4	70	-6	88	6
PBLG$_{50}$	280	290,320	17	20	-	-	118	9	-	-	-	-
PPDL$_{20}$	285	430, 470	1	-	90	151	-	-	75	-119	90	123
PPDL$_{20}$-b-PZLL$_{30}$	200	260-470	10	21	83	33	-	-	63	-37	84	30
PPDL$_{20}$-b-PZLL$_{70}$	210	230-410	9	21	84	23	~140	nd	67	-32	84	23
PPDL$_{20}$-b-PZLL$_{100}$	215	250-410	9	20	84	18	~140	nd	66	-22	84	15
PPDL$_{20}$-b-PZLL$_{190}$	240	270-410	5	20	90	2	-	-	77	-0.7	91	0.62
PZLL$_{50}$	260	290, 430	9	21	-	-	~140	nd	-	-	-	-

[a]Onset temperature for 5% of weight loss (^oT_d), maximum rate ($^{max}T_d$) decomposition temperatures and remaining weight (R_w) after heating at 600 ºC.
[b]Glass transition (T_g), melting (T_m and ΔH_m) and crystallization (T_c and ΔH_c) temperatures and enthalpies measured by DSC.
[c]T_{LC} is the temperature for the helical transition undergone by the polypeptide block. Values given for PPDL$_{20}$-b-PZLL$_{70}$ and PPDL$_{20}$-b-PZLL$_{100}$ are approximate.

The DSC traces registered from copolymers displayed typical melting and crystallization peaks corresponding to the PPDL block for the two series and for whichever composition, and the second heating traces reproduced the endothermal peak observed on the first heating traces with acceptably close values in both melting temperature and enthalpy (see Figure B5 in the Annex B). It is worth noting that in the PPDL$_x$-b-PBLG$_y$ series, the PPDL block melting peak appeared at the same temperature than in the homopolymer, but showing a shoulder at lower temperature that may be attributed to the fraction of polyester generated by secondary crystallization. On the contrary, the PPDL block in the PPDL$_x$-b-PZLL$_y$ series melted at a few degrees lower than the homopolymer with a shoulder around 90 ºC indicating that the PZLL block exerts a greater distorting effect on PPDL crystallization than the PBLG$_y$ block.
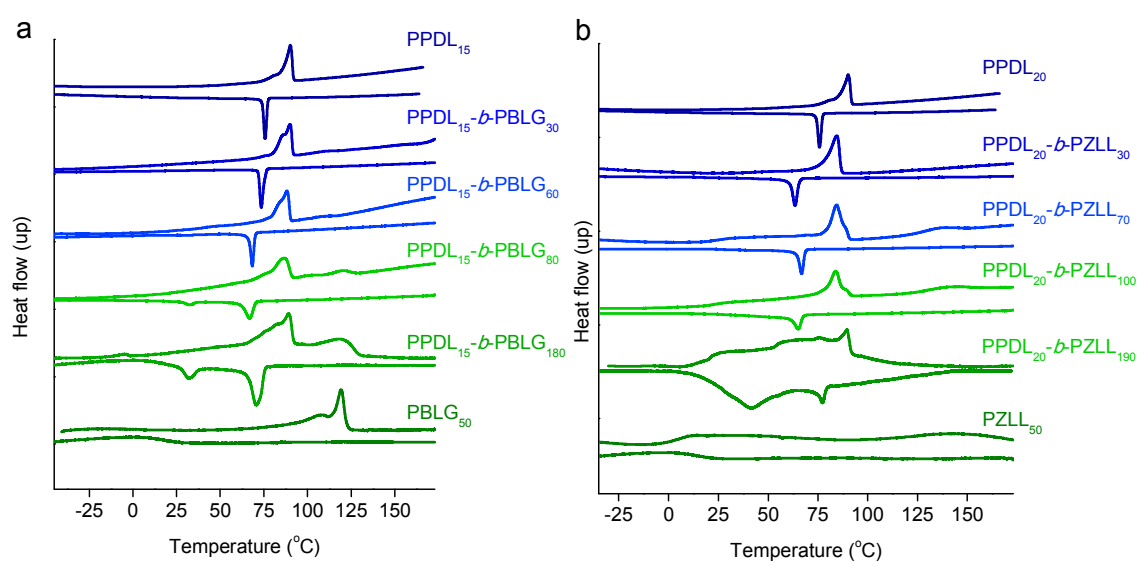
Figure 5.3. DSC first heating and cooling traces of PPDL$_x$-b-pPAA$_y$ diblock copolymers a) BLG-containing copolymers and b) ZLL-containing copolymers.

On the contrary the DSC traces of PBLG and PZLL, which are polypeptides known to be unable to crystallize, displayed an endotherm in the 100-150 ºC range. According to literature [16, 33] such peak is attributed to a conformational transition involving the conversion of the 7/2 helix to the 18/5 α-helix characteristic of poly(α-amino acid)s. The transition was clearly observed for PBLG as a sharp peak at 120 ºC whereas it was much less noticeable in PZLL where only a smooth wide hill was shown

in its heating trace. The occurrence of such transition in the PPDL$_x$-b-PBLG$_y$ series was evidenced for both 15/80 and 15/180 compositions by the presence of an endothermal peak appearing at 110-120 ºC. Heat exchanges with similar meaning were observed nearby 140-150 ºC for the PPDL$_x$-b-PZLL$_y$ copolymers with x/y values of 20/70 and 20/100 but not for 20/190, which is a highly striking result without apparent explanation.

5.2.4 Solid-state structure of the PPDL$_x$-b-pPAA$_y$ diblock copolymers

The occurrence of regular arrangements in the polypeptide chain of the PPDL$_x$-b-pPAA$_y$ copolymers and its dependence on the amino acid constitution was clearly demonstrated by FTIR analysis. The spectra of all the polymers studied in this work are comparatively represented in Figure 5.4. Bands at 1650 and 1545 cm^{-1} characteristic of α-helix type were conspicuous in the spectra recorded from all the PPDL$_x$-b-PBLG$_y$. In the case of the PPDL$_x$-b-PZLL$_y$, the spectra showed the absorption characteristic of the β-sheet at 1625 cm^{-1} in addition to the α-helix bands indicating that both forms coexist in this series. It should be noted that cannot be disregarded that the observed β-sheet structure may arise, at least in part, from homo-oligopeptides that could be present in the copolymer as a minor impurity. Nevertheless, in the two series, the relative amount of helical arrangement present in the copolymer is largely predominant and it increased with the length of the polypeptide block.
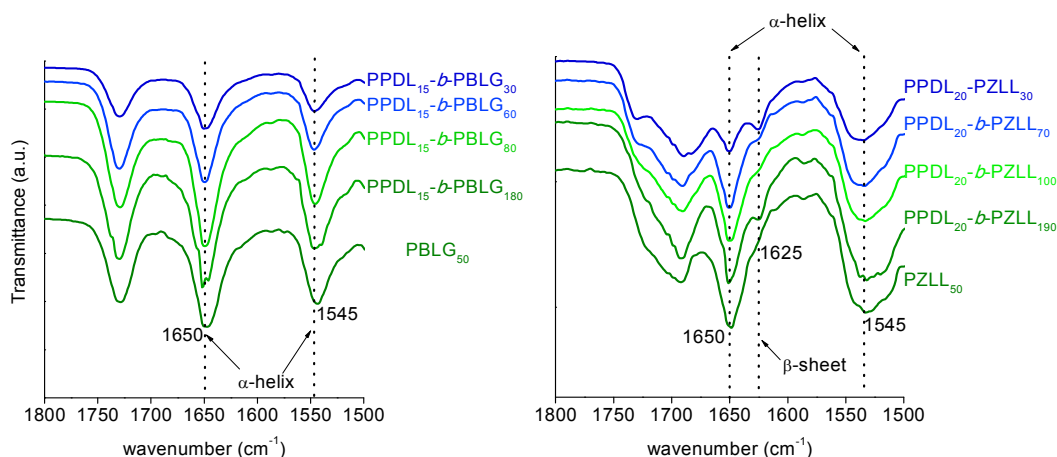

Figure 5.4. 1800-1500 cm^{-1} region of FTIR spectra of PPDL$_x$-b-pPAA$_y$ diblock copolymers and the PBLG and PZLL homopolymers showing bands characteristic of α-helix and β-sheet secondary structures

The large difference between the PPDL and pPAA blocks in chemical constitution leads to expect that the PPDL$_x$-*b*-pPAA$_y$ copolymers are able to self-assembly in the solid state in a biphasic structure at the nanometric scale. To get insight into this structure, a real-time X-ray diffraction study was carried out by using synchrotron radiation with samples subjected to variable temperature. Both wide and small angle scattering were simultaneously recorded at either heating or cooling within the 10-150 ºC temperature range. The evolution followed by the scattering profile of a pristine sample of PPDL$_{15}$-*b*-PBLG$_{80}$ with temperature changes is displayed in Figure 5.5.
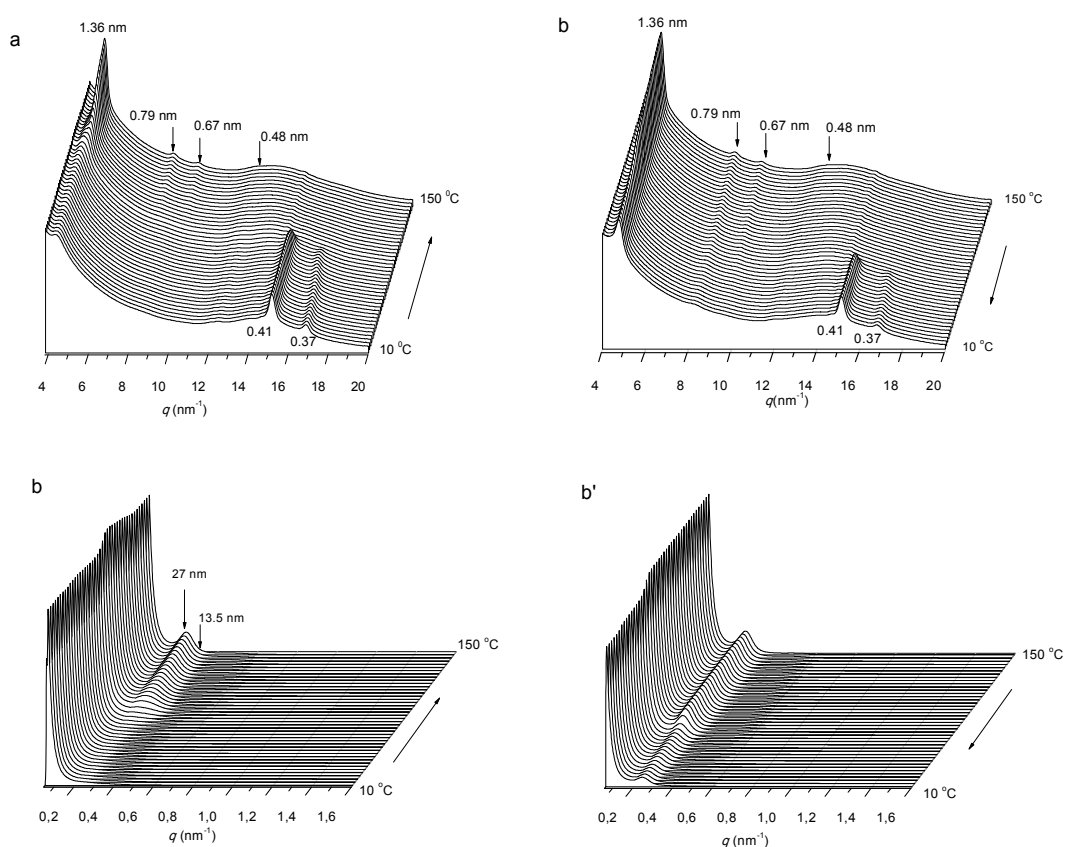
Figure 5.5. Evolution of the X-ray diffraction profiles of PPDL$_{15}$-*b*-PBLG$_{80}$ recorded at heating and cooling over the 10-150 ºC range. a, a') WAXS and b,b') SAXS (details may be clearly seen in the enlarged Figure B6 of the Annex B).

The WAXS recorded at 10 ºC shows exclusively the 0.41 nm and 0.37 nm reflections arising from the 110 and 200 planes of the pseudo-rhombic unit cell of PPDL with approximate dimensions a = 0.75 nm, b = 5.0 nm, and c = 20.0 nm and α = 90.0° [34] indicating that the polyester block is the only one crystallized in this sample.

This profile remained essentially unchanged under heating until temperature reached approximately 90 ºC where both peaks disappeared and new reflections with Bragg spacings of 1.36 nm, 0.79 nm and 0.67 nm started to emerge and became more pronounced as temperature increased. These spacing values are related as $1:3^{1/2}:2$ and according to literature, they must arise from a two-dimensional columnar hexagonal packing of PBLG α-helices of 1.55 nm diameter. After cooling from 150 ºC these peaks decreased in intensity as soon as crystallization of the PPDL block started, a fact that happened around 50 ºC, so that the 1.36 nm peak was the only one remained at 10 ºC. The presence of the crystalline and liquid crystal structures could be further evidenced by polarizing optical microscopy (Figure B7 in the Annex B).

The SAXS profiles recorded from PPDL$_{15}$-b-PBLG$_{80}$ at heating up to 150 ºC revealed the appearing of discrete reflections at 27 nm (main peak) and 13.5 nm simultaneously to the development of the columnar phase evidenced by WAXS. According to what has been reported for copolymers composed of PBLG and PLA blocks [6], such spacings are interpreted to arise from a nano-structure of alternating layers made of PBLG helices and liquid PPDL. After cooling from 150 ºC the nanostructure remained essentially unchangeable until crystallization of the PPDL block was initiated. It seems therefore that the occurrence of the nanometric structure is concomitant with the two-dimensional packing of the PBLG helices, and that the adoption of these ordered arrangements is disfavored by the presence of PPDL in the crystallized state.

The XRD analysis of PPDL$_{20}$-b-PZLL$_{100}$ was then carried out to get information from the copolymers containing lysine. The cumulative graphs showing the evolution of the WAXS profile of such copolymer with temperature changes along the 10-130 ºC range are provided in Figure 5.6. The response of this copolymer to the thermal treatment was significantly different to that observed for PPDL$_{15}$-b-PBLG$_{80}$. In this case, both the monoclinic crystal phase of PPDL and the 2D-hexagonal columnar phase of PZLL (with spacings at 1.5 nm, 0.86 nm and 0.74 nm [3,5,35]) are coexisting in the

original sample, and peaks arising from the later remained unchanged over the whole range of temperatures. The broad scattering observed around 0.47 nm at high temperature is attributed not only to the amorphous state of PPDL but also to PZLL in β-sheet form that remains unaffected by temperature along the range of the treatment. It is concluded therefore that, at difference with that happens in the PBLG containing copolymers, the formation and stability of the columnar structure made of the polypeptide block based on lysine is essentially independent on the state adopted by the PPDL phase. The weak conformational response to temperature given by PPDL$_{15}$-*b*-PBLG$_{80}$ and PPDL$_{20}$-*b*-PZLL$_{100}$ copolymers was supported by FTIR evidences (Figure B8 of Annex B).

On the other hand, the results obtained by SAXS were radically different since no discrete reflections were detected in these profiles (Figure B6 in Annex B) within the recording limits (up to approximately 40 nm). It may be concluded therefore that no segregation in ordered domains takes place in the PPDL$_{20}$-*b*-PZLL$_{100}$ copolymer in spite of that the liquid crystal structure was in this case readily formed.
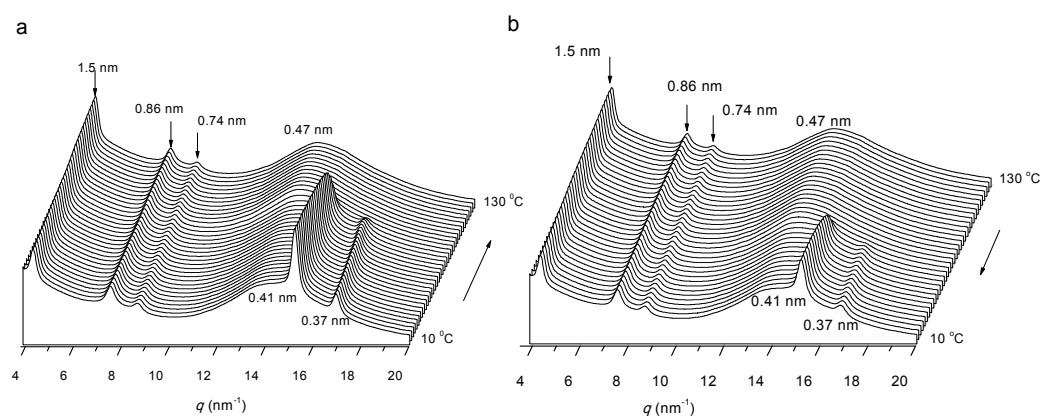
Figure 5.6. Evolution of the WAXS profiles of PPDL$_{20}$-*b*-PZLL$_{100}$ recorded at heating (a) and cooling (b) over the 10-130 °C range.

A crystallization kinetics analysis was carried out in order to investigate the possible influence of both the polypeptide block length and the thermal history of the sample on the crystallizability of the PPDL block. For such a purpose isothermal crystallizations of PPDL$_{15}$-*b*-PBLG$_y$ copolymers for y = 30, 80 and 180 and PPDL$_{20}$-*b*-

PZLL$_y$ for y= 30, 100 and 190 were carried out at 77 °C. Samples were previously heated at 150 °C to ensure that both PPDL melting and PAA helical transition had taken place. As it is shown in Figure 5.7, where relative crystallinity *vs.* time is comparatively represented for the two series and compared with their respective PPDL homopolyester, the crystallization rate of the PPDL block is notably enhanced by the presence of the polypeptidic counterpart. Furthermore the enhancing effect appeared to be independent from the polypeptide block length. It is a striking result that is however in agreement with both DSC and thermal XRD observations. Similar results were obtained when the sample was previously heated at 93 °C, *i.e.* between the PPDL melting and helical transition temperatures (see Figure B9 in Annex B) indicating that the polypeptide block conformation does not exert appreciable effect on the crystallizability of the PPDL block. These results allow extending the conclusions drawn in the XRD analysis of PPDL$_{15}$-*b*-PBLG$_{80}$ and PPDL$_{20}$-*b*-PZLL$_{100}$ (Figures 5.5 and 5.6) to other compositions.
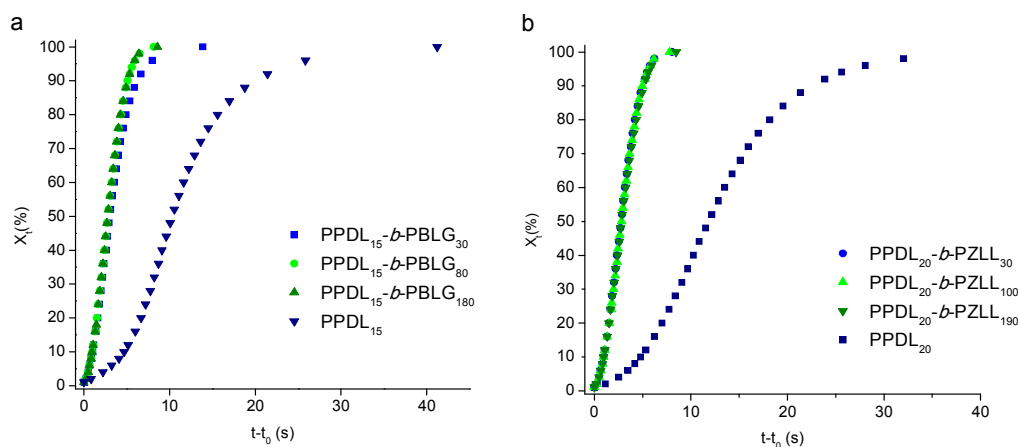
Figure 5.7. Evolution of the relative crystallinity as a function of time in the isothermal crystallization at 77 °C of PPDL$_x$-*b*-PBLG$_y$ (a) and PPDL$_x$-*b*-PZLL$_y$ (b) copolymers from samples melted at 150 °C.

5.2.5 Nanoparticles made of PPDL$_x$-*b*-pPAA$_y$ copolymers.

As the last stage in our examination of the PPDL$_x$-*b*-pPAA$_y$ copolymers, their capacity to form stable nano-aggregates was preliminary explored for one pair of selected copolyesters of each series differing in the length of the polypeptide segment.

Since these copolymers are non-soluble in water but soluble in volatile organic solvents as CHCl$_3$, the well-settled emulsion-evaporation technique was applied for creating the particles. The sizes and surface charges of the entities obtained by such method were determined by DLS measurements and the resulting values are compared in Table 5.3. Monomodal DLS curves were recorded for every case (Figure 5.8) with average diameters (*D*) in the 200-340 nm range with values being very close similar for the two series when copolymers with similar PDL/AA ratio are compared. All particles displayed small negative zeta potentials (ζ) with insignificant differences between the two copolymers integrating each pair. The morphology of these NPs was examined by SEM and illustrative pictures from selected copolymers are shown in Figure 5.9. A well-defined spherical shape is displayed in all cases with sizes in acceptable consistency with values measured by DLS.

Table 5.3. Nanoparticles made of PPDL$_x$-*b*-pPAA$_y$ copolymers.

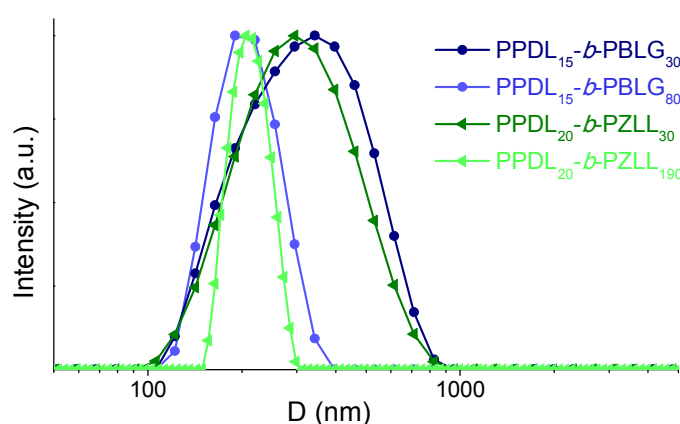| Polymer	D (nm)	PDI	ζ (mV)
PPDL$_{15}$-*b*-PBLG$_{30}$	340	0.40	-8.6
PPDL$_{15}$-*b*-PBLG$_{80}$	220	0.12	-8.4
PPDL$_{20}$-*b*-PZLL$_{30}$	300	0.18	-1.4
PPDL$_{20}$-*b*-PZLL$_{190}$	200	0.14	-1.7

Figure 5.8. DLS curves of PPDL-*b*-pPAA nanoparticles.

The chemical modification of the –COOH group of glutamic acid as benzyl ester and the –NH$_2$ group of lysine as carbobenzoxy amide greatly decreased the genuine

hydrophilic character of the amino acids and consequently the amphiphilic nature of the PPDL$_x$-b-pPAA$_y$ copolymers too. Nevertheless, clear evidences have been provided by DSC and XRD to demonstrate that the polyester and the polypeptide phases must be segregated in the PPDL$_x$-b-pPAA$_y$ copolymers when they are in the solid state, at least in the BLG-based copolymers. It should be expected therefore that these nanoparticles have a certain degree of heterogeneity with the polypeptide block being preferentially located at the outer region. It is however striking that the particle size notably decreased in each series with the increasing length of the polypeptide block. No simple explanation can be given at this moment for this apparent inconsistency.
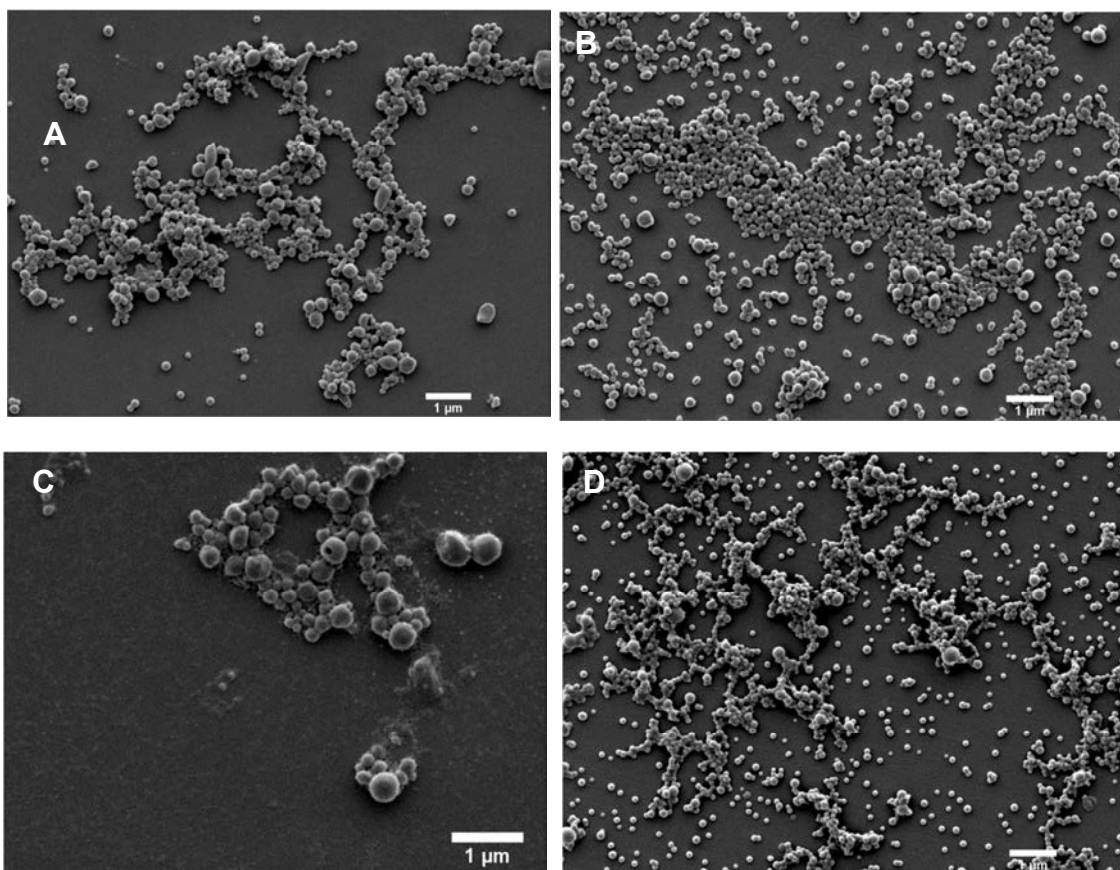
Figure 5.9. SEM images of nanoparticles made of PPDL-b-pPAA: A) PPDL$_{15}$-b-PBLG$_{30}$, B) PPDL$_{15}$-b-PBLG$_{80}$, C) PPDL$_{20}$-b-PZLL$_{30}$ and D) PPDL$_{20}$-b-PZLL$_{190}$.

5.3. Conclusions

Two series of diblock copolymers (PPDL-b-pPAA) made of ω-pentadecalactone (PDL) and γ-benzyl L-glutamate (BLG) or $^\varepsilon$N-carbobenzoxy-L-lysine (ZLL) were successfully synthesized by using a copolymerization approach based on the amino-

initiated ring-opening polymerization (ROP) of *N*-carboxyanhydrides (NCA) that avoided the use of organometallic compounds. CALB has been proved to be an efficient catalyst for the ROP of PDL leading to polyester blocks of well-defined lengths and exempted of undesirable side reaction products. The amino mediated opening of NCA allowed polypeptide segments of predetermined length according to the relative amount of macroinitiator that was used. PPDL-*b*-pPAA copolymers started to decompose noticeably at temperatures above 200 ºC to undergo major weight losses at much higher values. Despite that the genuine hydrophilicity was significantly diminished in the protected amino acids, the copolymers showed DSC characteristic of biphasic material indicating that even so, the PDL and AA blocks are still incompatible. Both phases were found to be organized in ordered arrangements, the polyester in the typical monoclinic crystal lattice of PPDL with chains in extended conformation, and the polypeptides in a 2D columnar pseudo-hexagonal liquid-crystal phase made of α-helices. The two phases are strongly interactive as it is revealed by the enhancing influence of the polypeptide on the crystallizability of the PPDL block and the occurrence of a nanometric periodical structure at temperatures above melting of the PPDL phase. These copolyesters are able to form well-defined quasi-spherical shape nanoparticles with diameters in the ~200-350 nm range and slight negative zeta-potential. It should be remarked that these PPDL-*b*-pPAA diblock copolymers are exempted of metallic contamination and they are therefore well-suited to build drug nanocarriers for biomedical applications. Furthermore, as the protected amino acids may be easily liberated, they stand as immediate precursors of electrostatic charged copolymers suitable for efficient loading and controlled release of ionic drugs and nucleic acids.

5.4. References

[1]   A. Carlsen, S. Lecommandoux, Self-assembly of polypeptide-based block copolymer amphiphiles, Curr. Opin. Colloid Interface Sci. 14 (2009) 329-339.

[2]   H.A. Klok, S. Lecommandoux, Solid-state structure, organization and properties of peptide-synthetic hybrid block copolymers, Adv. Polym. Sci. 202 (2006) 75-111.

[3]   J. Babin, J. Rodriguez-Hernandez, S. Lecommandoux, H.-A. Klok, M.-F. Achard, Self-assembled nanostructures from peptide–synthetic hybrid block copolymers: complex, stimuli-responsive rod–coil architectures, Faraday Discuss. 128 (2005) 179–192.

[4]   B.D. Olsen, R.A. Segalman, Self-assembly of rod-coil block copolymers, Mater. Sci. Eng. R Reports. 62 (2008) 37–66.

[5]   C.-J. Huang, F.-C. Chang, Polypeptide diblock copolymers: syntheses and properties of poly(N-isopropylacrylamide)-*b*-polylysine, Macromolecules 41 (2008) 7041–7052.

[6]   S. Caillol, S. Lecommandoux, A.-F. Mingotaud, M. Schappacher, A. Soum, N. Bryson, R. Meyrueix, Synthesis and self-assembly properties of peptide-polylactide block copolymers, Macromolecules 36 (2003) 1118–1124.

[7]   F. Chécot, A. Brûlet, J. Oberdisse, Y. Gnanou, O. Mondain-Monval, S. Lecommandoux, Structure of polypeptide-based diblock copolymers in solution: stimuli-responsive vesicles and micelles, Langmuir 21 (2005) 4308–4315.

[8]   J.J. Cornelissen, Helical superstructures from charged poly(styrene)-poly(isocyanodipeptide) block copolymers, Science 280 (1998) 1427–1430.

[9]   S. Hehir, N.R. Cameron, Recent advances in drug delivery systems based on polypeptides prepared from *N*-carboxyanhydrides, Polym. Int. 63 (2014) 943–954.

[10]   A. Shah, M.S. Malik, G.S. Khan, E. Nosheen, F.J. Iftikhar, F.A. Khan, S.S. Shukla, M.S. Akhter, H.B. Kraatz, T.M. Aminabhavi, Stimuli-responsive peptide-based biomaterials as drug delivery systems, Chem. Eng. J. 353 (2018) 559–583.

[11]   K. Bauri, M. Nandi, P. De, Amino acid-derived stimuli-responsive polymers and

their applications, Polym. Chem. 9 (2018) 1257–1287.

[12]   M. Gotsche, Amino-termined poly(L-lactide)s as initiators for the polymerization of *N*-carboxyanhydrides: synthesis of poly(L-lactide)-*block*-poly(α-amino acid)s, Macromol. Chem. Phys. 196 (1995) 3891–3903.

[13]   H.R. Kricheldorf, K. Hauser, Polylactones. 55. A-B-A triblock copolymers of various polypeptides. Syntheses involving 4-aminobezoyl-terminated poly(ε-caprolactone) as B block, Biomacromolecules 2 (2001) 1110–1115.

[14]   Y.F. Fan, G. Chen, J. Tanaka, T. Tateishi, L-Phe end-capped poly(L-lactide) as macroinitiator for the synthesis of poly(L-lactide)-*b*-poly(L-lysine) block copolymer, Biomacromolecules 6 (2005) 3051–3056.

[15]   Y. Li, Q. Li, F. Li, H. Zhang, L. Jia, J. Yu, Q. Fang, A. Cao, Amphiphilic poly(L-lactide)-*b*-dendritic poly(L-lysine)s synthesized with a metal-free catalyst and new dendron initiators: chemical preparation and characterization, Biomacromolecules 7 (2006) 224–231.

[16]   M. Schappacher, A. Soum, S.M. Guillaume, Synthesis of polyester-polypeptide diblock and triblock copolymers using amino poly(ε-caprolactone) macroinitiators, Biomacromolecules 7 (2006) 1373–9.

[17]   Y. Tsukahara, K. Adachi, Telechelic polymers: preparation and application, in: S. Kobayashi, K. Mullen (Eds.), Encyclopedia of Polymeric Nanomaterials, Springer, Berlin, Heidelberg, 2014, pp. 1–8.

[18]   S. Motala-Timol, D. Jhurry, J. Zhou, A. Bhaw-luximon, G. Mohun, H. Ritter, Amphiphilic poly(L-lysine-*b*-caprolactone) block copolymers : synthesis, characterization and solution properties, Macromolecules 18 (2008) 5571–5576.

[19]   L. Simón, J.M. Goodman, The mechanism of TBD-catalyzed ring-opening polymerization of cyclic esters, J. Org. Chem. 72 (2007) 9656–9662.

[20]   M. de Geus, R. Peters, C.E. Koning, A. Heise, Insights into the initiation process of enzymatic ring-opening polymerization from monofunctional alcohols using

liquid chromatography under critical conditions, Biomacromolecules 9 (2008) 752–757.

[21] E. Tinajero-Díaz, A. Martínez-de Ilarduya, S. Muñoz-Guerra, M. V. de-Paz, E. Galbis, Metal-free catalyzed ring-opening polymerization and block copolymerization of ω-pentadecalactone using amino-ended initiators, Eur. Polym. J. 108 (2018) 380–389.

[22] J. A. Wilson, Z. Ates, R.L. Pflughaupt, A.P. Dove, A. Heise, Polymers from macrolactones: from pheromones to functional materials, Prog. Polym. Sci. 91 (2019) 29–50.

[23] X. Zhang, B. Liu, Z. Yang, C. Zhang, H. Li, X. Luo, H. Luo, D. Gao, Q. Jiang, J. Liu, Z. Jiang, Micelles of enzymatically synthesized PEG-poly(amine-*co*-ester) block copolymers as pH-responsive nanocarriers for docetaxel delivery, Colloids Surfaces B Biointerfaces. 115 (2014) 349–358.

[24] E.M. Chen, A.R. Quijano, Y.E. Seo, C. Jackson, A.D. Josowitz, S. Noorbakhsh, A. Merlettini, R.K. Sundaram, M.L. Focarete, Z. Jiang, R.S. Bindra, W.M. Saltzman, Biodegradable PEG-poly(ω-pentadecalactone-*co*-*p*-dioxanone) nanoparticles for enhanced and sustained drug delivery to treat brain tumors, Biomaterials 178 (2018) 193–203.

[25] B. Liu, X. Zhang, Y. Chen, Z. Yao, Z. Yang, D. Gao, Q. Jiang, J. Liu, Z. Jiang, Enzymatic synthesis of poly(ω-pentadecalactone-*co*-butylene-*co*-3,3′-dithiodipropionate) copolyesters and self-assembly of the PEGylated copolymer micelles as redox-responsive nanocarriers for doxorubicin delivery, Polym. Chem. 6 (2015) 1997–2010.

[26] Y. Huang, Z. Tang, X. Zhang, H. Yu, H. Sun, X. Pang, X. Chen, pH-triggered charge-reversal polypeptide nanoparticles for cisplatin delivery: Preparation and in vitro evaluation, Biomacromolecules 14 (2013) 2023–2032.

[27] X. Guan, Y. Li, Z. Jiao, L. Lin, J. Chen, Z. Guo, H. Tian, X. Chen, Codelivery of

antitumor drug and gene by a ph-sensitive charge-conversion system, ACS Appl. Mater. Interfaces. 7 (2015) 3207–3215.

[28] J. Liu, Z. Jiang, S. Zhang, W.M. Saltzman, Poly(ω-pentadecalactone-*co*-butylene-*co*-succinate) nanoparticles as biodegradable carriers for camptothecin delivery, Biomaterials 30 (2009) 5707–5719.

[29] G.J.M. Habraken, M. Peeters, C.H.J.T. Dietz, C.E. Koning, A. Heise, How controlled and versatile is *N*-carboxyanhydride (NCA) polymerization at 0 ºC? Effect of temperature on homo-, block- and graft (co)polymerization. Polym. Chem. 1 (2010) 514–524.

[30] W.H. Daly, D. Poché, The preparation of *N*-carboxyanhydrides of α-amino acids using bis(trichloromethyl)carbonate, Tetrahedron Lett. 29 (1988) 5859-5862.

[31] Ph. Degée, Ph. Dubois, R. Jerôme, Ph. Teyssie, Synthesis and characterization of biocompatible and degradable poly(ε-caprolactone-*b*-γ-benzyl-L-gluamate) diblock copolymers. J. Polym. Sci.,Part A: Polym. Chem. 31 (1993), 275-278.

[32] M.L. Focarete, M. Scandola, A. Kumar, R. Gross, Physical characterization of poly(pentadecalactone) synthesized by lipase-catalyzed ring-opening polymerization, J. Polym. Sci. Part B Polym. Phys. 39 (2001) 1721–1729.

[33] G. Rong, M. Deng, C. Deng, Z. Tang, L. Piao, X. Chen, X. Jing, Synthesis of poly(ε-caprolactone)-*b*-poly(γ-benzyl-L-glutamic acid) block copolymer using amino organic calcium catalyst, Biomacromolecules 4 (2003) 1800–1804.

[34] M. Gazzano, M.L. Focarete, M. Scandola, R. a Gross, Crystal structure of poly (ω-pentadecalactone), J. Polym. Sci. Part B Polym. Phys. 41 (2003) 1009–1013.

[35] S. Lecommandoux, M.-F. Achard, J.F. Langenwalter, H.-A. Klok, Self-assembly of rod-coil diblock oligomers based on α-helical peptides, Macromolecules 34 (2001) 9100–9111.

Chapter 6. Poly(amino acid)-grafted polymacrolactones. Synthesis, self-assembling and ionic coupling properties

Abstract

Polyglobalide (PGl) with number average polymerization degree of ~20 was prepared by enzymatic ROP and then polyfunctionalized at 60% with aminothioethylene groups. The PGl_{20}-$(NH_2)_{12}$ copolymer was used as macroinitiator for the ROP of NCAs of Bn-LGA (γ-benzyl L-glutamate) and Z-LL ($^{\varepsilon}N$-carbobenzoxy-L-lysine) protected amino acids to produce neutral polypeptide-grafted polyglobalides poly[Gl_{20}-*graft*-$(AA)_z$] with z = 5 and 12, which upon deprotection, afforded anionic and cationic copolymers, respectively. Both protected and deprotected graft copolymers were characterized in full detail by NMR, and their thermal properties were evaluated by TGA and DSC. The structure of these copolymers in the solid-state was examined by FTIR and XRD using synchrotron radiation. All grafted polyglobalides were amorphous but the polypeptide side chains were arranged in either alpha-helix or beta-sheet conformation, and reliable indications on the occurrence of supramolecular structures were frequently found. The capacity of poly[Gl_{20}-*graft*-$(AA)_z$] copolymers to self-assemble in aqueous medium was evidenced by the preparation of well-shaped spheroidal nanoparticles with a diversity of sizes depending on copolymer composition and charge. Loading and release of doxorubicin (DOX) from nanoparticles made of negatively charged poly[Gl_{20}-*graft*-$(LGA)_{12}$] as well as DNA complexation with cationic poly[Gl_{20}-*graft*-$(LL)_5$] were explored to appraise the potential of these copolymers for building drug delivery systems.

Publication derived from this work:

Supporting information to this chapter in Annex C

6.1 Introduction

In chemotherapy, polymeric nanoparticles and nanocapsules are unique systems able to carry drugs in vivo with release at a target site thereby minimizing negative side effects associated with a prolonged administration [1,2]. Polyesters in particular [3-5] and more recently poly(amino acid)s (PAA) [6-8], have been highlighted as promising vehicles for drug delivery controlled by external stimuli and mediated by polymer degradation.

Poly(amino acid)s (PAA) are attractive candidates for drug delivery because they are biocompatible, are easily available in a wide variety of chemical structures, and may adopt different regular molecular conformations depending on the environment. In addition, some amino acids are readily ionized to become either positively or negatively charged, a quality that makes them particularly suitable as stimuli-responsive materials [9-13]. PAA are commonly prepared by ROP of amino acid *N*-carboxyanhydrides (AA NCA) [14]. On the other hand, aliphatic polyesters are mostly non-functional polymers without noticeable molecular activity. They are however susceptible to enzymatic degradation at a rate that depends on their hydrophilic-hydrophobic balance. Polyesters generally display a good biocompatibility, and they may be created with a great diversity of structures by relatively easy synthetic procedures. Given the complementary properties of PAA and polyesters, their combination in the form of copolymers constitutes an attractive approach for the design of nanocarriers for controlled drug delivery.

A fair set of linear block copolymers made of polypeptide and polyester blocks has been reported to date. Block copolymer structures are usually obtained by the ROP of the AA NCA initiated from an amino-capped polyester that was previously synthesized using a suitable functionalized initiator for the ROP of the lactone [14]. In most cases the polyester is generated from medium-size lactones (up to 11 atoms) such as ε-caprolactone (CL) and L-lactide (LA), and the homopolypeptide block is derived from different common amino acids such as L-glutamic acid, L-lysine, L-alanine,

etc. [15-21]. Macrolactones (MLs), *i.e.* lactones consisting in 12 or more atoms, have recently emerged as a new family of building blocks for creating novel polymer functional materials [22]. The polyesters made of MLs have hydrophobic character comparable to paraffins and display a strong tendency to crystallize. Such features have motivated their use for the design of biodegradable nanoparticles and fibres suitable for drug dispensing applications including in several cases the loading and controlled delivery of doxorubicin (DOX) [23-26]. Despite the potential of MLs, only one example recently reported by us explored their marriage with PAA with the goal to render the copolymer properties [27]. Block copolymers of pentadecalactone and L-glutamic acid or L-lysine with predetermined block lengths and the amino acids either in the free or protected form, were synthesized by sequential ROP. These copolymers were able to self-assemble in well-shaped nanospheres with a diameter in the ~200-400 nm range and a negative zeta-potential.

Some combinations of PAA and polyester from medium size lactones for the design of amphiphilic graft copolymers have also been explored. Mostly the polyester chains were grafted onto the polypeptide backbone taking advantage of the amino acid side groups, as is the case of PLL grafted with PLA [28,29]. Recently Thornton et al. [30] combined *N*-carboxyanhydride and *O*-carboxyanhydride ROP to synthesize poly(L-serine grafted with a poly(α-hydroxy acid). These copolymers were used to form nanoparticles capable of loading and subsequent releasing DOX via acid-mediated hydrolysis. Inverse structures consisting of the polyester backbone grafted with poly(amino acid)s are less accessible due to the lack of functionalization of the common polyesters. PLLs grafted with chains of L-alanine, L-aspartic acid or L-lysine have been prepared but in all these cases a copolymer of PLA containing minor amounts of Lys had to be used in a "grafting-from" approach [31,32]. The only example of PCL grafted with poly(amino acid)s was provided by Vert et al. [33], who reported (PCL-*graft*-PLL) copolymers that were synthesized following either the "grafting-onto" or the "grafting-from" method both applied to a macropolycarbanionic PCL derivative.

Pendant functions may be readily introduced into polyesters via ROP of lactones bearing some functionality [34,35]. Globalide (Gl) (oxacyclohexadecen-2-one) is a 16-membered macrolactone that is widely used in perfumery. It is in fact a mixture of two different constitutional isomers with the double bond at the 11 or 12 position. As it is well known to happen with its saturated analogue PDL (36-37), Gl readily polymerizes enzymatically or catalytically to produce polyglobalide (PGl), an unsaturated polyester that is semicrystalline (T_m = 46 ºC) and non-cytotoxic [22,38]. The double bond present in the repeating unit of PGl has been used for thiol-ene addition reactions addressed to obtain cross-linked polymers, grafted copolymers and bioconjugates for drug loading [39-41].

In this work we have used PGl to prepare poly[(Gl-*graft*-(AA)] copolymers, specifically those made of L-glutamic acid (LGA) and L-lysine (LL) with their pendant function (carboxyl or amino) either protected or in the free form. The structure in the solid-state of these copolymers and their capability to self-assemble in nanoparticles when placed in aqueous media has been assessed. Finally, the potential of the ionic poly[Gl-*graft*-(LGA)] and poly[Gl-*graft*-(LL)] water soluble copolymers to load DOX and to condensate DNA has been explored. To our knowledge it is the first time that the synthesis, structure and properties of a polymacrolactone grafted with amino acids is reported.

6.2. Results and Discussion

6.2.1 Synthesis of polypeptide-grafted poly(globalide)s

The pathway followed in this work to synthesize the polypeptide-grafted poly(globalide)s, abbreviated as poly[Gl$_{20}$-*graft*-(AA)$_z$] where AA is γ-benzyl L-glutamate (BLG)/L-glutamic acid (LGA) or $^\varepsilon N$-carbobenzoxy L-lysine (ZLL)(L-lysine (LL), and the z subscript stands for the average number of amino acid units in the grafting polypeptide chains, is depicted in Scheme 6.1 The results of these syntheses including the

compositions and molecular weights of both intermediate and final copolymers are collected in Table 6.1

Scheme 6.1. Synthesis of poly[(Gl$_x$-*graft*-(AA)$_z$] copolymers. Only the 11-ene isomer of Gl is represented for simplicity.

Firstly the polyamine macroinitiator poly[(Gl$_8$-*co*-(GlNH$_2$)$_{12}$] was synthesized. The PGl sample used for this synthesis was obtained with an average length of 20 units (M_n ~4750 g·mol^{-1}) by enzymatic ROP of globalide. Amine polyfunctionalization of PGl was accomplished by thiol-ene reaction with 2-(Boc-amino)ethanethiol (BAET) catalyzed by

AIBN. The minimum amount of solvent necessary to enable complete reactants miscibility was used in order to maximize conversion [44]. The amount of BAET that became inserted in the PGl chain was measured by ^{1}H NMR. The relative remaining area of the signal arising from the double bond protons at around 5.4 ppm indicated that 60% of the Gl units were modified. Removal of the Boc group by treatment with TFA led to the random copolyester poly[(Gl$_8$-co-(GlNH$_2$)$_{12}$] which was then used as macroinitiator for amino acid grafting. The ^{1}H NMR spectra of initial PGl, the BAET-modified PGl and the multifunctionalized macroinitiator are shown in Figure C1 of the Annex C.

Table 6.1. Results of the synthesis of poly[Gl$_{20}$-graft-(AA)$_z$] copolymers.

Polymer[a]	Feed[c] [NH$_2$]/[NCA]	Yield (%)	M_n[d] (g·mol^{-1})	Composition[e] [Gl]/[AA]	Grafted Gl[f] (%)
PGl$_{20}$	-	97	4750	-	-
Poly[Gl$_x$-co-(TGl)$_y$][a]					
Poly[Gl$_8$-co-(BAET-Gl)$_{12}$]	-	90	6880	-	-
Poly[Gl$_8$-co-(AET-Gl)$_{12}$]	-	90	5680	-	-
Poly[Gl$_x$-graft-(AA)$_z$][b]					
Poly[Gl$_{20}$-graft-(BLG)$_5$]	1/6	80	16,850	27/73	60
Poly[Gl$_{20}$-graft-(BLG)$_{12}$]	1/15	79	35,690	12/88	60
Poly[Gl$_{20}$-graft-(ZLL)$_5$]	1/5	80	20,090	26/74	60
Poly[Gl$_{20}$-graft-(ZLL)$_{12}$]	1/12	83	40,000	13/87	60
Poly[Gl$_{20}$-graft-(LGA)$_5$]	1/6	50	12,260	27/73	60
Poly[Gl$_{20}$-graft-(LGA)$_{12}$]	1/15	60	27,350	12/88	60
Poly[Gl$_{20}$-graft-(LL)$_5$]	1/6	75	12,720	26/74	60
Poly[Gl$_{20}$-graft-(LL)$_{12}$]	1/112	75	22,450	13/87	60

[a]Subscripts refer to the number of pristine Gl (x) and modified Gl (y) units.
[b]Subscripts refer to the total number of Gl units in the polyester chain (x) and the average number of amino acids contained in the polypeptide side chains (z).
[c]Molar ratio of amine groups to AA-NCA in the feed.
[d]Number-average molecular weight determined by ^{1}H NMR.
[e]Globalide to amino acid units ratio present in the graft copolymers.
[f]Percentage of grafted Gl units in the copolymer.

L-Glutamic acid and L-lysine were selected as amino acids for the grafting due to their anionic and cationic character, respectively. The "grafting-from" procedure was accomplished by ROP of the N-carboxyanhydrides of the two protected amino acids, i.e. as γ-benzyl ester and $^\varepsilon$N-carbobenzyl benzoxy, respectively, from the amino groups

present in poly[(GI$_8$-*co*-(GINH$_2$)$_{12}$]. These reactions were performed in DMF at 0 $^\circ$C to avoid end-group termination and minimize side-reactions [44]. Subsequently, full removal of the Bn and Z protecting groups was attained by treatment with TFA/HBr. Poly[GI$_{20}$-*graft*-(LL)$_z$] copolymers were recovered as hydrobromide salts whereas poly[GI$_{20}$-*graft*-(LGA)$_z$] copolymers were converted in their sodium salts for a more convenient handling.

^{1}H and ^{13}C NMR analyses were used to follow the grafting process and determine the copolymer molecular weights, and a representative selection of the spectra recorded from the graft copolymers is provided in Figures 6.1 and 6.2 and Figure C2 in the Annex C. ^{1}H NMR signals arising from the $\underline{C}$H$_2$-OH end-groups were quantitatively compared with signals arising from internal methylenes to determine the number of GI units in PGI (~20) corresponding to a $M_n\approx$, 4750 g·mol^{-1}. The grafting reaction was evidenced by the new signals appearing on the PGI spectrum in the 4.4-4.6 ppm range that are attributable to the α-proton of the inserted poly(amino acid) segment. Moreover, the protons of the methylene directly attached to the amino group (C$\underline{H}_2$-NH) in the thioethylene spacer are downfield shifted down to 3.5 ppm due to the formation of the amide bond. Such signal (d), which appears split into two broad multiplets due to the asymmetric carbon of the amino acid residue, is shared by all copolymers and it provides evidence of the successful attachment of amino acids to the PGI main chain *via* NCA ROP. By comparing the intensity of protons "d" with the intensity of protons "α" is possible to assess the average degree of polymerization attained in the polypeptide side chains which were calculated to be around 5 and 12. Furthermore, since no signal arising from the CH$_2$-NH$_2$ was detected in the grafted copolymers it is concluded that all amino side groups in the poly[GI$_8$-*co*-(GI-AET)$_{12}$] had reacted so the grafting degree was estimated to be 60% in every case.
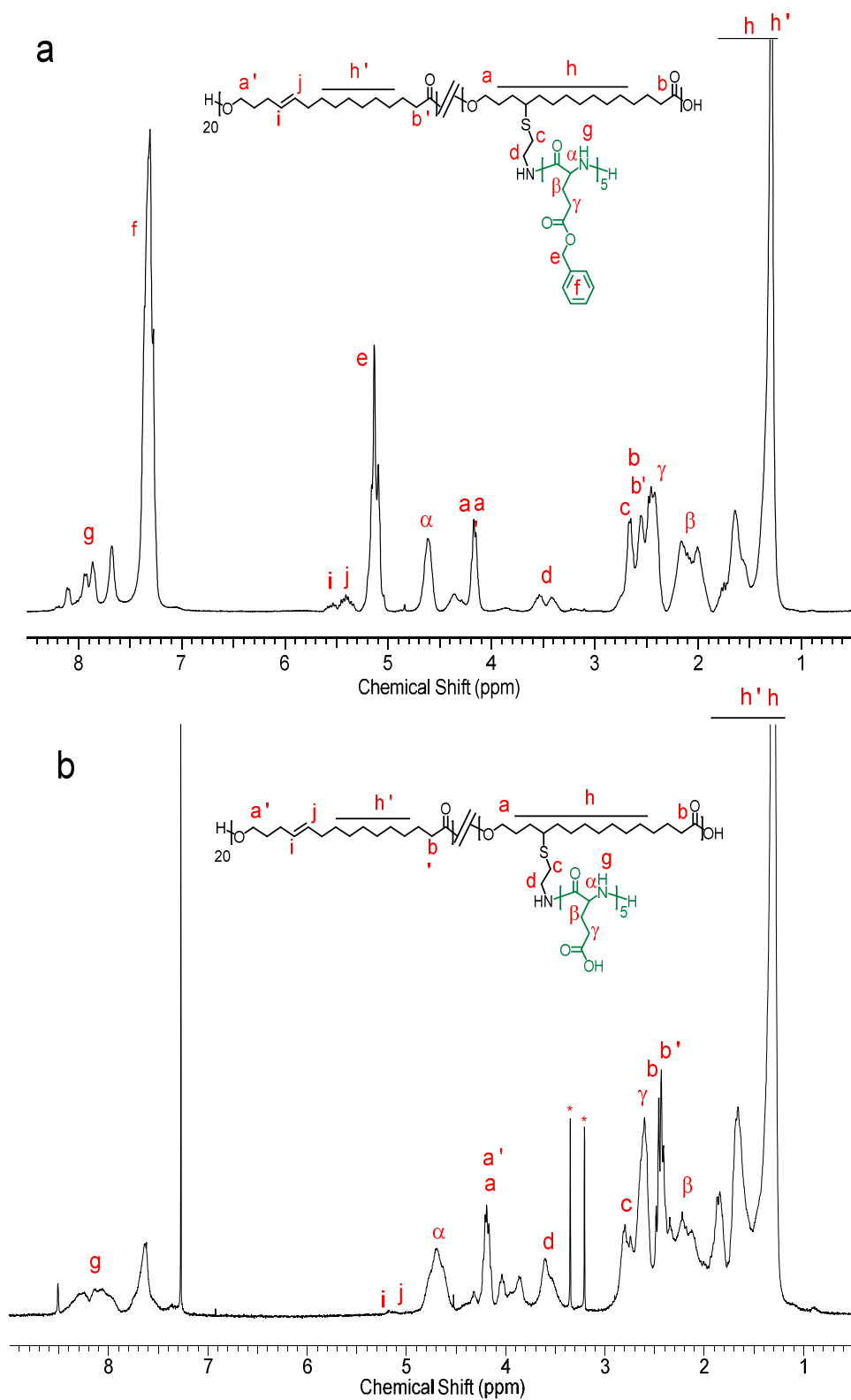
Figure 6.1. ^{1}H-NMR (CDCl$_3$/TFA) spectra of: (a) poly[Gl$_{12}$-*graft*-(BLG)$_5$] and (b) poly[Gl$_{12}$-*graft*-(LGA)$_5$] graft copolymers.
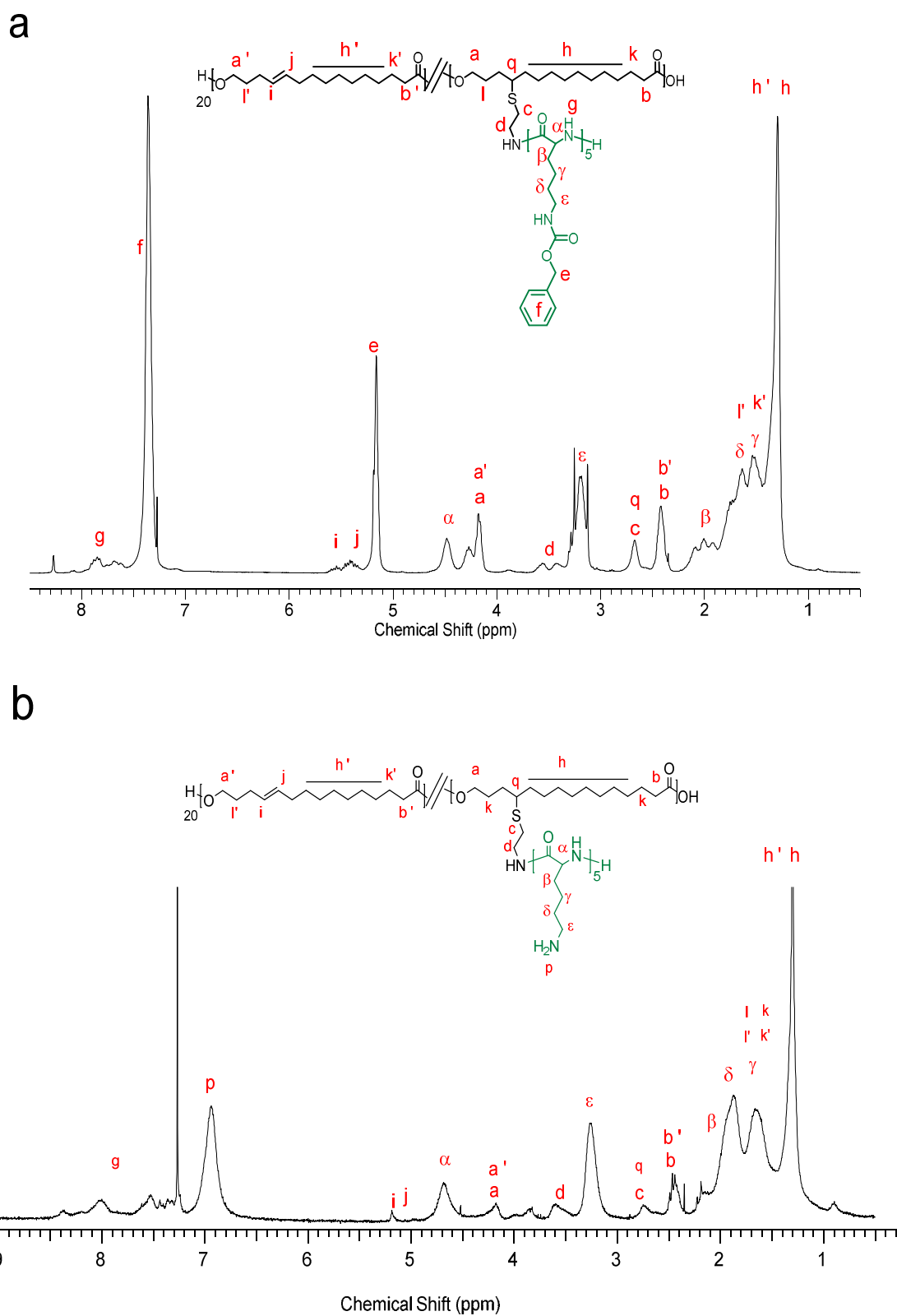
Figure 6.2. ^{1}H-NMR (CDCl$_3$/TFA) spectra of: (a) poly[Gl$_{12}$-*graft*-(ZLL)$_5$] and (b) poly[Gl$_{12}$-*graft*-(LL)$_5$] graft copolymers.

GPC of the intermediate and final copolymers showed monomodal peaks supporting the absence of homopolypeptide species in the graft copolymers (Figure C3 in the Annex C) highlighting that the PAA was indeed grafted to the PGl. A good agreement was found between the M_n values determined by ^{1}H NMR and GPC as far as the ungrafted copolymers where concerned whereas significant discrepancies appeared after grafting. Such discrepancies may be at least in part explained by the differences in hydrodynamic volume between the copolymers and the PMMA used as standard. It should also be noted that similar inconsistencies have been reported before for other polyester-polypeptide copolymers and attributed to the occurrence of specific interactions between the chromatography filler and the polypeptide moiety of the copolymer [19,45].

6.2.2 Thermal properties

The thermal properties of all copolymers were examined by TGA and DSC and the most relevant parameters are collected in Table 6.2. The TGA traces and their derivative curves are shown in Figures C4 and C5 of the Annex C. Upon heating polyglobalide starts to decompose at 370 ºC showing a sharply decay in weight at 420 ºC with less than 2% of material remaining at 600 ºC. Grafted copolymers showed a considerable decrease in thermal stability and their TGA profiles are complex indicating the occurrence of several decomposition steps as it could be expected from the presence of the polypeptide counterpart.

At clear difference with PGl, none of the graft copolymers displayed melting by DSC, as it could be largely expected from their non-regular branched architecture (Figure 6.3). The only heat exchange observed on DSC traces was a weak broad endotherm located at temperatures around 113-119 ºC for the BLG-grafted copolymers which could not be reproduced at the second heating. A peak with similar characteristics appears at 118 ºC for PBLG. This peak is reported in literature to be

due to an irreversible transition involving a rearrangement from the 7/2 to the 18/5 α-helical conformation [46].

Table 6.2. Thermal properties of poly[GI_{20}-*graft*-$(AA)_z$] copolymers.

	TGA[a]			DSC[b]							
				First heating					Second heating		
	^oT_d (ºC)	$^{max}T_d$ (ºC)	R_w (%)	T_g (ºC)	T_m (ºC)	ΔH (J·g^{-1})	T_{LC} (ºC)	ΔH (J·g^{-1})	T_g (ºC)	T_m (ºC)	ΔH (J·g^{-1})
PGI_{20}	370	420, 464	2	-	54	83	-	-	-	49	51
Poly[GI_x-*co*-$(TGI)_y$]											
Poly[GI_8-*co*-(BAET-GI)$_{12}$]	235	400, 460	3	-	-	-	-	-	-	-	-
Poly[GI_8-*co*-(AET-GI)$_{12}$]	190	270	20	-	-	-	-	-	-	-	-
Poly[GI_x-*graft*-$(AA)_z$]											
Poly[GI_{20}-*graft*-(BLG)$_5$]	370	310,400	13	21	-	-	113	0.4	21	-	-
Poly[GI_{20}-*graft*-(BLG)$_{12}$]	255	310	14	21	-	-	120	0.6	21	-	-
PBLG	280	290	16	21	-	-	118	9	21	-	-
Poly[GI_{20}-*graft*-(ZLL)$_5$]	245	410	2	-	-	-	-	-	-	-	-
Poly[GI_{20}-*graft*-(ZLL)$_{12}$]	230	410	10	-	-	-	-	-	-	-	-
PZLL	260	330	9	21	-	-	-	-	21	-	-
Poly[GI_{20}-*graft*-(LGA)$_5$]	235	360	36	-	-	-	-	-	-	-	-
Poly[GI_{20}-*graft*-(LGA)$_{12}$]	190	350	30	-	-	-	-	-	-	-	-
Poly[GI_{20}-*graft*-(LL)$_5$]	233	340, 430	16	-	-	-	-	-	-	-	-
Poly[GI_{20}-*graft*-(LL)$_{12}$]	242	330	2	-	-	-	-	-	-	-	-

[a]Onset temperature for 5% of weight loss (^oT_d), maximum rate decomposition temperature ($^{max}T_d$) and remaining weight (R_w) after heating at 600 ºC. Only $^{max}T_d$ main peaks are indicated (see Figures C4 and C5 for a graphical description.
[b]Glass transition temperature (T_g) and melting temperature and enthalpy (T_m and ΔH_m) measured from pristine samples (first heating) and from molten samples (second heating).
[c]T_{LC} is a solid state phase transition temperature caused by a conformational change taking place in the PBLG segment.

This interpretation is reasonable for explaining the peak displayed by the BLG-grafted copolymers and is supported by the fact that it decreases in both temperature and enthalpy when the length of the BLG-grafts decreases from 12 to 5. The glass transition was only observed for the BLG-grafted copolymers at 21 ºC, which is surprisingly the same value displayed by the PBLG polypeptide, and it was also present in the second melting traces. No other transition was observed either at cooling or at heating from the melt (see Figure C6 in the Annex C).
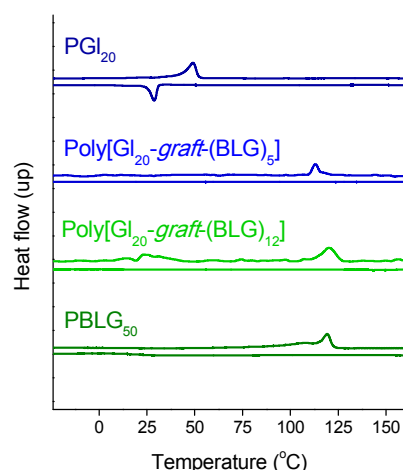
Figure 6.3. DSC registered at the first heating from poly[GI$_{20}$-*graft*-(BLG)$_z$] copolymers.

To support the interpretation made for DSC, poly[GI$_{20}$-*graft*-(AA)$_z$] copolymers bearing the amino acids protected were analyzed by FTIR, and their spectra compared with those registered from their respective homopolypeptides PBLG and PZLL. The spectral region containing both Amide I and Amide II bands characteristic of polypeptides, which are commonly used for detecting the presence of α-helix and β-sheet structures, is depicted in Figure 6.4 for both BLG- and ZLL-grafted copolymers. It is observed that whereas the helical conformation is that exclusively adopted by the two homopolypeptides (the absorption attributable to the β-sheet is very weak), the two structures become clearly visible in the copolymers with side chains containing 12 amino acids in average. The relative importance of the two forms reversed in copolymers with short side chains (with 5 amino acids in average) so that the β-sheet structure becomes preponderant in poly[GI$_{20}$-*graft*-(BLG)$_5$] and almost unique in poly[GI$_{20}$-*graft*-(ZLL)$_5$]. It can be concluded therefore that the layered structure is favored by longer amino acid sequences and also that its relative importance is higher in the ZLL-grafted copolymers. These observations are fully consistent with the well-known general structural behavior of polypeptides [47] and in good agreement with what has been reported for other copolymers containing segments made of BLG or ZLL units [48].
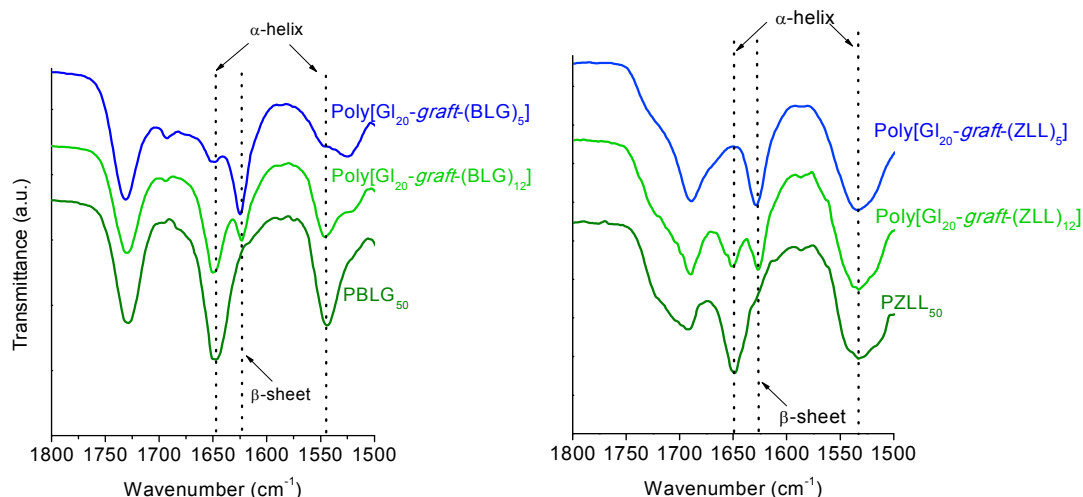
Figure 6.4. Amide I and II region of the FTIR spectra registered from poly[Gl$_{20}$-*graft*-(pAA)$_z$] copolymers and PBLG and PZLL homopolypeptides.

6.2.3 Supramolecular structure

The supramolecular organization of the poly[Gl$_{20}$-*graft*-(AA)$_z$] copolymers was examined by X-ray diffraction (XRD) at variable temperature using synchrotron radiation. The WAXS and SAXS results obtained in the analysis of poly[Gl$_{20}$-*graft*-(BLG)$_{12}$] are shown in Figure 6.5. At low temperature the discrete scattering produced by the copolymer was poor and uncertainly interpreted. The profile registered at 10 ºC in the WAXS region displayed broad peaks at approximately 1.5 and 0.5 nm whereas in the SAXS region a shoulder at 5.4 nm was the only signal observed. Since the FTIR spectra revealed the presence of both α- and β-sheet forms in this copolymer at room temperature, such signals should be associated to supramolecular structures defectively formed by the copolymer with the polypeptide branches arranged in one or other of these two conformations. Conversely, the scattering produced at 200 ºC in the medium-angle region displayed meaningful discrete information consisting of a set of Bragg reflections at 1.35, 0.77 and 0.68 nm which fit well into a 1:3$^{1/2}$:2 ratio.
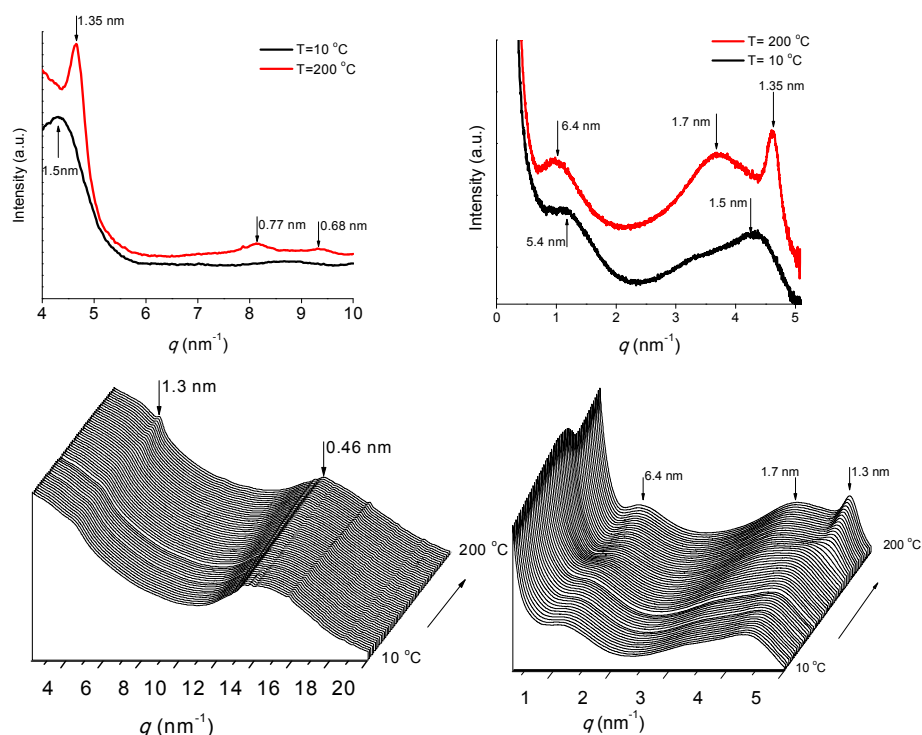
Figure 6.5. WAXS (left) and SAXS (right) profiles registered from poly[Gl$_{20}$-*graft*-(BLG$_{12}$)] at different temperatures. The profiles registered at 10 ºC and 200 ºC are compared in the top plots. The evolution of the profiles recorded at real time u heating over the 10-200 ºC range is displayed in the bottom figures.

According to literature [49] and to our own previous studies on block polyester-polypeptide copolymers as well [27], such diffraction pattern must be interpreted as arising from a columnar-hexagonal packing of (BLG)$_{12}$ α-helices of approximately 1.6 nm diameter. On the other hand, the scattering observed in the SAXS region at 10 ºC was essentially retained after heating at 200 ºC but with intensity increased and slightly displaced to lower *q* values.

The XRD analysis of the poly[Gl$_{20}$-*graft*-(ZLL)$_{12}$] copolymer provided profiles as those depicted in Figure 6.6. According to FTIR, the relative importance of the β-form to the α-helical form is higher in ZLL-grafted than in BLG-grafted copolymers and it is corroborated by XRD results. In fact, the WAXS profiles obtained for poly[Gl$_{20}$-*graft*-(ZLL)$_{12}$] at any temperature do not display any significant discrete scattering except the 0.46 nm broad peak which can be assumed to arise, at least in part, from the average interchain distance present in the β-sheet structure. In the SAXS region, two peaks at 2.4 and 4.8 nm are observed at low temperature whereas only the former remains after
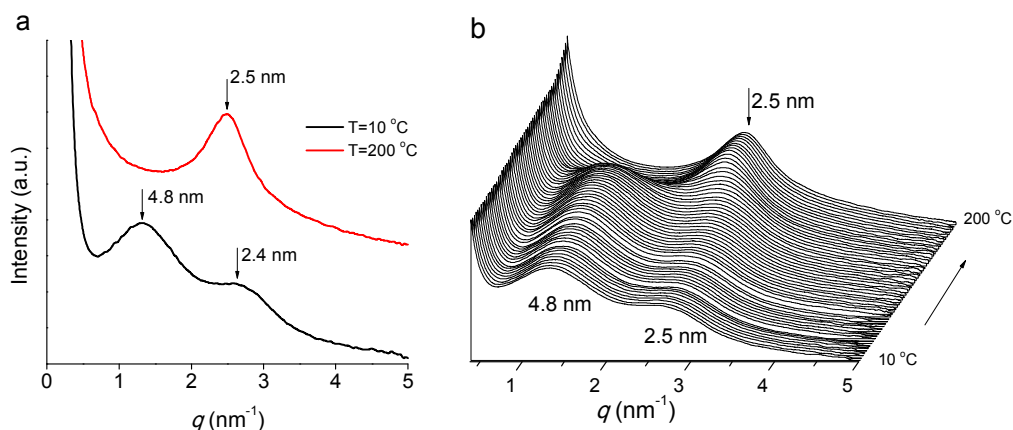
Figure 6.6. XRD profiles registered from poly[Gl$_{20}$-*graft*-(ZLL$_{12}$)] at different temperatures. The profiles registered in the SAXS region (q = 0.5-5 nm^{-1}) at 10 °C and 200 °C are compared in a). The evolution followed by the profiles when heated from 10 to 200 °C is displayed in b).

heating at 200 °C although slightly displaced up to 2.5 nm. The 2.3-2.4 nm peak could be attributed to the lamellar thickness made of ZLL-segments crystallized in β-sheet conformation. It seems therefore that at difference with poly[Gl$_{20}$-*graft*-(BLG)$_{12}$] and also with data reported by Lecommandoux et al. [48] for block copolymers made of styrene and ZLL, the α-helices adopted by PZLL in poly[Gl$_{20}$-*graft*-(ZLL)$_{12}$] are unable to form columnar liquid-crystal structures.

6.2.4 Self-assembling of poly[Gl$_{20}$-*graft*-(AA)$_z$] copolymers in aqueous medium

As it could be reasonably expected, the poly[Gl$_{20}$-*graft*-(AA)$_z$] copolymers grafted with protected amino acids are non-water soluble due to the high hydrophobic character of the aromatic groups used for protection. The situation is just the opposite when unprotected copolymers are concerned. The presence of multiple carboxylic or amino groups makes the copolymers to be water-soluble in greater or lesser extension depending on the length of the branches. In relation to the potential applications envisaged for these copolymers, their behavior in aqueous environments and in particular their capacity to generate organized aggregates, has been examined. Data relative to critical micelle concentration (*cmc*), particle diameter and dispersity (*D* and *PDI*) and zeta potential (ζ) of the aggregates spontaneously formed when poly[Gl$_{20}$-*graft*-(AA)$_z$] copolymers were placed in water are collected in Table 6.3.

The *cmc* of the water-soluble copolymers was measured by DLS and the plots used for determination are shown in Figure C7 of the Annex C. The *cmc* was found to decrease as the length of the grafted peptide branch increased, which is contrary to expectations since water solubility of these copolymers increased with larger contents in free amino acids. This is a pending issue of this work that needs further specific attention to be explained.

Table 6.3. Characterization of NPs made of poly[Gl_{20}-*graft*-$(AA)_z$] copolymers ansd polyplexes.

Polymer	*cmc* (mg·mL^{-1})	Conc (mg·mL^{-1})	*D* (nm)	*PDI*	ζ (mV)
Poly[Gl_{20}-*graft*-$(BLG)_5)$][a]	-	1.5	165	0.30	-47
Poly[Gl_{20}-*graft*-$(ZLL)_{12})$][a]	-	1.5	130	0.29	-24
Poly[Gl_{20}-*graft*-$(LGA)_5)$][a]	0.51	1.0	50-300	0.36	-12
Poly[Gl_{20}-*graft*-(LL_{12})][a]	1.62	1.0	80-400	0.31	27
Poly[Gl_{20}-*graft*-$(LGA)_5)$][b]	0.51	1.0	25/106	0.40	-11
Poly[Gl_{20}-*graft*-(LGA_{12})][b]	1.62	1.0	20/140	0.44	-36
Poly[Gl_{20}-*graft*-$(LL)_5$][b]	0.30	0.5	140	0.40	46
Poly[Gl_{20}-*graft*-(LL_{12})][b]	0.43	2.0	20/150	0.56	51
Poly[Gl_{20}-*graft*-$(LGA)_5)$] + Poly[Gl_{20}-*graft*-$(LL)_5$][c]	-	5:1.5	500	0.12	7.0

[a]Prepared by nanoprecipitation.
[b]Prepared by dissolution in deionized water.
[c]Prepared by ionotropic gelation in water with the LL-grafted copolymer solution (1.5 g·mL^{-1}) added dropwise to the LGA-grafted copolymer solution (5 mg·mL^{-1}).

The nanoprecipitation method from DMF solutions at 1.5 mg·mL^{-1} copolymer concentration was applied to prepare nanoparticles from poly[Gl_{20}-*graft*-$(BLG)_5$] and poly[Gl_{20}-*graft*-$(ZLL)_{12}$] copolymers in which the COOH and NH_2 groups are protected. As it is illustrated in Figure 6.7, almost monomodal distributions of entities with average diameters of 165 and 130 nm, respectively, and negative zeta-potential were obtained. TEM observations of these aggregates showed more or less rounded particles that are frequently collapsed most likely due to their deposition on the supporting film used for observation.

The application of the nanoprecipitation method to copolymers poly[Gl_{20}-*graft*-$(LGA)_5$] and poly[Gl_{20}-*graft*-$(LL)_{12}$] with the amino acids constitutive of the polypeptide side chains in the free form produced nanoparticles displaying a bimodal distribution of

sizes with respective average diameters of 50/80 nm and 300/400 nm. The zeta potential sign of the particles made of lysine-grafted copolymers was inverted upon deprotection, as it should be expected from the cationic charge that is created on the lysine residues.   DLS data and TEM micrographs recorded for these copolymers illustrating vividly the bimodal composition are included in Figure C8 of the Annex C.
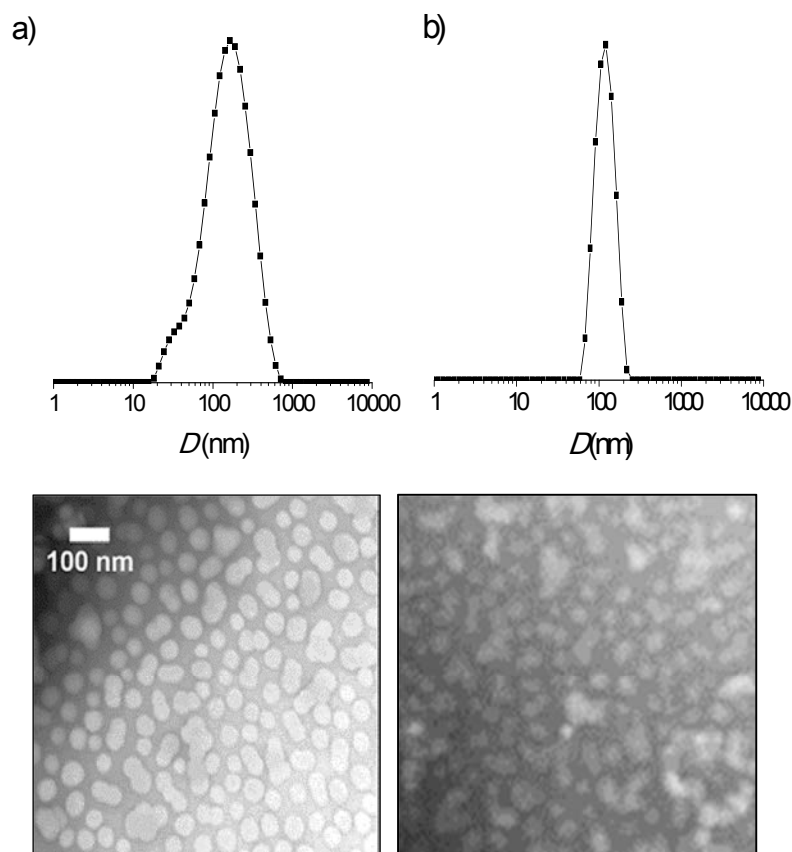
Figure 6.7. Size distribution profiles and TEM images of nanoparticles made of: a) poly[Gl$_{20}$-*graft*-(BLG)$_5$] and b) poly[Gl$_{20}$-*graft*-(ZLL)$_{12}$].

To investigate copolymer aggregation in water without mediation of organic solvents, poly[Gl$_{20}$-*graft*-(LGA)$_5$] and poly[Gl$_{20}$-*graft*-(LL)$_5$] were dissolved in water at concentrations above their respective *cmc* and their solutions were examined by DLS to measure size and zeta potential of the aggregates as a function of concentration. Size distribution traces and representative TEM images of these preparations are shown in Figure 6.8 and average diameters, dispersities and zeta-potentials are

compared in Table 6.3. To explore the stability of these NPs with time, aliquots were withdrawn every 24 h for one week, and the changes taking place in size were assessed by DLS. Both types of particles were found to be fairly stable with sizes remaining essentially constant over the whole period of experimentation.
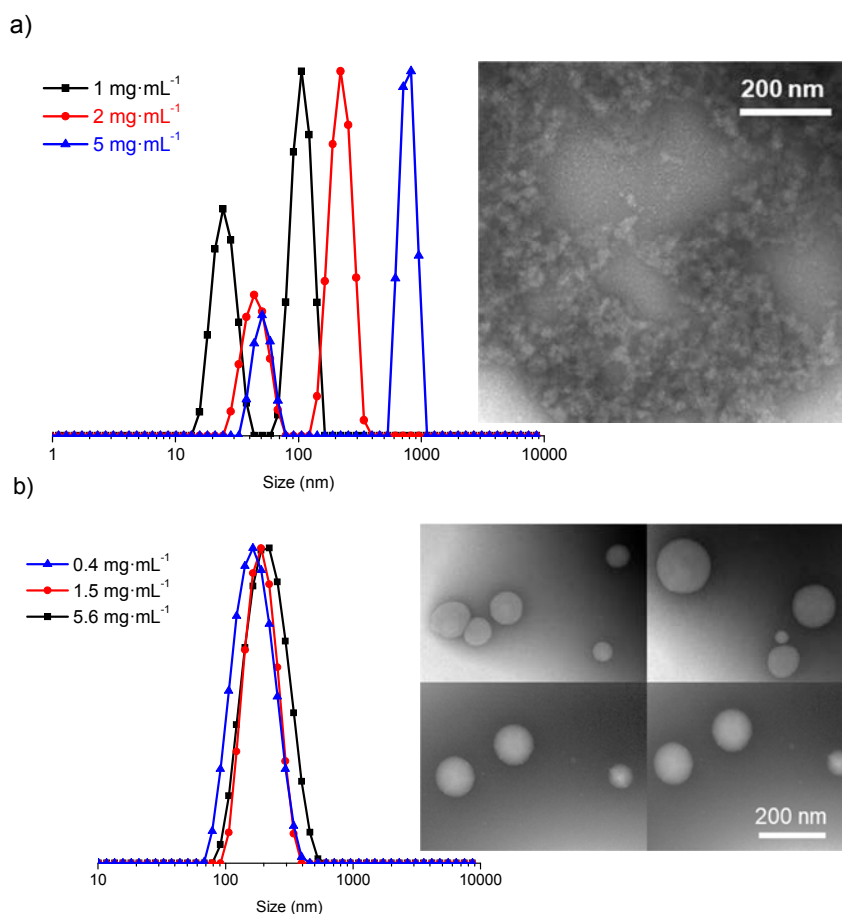
Figure 6.8. Size distribution profiles and TEM images of micelles made of (a) poly[Gl$_{20}$-*graft*-(LGA)$_5$] (a) and poly[Gl$_{20}$-*graft*-(LL)$_5$] at different copolymer concentrations. (b) TEM images taken from the lowest concentration solutions (1 mg·mL^{-1} and 0.4 mg·mL^{-1}, respectively).

The DLS profiles obtained for the different scheduled incubation times and the plot of nanoparticles average diameters as a function of time are shown in the Annex C as Figure C9.

6.2.5 Ionic coupling of deprotected copolymers: drug conjugates and polyplexes

6.2.6 DOX loading and delivery

DOX is an amphiphilic compound that may be positively charged due to the protonable amino group contained in its sugar moiety. DOX is today one of the most used drugs for cancer therapy and frequently taken as model to assess the potential of novel drug delivery systems that are designed with such purpose. To evaluate the capacity of poly[Gl$_{20}$-*graft*-(LGA)$_{12}$] to load DOX, the NPs formed from an aqueous solution of the copolymer (1.2 mg·mL^{-1}) to which a DOX solution was simultaneously added were examined by DLS and compared with those prepared from the copolymer alone. Results are graphically depicted in Figure 6.9 indicating that upon conjugation, the bimodal distribution of sizes became monomodal and increased in diameter from 20/150 nm up to 260 nm. The zeta-potential changed also to become less negative (from -34 mV to -22 mV). These results are according with the coupling mechanism that is expected to operate for the loading of positively charged DOX onto the carboxylate-free copolymer. Drug loading efficiency (DLE) and drug loading content (DLC) were measured for different copolymer/drug proportions used for preparing the loaded NPs and their values are represented in Figure 6.10. Both indexes increased steadily with the relative amount of DOX up to DOX:copolymer ratio of 0.6. At this point, 63% and 38%, were the values attained by DLE and DLC, respectively. For higher amounts of DOX, a significant decreasing was observed for DLE whereas DLC slightly changed. It can be inferred that ionic coupling attained its maximum at the 0.6 ratio. Although not all the negative charges present in poly[Gl$_{20}$-*graft*-(LGA)$_{12}$] have been neutralized at such ratio, it is reasonable to assume that a good number of carboxylate groups present in the copolymer are not accessible to DOX. This is in agreement with the fact the zeta-potential of the DOX loaded NPs is still negative.
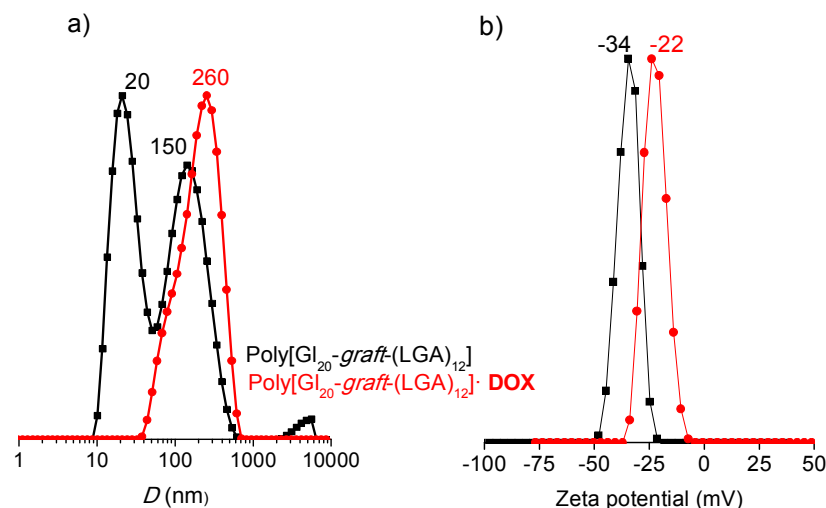
Figure 6.9. DLS (a) and zeta potential (b) profiles of poly[Gl$_{20}$-*graft*-(LGA)$_{12}$]·nanoparticles unloaded and loaded with DOX.
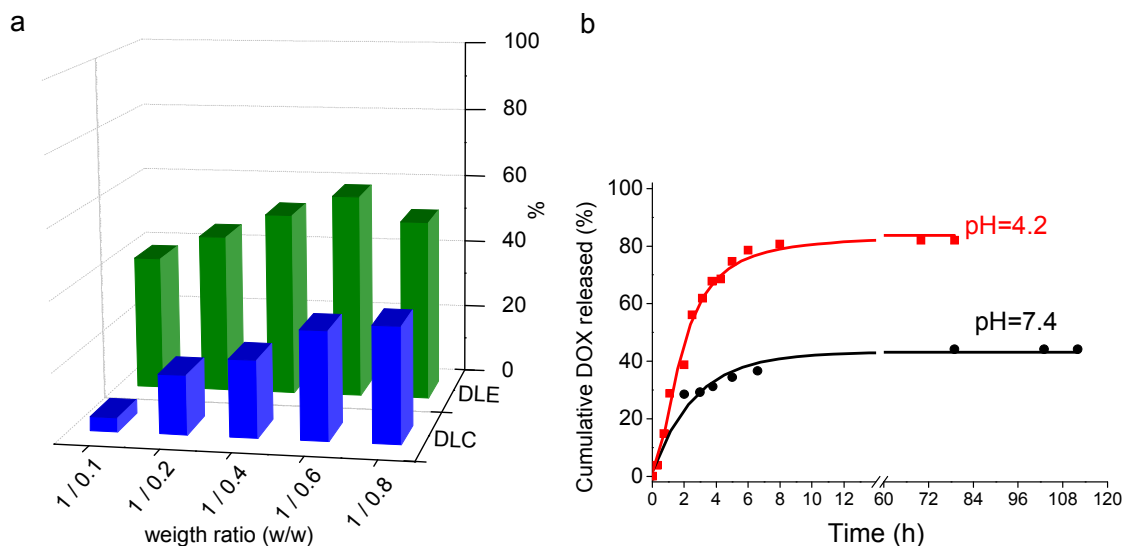
Figure 6.10. a) DLE and DLC for different poly[Gl$_{20}$-*graft*-(LGA)$_{12}$]·copolymer: DOX ratios. b) *In vitro* release profiles of poly[Gl$_{20}$-*graft*-(LGA)$_{12}$]·DOX nanoparticles at pH 7.4 and 4.2.

The *in vitro* release profiles of poly[Gl$_{20}$-*graft*-(BLG)$_{12}$]·DOX NPs that were loaded at a DOX:copolymer feed ratio of 0.6 are shown in Figure 6.10 for two different pHs (4.2 and 7.4). These pH values were selected because tumor extracellular pH values range from pH 6.5 to pH 7.2, whereas the pH within cancerous cells may be between pH 4.0 and 5.0 depending on location [50]. In both cases, DOX delivery happened within the first eight hours of incubation but the total amount of released drug and releasing rate were noticeably higher in the acid medium. These results are consistent with the ionic coupling that is assumed to occur between DOX and the copolymer. At

pH 4.2 a significant reduction in the ionization degree of LGA moieties must take place with the subsequent disruption of the electrostatic interactions.

6.2.7 Polyplex formation and DNA complexation

At the last stage of this work and as a preliminary assessment of the capability of the cationic poly[Gl$_{20}$-*graft*-(LL)$_z$] copolymers to condensate DNA, aggregates formed from mixtures of LGA- and LL-grafted copolymers were investigated. Since they are oppositely charged it is expected that they become spontaneously assembled in definite objects stabilized by electrostatic interactions. Water solutions of poly[Gl$_{20}$-*graft*-(LGA)$_5$] and poly[Gl$_{20}$-*graft*-(LL)$_5$] were mixed at room temperature by adding dropwise one to the other, and the resulting solution was examined by DLS and TEM. Results obtained when the Lys-grafted copolymer solution (1.5 g·mL^{-1}) was added dropwise to a similar volume of LGA-grafted copolymer solution (5 mg·mL^{-1}) are graphically shown in Figure 6.11 and numerically collected in Table 6.3. As it is clearly illustrated in Figure 6.11, a monomodal population of polyplex particles with an average diameter around 500 nm were formed, which is a size about four-five times larger than those displayed by the particles detected in each separate solution. The zeta-potential measured for these particles was intermediate between the values displayed by the single copolymer particles, and TEM observations showed that they are essentially round. The addition order followed for mixing was not critical since similar results were obtained when the LGA-grafted copolymer was added to the LL-grafted one with the only difference being that a somewhat larger particle size resulted in this case (Figure C10 of the Annex C). Conversely, solutions concentrations seem to be critical for the formation of the polyplex since no particles were detected when the same concentration was used for the two mixing solutions but a precipitate was obtained instead.
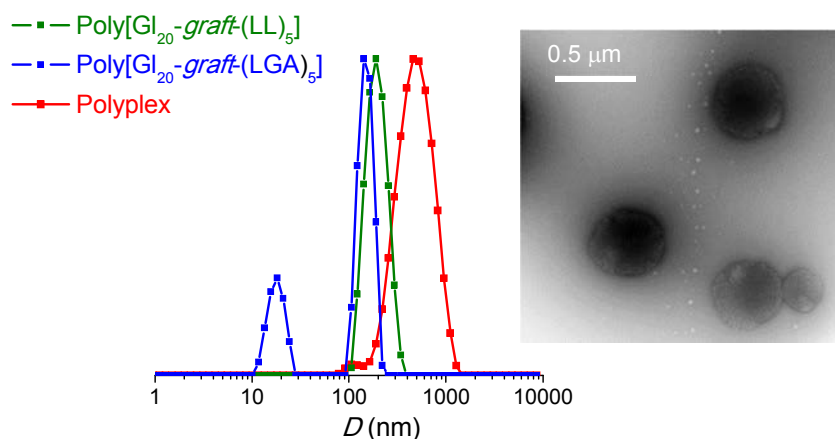
Figure 6.11. DLS profile recorded from the polyplex generated by mixing equal amounts of the LGA-grafted the LL-grafted copolymer solutions at a concentration of 5 mg·mL^{-1}. Profiles obtained from the separate solutions are included for comparison. A TEM representative picture of the polyplex particles is shown in the inserted image.

The capability of the anionic poly[Gl$_{12}$-*graft*-(LL)$_5$] copolymer for condensing DNA was assessed by examining the formation of polyplexes with salmon testes DNA (*st*DNA, 2000 bp). For this, aqueous polymer solutions of copolymer and *st*DNA) were mixed at different proportions expressed as nitrogen/phosphorous ratio (N/P). N and P values were determined by considering that the poly[Gl$_{12}$-*graft*-(LL)$_5$] mass per cationic charge (one per amino N atom) is 225 g·mol^{-1} and the DNA mass per anionic charge (one per P atom) is ~325 g mol^{-1}. The copolymer/DNA polyplexes were formed at room temperature upon dropwise addition of the copolymer solution to the DNA one followed by incubation of the mixture for 20 min at room temperature.
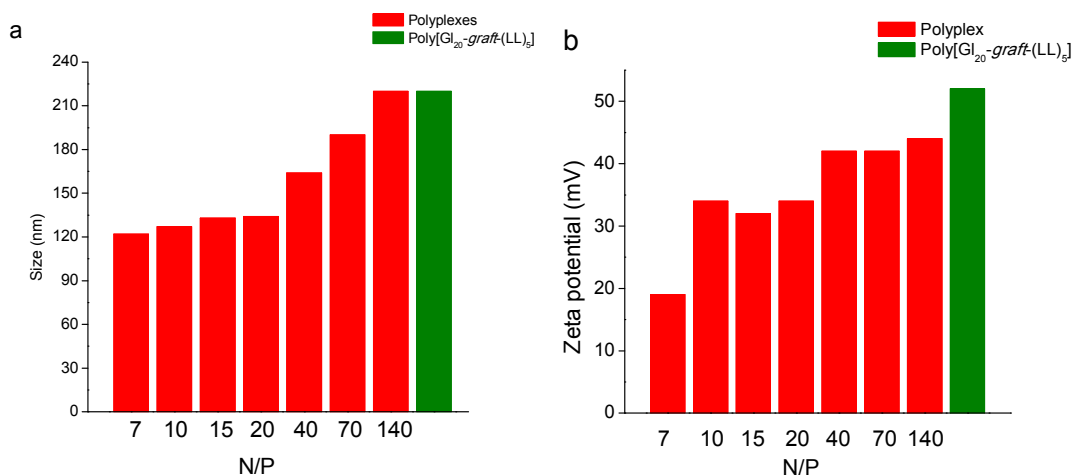
Figure 6.12. Diameter (a) and zeta potential (b) of polyplexes nano-objects formed from poly[Gl$_{12}$-*graft*-(LL)$_5$] and *st*DNA at different N/P ratios.

A wide N/P range going from 5 to 100 was tested and the mixed solutions were analyzed by DLS. Monomodal profiles registered from these mixtures are shown in Figure C11 of the Annex C. As it is represented in the bar plot of Figure 6.12, the stable nanoaggregates formed by ionic coupling of poly[Gl$_{12}$-*graft*-(LL)$_5$] with *st*DNA showed average diameters steadily decreasing from 220 nm, which is the size of the particles formed from the single copolymer, to 120 nm for a N/P ratio of 7. The zeta-potential showed a similar trend with a decrease from around 50 mV for the poly[Gl$_{12}$-*graft*-(LL)$_5$] NPs down to less than 20 mV. N/P ratios lower than 7 produced precipitates presumably consisting of unspecific NP aggregates caused by DNA interlocking. Since the length of the *st*DNA used in this study is near to 1000 nm, the drastic reductions observed in diameter and Z-potential of NPs are taken as clear evidences for the DNA condensating capacity of poly[Gl$_{12}$-*graft*-(LL)$_5$] copolymer [51].

6. 3 Conclusions

A polyglobalide (PGl) made of 20 monomeric units in average was obtained by enzymatic ROP using Novozyme 435. This PGl was made to react with 2-(Boc-amino)ethanethiol to afford a PGl copolymer containing about 60% of globalide units bearing a pendant amino group. The aminated polyglobalide was effective in initiating conveniently protected L-Glu and L-Lys NCA ROP to produce poly[Gl$_{20}$-*graft*-(AA)$_z$] copolymers with side chains made of either 5 or 12 units of each one of these two amino acids. These neutral copolymers could be readily deprotected to render polycharged anionic and cationic copolymers respectively. Both protected and deprotected poly[Gl$_{20}$-*graft*-(AA)$_z$] copolymers were amorphous but the poly(amino acid) side chains were arranged in either α-helix of β-sheet regular conformation. Powder XRD of poly[Gl$_{20}$-*graft*-(AA)$_z$] showed discrete scattering in the 2.5-6.5 nm range of spacings indicating the presence of organized supramolecular structures in these copolymers when they are in the solid state. In aqueous medium all the copolymers were arranged in nano-objects with a size and surface charge depending

on their constitution. The capacity of anionic poly[Gl$_{20}$-*graft*-(LGA)$_5$] and cationic poly[Gl$_{20}$-*graft*-(LL)$_5$] nanoparticles for loading and releasing DOX and condensing DNA, respectively, was assessed in vitro essays. DLE and DLC values found for DOX were around 60% and 40%, and DNA was efficiently packed in the NPs over a wide range of cationic/anionic charges ratio.

6.4 References

[1]   A. Kumari, S.K. Yadav, S.C. Yadav, Biodegradable polymeric nanoparticles based drug delivery systems., Colloids Surf. B. Biointerfaces. 75 (2010) 1–18.

[2]   C.E. Mora-Huertas, H. Fessi, A. Elaissari, Polymer-based nanocapsules for drug delivery, Int. J. Pharm. 385 (2010) 113–142.

[3]   H. Seyednejad, A.H. Ghassemi, C.F. Van Nostrum, T. Vermonden, W.E. Hennink, Functional aliphatic polyesters for biomedical and pharmaceutical applications, J. Control. Release. 152 (2011) 168–176.

[4]   H. Seyednejad, A.H. Ghassemi, C.F. Van Nostrum, T. Vermonden, W.E. Hennink, Functional aliphatic polyesters for biomedical and pharmaceutical applications, J. Control. Release. 152 (2011) 168–176.

[5]   K.E. Washington, R.N. Kularatne, V. Karmegam, M.C. Biewer, M.C. Stefan, Recent advances in aliphatic polyesters for drug delivery applications, Wiley Interdiscip. Rev. Nanomedicine Nanobiotechnology 9 (2017).

[6]   C. He, X. Zhuang, Z. Tang, H. Tian, X. Chen, Stimuli-sensitive synthetic polypeptide-based materials for drug and gene delivery, Adv. Healthc. Mater. 1 (2012) 48–78.

[7]   K. Bauri, M. Nandi, P. De, Amino acid-derived stimuli-responsive polymers and their applications, Polym. Chem. 9 (2018) 1257–1287.

[8]   J.V. González-Aramundiz, M.V. Lozano, A. Sousa-Herves, E. Fernandez-Megia, N. Csaba, Polypeptides and polyaminoacids in drug delivery, Expert Opin. Drug Deliv. 9 (2012) 183–201.

[9]   C. Lavilla, M. Byrne, A. Heise, Block-sequence-specific polypeptides from α-amino acid *N*-carboxyanhydrides: synthesis and influence on polypeptide properties, Macromolecules 49 (2016) 2942–2947.

[10]   D.P. Walsh, R.D. Murphy, A. Panarella, R.M. Raftery, B. Cavanagh, J.C. Simpson, F.J. O'Brien, A. Heise, S.A. Cryan, Bioinspired star-shaped poly(L-lysine) polypeptides: efficient polymeric nanocarriers for the delivery of DNA to mesenchymal stem cells, Mol. Pharm. 15 (2018) 1878–1891.

[11]   M. Byrne, R. Murphy, A. Kapetanakis, J. Ramsey, S.-A. Cryan, A. Heise, Star-shaped polypeptides: synthesis and opportunities for delivery of therapeutics, Macromol. Rapid Commun. 36 (2015) 1862–1876.

[12]   B.S. McAvan, M. Khuphe, P.D. Thornton, Polymer hydrogels for glutathione-mediated protein release, Eur. Polym. J. 87 (2017) 468–477.

[13]   W. Gao, B. Xiang, T.T. Meng, F. Liu, X.R. Qi, Chemotherapeutic drug delivery to cancer cells using a combination of folate targeting and tumor microenvironment-sensitive polypeptides, Biomaterials 34 (2013) 4137–4149.

[14]   S. Hehir, N.R. Cameron, Recent advances in drug delivery systems based on polypeptides prepared from *N*-carboxyanhydrides, Polym. Int. 63 (2014) 943–954.

[15]   S. Caillol, S. Lecommandoux, A.-F. Mingotaud, M. Schappacher, A. Soum, N. Bryson, R. Meyrueix, Synthesis and self-assembly properties of peptide-polylactide block copolymers, Macromolecules 36 (2003) 1118–1124.

[16]   M. Gotsche, Amino-termined poly(L-lactide)s as initiators for the polymerization of *N*-carboxyanhydrides: synthesis of poly(L-lactide)-*block*-poly(α-amino acid)s, Macromol. Chem. Phys. 196 (1995) 3891–3903.

[17]   H.R. Kricheldorf, K. Hauser, Polylactones. 55. A-B-A triblock copolymers of various polypeptides. Syntheses involving 4-aminobezoyl-terminated poly(ε-caprolactone) as B block, Biomacromolecules 2 (2001) 1110–1115.

[18] Y.F. Fan, G. Chen, J. Tanaka, T. Tateishi, L-Phe end-capped poly(L-lactide) as macroinitiator for the synthesis of poly(L-lactide)-*b*-poly(L-lysine) block copolymer, Biomacromolecules 6 (2005) 3051–3056.

[19] M. Schappacher, A. Soum, S.M. Guillaume, Synthesis of polyester−polypeptide diblock and triblock copolymers using amino poly(ε-caprolactone) macroinitiators, Biomacromolecules 7 (2006) 1373–1379.

[20] S. Motala-Timol, D. Jhurry, J. Zhou, A. Bhaw-Luximon, G. Mohun, H. Ritter, Amphiphilic poly(L-lysine-*b*-caprolactone) block copolymers : synthesis, characterization, and solution properties, Macromolecules 41 (2008) 5571–5576.

[21] H. Arimura, Y. Ohya, T. Ouchi, The formation of biodegradable polymeric micelles from newly synthesized poly(aspartic acid)-*block*-polylactide AB-type diblock copolymers, Macromol. Rapid Commun. 25 (2004) 743–747.

[22] J.A. Wilson, Z. Ates, R.L. Pflughaupt, A.P. Dove, A. Heise, Polymers from macrolactones: from pheromones to functional materials, Prog. Polym. Sci. 91 (2019) 29-50.

[23] J. Liu, Z. Jiang, S. Zhang, C. Liu, R.A. Gross, T.R. Kyriakides, W.M. Saltzman, Biodegradation, biocompatibility, and drug delivery in poly(ω-pentadecalactone-*co-p*-dioxanone) copolyesters, Biomaterials 32 (2011) 6646–6654.

[24] J.C. Chen, J.Z. Li, J.H. Liu, L.Q. Xu, Amphiphilic poly(ethylene glycol)-*b*-poly(ethylene brassylate) copolymers: One-pot synthesis, self-assembly, and controlled drug release, Chinese Chem. Lett. 26 (2015) 1319–1321.

[25] B. Liu, X. Zhang, Y. Chen, Z. Yao, Z. Yang, D. Gao, Q. Jiang, J. Liu, Z. Jiang, Enzymatic synthesis of poly(ω-pentadecalactone-*co*-butylene-co-3,3′-dithiodipropionate) copolyesters and self-assembly of the PEGylated copolymer micelles as redox-responsive nanocarriers for doxorubicin delivery, Polym. Chem. 6 (2015) 1997–2010.

[26] L. Xu, J. Chen, B. Weng, J. Liu, J. Li, Synthesis and self-assembly of four-armed star copolymer based on poly(ethylene brassylate) hydrophobic block as potential drug carries, J. Nanoparticle Res. 18 (2016) 1-9.

[27] E. Tinajero-Díaz, A. Martínez de Ilarduya, S. Muñoz-Guerra, Synthesis and properties of diblock copolymers of ω-pentadecalactone and α-amino acids, Eur. Polym. J. 116 (2019) 169–179.

[28] F. Tasaka, H. Miyazaki, Y. Ohya, T. Ouchi, Synthesis of comb-type biodegradable polylactide through depsipeptide-lactide copolymer containing serine residues, Macromolecules 32 (1999) 6386-6389.

[29] J.H. Jeong, Y. Byun, T.G. Park, Synthesis and characterization of poly(L-lysine)-*g*-poly(D,L-lactic-*co*-glycolic acid) biodegradable micelles, J. Biomater. Sci. Polym. Ed. 14 (2003) 1–11.

[30] D.J. Price, M. Khuphe, R.P.W. Davies, J.R. McLaughlan, N. Ingram, P.D. Thornton, Poly(amino acid)-polyester graft copolymer nanoparticles for the acid-mediated release of doxorubicin, Chem. Commun. 53 (2017) 8687–8690.

[31] R. Langer, M. Poh, N. Lotan, J.S. Hrkach, P. Colombo, G. Caponetti, B. Kriwet, Microparticles of novel branched copolymers of lactic acid and amino acids: preparation and characterization, J. Pharm. Sci. 88 (2002) 136–141.

[32] J.S. Hrkach, J. Ou, N. Lotan, R. Langer, Synthesis of Poly(L-lactic acid-*co*-L-lysine) graft copolymers, Macromolecules 28 (1995) 4736-4739.

[33] B. Nottelet, A. El Ghzaoui, J. Coudane, M. Vert, Novel amphiphilic poly(ε-caprolactone)-*g*-poly(L-lysine) degradable copolymers, Biomacromolecules 8 (2007) 2594-2601.

[34] C. Jérôme, P. Lecomte, Recent advances in the synthesis of aliphatic polyesters by ring-opening polymerization, Adv. Drug Deliv. Rev. 60 (2008) 1056–1076.

[35] a) J. Wilson, S.A. Hopkins, P.M. Wright, A.P. Dove Synthesis and postpolymerization modification of one-pot ω-pentadecalactone block-like

copolymers, Biomacromolecules 16, (2015), 3191–3200; b) P. Bexis, A.W. Thomas, C.A. Bell, A.P. Dove, Synthesis of degradable poly(ε-caprolactone)-based graft copolymers via a "grafting-from" approach, Polym. Chem. 7 (2016) 7126–7134.

[36] a) K.S. Bisht, L.A. Henderson, R.A. Gross, D.L. Kaplan, G. Swift, Enzyme-catalyzed ring-opening polymerization of ω-pentadecalactone, Macromolecules 30 (2002) 2705–2711; b) A. Kumar, B. Kalra, A. Dekhterman, R.A. Gross, Efficient ring-opening polymerization and copolymerization of ε-caprolactone and ω-pentadecalactone catalyzed by candida antartica Lipase B, Macromolecules 33 (2002) 6303–6309.

[37] a) M. Bouyahyi, R. Duchateau, Metal-based catalysts for controlled ring-opening polymerization of macrolactones: high molecular weight and well-defined copolymer architectures, Macromolecules 47 (2014) 517–524; b) M.P.F. Pepels, I. Hermsen, G.J. Noordzij, R. Duchateau, Molecular structure-catalytic activity relationship in the ring-opening polymerization of (macro)lactones, Macromolecules 49 (2016) 796–806.

[38] I. Van Der Meulen, M. De Geus, H. Antheunis, R. Deumens, E.A.J. Joosten, C.E. Koning, A. Heise, Polymers from functional macrolactones as potential biomaterials: enzymatic ring opening polymerization, biodegradation, and biocompatibility, Biomacromolecules 9 (2008) 3404-3410.

[39] Z. Ates, A. Heise, Functional films from unsaturated poly(macrolactones) by thiol–ene cross-linking and functionalisation, Polym. Chem. 5 (2014) 2936.

[40] A. Heise, S.D. Kimmins, C. Kearney, T.E. da Silva, D. Olvera, S.-A. Cryan, F.C.S. de Oliveira, D.J. Kelly, M.J. Sawkins, G.P. Duffy, Direct UV-triggered thiol–ene cross-linking of electrospun polyester fibers from unsaturated poly(macrolactone)s and their drug loading by solvent swelling, Biomacromolecules 18 (2017) 4292–4298.

[41]   Z. Ates, F. Audouin, A. Harrington, B. O'Connor, A. Heise, Functional brush-decorated poly(globalide) films by ARGET-ATRP for bioconjugation, Macromol. Biosci. 14 (2014) 1600–1608.

[42]   W.H. Daly, D. Poché, The preparation of *N*-carboxyanhydrides of α-amino acids using bis(trichloromethyl)carbonate, Tetrahedron Lett. 29 (1988) 5859-5862.

[43]   G.J.M. Habraken, M. Peeters, C.H.J.T. Dietz, E. Koning, A. Heise, How controlled and versatile is *N*-carboxyanhydride (NCA) polymerization at 0 ºC? effect of temperature on homo-, block and graft (co) polymerization, Polym.Chem. (2010) 514–524.

[44]   V. Darcos, S. Antoniacomi, C. Paniagua, J. Coudane, Cationic polyesters bearing pendent amino groups prepared by thiol–ene chemistry, Polym. Chem. 3 (2012) 362–368.

[45]   Y.L. Tu, C.-C-. Wang, C.-Y. Chen, Synthesis and characterization of a poly(GMA)-*graft*-poly(Z-L-lysine) graft copolymer with a rod-like structur., J. Polym. Sci. Part A Polym. Chem. 47 (2009) 4655–4669.

[46]   J. Watanabe, I. Uematsu, Anomalous properties of poly(γ-benzyl-L-glutamate) film composed of unusual 7/2 helices, Polymer 25 (1984) 1711–1717.

[47]   J. Babin, J. Rodriguez-Hernandez, S. Lecommandoux, H.-A. Klok, M.-F. Achard, Self-assembled nanostructures from peptide–synthetic hybrid block copolymers: complex, stimuli-responsive rod–coil architectures, Faraday Discuss. 128 (2005) 179–192.

[48]   S. Lecommandoux, M. Achard, J.F. Langenwalter, H. Klok, Self-assembly of rod-coil diblock oligomers based on α-helical peptides, Macromolecules 34 (2001) 9100–9111.

[49]   P. Papadopoulos, G. Floudas, H.A. Klok, I. Schnell, T. Pakula, Self-assembly and dynamics of poly(γ-benzyl-L-glutamate) peptides, Biomacromolecules 5 (2004) 81–91.

[50] Y. Liu, W. Wang, J. Yang, C. Zhou, J. Sun, pH-Sensitive polymeric micelles triggered drug release for extracellular and intracellular drug targeting delivery, Asian J. Pharm. Sci. 8 (2013) 159–167.

[51] D. Ulkoski, C. Scholz, Impact of cationic charge density and PEGylated poly(amino acid) tercopolymer architecture on their use as gene delivery vehicles. Part 1: synthesis, self-assembly, and DNA complexation, Macromol. Biosci. 18 (2018) 1800108.

Chapter 7. pH-Responsive diblock copolymers made of ω-pentadecalactone and ionically charged α-amino acids

Abstract

Two sets of ionically charged polypentadecalactone-polypeptide diblock copolymers (PPDL$_x$-*b*-PAA$_y$, with x= 15 or 20 and y ranging from 30 to 200), one containing α-L-glutamic acid (LGA) and the other containing α-L-lysine (LL), were obtained from their respective precursors with the side groups of LGA and LL protected as $^\gamma$*O*-benzyl and $^\varepsilon$*N*-carbobenzoxy, respectively. The copolymers were semicrystalline with the polyester block crystallized in the usual pseudo-rhombic lattice and the polypeptide in the α-helix or β-sheet conformation depending on the amino acid and the length of the block. The copolymers with PAA blocks with y ≥ 80 were water-soluble and they adopted the α-helix conformation in the aqueous medium when they are in the non-ionized state. Both LGA and LL containing copolymers self-assembled in nanoparticles with a size between 150 and 180 nm in diameter. PPDL-*b*-PLGA nanoparticles were able to load DOX with an efficiency of ~70% whereas PPDL-*b*-PLL displayed a noticeable capacity for condensing DNA. In both cases hosting was based on the ionic complexation taking place between the ionized copolymer and the guest compound. Accordingly DOX release rate was found to be depending on pH.
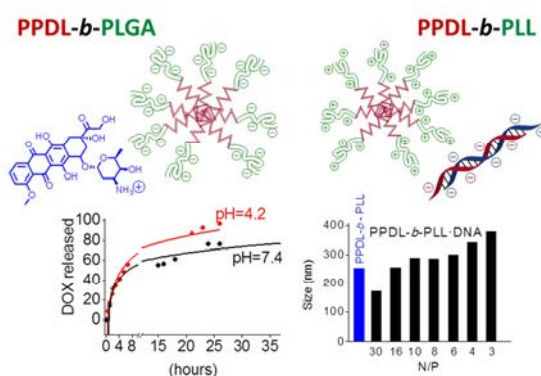
Publication derived from this work:

7.1 Introduction

Among the polymer materials that are addressed to the design of drug delivery systems, amphiphilic block copolymers are particularly appreciated [1,2]. This is so because the combination of two polymer blocks showing opposite water affinity renders biphasic systems prone to self-assemble in nano-morphologies well suited for encapsulation and transportation of drugs [3]. A distinguished class of these copolymers is that consisting of hydrophobic polyester and hydrophilic polypeptide blocks [4]. Aliphatic polyesters are the polymers of choice because their chemical versatility together with their friendly behavior in physiological environments provide a broad portfolio of materials with appealing properties in the biomedical field [5,6]. On the other hand, polypeptides are widely recognized for their good biocompatibility and biodegradability *in vivo* mediated by specific enzymes whereas they show high stability against chemical hydrolysis [7]. Additionally they are exceptional for their ability of taking up precise secondary conformations [8,9]. Nevertheless it is the pendant functionality provided by certain amino acids that makes polypeptides particularly interesting as building blocks for the synthesis of stimuli-responsive copolymers [10-12].

Many polyester-polypeptide block copolymers are readily attainable by ring opening polymerization of a wide collection of both lactones [13] and α-amino acid *N*-carboxyanhydrides [14]. Representative examples are those made of common aliphatic polyesters coming from medium-size lactones as poly(glycolic acid), polylactides, poly(ε-caprolactone) and polycarbonates [15-18]. More recently, macrolactones (rings with 11 or more atoms) have been included as polyester comonomers to generate amphiphilic polyester-polypeptide block and graft copolymers with the hydrophobic moiety displaying properties close to paraffins [19-21]. An outstanding subclass of hybrid polyester-polypeptide copolymers are those made of acid or basic amino acids, namely, aspartic and glutamic acids or lysine, arginine and histidine, which may be negatively or positively charged, respectively, depending on pH. When these

chargeable polypeptides are covalently coupled with neutral polypeptides or synthetic hydrophobic polymers, the physico-chemical behavior of the resulting copolymers, including their conformation and assembling properties, turns out to be highly sensitive to external stimuli, in particular to pH changes. A number of chargeable block copolymers entirely made of α-amino acids [11] as well as those combining polypeptide with a variety of synthetic polymer segments have been reported [22-26] including several examples containing polyester blocks [27-31]. The situation is more precarious when the polyester block is made from macrolactones with no case reported to date.

We have recently reported on polyester-polypeptide diblock copolymers (PPDL-*b*-pPAA) made of ω-pentadecalactone (PDL) and protected α-amino acids (pAA), either benzyl L-glutamate (BLG) or $^\varepsilon N$-carbobenzoxy L-lysine (ZLL) [20]. To our knowledge, this is the only example of polymacrolactone-*b*-polypeptide diblock copolymers described in the literature. PPDL-*b*-pPAAs were synthesized by ROP of their respective α-amino acid *N*-carboxyanhydrides initiated by an amino-ended polyester previously produced by enzymatically ROP of PDL. These neutral copolymers were extensively characterized and their capacity for generating nanoparticles was examined. The suitability of PPDL-*b*-pPAA to directly render ionizable copolymers by simple deprotection of their polypeptide moieties was there pointed out as an additional merit of such copolymers. Following our previous work, we wish to report in this occasion on the deprotected PPDL-*b*-PAA diblock copolymers and their potential as biomaterials for drug delivery. The paper covers their synthesis from PPDL-*b*-pPAA, their structure and thermal properties in the solid state, and their behavior in aqueous medium regarding their self-assembling properties. The capacity of the negatively and positively charged PPDL-*b*-PAA to load hydrophobic drug and to condense DNA respectively by ionic complexation has been preliminary assessed.

7.2 Results and discussion

7.2.1 Synthesis of ionic PPDL$_x$-*b*-PAA$_y$ diblock copolymers.

The PPDL$_x$-*b*-pPAA$_y$ diblock copolymers constituted by PDL and protected amino acids, either γ-benzyl L-glutamate or $^\varepsilon N$-carbobenzoxy L-lysine, were recently reported by us, and the chemical route followed for their synthesis is depicted in Scheme D1 of the Annex D. These copolymers have been used in the present work for preparing their corresponding deprotected PPDL$_x$-*b*-PAA$_y$ copolymers. Thus the removal of the benzyl ester group in PPDL$_x$-*b*-PBLG$_y$ and the benzyloxycarbonyl group in PPDL$_x$-*b*-PZLL$_y$ by treatment with HBr led to the PPDL$_x$-*b*-PLGA$_y$ and PPDL$_x$-*b*-PLL$_y$ copolymers, respectively, in which the polypeptide block bears either one free carboxylic side group or one free amino group in every repeating unit. The reactions involved in such modifications are formulated in Scheme 7.1 and the results attained are given in Table 7.2. Yields were in the 60-75% range with losses being mainly attributable to limitations in the recovery and purification of the final product. Number-average molecular-weights determined by NMR end-group analysis of deprotected copolymers were close to the values calculated by subtracting the protecting group mass from the M_n of their
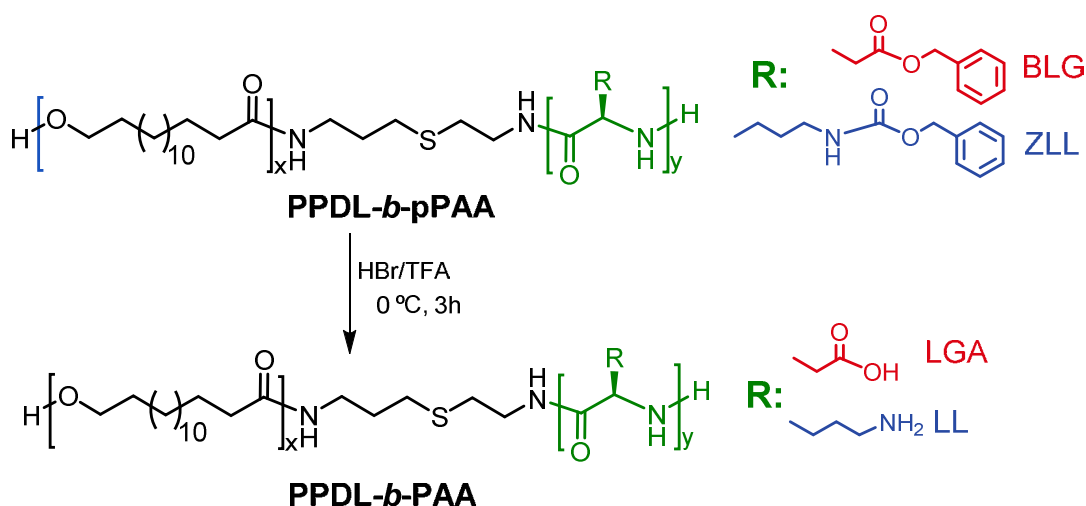
Scheme 7.1. Treatment applied for amino acid deprotection of diblock copolymers.

respective protected copolymers. Differences between M_n values obtained by the two methods were less than 5% for the case of PPDL$_x$-b-PLL$_y$ and around 12-13% for PPDL$_x$-b-PLGA$_y$ indicating that splitting of the main chain caused by the acidic treatment must be negligible in the former and of little significance in the latter. Additionally, the ^{1}H NMR analysis proved that full conversion was attained in the hydrolysis of the protected groups and also ascertained the composition of the deprotected copolymers. Representative spectra of the two series are shown in Figure 7.1 with indication of the assignments for all the observed signals. Additional examples are given in Figure D1 of the Annex D.

Table 7.2. Yield, M_n and thermal properties of deprotected PPDL$_x$-b-PAA$_y$ copolymers.

Copolymer[a]	Yield (%)	M_n[b] (g·mol^{-1})	TGA[c] $^o T_d$[a] $^o C$	$^{max}T_d$ $^o C$	R_w %	DSC[d] 1st heating T_m $^o C$	ΔH J·g^{-1}	1st cooling T_c $^o C$	ΔH J·g^{-1}	2nd heating T_m $^o C$	ΔH J·g^{-1}
PPDL$_{15}$	90	3600	285	430 470	1	90	151	75	-119	90	123
PPDL$_{15}$-b-PLGA$_{30}$	70	7500 (8450)	270	370	21	89	72	70	-23	90	29
PPDL$_{15}$-b-PLGA$_{60}$	70	10,500 (11,850)	290	325	40	86	89	68	-13	90	15
PPDL$_{15}$-b-PLGA$_{80}$	74	14,000 (15,950)	295	315	40	85	84	65	-4	92	3
PPDL$_{15}$-b-PLGA$_{180}$	60	27,400 (31,100)	300	300	70	100	110	n.o.	n.o.	n.o.	n.o.
PLGA$_{50}$	70	6550	290	300	49	74	51	-	-	-	-
PPDL$_{20}$	94	4800	285	430 470	1	90	151	75	-119	90	123
PPDL$_{20}$-b-PLL$_{30}$	72	8500 (8900)	228	470	12	91	112	72	-81	85	70
PPDL$_{20}$-b-PLL$_{70}$	70	13,200 (13,500)	272	450	10	87	65	78	-11	89	13
PPDL$_{20}$-b-PLL$_{100}$	70	17,400 (17,700)	180	300	15	85-90	35	78	-6	91	10.0
PPDL$_{20}$-b-PLL$_{190}$	65	28,800 (29,150)	300	340	18	85-90	7	72	-1	91	0.9
PLL$_{50}$	75	6500	270	325	16	85	48	-	-	-	-

[a]Subscripts have the same meaning as in Table 1.
[b]Number-average molecular weight determined by ^{1}H NMR. In parenthesis the molecular weight (rounded to ten) calculated for the composition given in Table 1.
[c]Onset temperature for 5% weight loss ($^o T_d$) and maximum rate ($^{max}T_d$) decomposition temperatures measured in the TGA analysis performed under inert atmosphere. R_w: weight (%) remaining after heating at 600 ºC.
[d]Melting (T_m and ΔH_m) and crystallization (T_c and ΔH_c) temperatures and enthalpies measured by DSC at heating (first and second run) and cooling.
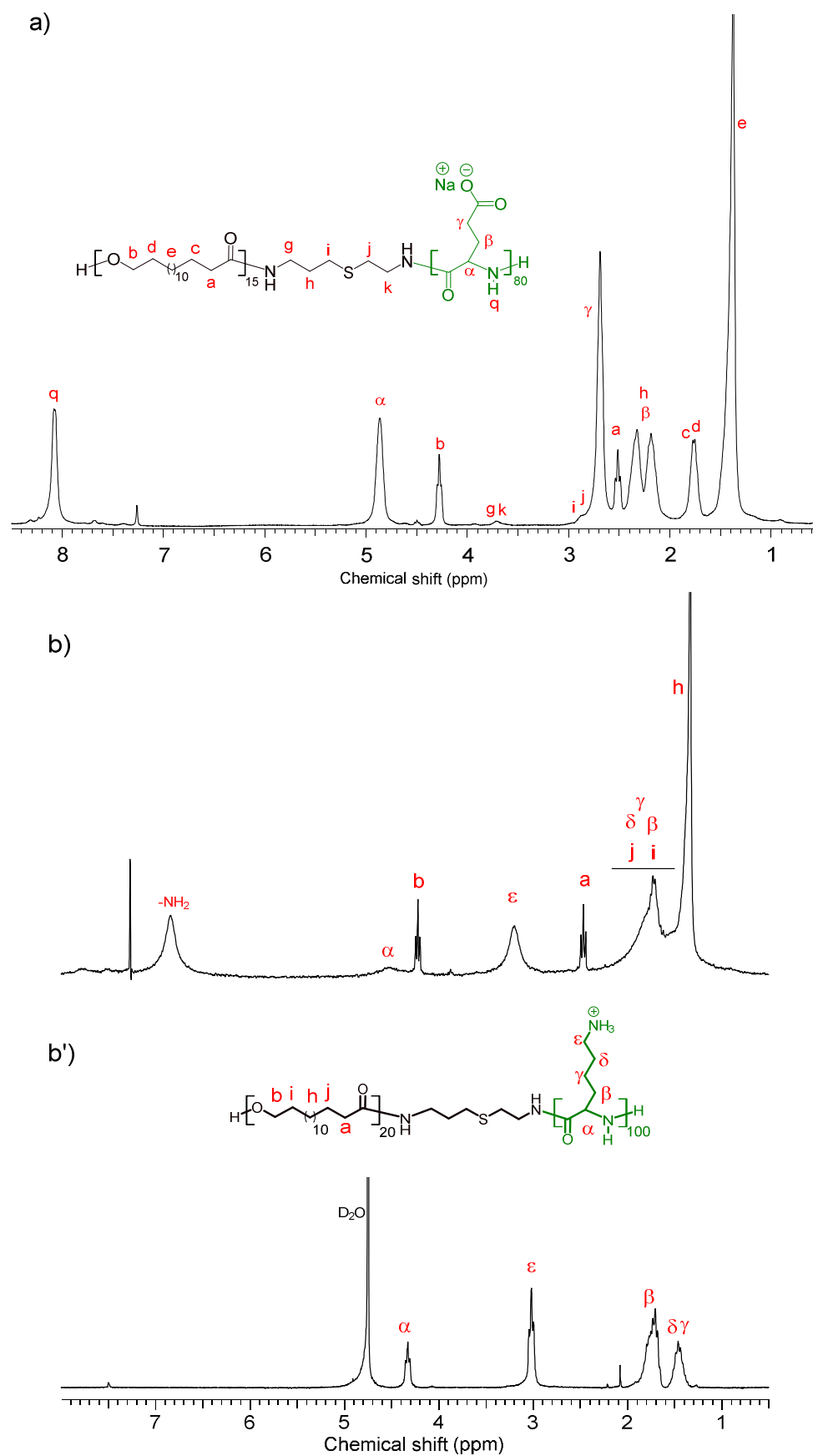
Figure 7.1. ^{1}H NMR spectra of PPDL$_{15}$-b-PLGA$_{80}$ in CDCl$_3$/TFA (a) and PPDL$_{20}$-b-PLL$_{100}$ in CDCl$_3$/TFA (b) and water (b').

7.2.2. Thermal properties of the PPDL$_x$-*b*-PAA$_y$ diblock copolymers

The TGA traces of the deprotected PPDL$_x$-*b*-PAA$_y$ diblock copolymers registered under a nitrogen atmosphere within the 20-600 ºC temperature range as well as their derivative curves are accessible in the Annex D as Figure D2. The most significant decomposition parameters of the two series provided by TGA analysis are listed in Table 7.2. Compared to the protected copolymers [20], the thermal stability in overall increased after deprotection. In fact, onset temperatures are observed well above 200 ºC and bulk decompositions take place around 300 ºC. The derivative curves showed that decomposition evolved through a rather complicate process consisting in several steps, the last one taking place at temperatures not far from 500 ºC which probably corresponds to the decomposition of the PPDL block. What is really different is the amount of weight remaining after heating at 600 ºC which appears to be much higher in the case of the deprotected copolymers with values reaching up to 70% in the case of PPDL$_{15}$-*b*-PLGA$_{180}$. No doubt such large differences must be due, at least in part, to the ionic nature of PPDL$_x$-*b*-PAA$_y$ copolymers.

The DSC heating and cooling traces recorded from the PPDLx-*b*-PLGA$_y$ and PPDL$_x$-*b*-PLL$_y$ copolymers are shown in Figure 7.2, and the thermal data provided by this analysis are gathered in Table 7.2.
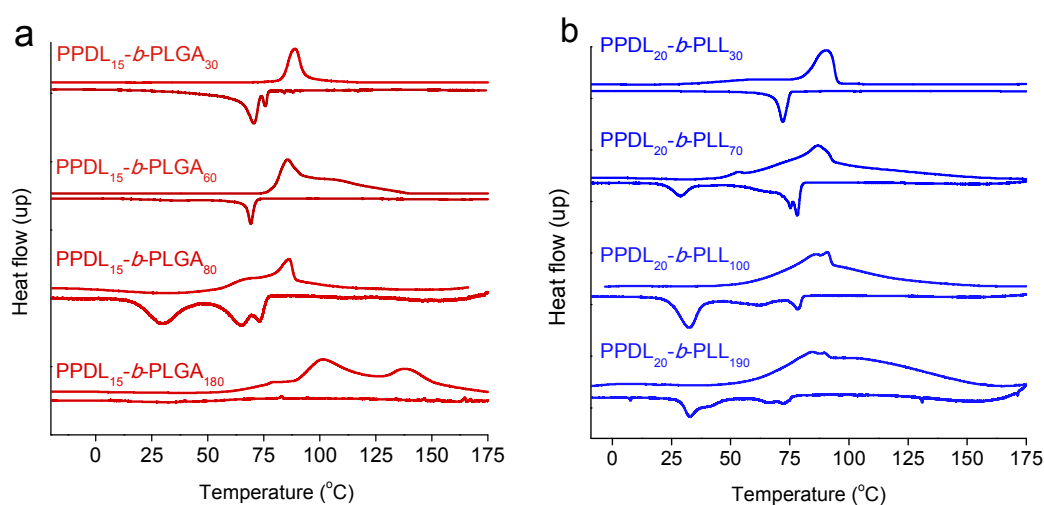
Figure 7.2. DSC traces recorded at heating from pristine samples of PPDL$_x$-*b*-PLGA$_y$ (a) and PPDL$_x$-*b*-PLL$_y$ (b) diblock copolymers.

The heating DSC traces displayed by these copolymers have in common the presence of the melting peak of the PPDL block in the 80-90 ºC temperature range followed by a more or less prominent endotherm that, according to related antecedents, it could be associated to a conformational transition taking place in the polypeptide block. The occurrence of conformational transitions in the unprotected PLGA and PLL blocks of polypeptide-based block copolymers has been reported previously by other authors [32] and is consistent with the presence of ordered conformations. One or two exothermal peaks corresponding to one or two-step crystallization of the PPDL block were observed in the cooling traces. A critical inspection of Table 7.2 reveals that T_m values recorded at the first heating fluctuates inconsistently along the two series, which is in contrast with the rather steady variation and peak sharpness that is observed for such transition when recorded at the second heating (see Figure D3 in the Annex C). These results indicate that crystallization of the PPDL must be sensitively affected by the history of the samples, a fact that is uncontrolled when they come directly from synthesis but that is essentially the same when they are crystallized from the melt.

7.2.3. Solid-state structure of the PPDL$_x$-b-PAA$_y$ copolymers

FTIR analysis of powder samples of PPDL$_x$-b-PAA$_y$ was performed to get insight the molecular arrangement that is adopted by the polypeptide block in these copolymers in the solid-sate. The spectra of the two series are compared in Figure 7.3 which shows intensity variations in the characteristic absorptions of the copolymers that are consistent with composition. Thus the broad band appearing around 3500 cm^{-1} due to the stretching vibration of O-H or/and N-H bonds increased steadily with the AA/PDL ratio whereas exactly the opposite happenned with the 2950-2800 cm^{-1} and 1750 cm^{-1} bands arising from the methylene and carbonyl ester groups present in the PPDL block. Additionally a close inspection of the absorption pattern recorded in the 1700-1500 cm^{-1} region revealed significant differences not only between the two series but

also for the different compositions within each of them. The spectra of PPDL$_{15}$-*b*-PLGA$_y$ copolymers show a band a 1645-1650 cm^{-1} with transmittance practically constant along the series. This band is commonly assigned to the Amide II band of the PLGA block in α-helix conformation although the presence of random coil arrangement cannot be discarded. On the other hand, the PPDL$_{20}$-*b*-PLL$_y$ series displays in addition to such band, a second Amide II band at ~1625 nm^{-1} whose intensity increased with y. This band is characteristic of the β-sheet form and its presence reveals that the PLL block in these copolymers must be partially arranged with chains in almost extended conformation and intermolecularly hydrogen bonded in a proportion that increases with the length of the polypeptide block.
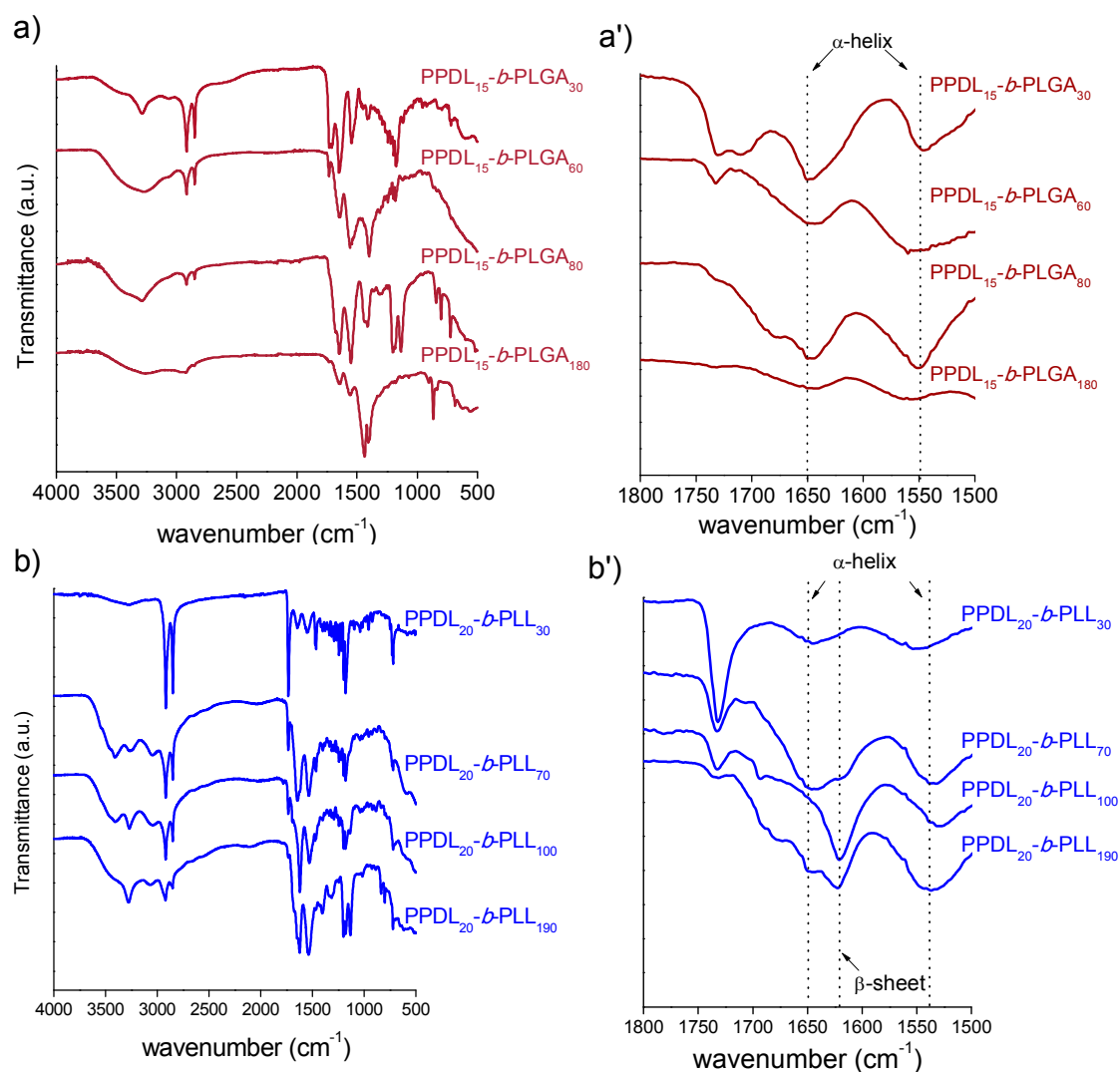
Figure 7.3. FTIR of PPDL$_x$-*b*-PAA$_y$ diblock copolymers. In a' and b' plots, the 1800-1500 cm^{-1} region has been enlarged for a better comparison of characteristic absorptions of the helical and β-sheet forms.

The structure of the PPDL-*b*-PAA copolymers in the solid-state was then examined by XRD at variable temperature using synchrotron radiation and covering both WAXS and SAXS regions. The WAXS scattering profiles recorded for PPDL$_{15}$-*b*-PLGA$_{80}$ and PPDL$_{20}$-*b*-PLL$_{100}$ at both heating and cooling in the 10-150 ºC temperature range are plotted in Figure 7.4. The reflections at 0.41 and 0.37 nm indexed as 110 and 200, which are characteristic of the pseudo-rhombic monoclinic unit cell of PPDL with approximate dimensions a = 0.75 nm, b = 0.5 nm, and c = 2.0 nm and α = 90.0°[33,34], are apparent in the profiles of the two copolymers recorded at 10 ºC. Upon heating the two reflections were initially unaltered but they disappeared abruptly when temperature reached the proximities of 90 ºC. The same behavior was displayed by the weak refection at ~0.71 nm observed in the diffraction profiles of PPDL$_{20}$-*b*-PLL$_{100}$ which could be tentatively indexed as the 101 of the PPDL crystal lattice. The two *hk*0 reflections were fully recovered upon cooling when temperature arrived to around 65 ºC and 80 ºC for the LGA and the LL containing copolymers, respectively. These results are in full agreement with those obtained by DSC confirming that the PPDL block was crystallized in all the PPDL$_x$-*b*-PAA$_y$ copolymers, and that this block is able to recrystallize from the melt at an undercooling that is significantly larger for the LGA containing copolymers. Since no sign of any other reflection is observed in the WAXS profiles recorded from PPDL$_{15}$-*b*-PLGA$_{80}$, it should be concluded that the order attained by the PLGA blocks in this copolymer must be low. Conversely, the WAXS profiles produced by PPDL$_{20}$-*b*-PLL$_{100}$ show additional reflections at 1.4 and 0.81 nm which could be attributed to the β-sheet structure in which the PLL block seems to be arranged as it was clearly revealed by FTIR. It is worth noting that the scattering due to the β-sheet form phase was attenuated at temperatures above melting of the PPDL phase so that the 0.81 reflection was the only remaining at 150 ºC. After cooling, the β-form was not be recovered whereas the PPDL crystallized so that its initial diffraction pattern became well reproduced. At difference with what was reported for the protected

PPDL-*b*-pPAA copolymers, no discrete scattering was observed in the SAXS profiles produced by the deprotected PPDL-*b*-PAA copolymers indicating that they are not assembled in any ordered nanostructure, at least below the 60 nm scale.
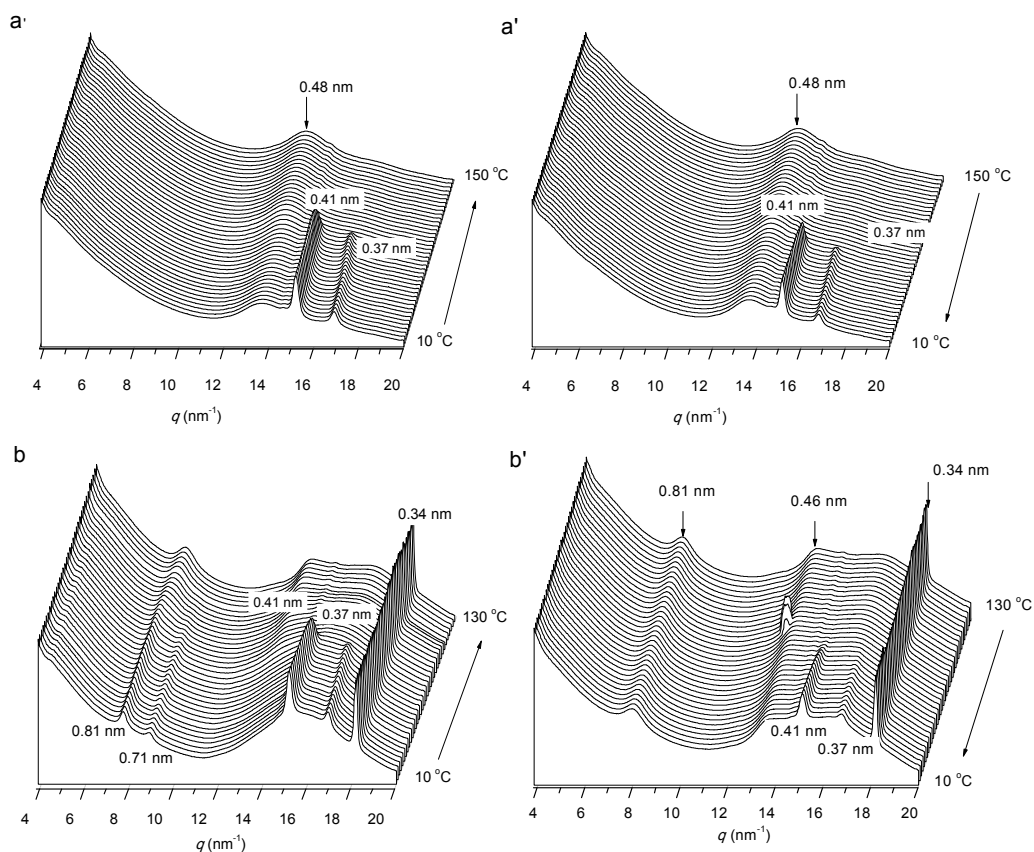
Figure 7.4. Evolution of the WAXS profiles of PPDL$_{15}$-*b*-PLGA$_{80}$ (a,a') and PPDL$_{20}$-*b*-PLL$_{100}$ (b,b') recorded at heating and cooling over the 10-150 $^{\circ}$C at a rate of 10 $^{\circ}$C·min^{-1}. The reflection at 1.4 nm that is cited in the text is hardly seen in b). For a better visualization, an enlarged region has been reproduced in Figure D4 of the Annex D. The peak observed at 0.34 nm is an artefact of unknown origin that was produced during the register of data.

7.2.4. Properties in water solution and self-assembling of PPDL-*b*-PAA.

The protected PPDL$_x$-*b*-pPAA$_y$ diblock copolymers were non-water soluble as it could be reasonably expected from the presence of the hydrophobic groups used for protection. Conversely, the solubility in water of the deprotected PPDL$_x$-*b*-PAA$_y$ copolymers is strongly dependent on both the x/y ratio and the ionic state of the polypeptide counterpart. In the non-ionized form none of these copolymers could be solubilized in water but PPDL$_{15}$-*b*-PLGA$_{80}$ and PPDL$_{15}$-*b*-PLGA$_{180}$ as well as PPDL$_{20}$-*b*-PLL$_{100}$ and PPDL$_{20}$-*b*-PLL$_{190}$ became water-soluble when they were in the sodium and hydrobromide salts, respectively. The high contrast between the strong hydrophobic

nature of the polyester block and the ionically charged polypeptide block in these copolymers make them to display a markedly amphiphilic behavior that should be reflected in their capacity to self-assemble in aqueous medium. The conformational preferences of the water-soluble $PPDL_x$-b-PAA_y copolymers when dissolved in water, their critical micelle concentrations (cmc), and the main features of the nanoparticles that they are able to form are compared in Table 7.3.

Table 7.3. Features of the water-soluble $PPDL_x$-b-PAA_y diblock copolymers in aqueous medium

Copolymer	CD		DLS			
	Secondary structure		cmc	D	PDI	ζ
	pH=2	pH=10	$(mg \cdot mL^{-1})$	(nm)		(mV)
$PPDL_{15}$-b-$PLGA_{80}$	helix	coil	0.37	146	0.26	-4.12
$PPDL_{15}$-b-$PLGA_{180}$	helix	coil	0.79	153	0.26	-45.3
$PPDL_{20}$-b-PLL_{100}	coil	helix	0.26	180	0.12	39.5
$PPDL_{20}$-b-PLL_{190}	coil	helix	0.30	176	0.24	70.8

Firstly the determination of the cmc was carried out by measuring the variation in light scattering intensity with polymer concentration in aqueous solution. As expected, the resulting plots (see Figure D5 in Annex D) clearly indicated a sharp change in the slope of the straight line at a concentration that increased with the PAA to PPDL ratio. Secondly the occurrence of regular conformations of $PPDL_x$-b-PAA_y in aqueous solution and their dependence on pH and temperature were investigated by CD spectroscopy at concentrations well below the cmc. The CD traces recorded for $PPDL_{15}$-b-$PLGA_{80}$ and $PPDL_{20}$-b-PLL_{100} under different conditions are shown in Figure 7.5. The maxima dichroic pair appearing at 212 and 222 nm with negative sign, which is the profile characteristic of α-helix, became well appreciated in these compounds at pH 2 and 10 respectively in agreement with to their non-ionized states. As it should be expected, the helical dichroism profile disappeared when pH changed from acid to basic in the former and in the opposite sense in the latter. The heating effect was zimilar in both cases with the helical structure being progressively disrupted as temperature increased.
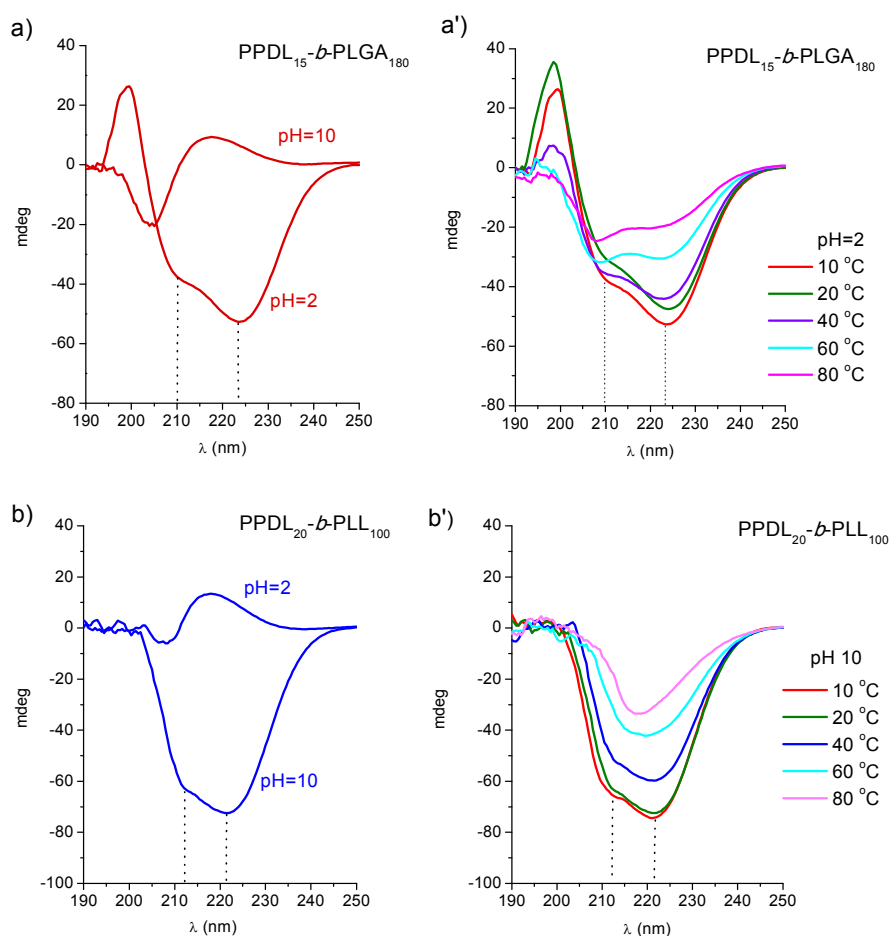
Figure 7.5. CD spectra of PPDL$_x$-*b*-PAA$_y$ diblock copolymers in aqueous solution at a concentration of 50 μg·mL^{-1}.

The DLS plots of the aqueous solutions of the PDDL$_x$-*b*-PAA$_y$ copolymers at concentrations above the *cmc* are shown in Figure 7.6 (a and b). These plots evidence the presence of aggregates of nanometric size with a diameter that is dependent on the amount of dissolved copolymer. Bimodal distributions were occasionally obtained indicating that aggregation take place in more than one specific manner. The ζ-potential displayed by these nanoparticles was positive or negative for LGA and LL containing copolymers respectively in agreement with the sign charge of the polypeptide present in each case. In both cases, the absolute value of ζ increased with the length of the polypeptide block, as expected.
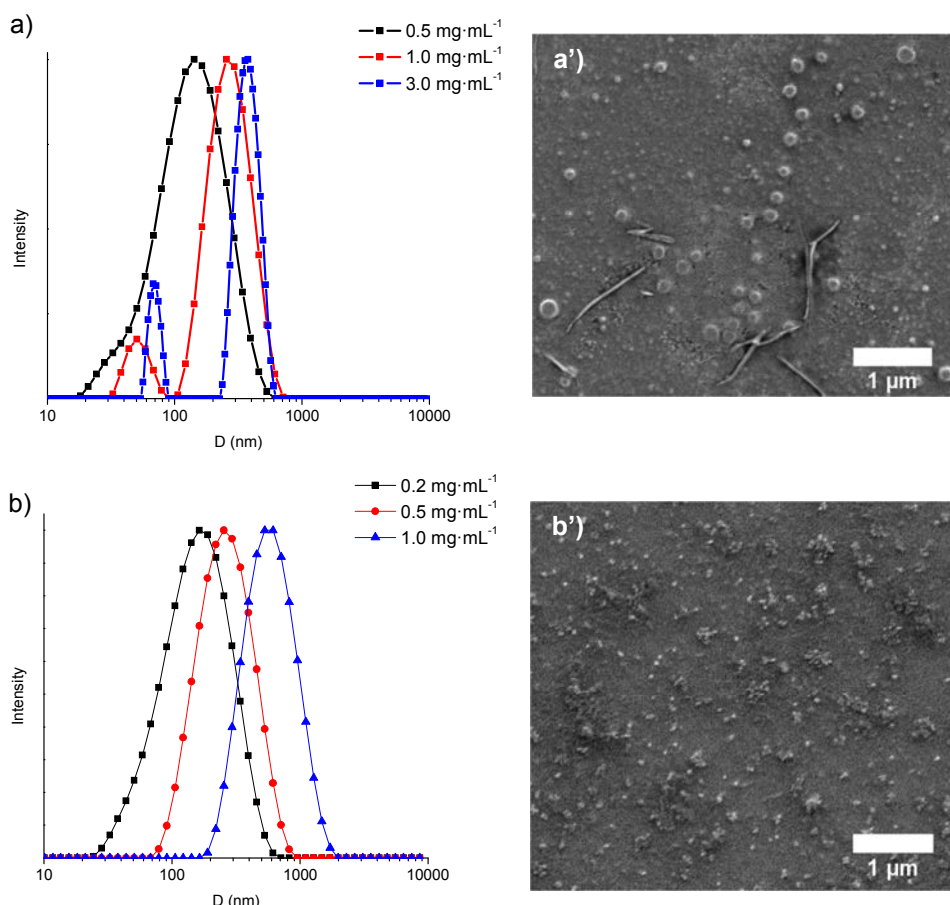
Figure 7.6. DLS plots of aqueous solutions of PPDL$_{15}$-*b*-PLGA$_{180}$ (a) and PPDL$_{20}$-*b*-PLL$_{190}$ (b) at different concentrations, and SEM images of the nanoparticles (a' and b') left upon water evaporation of the lowest concentration solutions.

The morphology of the nanoaggregates formed in aqueous solution at concentrations above *cmc* was examined by SEM. The significance of the resulting nanoparticles in terms of size is not reliable since aggregation is highly sensitive to concentration and therefore it will be enhanced during the evaporation of the drop. Nevertheless the SEM images (Figure 7.6a' and 7.6b') showed homogeneous populations of nanoparticles well separated from each other that could be clearly differentiated.

7.2.5. Preliminar evaluation of PPDL$_x$-*b*-PAA$_y$ copolymers as drug nanocarriers

7.2.6. PPDL$_x$-*b*-PLGA$_y$ copolymers: Doxorubucin loading and release

Doxorubicin (DOX), a widely-known antineoplasic compound [35], was used as model to evaluate the potential of the anionic PPDL$_x$-*b*-PLGA$_y$ copolymers to be used as drug delivery systems. Two LGA-containing copolymers differing in the length of the

PLGA block were selected for this study, namely PPDL$_{15}$-*b*-PLGA$_{80}$ and PPDL$_{15}$-*b*-PLGA$_{180}$. In these copolymers, ionic coupling between DOX and the carboxylate side groups of the LGA units should be expected to be the main mechanism responsible for entrapping.

The DLS experimental traces registered from (PPDL$_x$-*b*-PLGA$_y$)·DOX conjugates for a LGA/DOX ratio of 5:1 and 8:1 and blanks (pristine copolymer) nanoparticles are shown in Figure 7.7 and their diameters (*D*), polydispersity indexes (*PDI*) and zeta potentials (ζ) measured by this technique are compared in Table 7.4. In both cases, the monomodal traces observed for the unloaded NPs made of pristine copolymers became split when they were loaded with DOX. The two new signals corresponded to NPs sizes smaller and greater than that of the unloaded ones, and the negative zeta potential significantly decreased upon DOX loading in both cases.
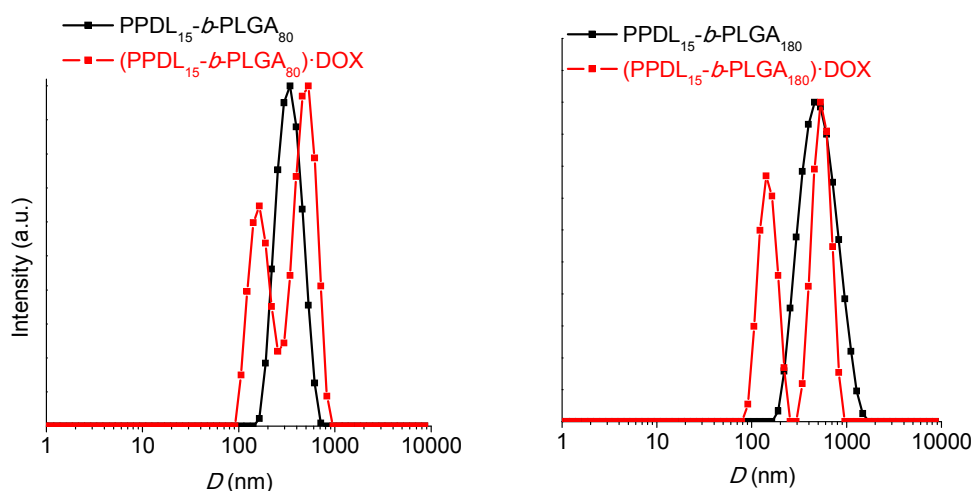
Figure 7.7. DLS profiles of DOX-charged NPs made of PPDL$_{15}$-*b*-PLGA$_y$ diblock copolymers.

Table 7.4. Characterization of DOX-loaded nanoparticles.

Copolymer or conjugate	LGA/DOX (mol/mol)	*D* (nm)	*PDI*	ζ (mV)
PPDL$_{15}$-*b*-PLGA$_{80}$	-	360	0.32	-39
(PPDL$_{15}$-*b*-PLGA$_{80}$)·DOX	5/1	160/490	0.53	-20
PPDL$_{15}$-*b*-PLGA$_{180}$	-	460	0.14	-45
(PPDL$_{15}$-*b*-PLGA$_{180}$)·DOX	8/1	140/550	0.60	-29

To assess the influence of the feed composition on coupling efficiency, a set of $(PPDL_{15}$-b-$PLGA_{80})\cdot DOX$ conjugates were prepared using different LGA/DOX ratios. Copolymer/drug mixtures prepared at the selected ratios were dialyzed against water to remove non-associated DOX and the absorption of the dialysate at 480 nm was measured to estimate the amount of DOX that remained attached to the copolymer. Additionally, the residue recovered upon lyophilization of the dialysate was examined by ^{1}H NMR using external calibration to determine the absolute amount of DOX present in the nanoparticles (an illustrative spectrum is shown in Figure D6 in the Annex D) The values obtained for DLE (Drug Loaded Efficiency) and DLC (Drug Loaded Content), as well as for the zeta-potential are graphically shown in Figure 7.8 for the different tested LGA/DOX ratios. For low values the two parameters increased with the proportion of drug used to form the conjugate but this trend vanished for ratios lower than 5/2. All DOX-loaded particles exhibited a negative surface charge around 20 mV lower than that of the unloaded which is consistent with the neutralization of part of the LGA carboxylate groups by the loaded drug molecules [36].
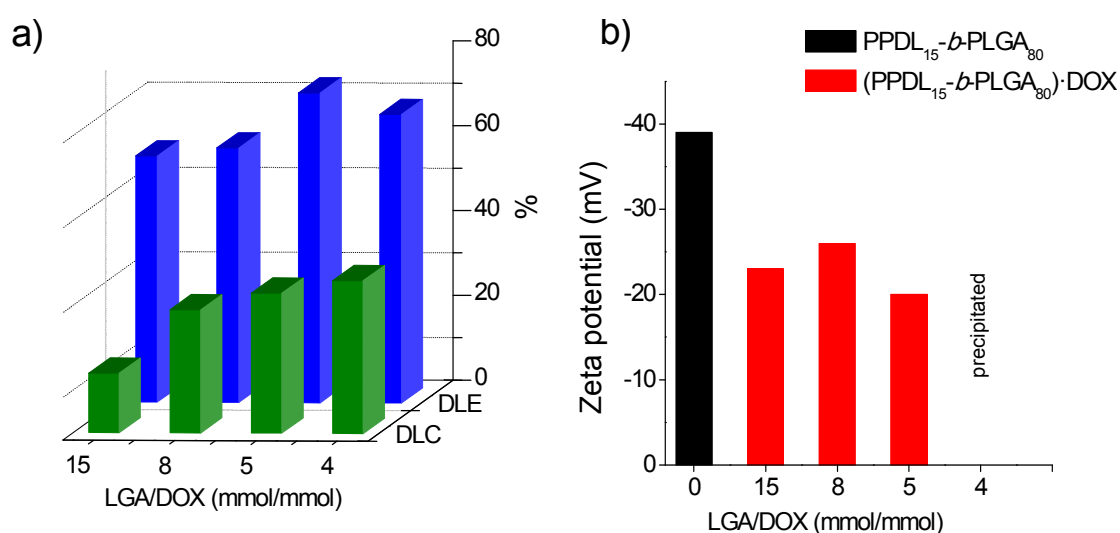
Figure 7.8. $PPDL_{15}$-b-$PLGA_{80}\cdot DOX$ conjugates obtained at different LGA/DOX ratios. a) DLE and DLC, and b) zeta potential.

Release of DOX from the $(PPDL_{15}$-b-$PLGA_y)\cdot DOX$ conjugates incubated in aqueous medium is expected to happen as a consequence of the dissociation of the

ionic complex, a process that must be pH-dependent. DOX-loaded NPs prepared from PPDL$_{15}$-b-PLGA$_{80}$ and PPDL$_{15}$-b-PLGA$_{180}$ using a feed with a LGA/DOX ratio of 5 were chosen to evaluate the release of DOX at 37 $^{\circ}$C at two different pHs, $i.e.$ in PBS, pH 7.4 and citrate-phosphate buffer, pH 4.2. The plots of the cumulative DOX release obtained over a period of one day and a half are shown in Figure 7.9. In all cases the release of the drug happened fast in the first several hours of incubation to slow down later to the point that the 100% of delivery was not reached. No significant differences in the profiles obtained for the two tested copolymers were observed indicating that the influence of the PLGA block length is not significant. On the contrary, the release at pH 4.2 took place at a noticeably high rate than at pH 7.4 as it could be reasonably expected from the enhancing effect of pH on the dissociation of the LGA·DOX ionic complex. This effect was clearly evidenced in the ^{1}H NMR spectra shown in Figure 7.10 which were registered from PPDL$_{15}$-b-PLGA$_{80}$ copolymer and its DOX conjugate at neutral and acidic aqueous media. It is noteworthy that signals from DOX were almost undetectable at neutral pH whereas they became clearly visible at pH 2 indicating that an extensive dissociation of the complex must occur in the acidic medium.
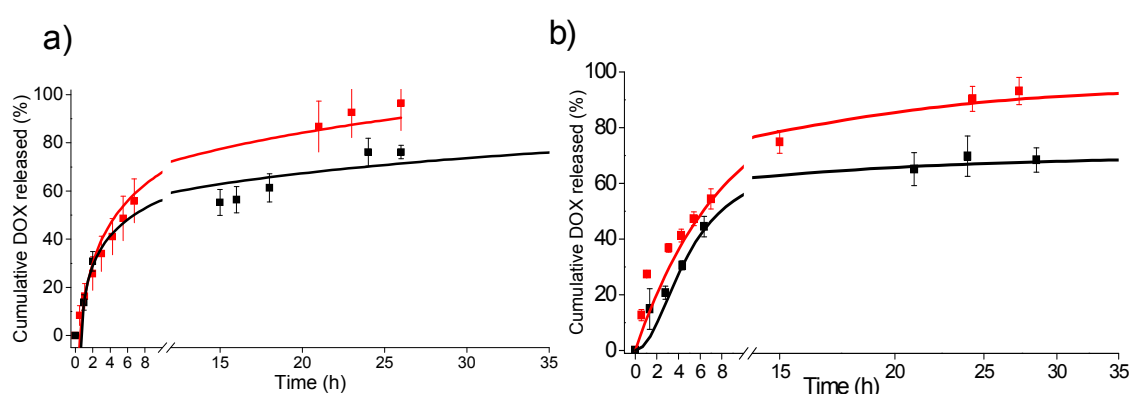
Figure 7.9. Cumulative release (%) of DOX from loaded micelles of: (a) PPDL$_{15}$-b-PLGA$_{80}$ and (b) PPDL$_{15}$-b-PLGA$_{180}$ diblock copolymers at pH 7.4 (black line) and pH 4.2 (red line). The release study was performed using the dialysis method and DOX concentration was estimated by UV absorption at 480 nm. Data are given as mean ±SD of triplicates.
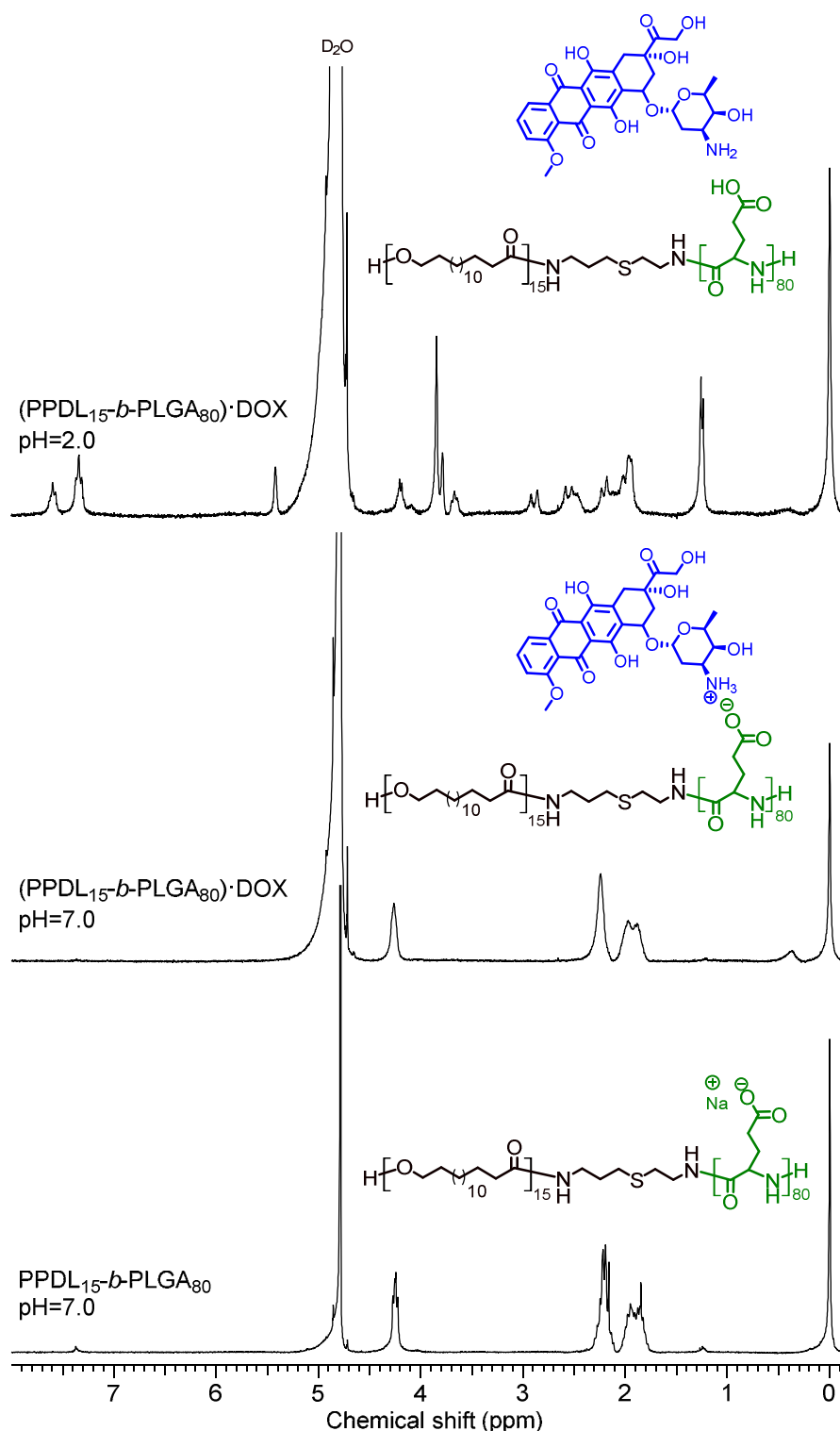
Figure 7.10. ^{1}H NMR spectra (D$_2$O) of the PPDL$_{15}$-b-PLGA$_{80}$ copolymer and (PPDL$_{15}$-b-PLGA$_{80}$)·DOX conjugate at neutral and acidic pH.

7.2.7. PPDL$_x$-b-PLL$_y$ copolymers: DNA complexation

The formation of complexes between LL-containing copolymers and DNA was examined using the PPDL$_{20}$-b-PLL$_{100}$ copolymer and salmon testes DNA (*st*DNA,

M_w~2,000 bp) in aqueous medium. The polyplexes were prepared at room temperature using deionized water by addition of the copolymer solution to that of DNA and subsequent incubation of the mixture for 20 min. A range of N to P ratios (N/P, mol/mol) going from 30 to 3 was tested. N/P values were determined by considering that the $PPDL_{20}$-b-PLL_{100} and DNA mass per N and P atom is 225 g·mol^{-1} and 325 g mol^{-1}, respectively. The polyplex solution was subjected to DLS analysis and scattering data compared to those obtained for the pristine copolymer. As it is seen in Figure 7.11, the original size of copolymer nanoparticles of ~250 nm decreased with addition of moderate amounts of DNA (N/P =30) down to ~150 nm indicating that complexation with concomitant condensation of the DNA molecule has taken place. Further addition of DNA entailed a steadily increase in particle size to reach a diameter near 400 nm for N/P = 3. This is consistent with previous observations reporting that the largest aggregates are formed for N/P values close to 1 [37]. Polyplex formation also entailed a decrease in the positive zeta-potential of the copolymer for all compositions, as it should be expected from the charge compensation that must take place upon coupling. However the variation of ζ with composition does not display a logical trend. It decreased about 10 mV for small amounts of DNA (N/P = 30 and 16) and recovered almost totally for N/P = 10. From this value onwards ζ decayed slightly but steadily for increasing content in DNA.
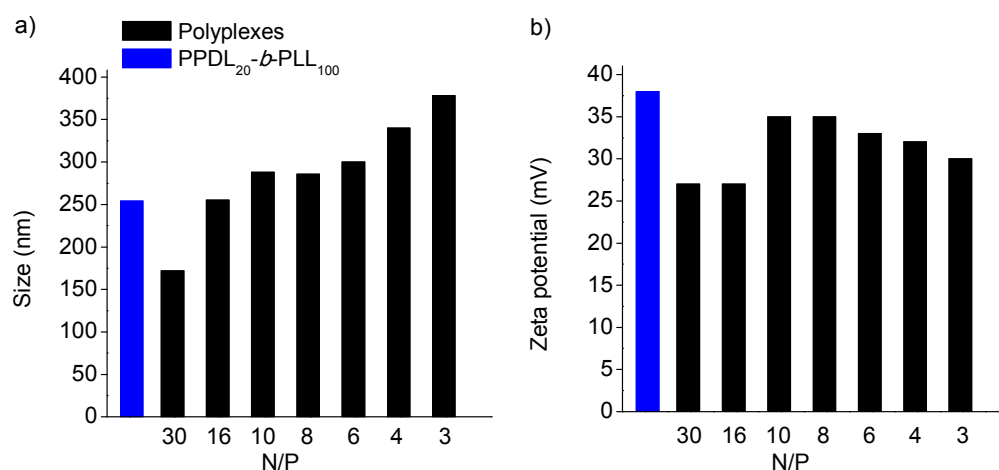
Figure 7.11. Diameter (a) and zeta potential (b) of the ($PPDL_{20}$-b-PLL_{100})·DNA polyplexes.

7.3. Conclusions

Diblock copolymers (PPDL$_x$-b-PAA$_y$), either negatively or positively charged, made of polypentadecalactone (PDL) and L-polyglutamic acid (PLGA) or L-polylysine (PLL), respectively, have been successfully prepared. Neutral copolymer precursors obtained by sequential ROP of PDL and amino acid NCA, in which LGA or LL units were duly protected, have shown to be appropriate for this synthesis. Deprotection was easily accomplished to render copolymers with the same PDL/AA composition as the parent precursors. In all PPDL$_x$-b-PAA$_y$ copolymers, the PPDL block was crystallized and the polypeptidic block was arranged in α-helix or β-sheet conformation depending on the amino acid and the length of the block. These copolymers displayed water solubility for long amino acid blocks in the ionized state and showed helix-coil transition in aqueous solution mediated by pH changes. PPDL$_x$-b-PAA$_y$ copolymers were able to self-assembled in nanoparticles with sizes between 100 and 200 nm with presumed good stability due to the tight effect provided by the polyester core. The peripheral location of the ionic block made these nanoparticles particularly suitable for anchoring charged molecules by ionic coupling mechanism. DOX was entrapped in the PLGA-based copolymer particles with a loading efficiency near 80% to attain contents of the drug up to 20% and it was released in hours at a pH-depending rate. A preliminary examination of the capacity of the PLL-based copolymers to couple DNA revealed the formation of nanometric ionic polyplexes with apparent condensation for high copolymer/biopolymer ratios.

7.4 References

[1]   M.L. Adams, A. Lavasanifar, G.S. Kwon, Amphiphilic block copolymers for drug delivery, J. Pharm. Sci. 92 (2003) 1343–1355.

[2]   J.K. Kim, S.Y. Yang, Y. Lee, Y. Kim, Functional nanomaterials based on block copolymer self-assembly, Prog. Polym. Sci. 35 (2010) 1325–1349.

[3]   Z.L. Tyrrell, Y. Shen, M. Radosz, Fabrication of micellar nanoparticles for drug

delivery through the self-assembly of block copolymers, Prog. Polym. Sci. 35 (2010) 1128–1143.

[4] K.E. Uhrich, S.M. Cannizzaro, R.S. Langer, K.M. Shakesheff, Polymeric systems for controlled drug release, Chem. Rev. 99 (1999) 3181–3198.

[5] H. Seyednejad, A.H. Ghassemi, C.F. Van Nostrum, T. Vermonden, W.E. Hennink, Functional aliphatic polyesters for biomedical and pharmaceutical applications, J. Control. Release. 152 (2011) 168–176.

[6] K.E. Washington, R.N. Kularatne, V. Karmegam, M.C. Biewer, M.C. Stefan, Recent advances in aliphatic polyesters for drug delivery applications, Wiley Interdiscip. Rev. Nanomed. Nanobiotechnol. 9 (2017) e1446.

[7] T.J. Deming, Synthetic polypeptides for biomedical applications, Prog. Polym. Sci. 32 (2007) 858–875.

[8] C. Bonduelle, Secondary structures of synthetic polypeptide polymers, Polym. Chem. 9 (2018) 1517–1529.

[9] K.E. Gebhardt, S. Ahn, G. Venkatachalam, D.A. Savin, Role of secondary structure changes on the morphology of polypeptide-based block copolymer vesicles, J. Colloid Interface Sci. 317 (2008) 70–76.

[10] C. Deng, J. Wu, R. Cheng, F. Meng, H.A. Klok, Z. Zhong, Functional polypeptide and hybrid materials: precision synthesis via α-amino acid *N*-carboxyanhydride polymerization and emerging biomedical applications, Prog. Polym. Sci. 39 (2014) 330–364.

[11] K. Bauri, M. Nandi, P. De, Amino acid-derived stimuli-responsive polymers and their applications, Polym. Chem. 9 (2018) 1257–1287.

[12] A. Carlsen, S. Lecommandoux, Current Opinion in Colloid & Interface Science Self-assembly of polypeptide-based block copolymer amphiphiles, Curr. Opin. Colloid Interface Sci. 14 (2009) 329–339.

[13] A.C. Albertsson, I.K. Varma, Recent developments in ring opening polymerization of lactones for biomedical applications, Biomacromolecules 4

(2003) 1466–1486.

[14] H.R. Kricheldorf, Polypeptides and 100 years of chemistry of α-amino acid *N*-carboxyanhydrides, Angew. Chemie - Int. Ed. 45 (2006) 5752–5784.

[15] Š. Gradišar, E. Žagar, D. Pahovnik, Hybrid block copolymers of polyesters/polycarbonates and polypeptides synthesized via one-pot sequential ring-opening polymerization, Polym. Chem. 9 (2018) 4764–4771.

[16] S. Caillol, S. Lecommandoux, A.F. Mingotaud, M. Schappacher, A. Soum, N. Bryson, R. Meyrueix, Synthesis and self-assembly properties of peptide-polylactide block copolymers, Macromolecules 36 (2003) 1118–1124.

[17] M. Gotsche, Amino-termined poly(L-lactide)s as initiators for the polymerization of *N*-carboxyanhydrides: synthesis of poly(L-lactide)-*block*-poly(α-amino acid)s, Macromol. Chem. Phys. 196 (1995) 3891–3903.

[18] M. Schappacher, A. Soum, S.M. Guillaume, Synthesis of polyester−polypeptide diblock and triblock copolymers using amino poly(ϵ-caprolactone) macroinitiators, Biomacromolecules 7 (2006) 1373–1379.

[19] J.A. Wilson, Z. Ates, R.L. Pflughaupt, A.P. Dove, A. Heise, Polymers from macrolactones: from pheromones to functional materials, Prog. Polym. Sci. 91 (2019) 29–50.

[20] E. Tinajero-Díaz, A. Martínez de Ilarduya, S. Muñoz-Guerra, Synthesis and properties of diblock copolymers of ω-pentadecalactone and α-amino acids, Eur. Polym. J. 116 (2019) 169–179.

[21] E. Tinajero-Díaz, A. Martínez-de Ilarduya, B. Cavanagh, A. Heise, S. Muñoz-Guerra, Poly(amino acid)-grafted polymacrolactones. Synthesis, self-assembling and ionic coupling properties, React. Funct. Polym. (2019) (submitted).

[22] K. Osada, R.J. Christie, K. Kataoka, Polymeric micelles from poly(ethylene glycol)-poly(amino acid) block copolymer for drug and gene delivery, J. R. Soc. Interface 6 (2009) S325-S339.

[23] F. Chécot, A. Brûlet, J. Oberdisse, Y. Gnanou, O. Mondain-Monval, S. Lecommandoux, Structure of polypeptide-based diblock copolymers in solution: stimuli-responsive vesicles and micelles, Langmuir 21 (2005) 4308–4315.

[24] S. Lecommandoux, R. Borsali, On the physics of block copolymers, Polym. Int. 55 (2006) 1161–1168.

[25] F. Chécot, J. Rodríguez-Hernández, Y. Gnanou, S. Lecommandoux, pH-Responsive micelles and vesicles nanocapsules based on polypeptide diblock copolymers, Biomol. Eng. 24 (2007) 81–85.

[26] K. Hales, D.J. Pochan, Using polyelectrolyte block copolymers to tune nanostructure assembly, Curr. Opin. Colloid Interface Sci. 11 (2006) 330–336.

[27] E.B. Lavik, J.S. Hrkach, N. Lotan, R. Nazarov, A simple synthetic route to the formation of a block copolymer of poly(lactic-*co*-glycolic acid) and polylysine for the fabrication of functionalized, degradable structures for biomedical applications, J. Biomed. Mater. Res. 58 (2001) 291–294.

[28] H. Arimura, Y. Ohya, T. Ouchi, The formation of biodegradable polymeric micelles from newly synthesized poly(aspartic acid)-*block*-polylactide AB-type diblock copolymers, Macromol. Rapid Commun. 25 (2004) 743–747.

[29] Y.F. Fan, G. Chen, J. Tanaka, T. Tateishi, L-Phe end-capped poly(L-lactide) as macroinitiator for the synthesis of poly(L-lactide)-*b*-poly(L-lysine) block copolymer, Biomacromolecules 6 (2005) 3051–3056.

[30] S. Motala-Timol, D. Jhurry, J. Zhou, A. Bhaw-Luximon, G. Mohun, H. Ritter, Amphiphilic poly(L-lysine-*b*-caprolactone) block copolymers : synthesis, characterization, and solution properties, Macromolecules 41 (2008) 5571–5576.

[31] M. Le Hellaye, N. Fortin, J. Guilloteau, A. Soum, S. Lecommandoux, S.M. Guillaume, Biodegradable polycarbonate-*b*-polypeptide and polyester-*b*-polypeptide block copolymers: synthesis and nanoparticle formation towards biomaterials, Biomacromolecules 9 (2008) 1924–1933.

[32] H. Wu, N. Reeves-McLaren, S. Jones, R.I. Ristic, J.P.A. Fairclough, A.R. West, Phase transformations of glutamic acid and its decomposition products, Cryst. Growth Des. 10 (2010) 988–994.

[33] Z. Jiang, H. Azim, R.A. Gross, M.L. Focarete, M. Scandola, Lipase-catalyzed copolymerization of ω-pentadecalactone with *p*-dioxanone and characterization of copolymer thermal and crystalline properties, Biomacromolecules 8 (2007) 2262–2269.

[34] M. Gazzano, M.L. Focarete, M. Scandola, R.A. Gross, Crystal structure of poly(ω-pentadecalactone), J. Polym. Sci. Part B Polym. Phys. 41 (2003) 1009–1013.

[35] S. Rivankar, An overview of doxorubicin formulations in cancer therapy, J. Cancer Res. Ther. 10 (2014) 853–858.

[36] M. Li, W. Song, Z. Tang, S. Lv, L. Lin, H. Sun, Q. Li, Y. Yang, H. Hong, X. Chen, Nanoscaled poly(L-glutamic acid)/doxorubicin-amphiphile complex as pH-responsive drug delivery system for effective treatment of nonsmall cell lung cancer, ACS Appl. Mater. Interfaces. 5 (2013) 1781–1792.

[37] S.C. De Smedt, J. Demeester, W.E. Hennink, Cationic polymer based gene delivery systems, Pharm. Res. 17 (2000) 113–126.

Chapter 8. Block and graft copolymers made of 16-membered macrolactones and L-alanine: A comparative study

ABSTRACT

Block and graft poly(macrolactone)-poly(α-amino acid) copolymers made of L-alanine and pentadecalactone or globalide respectively, were prepared. A sequential ROP copolymerization route consisting of two stages, the first devoted to the preparation of the amino-functionalized poly(macrolactone) and the second to the amino-initiated polymerization of Ala-NCA, was followed for the synthesis of both types of copolymers. Poly(L-alanine) segment lengths were accurately controlled by adjusting the macroitiator/Ala NCA ratio used for reaction in the second stage. Block copolymers were semicrystalline with the poly(pentadecalactone) block well crystallized in a separate phase and the poly(α-amino acid) block arranged in either the α-helical or β-sheet structure in a ratio that was depending on composition and temperature. Graft copolymers were amorphous but with the poly(α-amino acid) side chains in a more or less regular conformation. Nanoparticles with a diameter of around 300 nm and moderate positive *Z*-potential could be obtained from the block copolymers by self-assembling in water whereas graft copolymers were unable to render recognizable objects of nanometer-dimension under similar conditions.

Publication derived from this work:

Supporting information to this chapter in Annex E

8.1 Introduction

Block and graft copolymers in which homogeneous monomer sequences are incompatible and therefore able to spontaneously self-assemble in organized arrangements, are the preferred compounds for building nanostructured polymeric systems [1-3]. In this regard, amphiphilic copolymers made of hydrophilic and hydrophobic segments are particularly interesting given their capacity to form biphasic nanoparticles including compact, hollow and core-shell objects, when they are free to self-assemble in aqueous media [4-6]. As a subfamily of heterogeneous copolymers, those integrated by aliphatic polyester and poly(α-amino acid) segments are receiving great attention in these last years due to the outstanding assortment of properties that may be attained by such combination. As a matter of fact, this paper deals with diblock and graft copolymers made of polyesters derived from macrolactones (ML) and the poly(α-amino acid) poly(L-alanine) (PAla).

Poly(α-amino acid)s are biocompatible polymers that exist in a wide variety of chemical structures, many of them ready accessible by ring-opening polymerization (ROP) of α-amino acid N-carboxyanhydrides [7]. These polymers display high conformational versatility and may adopt different structures depending on the surrounding conditions [8]. Aliphatic polyesters are mostly non-functional synthetic polymers usually lacking molecular activity but displaying an enormous potential for drug delivery applications [9-11]. These polyesters can be synthesized by relatively simple polymerization procedures; the most used one being the ring-opening polymerization (ROP) of lactones [12]. Polyesters generally display a good biocompatibility and are more or less vulnerable to enzymatic degradation depending mainly on their hydrocarbon/ester ratio. A good number of polyester-poly(α-amino acid) block copolymers has been described in the literature, and their capacity to form nanoparticles with potential utility as drug carrier and delivery systems has been extensively explored [13-17]. The number of cases dealing with polyester-poly(α-amino

acid) graft copolymers that has been studied appear to be much lower [18-21], in particular when grafting is made on the polyester counterpart. In both cases, diblock and graft systems, the polyester invariably derived from a medium-size lactone (up to 11 atoms) such as ε-caprolactone or L-lactide, and the polypeptide was made of a three-functional α-amino acid such as aspartic or glutamic acid, lysine or serine.

The polyesters made of macrolactones (large-size lactones containing more than 11 atoms) have hydrophobic character comparable to paraffins, and their potential for the design of biodegradable carriers suitable for drug dispensing applications has been extensively explored along the last decade [22-25]. However ML-based hybrid copolymers have been scarcely studied and the number of poly(macrolactone-*co*-α-amino acid) copolymer systems known to date reduces to a couple of examples recently reported by us [26-27]. In these works, ω-pentadecalactone (PDL) and globalide (Gl) were the MLs chosen for the synthesis of block and graft copolymers, respectively, and the α-amino acids were L-glutamic and L-lysine in both cases. The copolymers were prepared by enzymatic ROP of the ML and subsequent coupling by amino-initiated ROP of the conveniently protected α-amino acid. By this method, the length of the blocks and grafted chains of the copolymers could be precisely adjusted. Most of these copolymers were shown to be able to self-assemble in well-shaped nanoparticles with a diameter in the ~200-400 nm range and displayed negative zeta-potential.

L-Alanine is a neutral α-amino acid that has a strong helix-stabilizing effect when incorporated in a polypeptide chain. The small size of the methyl side chain of L-alanine allows high chain flexibility while retaining enough bulk to stabilize the secondary structure through side-chain/side-chain interactions and van der Waals forces. In polymer design, L-alanine has been mostly copolymerized with hydrophilic monomers such as ethylene glycol [28-32] to build amphiphilic block copolymers showing nanophase separation. Although L-alanine is catalogued as a hydrophobic α-amino

acid, the capacity of the amide group to be hydrogen-bonded with itself or directly to water enables this amino acid to play a relatively hydrophilic function when inserted in highly hydrophobic molecules. Thus block copolypeptides made of alanine and γ-benzyl-L-glutamate have been synthesized and described to be structurally heterogeneous with the two integrating amino acids taking up the α-helical and the β-sheet structure, respectively [33,34]. Furthermore L-alanine is known to play a critical role in regulating the secondary structure of spider silks polypeptides due to the influence exerted by the poly(L-alanine) domains arranged in β-sheet form [35,36]. Copolymers based on the combination of polyalanine and polyester sequences are rare so that only L-lactide [14] and ε-caprolactone [15] have been used so far as comonomers of L-alanine in the synthesis of block copolymers. On the other hand, L-alanine has been recurrently used for grafting water-soluble polymers [37] and biopolymers [38,39] with the aim at making them more water-resistant. To our knowledge, neither block nor graft copolymers made of L-alanine and macrolactones have been investigated so far.

In this paper block and graft copolymers made of L-alanine and either PDL or Gl, are synthesized, and their structure, thermal properties and capacity to form self-assembled nanoparticles are assessed through a comparative study. The purpose of this work is to show the utility of the sequential ROP synthesis to produce well-defined heterogeneous copolymers from MLs and L-Ala and additionally to explore the capacity of such copolymers for building nanoparticles with potential application as nanocarriers. Since the crystallinity and conformation of the two counterparts play a crucial role in the eventual arrangement adopted by the copolymer, main efforts have been focused on the analysis of the structure by means of FTIR, DSC and XRD.

8.2 Results and discussion

8.2.1 Copolymer synthesis

The synthesis of diblock and graft copolymers based on 16-membered macrolactones, either oxacyclohexadecan-2-one (15-pentadecalactone, PDL) or oxacyclohexadecen-2-one (globalide, Gl), and the α-amino acid L-alanine (L-Ala) was carried out by the two-stages sequential ring opening polymerization (ROP) process previously used by us for the synthesis of analog macrolactone-based copolymers containing L-glutamic acid or L-lysine [26,27]. A detailed description of this chemical route with indication of all involved reagents and reaction conditions is depicted in Scheme 8.1.

The first stage of the synthesis was devoted to the enzymatic ROP of the macrolactone and ended with the preparation of the amino-functionalized poly(macrolactone) that was used in the second stage for initiating the ROP of the L-Ala-NCA. An amino-capped poly(pentadecalactone) $PPDL_{10}NH_2$ with an average length of ten units was the macroinitiator used for the synthesis of the diblock copolymers $PPDL_{10}$-b-$PAla_y$.
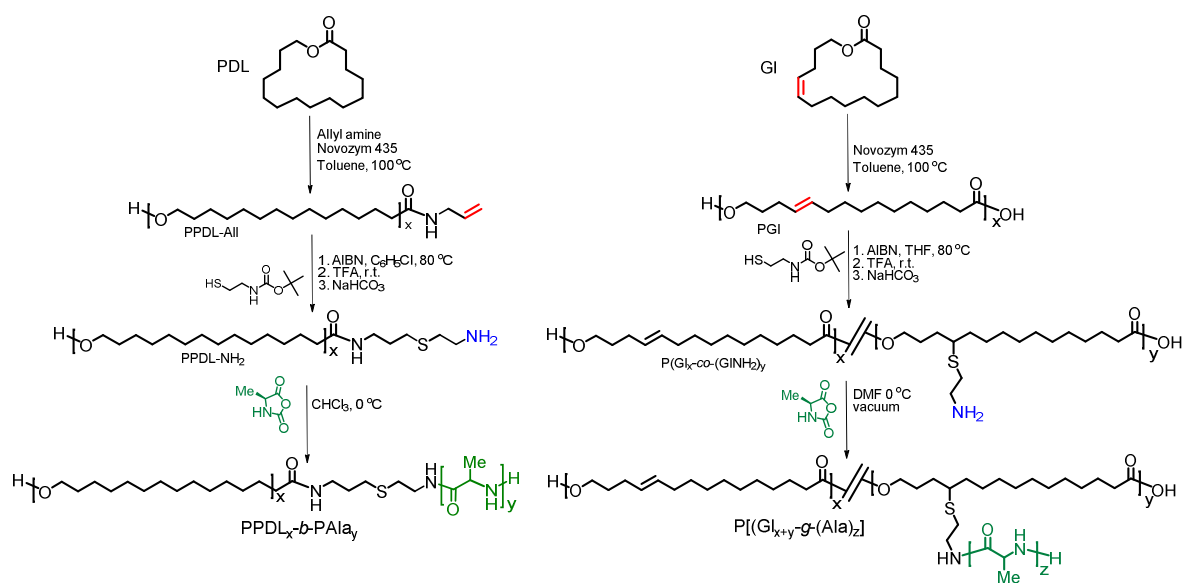
Scheme 8.1. Parallel routes followed for the synthesis of copolymers made of 16-membered macrolactones and L-alanine. Left: Block copolymers from pentadecalactone (PDL). Right: Graft copolymers from globalide (Gl).

Conversely, the unsaturated polyglobalide (PGl) obtained by enzymatic ROP of Gl with an average length of 20 units was amino multifunctionalized in the main chain by click reaction with 2-(Boc-amino)etanothiol (BAET) and subsequent removal of the Boc group. The resulting random copolymer $P[Gl_8\text{-}co\text{-}(GlNH_2)_{12}]$ containing around 60% of amino-functionalized Gl-units was the macroinitiator used in the second stage for the "grafting-from" synthesis of the $P[Gl_{20}\text{-}g\text{-}(Ala)_z]$ copolymers. ^{1}H NMR spectra of the two macroinitiators are available in Figure E4 of the Annex E. The ROP of Ala-NCA was triggered by the nucleophilic attack of the amino group of the macroinitiator onto the NCA carbamate carbonyl group. Different ML/Ala-NCA ratios were used for copolymerization in order to obtain a variety of copolymers with significant different Ala-segment lengths that allows a rational comparison regarding structure and properties. Synthesis results and compositions as well as molecular weight data of all the prepared copolymers are collected in Table 8.1.

Table 8.1. Synthesis results obtained for $PPDL_{10}\text{-}b\text{-}PAla_y$ and $P[Gl_{20}\text{-}g\text{-}(Ala)_z]$ copolymers.

Copolymer[a]	Feed ratio[b] ML-NH$_2$/NCA	Copolymer ratio[c] ML/Ala	Yield (%)	M_n[d] (g·mol^{-1})	M_n[e] (g·mol^{-1})	$Đ$[e]	$L_{PDL,Gl}$ /L_{Ala}[f] (nm)/(nm)
$PPDL_{10}\text{-}b\text{-}PAla_{30}$	1/30	26/74	80	4500	7300	2.1	19/11
$PPDL_{10}\text{-}b\text{-}PAla_{60}$	1/60	15/85	80	6700	10200	2.9	19/22
$PPDL_{10}\text{-}b\text{-}PAla_{200}$	1/200	5/95	70	16,600	14,000	1.4	19/73
$P[Gl_{20}\text{-}g\text{-}(Ala)_5]$	1/5	25/75	80	9900	9200	4.3	39/2
$P[Gl_{20}\text{-}g\text{-}(Ala)_{20}]$	1/25	8/92	60	23,500	19,700	3.9	39/8

[a]Copolymer composition (in mole) expressed by subscripts are those given by NMR and rounded to the nearest five units. The subscript for Ala refers to block and side chain average number of units for block and graft copolymers, respectively.
[b]Molar ratio of amino-functionalized macrolactone unit (ML-NH$_2$, ML being PDL or Gl) to L-Ala NCA used in the feed for NCA ROP.
[c]Copolymer composition (%-mole) determined by ^{1}H NMR.
[d]Number-average molecular weight determined by ^{1}H NMR.
[e]Number-average molecular weight and molar dispersity determined by GPC against PMMA standards.
[f]Average lengths of the PDL and Ala segments in the copolymers estimated on the basis of a fully extended conformation with an average projected bond length of 0.120 nm.

All the copolymerization products were analyzed by GPC using HFIP as solvent. As it is shown in Figure 8.1, monomodal chromatograms were obtained which allow discarding the presence of homo-oligopeptides generated by uncontrolled initiation

caused by other nucleophiles that could be present in the reaction medium as it is water. The NMR analysis of the copolymers in TFA ascertained the hybrid constitution of the copolymers and afforded their molar composition in ML and Ala units which allowed appraising the coupling efficiency of the ROP reaction. For this purpose, the areas of the alpha proton arising from the alanine moiety at 4.3 ppm and the ML $CH_2C\underline{H}_2O$ signal of either PDL or Gl at 4.2 ppm were compared. Differences in composition between the block copolymer and their feeds were in all cases less than 5% indicating that an almost complete incorporation of the α-amino acid was attained by block copolymerization. In the case of the $P[Gl_{20}\text{-}g\text{-}(Ala)_5]$, copolymer and feed compositions were the same but strikingly about 20% of the fed amino acid was lost in the grafting ROP when the ML-NH_2/Ala-NCA ratio was 1/25. Nevertheless the fact that Ala grafting took place on each amino-functionalized Gl unit demonstrated that the efficiency of the initiation reaction in this case is also high, and led to infer that chain growth must be the process that becomes hindered for high Ala-NCA conversions. Illustrative ^{1}H NMR spectra illustrative of each copolymer type are reproduced in Figure 8.2 with full assignment of all observed signals, and complementary ^{1}H and ^{13}C NMR spectra are available in Figures E5 and E6 of the Annex E.
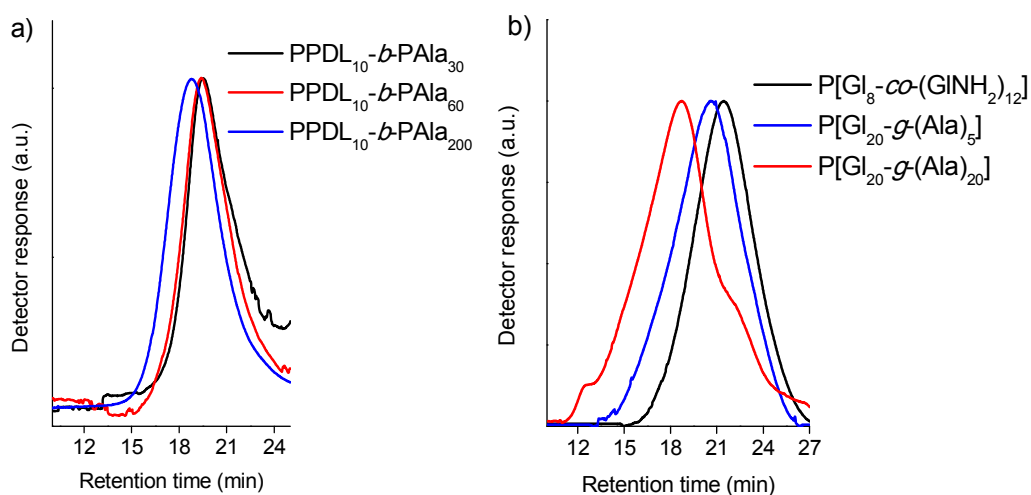
Figure 8.1. GPC traces of the PPDL$_{10}$-b-PAla$_y$ diblock (a), and P[Gl$_{20}$-g-(Ala)$_z$] graft copolymers.
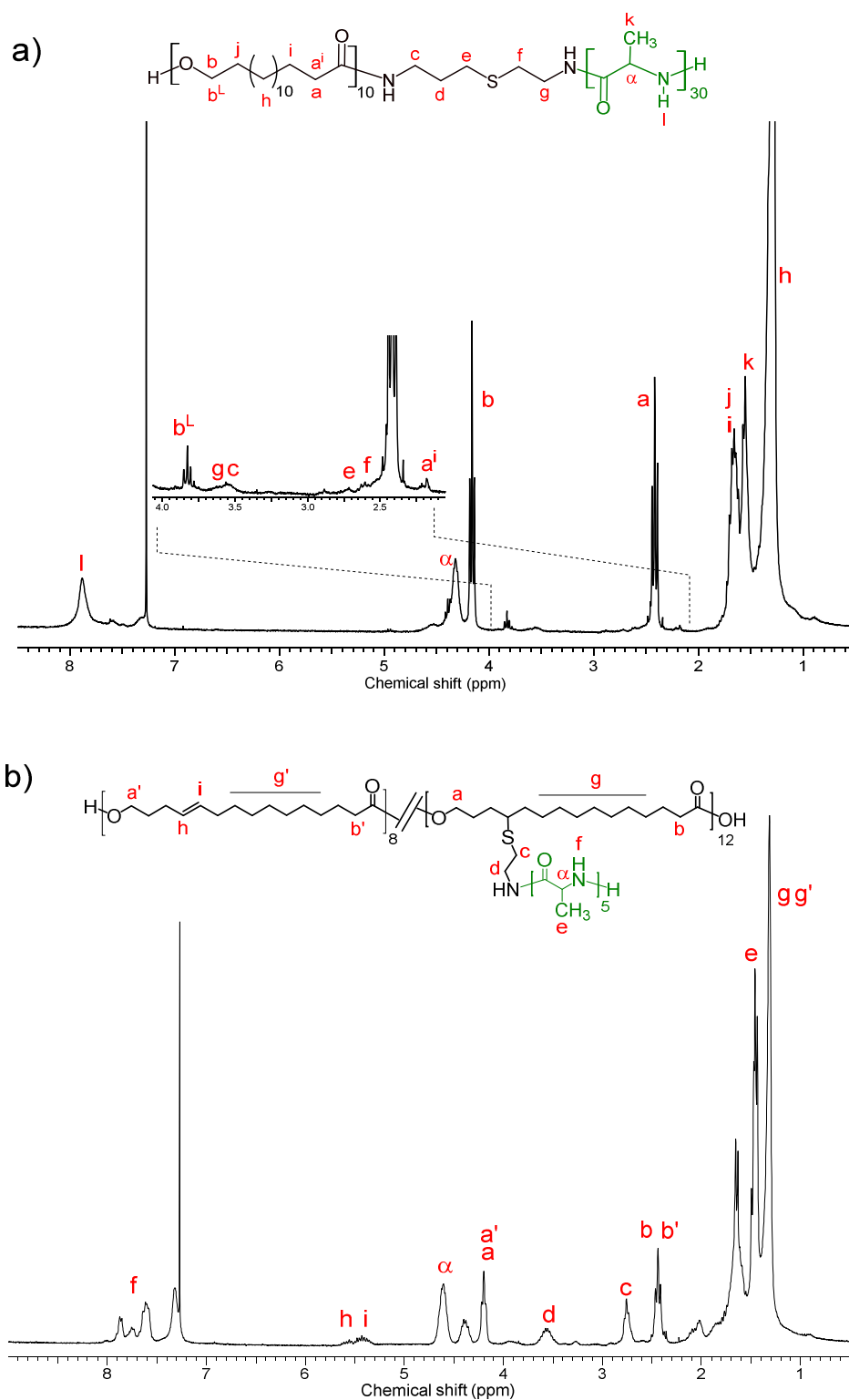
Figure 8.2. ^{1}H NMR (CDCl$_3$/TFA) spectra of PPDL$_{10}$-*b*-PAla$_{30}$ diblock (a), and P[Gl$_{20}$-*g*-(Ala)$_5$] graft copolymers (b). a^i and b^L correspond to the first and last repeating unit, respectively.

8.2.2 Thermal properties

The thermal properties of the $PPDL_{10}$-b-$PAla_y$ diblock and $P[(Gl_{20}$-g-$(Ala)_z]$ graft copolymers were evaluated by TGA and DSC and compared with those of their parent homopolymers $PPDL_{10}$ or PGL_{20} and $PAla_{50}$ taken as references. All the decomposition and transition temperatures detected in these assays are listed in Table 8.2. Representative thermograms illustrating the thermal behavior are shown in Figures 8.3 and 8.4 and this information is complemented with additional thermograms provided in Figures E7 and E8 of the Annex E.

Table 8.2. Thermal properties of the $PPDL_{10}$-b-$PAla_y$ and $P[(Gl_{20}$-g-$(Ala)_z$ copolymers.

Polymer	TGA[a]			DSC[b]					
				1st heating		cooling		2nd heating	
	^oT_d	$^{max}T_d$	R_w	^1T_m	$^1\Delta H$	T_c	ΔH	^2T_m	$^2\Delta H$
	^oC	^oC	%	^oC	$J\cdot g^{-1}$	^oC	$J\cdot g^{-1}$	^oC	$J\cdot g^{-1}$
$PPDL_{10}$	285	425	1	90	148	76	-115	91	134
$PPDL_{10}$-b-Ala_{30}	210	415	11	79, 90	54	78	-19	89	24
$PPDL_{10}$-b-Ala_{60}	255	328	18	75, 91	34	67	-9	90	2
$PPDL_{10}$-b-Ala_{200}	267	340	21	73, 91	10	-	-	-	-
PGl_{20}	370	420	2	54	84	29	-48	49	50
$Poly[Gl_{20}$-g-$(Ala)_5]$	228	355	9	-	-	-	-	-	-
$Poly[Gl_{20}$-g-$(Ala)_{20}]$	190	380	7	-	-	-	-	-	-
$PAla_{50}$	225	375	8	-	-	-	-	-	-

[a]Onset for 5% weight loss (^oT_d) and maximum rate ($^{max}T_d$) thermal decomposition temperatures measured in the TGA analysis performed under inert atmosphere. R_w: weight (%) remaining after heating at 600 ºC.
[b]Melting (T_m and ΔH_m) and crystallization (T_c and ΔH_c) temperatures and enthalpies measured by DSC.

The TGA analysis of $PPDL_{10}$ and PGl_{20} evidenced the high thermal resistance inherent to these polyesters. As it is seen in Figure 8.3, they decompose through a rather simple process that does not begin to be clearly perceivable up to above 400 ºC. $PAla_{50}$ is also fairly stable to heat displaying a single decomposition temperature with maximum rate at 375 ºC. The thermal decomposition traces recorded for the copolyesters are in general more complex and show significant weight losses at temperatures intermediate of those registered for their corresponding homopolymers.

The derivative curves of these traces (Figure E7 in the Annex E) contain 3-4 peaks corresponding to other so many decomposition steps (only the $^{max}T_d$ for the main peak has been listed in Table 2). The onset temperatures of the copolyesters (^oT_d measured for 5% of weight loss) were markedly lower than those of the poly(macrolactone)s and they tend to approach in general to that of PAla$_{50}$. The onset decomposition temperatures also diminished with copolymerization but their values should be taken with caution since the presence of minor amounts of water, which is difficult to remove, may alter significantly their determination.
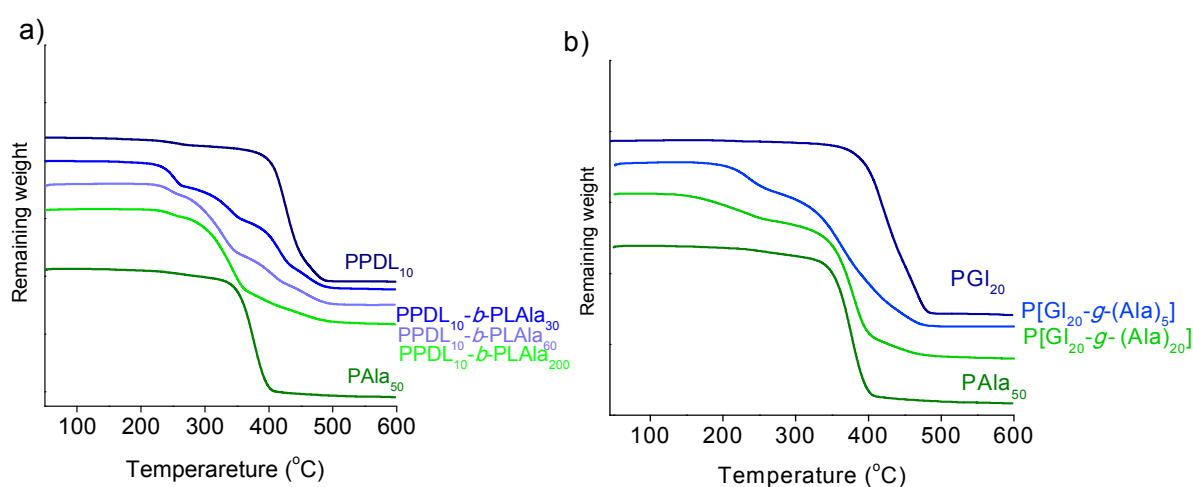
Figure 8.3. TGA traces of PPDL$_{10}$-b-PAla$_y$ and P[Gl$_{20}$-g-(Ala)$_z$] copolymers compared to those of their parent homopolymers.

The occurrence of thermal transitions taking place in the copolymers was examined by DSC of samples subjected to heating/cooling/heating cycles within the 25-170 ºC range. The cycle traces recorded for PPDL$_{10}$-b-PLAla$_{30}$ diblock and P[(Gl$_{20}$-g-(Ala)$_5$] graft copolymers, which may be taken as representatives, as well as those recorded for their parent homopolymers are depicted in Figure 8.4. The DSC traces obtained for the other copolymers synthesized in this work have been added to the Annex E (Figure E8). The traces registered for PPDL$_{10}$ and PGl$_{20}$ were characteristic of semicrystalline polymers showing ^1T_m's at 90 ^{o}C and 54 at the first heating ºC, and ^1T_c's at 76 ºC and 29 ºC, upon cooling, respectively. The recrystallized samples displayed melting peaks comparable to those observed for the pristine samples with

small deviations in temperatures and enthalpies. These results are in full agreement with data published on the high molecular weight PPDL [45] and PGl homologues [43]. On the other hand, the thermogram produced by a sample of PAla$_{50}$ coming directly from synthesis showed a broad endotherm with its maximum at 70-80 ºC that was attributed to solvent volatilization since it almost fully disappeared when the sample was previously dried at 45 ºC for several hours under vacuum. No other heat exchange was detected for PAla$_{50}$, neither at heating nor at cooling through the analyzed range of temperatures. This is in agreement with that has been reported for the thermal behavior of PAla in the solid state which is characterized by the occurrence of a phase transition from the α-form to the β-form taking place at temperatures above 300 ºC. Melting of PAla cannot be experimentally observed because it would take place at temperatures above decomposition.

The DSC pattern characteristic of PPDL$_{10}$-b-PAla$_y$ copolymers may be represented by that recorded for PPDL$_{10}$-b-PAla$_{30}$ which is shown in Figure 8.4a. The first heating trace taken from the copolymer (previously dried as it was indicated for PAla$_{50}$) showed two endothermic peaks at 77 ºC and 90 ºC with similar intensities which are attributed to the respective melting of two copolymer populations differing in crystallite size. At cooling from 170 ºC, a crystallization peak was observed at 78 ºC, and at the second heating, the initial melting peak appearing at 90 ºC was recovered accompanied of a broad weak endotherm that spread over a 70-80 ºC range. These results doubtlessly indicate that the PPDL block in this copolymer is crystallized and that it can be reversibly melted and recrystallized. Similar results were observed for the other two block copolymers with the only difference that no recrystallization was observed for PPDL$_{10}$-b-PAla$_{200}$ which must be interpreted as due to the high diluent effect exerted by the long PAla block present in this copolymer (Figure E8). The DSC results obtained for the P[Gl$_{20}$-g-(Ala)$_z$] graft copolymers differed noticeably from those described for PPDL$_{10}$-b-PAla$_y$ block copolymers in spite of that the melting-crystallization behavior displayed by PGl$_{20}$ and PPDL$_{10}$ was very similar. The heating-cooling traces registered

for P[GI$_{20}$-g-(Ala)$_5$] (Figure 8.4b) did not display any sign of crystallinity indicating that PGI$_{20}$ became unable to crystallize after grafting. The same result was obtained in the analysis of P[GI$_{20}$-g-(Ala)$_{20}$] (Figure E8). It can be therefore concluded that, as expected, the graft copolymers are essentially amorphous whereas the block copolymers are able to show crystallinity whichever is their composition.
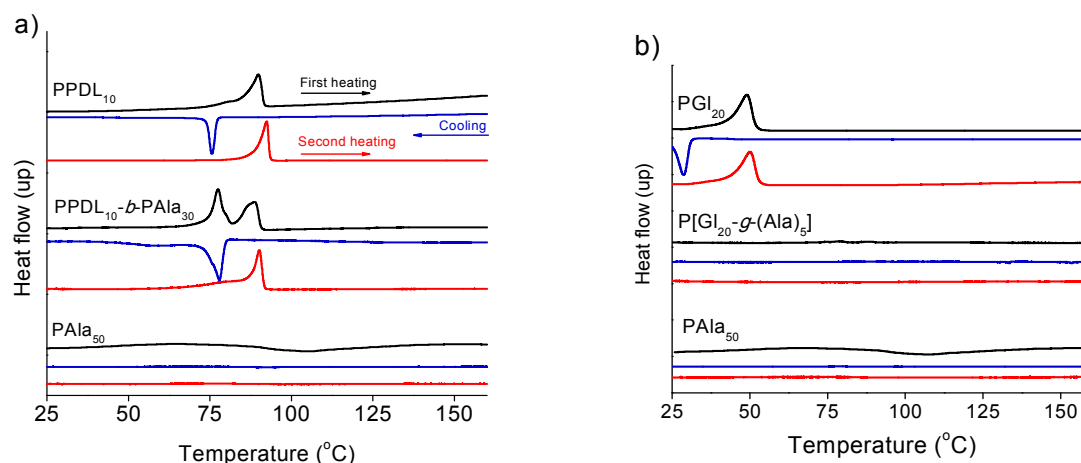
Figure 8.4. DSC traces recorded for a) PPDL$_{10}$-b-PLAla$_{30}$ diblock and b) P[GI$_{20}$-g-(Ala)$_5$] graft copolymers and for their parent homopolymers.

The influence of the PAla$_y$ block on the crystallizability of the PPDL$_{10}$ block in PPDL$_{10}$-b-PAla$_y$ copolymers was examined by measuring the increment of the relative crystallinity produced in their isothermal crystallization as a function of time. Results obtained for the three block copolymers studied in this work as well as for the poly(pentadecalactone) homopolymer are plotted in Figure 8.5, where it is clearly shown that the presence of the PAla$_y$ block whatever its length enhanced the crystallization rate of the PPDL$_{10}$ block. Such an enhancing effect seems to be however something more intense for shorter PAla$_y$ blocks, a fact that may be due to the high dilution produced by the PAla$_{200}$ block. This result is in line with the non-observance of recrystallization for the PPDL$_{10}$-b-PAla$_{200}$ copolymer when it was cooled at constant rate from the melt to room temperature (Figure E8).
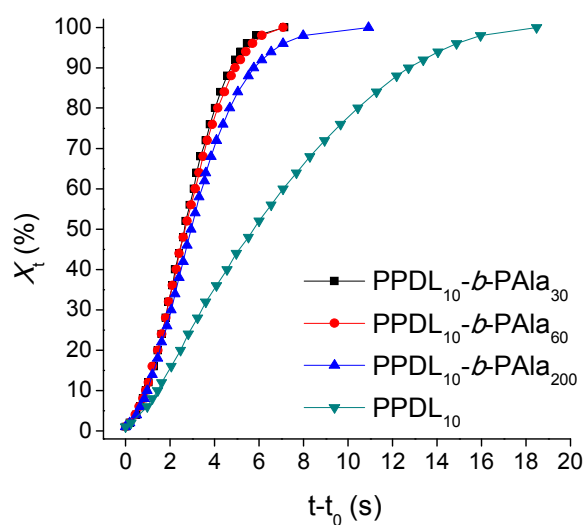
Figure 8.5. Evolution of the relative crystallinity as a function of time in the isothermal crystallization at 82 °C of the $PPDL_{10}$-b-$PAla_y$ diblock copolymers.

8.2.3 Chain conformation and structure

The crystal structure of poly(macrolactone)s has been reported by different authors. PPDL is known to adopt a pseudo-rhombic monoclinic structure with a unit cell of approximate dimensions a = 0.75 nm, b = 0.5 nm, and c = 2.0 nm and α = 90.0° [42,46]. The X-ray diffraction spacings characteristic of this structure are those at 0.40 nm and 0.37 nm corresponding to 110 and 200 interplanar distances. On the contrary, the crystal structure of PGI has not yet been resolved but there indications that it must not be significantly dissimilar to that of PPDL [25]. On the other hand, the polypeptide $PAla_n$ is known to be usually arranged in one of the two ordered structures commonly found in polypeptides, *i.e.* the α-helical or the β-sheet forms, with preference for one or the other depending on both chain length and crystallization conditions. The helical structure consists of a hexagonal arrangement of 13/5 helices that is characterized by a strong reflection at about 0.75 nm. The β-form is a layered structure made of nearly fully extended chains with characteristic X-ray reflections at 0.53 nm and 0.45 nm [47]. FTIR spectra are usually taken to support the chain arrangement adopted by polypeptides. The absorption bands at 1650 cm^{-1} (Amide I) and 1545 cm^{-1} (Amide II) are taken as characteristic of the α-helix whereas bands at 1630 (Amide I), 1535

(Amide II) and 700 cm^{-1} (Amide V) are used for identifying the β-form. The helical form is known to be favored by high molecular weights and temperatures. It has been also reported that the helical form is irreversibly converted into the layered form by heating at temperatures close to 300 °C, a transition that may be followed by both XRD and FTIR [47].

The arrangements adopted by the block and graft PML-PAla copolymers in the solid state and the changes that they may undertake by effect of heating were examined by FTIR and XRD at variable temperature. Firstly the FTIR study was carried out using powder samples in order to get insight into the secondary structure adopted by the polypeptide chains. The 1500-1800 cm^{-1} region of the FTIR spectra, in which Amide I and Amide II bands appear, is displayed in Figure 8.6 for PPDL$_{10}$-*b*-PAla$_y$ diblock and P[Gl$_{20}$-*g*-(Ala)$_z$] graft copolymers as well as for the homopolypeptide PAla$_{50}$. Just to note that the band due to the polyester C=O stretching is observed in this region at 1730 cm^{-1} with an intensity that correlates well with the relative content of ester groups in the copolymers. The spectrum of PAla$_{50}$ shows a main absorption peak at 1650 cm^{-1} with a prominent shoulder at 1630 cm^{-1} that correspond to the Amide I band of the helical and sheet forms, respectively. Accordingly, the Amide II band was found to consist of a broad absorption with a maximum at 1540 cm^{-1} and a poorly visible shoulder at around 1520 cm^{-1}. The spectra recorded from the copolymers displayed a pattern similar to that of PAla$_{50}$ but differing in the relative intensity of the Amide I and II bands arisen from each of the two
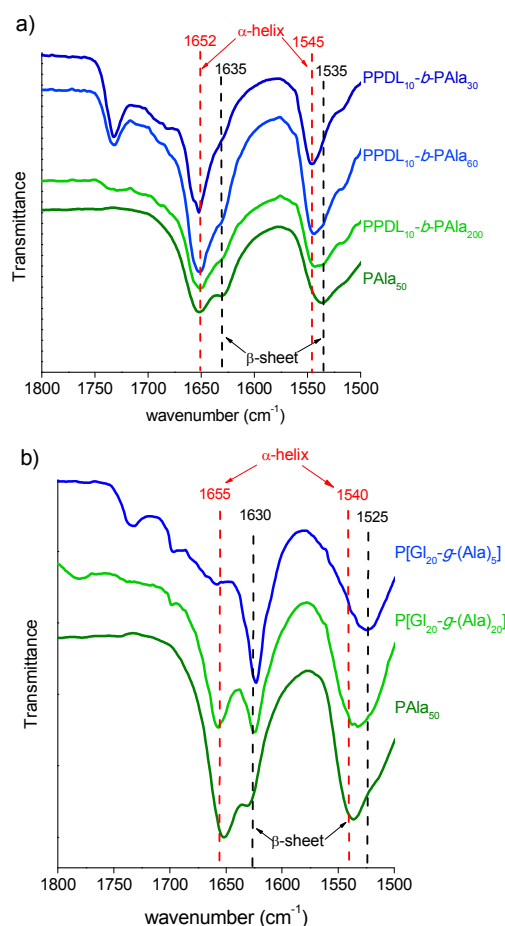
Figure 8.6. Amide I and II region of FTIR spectra of a) $PPDL_{10}$-b-$PAla_y$ diblock and b) $P[Gl_{20}$-g-$(Ala)_z]$ graft copolymers.

forms. In the case of the graft copolymers (Figure 8.6b) the amounts of polypeptide arranged in helical and extended conformation are comparable for a side chain length of 20 Ala units whereas the latter is the only almost conformation present when the length of the Ala segment reduced to 5 units. Strikingly the behavior observed for the block copolymers is just the opposite. In this case it is the α-form that is largely predominant for shorter polypeptide lengths although it is true also that the β-form seem to be minority along the whole series. It may be then speculated that the polyester in the crystallized state must exert certain influence on the molecular arrangement adopted by the polypeptide with the result of an inversion in its expected conformational preferences. The response given by FTIR spectra to heating is in line with these observations. The $PPDL_{10}$-b-$PAla_{200}$ copolymer containing similar amounts

of α and β-form at room temperature became entirely arranged in the α-form when heated at temperatures above 60 ºC which is close to the melting temperature of the polyester block. On the contrary, the α/β composition of P[Gl$_{20}$-g-(Ala)$_{20}$], in which the polyester counterpart is not ordered, appears to be invariable with temperature. Plots of the FTIR spectra of PPDL$_{10}$-b-PAla$_{200}$ and P[Gl$_{20}$-g-(Ala)$_{20}$], at temperatures increasing from 25 ºC to 250 ºC are shown in Figure E9 of the Annex E.

The X-ray diffraction study was performed on powder samples using synchrotron radiation at variable temperature and recording the scattered light at real time. WAXS and SAXS data were simultaneously registered and the changes taking place by effect of heating or cooling were visualized by comparative representation of the scattering profiles as a function of temperature (Figure 8.7 and Figures E10-E12 in the Annex E).
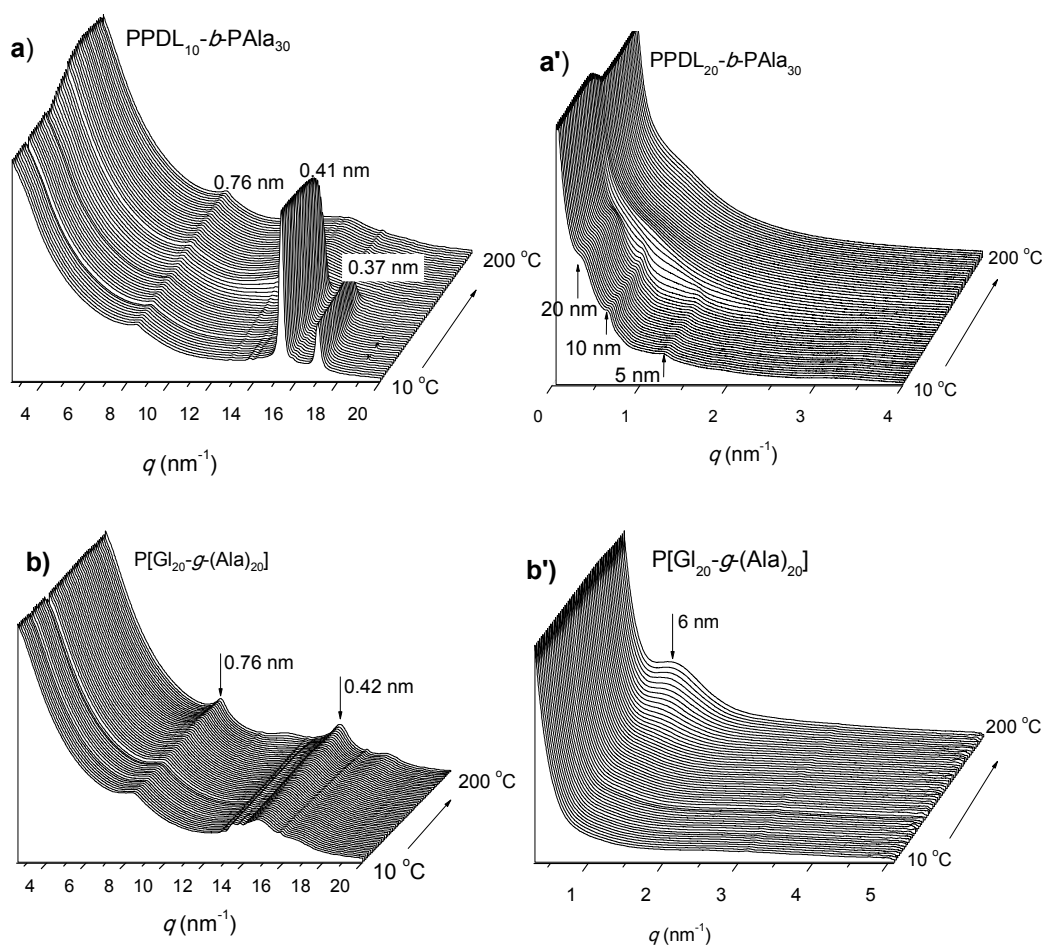
Figure 8.7. Evolution of the WAXS (a and b) and SAXS (a' and b') diffraction profiles of PPDL$_{10}$-b-PAla$_{30}$ diblock and P[Gl$_{20}$-g-(Ala)$_{20}$] graft copolymers recorded at increasing temperature from 10 ºC to 200 ºC.

The WAXS profile registered at 10 ºC from $PPDL_{10}$-b-$PAla_{30}$ (Figure 8.7a) clearly showed the two characteristic peaks of PPDL at 0.41 nm and 0.37 nm. At heating these peaks kept unaltered until temperature reached around 90 ºC where they completely disappeared. According to DSC data such behavior corresponds to the melting of the crystalline PPDL block. In fact, both peaks were almost completely recovered upon cooling at temperatures around 60 ºC (Figure E10). A reflection at 0.76 nm with a moderate intensity that slightly increased with temperature was also detected in the WAXS profiles. This reflection is made to correspond to the hexagonal packing of $PAla_{30}$ α-helices. Additionally a careful inspection of the low temperature profile revealed the presence of low intensity peaks at 0.49 nm and 0.45 nm that stayed invariable at 200 ºC, and which could be attributed to the presence of some amount of polyalanine in the β-form. The SAXS profile registered for $PPDL_{10}$-b-$PAla_{30}$ (Figure 8.7a') at 10 ºC displayed weak reflections at 20, 10 and 5 nm that remained unaltered up to temperatures near to that of PPDL melting was reached. It seems therefore that a 1D structure with a main spacing of 20 nm (second and fourth orders at 10 nm and 5 nm) and consisting of a biphasic alternating arrangement of the two blocks, is adopted by this copolymer. Since all SAXS signals disappeared upon heating at temperatures close to 90 ºC, it can be inferred that the nanometric structure becomes unstable as soon as the polyester phase is molten.

The X-ray diffraction results produced by the $P[Gl_{20}$-g-$(Ala)_{20}]$ graft copolymer were largely dissimilar. As it is seen in Figure 8.7b, no peaks characteristic of polyester were observed in these profiles so that all the discrete reflections there present have to be interpreted to arise from the polypeptidic phase. Peaks at 0.49 nm and 0.45 nm characteristic of β-form and 0.76 nm of α-form observed at low temperature remained almost invariable at heating up to 200 ºC. This behavior is in agreement with that observed by FTIR and confirms the thermal stability of the two forms in the graft copolymers over the studied range of temperatures. The SAXS produced by $P[Gl_{20}$-g-

(Ala)$_{20}$] and how it changed with temperature is shown in Figure 8.7b'. No scattering was observed below ~150 ºC indicating the absence of any order or discrete phase segregation in this copolymer at low temperature. At high temperature, *i.e.* above 160 ºC, a broad signal corresponding to a spacing of approximately 6.6 nm emerged and became more pronounced as temperature increased. Unfortunately, there are not enough data available nor accessible precedents that allow conjecturing with a minimum detail on the nature of the arrangement responsible for such scattering.

8.2.4 Copolymer self-assembly in aqueous environment

The copolymers studied in this work cannot be actually classified as amphiphilic since the PML block is highly hydrophobic and PAla, although its affinity for water is greater than that of the polyester, cannot not be considered a hydrophilic polypeptide. In fact, PAla segments have been combined with other segments made of charged α-amino acids or water-soluble monomers in order to generate well-defined amphiphilic block or graft copolymers able to display a strong tendency to phase separation [28-32].

Nevertheless, it was interesting to explore in a comparative manner the spontaneous assembling behavior that could display PPDL$_{10}$-*b*-PAla$_y$ block and P[Gl$_{20}$-*g*-(Ala)$_z$] graft copolymers when they are freely placed in an aqueous environment. Both the emulsion-evaporation solvent and the nanoprecipitation techniques were used to drive the self-assembly of a selection of PML-PAla copolymers in recognizable nano-objects and the obtained results are given in Table 8.3. Both PPDL$_{10}$-*b*-PAla$_{30}$ and PPDL$_{10}$-*b*-PAla$_{200}$ became self-assembled in nanoparticles with a low positive zeta-potential and diameters about 300 nm and 350 nm, respectively. The DLS profiles and SEM images of these nanoparticles are shown in Figure 8.8. On the other hand, neither the emulsion-solvent evaporation nor nanoprecipitation method induced the self-assembling of P[Gl$_{20}$-*g*-(Ala)$_5$] copolymer so that only unspecific aggregates of

large sizes were observed instead. The DLS profile recorded from this sample is available in Figure E13 of the Annex E.

Table 8.3. Characterization of nanoparticles by DLS.

Polymer	D (nm)	*DPI*	ζ (mV)	Used method
PPPL$_{10}$-*b*-PLAla$_{30}$	300	0.29	6.3	emulsion-evaporation
PPPL$_{10}$-*b*-PLAla$_{200}$	350	0.39	7.5	emulsion-evaporation
P[Gl$_{20}$-*g*-(Ala)$_5$]	60/3000	0.88	-	nanoprecipitation
P[Gl$_{20}$-*g*-(Ala)$_{20}$]	n.o.	n.o	-	nanoprecipitation

n.o. = not observed.
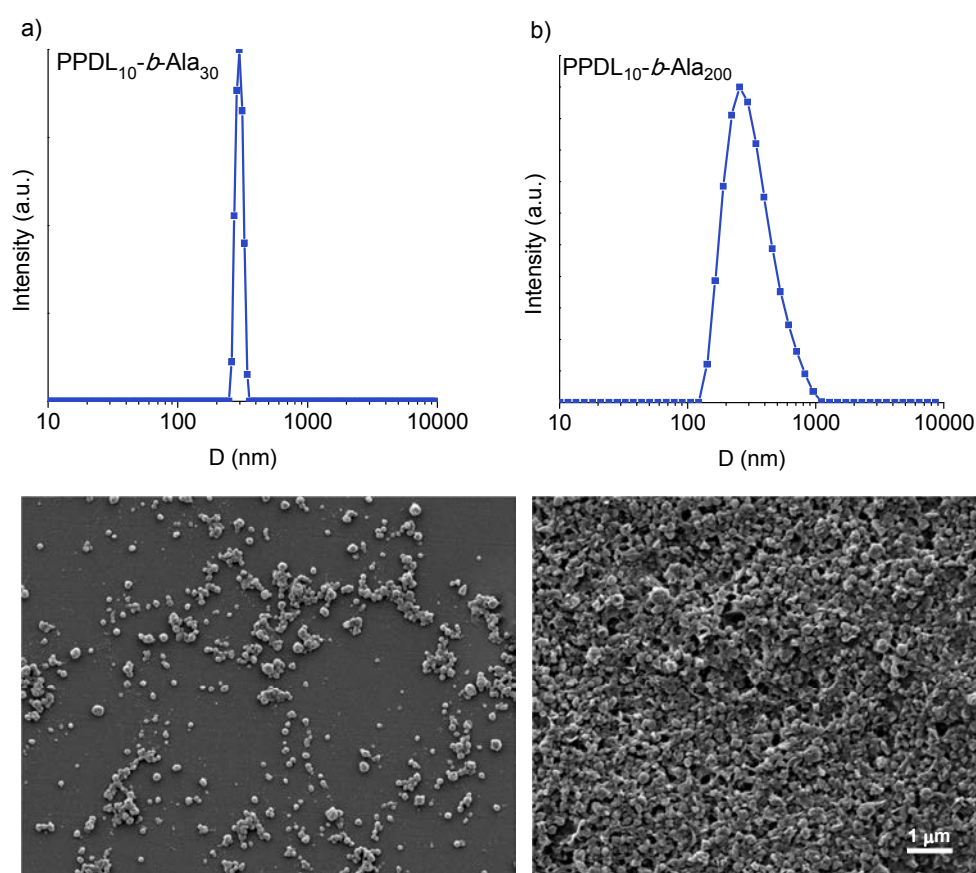
Figure 8.8. DLS profiles and SEM images of PPDL$_{10}$-*b*-PAla$_{30}$ (a) and PPDL$_{10}$-*b*-PAla$_{200}$ (b) diblock copolymers.

8.3 Conclusions

The sequencial ROP polymerization previously used by us for the synthesis of poly(macrolactone)-poly(α-amino acid) copolymers made of either L-Lys or L-Glu has

proven to be extensible to the preparation of block and graft copolymers made of L-Ala. The polyester block in the poly(pentadecalactone)-*block*-poly(α-L-alanine) copolymers was in the crystalline state and was able to crystallize from the melt at a crystallization rate enhanced by the presence of the polypeptide block. On the contrary, the polyester main chain of the poly[globalide-*grafte*-(α-L-alanine)] copolymers was invariably in the disordered state. Regarding the polypeptide counterpart, a conformational mixture of α-helical and β-forms was present in both types of copolymers but its dependence on the polypeptide length and its response to heating effect was found to be opposite. The conformational behavior observed in graft copolymers was in agreement with expectations but in block copolymers the α/β ratio decreased with the increasing length of the polypeptide chain and with decreasing temperature. The crystalline nature of the polyester domain and the melting-crystallization transition happening in the block copolymers could be invoked to be responsible for this anomalous behavior. Such differences in crystallinity and conformation become reflected in the different ability displayed by these copolymers to be self-assembled. Only the block copolymers were able to form nanometric particles, a property that could be associated to the expected tendency of the polyester block to build a crystalline core with subsequent outwards segregation of the poly(α-amino acid) segment arranged in the α-helical form. The incapacity of the graft copolymers to form nanoparticles may be attributed either to a defective separation of the poly(α-amino acid) and polyester domains or to an extensive primary particle aggregation caused by hydrogen-bonding interaction between the peripheral polypeptide arranged in the β-form.

8.4 References

[1]   Y. Mai, A. Eisenberg, Self-assembly of block copolymers, Chem. Soc. Rev. 41 (2012) 5969-5985.

[2]   L. Atanase, G. Riess, Self-assembly of block and graft copolymers in organic solvents: an overview of recent advances, Polymers 10 (2018) 62.

[3]   S. Sakuma, M. Hayashi, M. Akashi, Design of nanoparticles composed of graft

copolymers for oral peptide delivery, Adv. Drug Deliv. Rev. 47 (2001) 21–37.

[4]   M.L. Adams, A. Lavasanifar, G.S. Kwon, Amphiphilic block copolymers for drug delivery, J. Pharm. Sci. 92 (2003) 1343–1355.

[5]   A. Rösler, G.W.M. Vandermeulen, H.-A. Klok, Advanced drug delivery devices via self-assembly of amphiphilic block copolymers, Adv. Drug Deliv. Rev. 64 (2012) 270–279.

[6]   D. Wu, Y. Huang, F. Xu, Y. Mai, D. Yan, Recent advances in the solution self-assembly of amphiphilic "rod-coil" copolymers, J. Polym. Sci. Part A Polym. Chem. 55 (2017) 1459–1477.

[7]   H.R. Kricheldorf, Polypeptides and 100 Years of Chemistry of α-Amino Acid N-Carboxyanhydrides, Angew. Chemie Int. Ed. 45 (2006) 5752–5784.

[8]   C. Bonduelle, Secondary structures of synthetic polypeptide polymers, Polym. Chem. 9 (2018) 1517–1529.

[9]   K.E. Uhrich, S.M. Cannizzaro, R.S. Langer, K.M. Shakesheff, Polymeric systems for controlled drug release, Chem. Rev. 99 (1999) 3181–3198.

[10]   H. Seyednejad, A.H. Ghassemi, C.F. van Nostrum, T. Vermonden, W.E. Hennink, Functional aliphatic polyesters for biomedical and pharmaceutical applications, J. Control. Release. 152 (2011) 168–176.

[11]   K.E. Washington, R.N. Kularatne, V. Karmegam, M.C. Biewer, M.C. Stefan, Recent advances in aliphatic polyesters for drug delivery applications, Wiley Interdiscip. Rev. Nanomedicine Nanobiotechnology 9 (2017) e1446.

[12]   A.-C. Albertsson, I.K. Varma, Recent developments in ring opening polymerization of lactones for biomedical applications, Biomacromolecules 4 (2003) 1466–1486.

[13]   S. Caillol, S. Lecommandoux, A.-F. Mingotaud, M. Schappacher, A. Soum, N. Bryson, R. Meyrueix, Synthesis and self-assembly properties of peptide−polylactide block copolymers, Macromolecules 36 (2003) 1118–1124.

[14]   M. Gotsche, Amino-termined poly(L-lactide)s as initiators for the polymerization of N-carboxyanhydrides: synthesis of poly(L-lactide)-block-poly(α-amino acid)s, Macromol. Chem. Phys. 196 (1995) 3891–3903.

[15]   H.R. Kricheldorf, K. Hauser, Polylactones. 55. A−B−A triblock copolymers of various polypeptides. Syntheses involving 4-aminobenzoyl-terminated poly(ϵ-caprolactone) as B block, Biomacromolecules 2 (2001) 1110–1115.

[16]   M. Schappacher, A. Soum, S.M. Guillaume, Synthesis of polyester−polypeptide diblock and triblock copolymers using amino poly(ϵ-caprolactone) macroinitiators, Biomacromolecules 7 (2006) 1373–1379.

[17]   S. Motala-Timol, D. Jhurry, J. Zhou, A. Bhaw-Luximon, G. Mohun, H. Ritter, Amphiphilic poly(L-lysine-b-caprolactone) block copolymers: synthesis, characterization, and solution properties, Macromolecules 41 (2008) 5571–5576.

[18]   J.H. Jeong, Y. Byun, T.G. Park, Synthesis and characterization of poly(L-lysine)-g-poly(D,L-lactic-co-glycolic acid) biodegradable micelles, J. Biomater. Sci. Polym. Ed. 14 (2003) 1–11.

[19] D.J. Price, M. Khuphe, R.P.W. Davies, J.R. McLaughlan, N. Ingram, P.D. Thornton, Poly(amino acid)-polyester graft copolymer nanoparticles for the acid-mediated release of doxorubicin, Chem. Commun. 53 (2017) 8687–8690.

[20] G. Caponetti, J.S. Hrkach, B. Kriwet, M. Poh, N. Lotan, P. Colombo, R. Langer, Microparticles of novel branched copolymers of lactic acid and amino acids: preparation and characterization, J. Pharm. Sci. 88 (1999) 136–141.

[21] B. Nottelet, A. El Ghzaoui, J. Coudane, M. Vert, Novel amphiphilic poly(ε-caprolactone)-g-poly(L-lysine) degradable copolymers, Biomacromolecules 8 (2007) 2594–2601.

[22] J.A. Wilson, Z. Ates, R.L. Pflughaupt, A.P. Dove, A. Heise, Polymers from macrolactones: from pheromones to functional materials, Prog. Polym. Sci. 91 (2019) 29–50.

[23] J. Liu, Z. Jiang, S. Zhang, C. Liu, R.A. Gross, T.R. Kyriakides, W.M. Saltzman, Biodegradation, biocompatibility, and drug delivery in poly(ω-pentadecalactone-co-p-dioxanone) copolyesters, Biomaterials 32 (2011) 6646–6654.

[24] M.P.F. Pepels, I. Hermsen, G.J. Noordzij, R. Duchateau, Molecular structure-catalytic activity relationship in the ring-opening polymerization of (macro)lactones, Macromolecules 49 (2016) 796–806.

[25] I. van der Meulen, M. de Geus, H. Antheunis, R. Deumens, E.A.J. Joosten, C.E. Koning, A. Heise, Polymers from functional macrolactones as potential biomaterials: enzymatic ring opening polymerization, biodegradation, and biocompatibility, Biomacromolecules 9 (2008) 3404–3410.

[26] E. Tinajero-Díaz, A. Martínez de Ilarduya, S. Muñoz-Guerra, Synthesis and properties of diblock copolymers of ω-pentadecalactone and α-amino acids, Eur. Polym. J. 116 (2019) 169–179.

[27] E. Tinajero-Díaz, A. Martínez de Ilarduya, S. Muñoz-Guerra, Poly(amino acid)-grafted polymacrolactones. Synthesis, self-assembling and ionic coupling properties (2019) (submitted).

[28] Y.Y. Choi, J.H. Jang, M.H. Park, B.G. Choi, B. Chi, B. Jeong, Block length affects secondary structure, nanoassembly and thermosensitivity of poly(ethylene glycol)-poly(L-alanine) block copolymers, J. Mater. Chem. 20 (2010) 3416.

[29] M.K. Joo, D.Y. Ko, S.J. Jeong, M.H. Park, U.P. Shinde, B. Jeong, Incorporation of D-alanine into poly(ethylene glycol) and L-poly(alanine-co-phenylalanine) block copolymers affects their nanoassemblies and enzymatic degradation, Soft Matter. 9 (2013) 8014-8022.

[30] Z. Jiao, X. Wang, Z. Chen, Folate-conjugated methoxy poly (ethylene glycol)/poly (L-alanine) amphiphilic block copolymeric micelles for targeted delivery of paclitaxel, Drug Deliv. 18 (2011) 478–484.

[31] GL, Zhang, JB, Ma, YN, Wang, Micellization of poly(L-alanine)/poly(ethylene glycol) block copolymer, Chem. J. Chinese U. 27 (2006) 767-770.

[32] G.L. Wu, P.C. Sun, H. Lin, J.B. Ma, The secondary structures of poly (L-alanine) blocks in some diblock copolymers of poly(L-alanine)-b-poly(ethylene glycol) monomethyl ether in the solid state characterized by nuclear magnetic resonance and infrared spectrometry, J. Mol. Struct. 689 (2004) 143–146.

[33] M. Duerden, M.N. Jones, R.A. Badley, E.R. Morris, Synthesis, characterization and conformation of some block copolypeptides in aqueous solution, Int. J. Biol. Macromol. 2 (1980) 274–278.

[34] A. Gitsas, G. Floudas, M. Mondeshki, H.W. Spiess, T. Aliferis, H. Iatrou, N. Hadjichristidis, Control of peptide secondary structure and dynamics in poly(γ-benzyl-L-glutamate)-*b*-polyalanine peptides, Macromolecules 41 (2008) 8072–8080.

[35] O. Rathore, D.Y. Sogah, Self-assembly of β-sheets into nanostructures by poly(alanine) segments incorporated in multiblock copolymers inspired by spider silk, J. Am. Chem. Soc. 123 (2001) 5231–5239.

[36] O.S. Rabotyagova, P. Cebe, D.L. Kaplan, Role of polyalanine domains in β-sheet formation in spider silk block copolymers, Macromol. Biosci. 10 (2010) 49–59.

[37] M. Higuchi, J.P. Wright, K. Taguchi, T. Kinoshita, Structure and molecular recognition properties of a poly(allylamine) monolayer containing poly(L-alanine) graft chains, Langmuir 16 (2000) 7061–7065.

[38] G.H. Park, M.-S. Kang, J.C. Knowles, M.-S. Gong, Synthesis, characterization, and biocompatible properties of alanine-grafted chitosan copolymers, J. Biomater. Appl. 30 (2016) 1350–1361.

[39] M. Motiei, S. Kashanian, A. (Arman) Taherpour, Hydrophobic amino acids grafted onto chitosan: a novel amphiphilic chitosan nanocarrier for hydrophobic drugs, Drug Dev. Ind. Pharm. 43 (2017) 1–11.

[40] G.J.M. Habraken, M. Peeters, C.H.J.T. Dietz, C.E. Koning, A. Heise, How controlled and versatile is *N*-carboxy anhydride (NCA) polymerization at 0 °C? Effect of temperature on homo-, block- and graft (co)polymerization, Polym. Chem. 1 (2010) 514-524.

[41] W.H. Daly, D. Poché, The preparation of *N*-carboxyanhydrides of α-amino acids using bis(trichloromethyl)carbonate, Tetrahedron Lett. 29 (1988) 5859–5862.

[42] M. Letizia Focarete, M. Scandola, A. Kumar, R. a Gross, Physical characterization of poly(ω-pentadecalactone) synthesized by lipase-catalyzed ring-opening polymerization, J. Polym. Sci. Part B Polym. Phys. 39 (2001) 1721–1729.

[43] Z. Ates, P.D. Thornton, A. Heise, Side-chain functionalisation of unsaturated polyesters from ring-opening polymerisation of macrolactones by thiol-ene click chemistry, Polym. Chem. 2 (2011) 309–312.

[44] J. Liu, Z. Jiang, S. Zhang, C. Liu, R.A. Gross, T.R. Kyriakides, W.M. Saltzman, Biodegradation, biocompatibility, and drug delivery in poly(ω-pentadecalactone-*co*-*p*-dioxanone) copolyesters Biomaterials 32 (2011) 6646-6654.

[45] M. De Geus, I. Van Der Meulen, B. Goderis, K. Van Hecke, M. Dorschu, H. Van Der Werff, C.E. Koning, A. Heise, Performance polymers from renewable monomers: High molecular weight poly(pentadecalactone) for fiber applications, Polym. Chem. 1 (2010) 525–533.

[46] M. Gazzano, V. Malta, M.L. Focarete, M. Scandola, R. a Gross, Crystal structure of poly(ω-pentadecalactone), J. Polym. Sci. Part B Polym. Phys. 41 (2003) 1009–1013.

[47] M. Tsukada, M. Nagura, H. Ishikawa, Structural-changes in poly(L-alanine) induced by heat-treatment, J. Polym. Sci. Part B: Polym. Phys. 25 (1987) 1325.

Chapter 9. Isomorphic pentadecalactone-globalide random copolyesters grafted with L-glutamic acid. Synthesis and nanocarrier properties

Abstract

The enzymatic copolymerization of globalide (Gl) and pentadecalactone (PDL) was performed in solution from macrolactones mixtures covering the whole comonomeric composition. The thermal properties and structure in the solid state of the resulting random copolyesters PGl-*r*-PPDL were evaluated by DSC, FTIR and XRD. Interestingly, the copolyesters were found to have an isomorphic behavior in crystallization. They all are crystalline and adopt the same crystal structure as the reference homopolyesters PGl and PPDL. Grafting of amino-functionalized PGl-*r*-PPDL by ROP of benzyl-L-glutamate NCA provided neutral poly(γ-benzyl-L-glutamate) grafted copolyesters that could be then readily converted into negatively charged hybrid copolymers by hydrolysis of the benzyl carboxylate group. Both water soluble and non-soluble copolymers were produced depending on the copolymer charge and grafting degree, and their capacity to self-assemble in nano-objects was preliminarily comparatively examined. Well delineated 200-300 spherical nanoparticles were obtained by applying the solvent-evaporation technique to the chloroform soluble copolymers bearing benzyl glutamate chains. Conversely, micelle aggregates were spontaneously generated in the water solutions of the copolyesters grafted with side chains made of ten glutamic acid units in average. Copolymer micelles were able to load DOX with high efficiency by means of electrostatic interactions and to release the drug at a rate that was markedly depending on pH.

Publication derived from this work:

9.1 Introduction

Polypeptides can be regarded as a class of highly refined polymers that may have either natural or synthetic origin [1]. When synthetic polymers are married to polypeptides, the resulting hybrid conjugates are able to synergistically combine the properties of the individual components and overcome their separate limitations. Thus, the peptide component will provide functionality to the conjugate whereas the synthetic polymer component may improve the stability, solubility and biocompatibility of the system. The synthetic polymer can also introduce new properties such as amphiphilic character and heterophase behavior required for self-assembly, and it can even modulate the polypeptide   activity [2]. Particularly, the copolymers made of polypeptides and polyesters constitute a large family of hybrid materials with great interest in the biomaterial field [3]. The excellent complementing properties of these two types of polymers together with their good synthetic accessibility by means of ring-opening polymerization [4,5] made their copolymers to be one of the preferred systems that are today under study.

As monomers, macrolactones stand out as ideal candidates for green polymer chemistry [6]. They are produced from renewable materials and they are susceptible of ring-opening polymerization conducted by different methods specially including that mediated by enzymes. ω-Pentadecenlactone (Gl) and ω-pentadecalactone (PDL) are 16-membered macrolactones (ML) that only differ in the presence of one double bond located in the carbon chain of the former. Both ML are highly hydrophobic compounds that are commercially available because their traditional use in perfumery [7]. PDL has been extensively studied in these two last decades for the synthesis of aliphatic polyesters and copolyesters with high potential as biodegradable and bioresorbable medical materials whereas the interest for Gl has been so far much more contained. Copolymerization of PDL with other lactones constitutes the major approach towards the production of highly hydrophobic polyesters with adjusted thermal and mechanical properties, and it includes a variety of compounds such as L-lactide [8,9], ε-

caprolactone [10-12], *p*-dioxanone [13] δ-valerolactone and γ-butyrolactone [14] among others [15]. It is remarkable that in a good number of cases the copolymerization was accomplished by enzymatic catalysis using Novozyme 435 [10,11,13,15,16]. However a limitation of the polyesters coming from PDL is that they have no functionality other than chain ends. Dove and coworkers used a modified ε-caprolactone, *i.e*. menthide, to introduce side chain functionality into PPDL copolymers, which were able to undergo post-polymerization modification. However, the synthesis of the menthide was long and tedious [17].

The unsaturation present in Gl provides a chemical handle for functionalization. Gl has been homopolymerized in several occasions to produce polyglobalide (PGl), an unsaturated polyester [18] that could then be modified by click reaction to produce cross-linked polymers [19,20] or polypeptide grafted copolymers [21]. However Gl has never been copolymerized with PDL, as far as we know. The work here reported is focused on the copolymerization of Gl and PDL with the final purpose of using the resulting unsaturated copolyesters for preparing amphiphilic hybrid polypeptide-polyester graft copolymers with potential as drug nanocarriers. Several aspects were taken into consideration to justify such a choice. a) An entirely bio-based green system could be built by combining the enzymatic polymerization with the natural origin of all the implied monomers. b) Nothing has been reported on copolymerization of macrolactones, in particular of two macrolactones with the same number of carbons. The crystalline behavior of the PGl-PPDL copolyesters regarding possible isomorphism will be of general interest in the polymer crystallization field. c) The hybrid copolymers built by amino acid grafting of the PGl-PPDL copolyesters will exhibit a great hydrophilic character as a consequence of the combination of the high hydrophobicity provided by the macrolactone counterpart and the highly polar nature inherent to the polypeptide side chain, in special when it is in the charged state. The nanoparticles rendered by these systems should be expected to be well stable due to the occurrence

on interior strong hydrophobic interactions and to be capable of loading charged drugs with good efficiency and releasing it at pH depending rates.

9.2. Results and discussion

9.2.1 Synthesis of PGl-*r*-PDL copolyesters

The route followed for the overall synthesis of the L-Glu-grafted poly(globalide-*random*-pentadecalactone) copolyesters with the L-Glu either protected as benzyl ester (BLG) or with the carboxyl groups in the free form, i.e. $P[(Gl$-g-$BLG_z)_x$-r-$PDL_y]$ and $P[(Gl$-g-$LGA_z)_x$-r-$PDL_y]$, that have been studied in this work, is depicted in Scheme 9.1. Firstly, a series of random copolyesters made of globalide (Gl) and pentadecalactone (PDL), namely $P(PGl_x$-r-$PDL_y)$, covering the whole range of compositions, was prepared by enzymatic ring-opening polymerization (eROP) mediated by *Candida antarctica* Lipase B (CALB) (Novozymes 425). The results obtained in these copolymerizations are shown in Table 9.1. The eROP method, which had been previously used by different authors for the polymerization of both Gl and PDL separately [22-24] has afforded satisfactory results in the copolymerization of these two macrolactones with yields ranging between 75 and 90% and moderate deviations in the copolymer compositions respect to feed compositions. NMR was used for the chemical characterization of the copolymers including composition and chain length. The ^1H and ^{13}C NMR spectra of $P(Gl_{13\%}$-r-$PDL_{87\%})$ are given in Figure F1 of the Annex F associated to this Thesis, and ^1H NMR spectra for the whole series are compared in Figure F2. Number-average molecular weights (M_n) determined by end-group analysis were in the 9000-12,000 g·mol^{-1} range with differences being small and showing no apparent correlation with compositions. Determination of the comonomers distribution along the copolymer chain was not feasible because NMR spectra were scarcely sensitive to sequential effects due to the long distance between ester groups and also exceptionally complex due to the existence of both constitutional and steric isomerism. In fact, the Gl used in this work consisted of a mixture of two monounsaturated isomers

corresponding to the double bond placed at the 11 or 12 positions in a 81/19 ratio with an overall diastereomeric E/Z configuration ratio of 78/22. These ratios were approximately maintained in the PGl-r-PDL copolyesters. Compared ^{1}H NMR spectra of GI and PGI are afforded in Figure F3. Nevertheless, a random distribution may be assumed to be present in these copolymers since that should be expected from the well-known indiscriminate transesterase activity of lipases [25] and is also according with the microstructure generated in the eROP of diverse PPDL copolyesters previously reported [10,11,13,14].
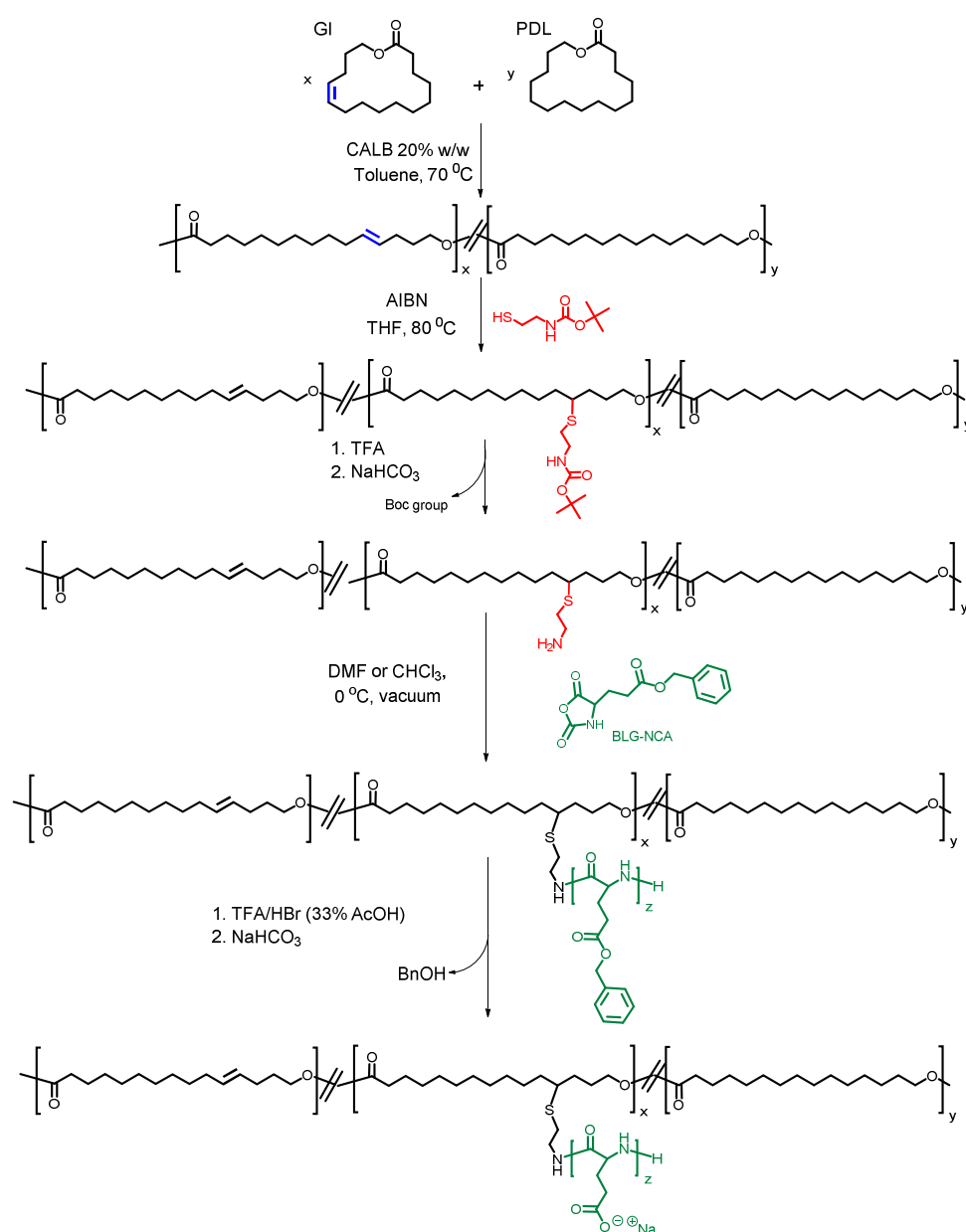
Scheme 9.1. Synthesis of P[(GI$_x$-*co*-PDL$_y$)-*g*-Glu$_y$] copolymers.

Table 9.1. Yield, composition and molecular weight of the P(PDL$_x$-r-Gl$_y$) copolyesters.

Polyester[a]	Yield (%)	Composition[b] (Gl)/(PDL)(mol/mol)		M_n[c] (g·mol^{-1})
		feed	copolymer	
PGl	70	100/0	100/0	9700
P(Gl$_{82}$-r-PDL$_{18}$)	80	90/10	82/18	10,500
P(Gl$_{73}$-r-PDL$_{27}$)	75	70/30	73/27	9450
P(Gl$_{48}$-r-PDL$_{52}$)	88	50/50	48/52	11,900
P(Gl$_{33}$-r-PDL$_{67}$)	80	30/70	33/67	10,650
P(Gl$_{13}$-r-PDL$_{87}$)	90	10/90	13/87	11,760
PPDL	90	0/100	0/100	12,300

[a]Subscripts x and y indicate the %-mole composition of the copolymer in Gl and PDL units, respectively.
[b]%-mole composition of the feed and the resulting copolymer determined by ^{1}H NMR.
[c]Number-average molecular weight of the resulting copolymer determined by end-group ^{1}H NMR analysis.

9.2.2. Thermal properties and crystallization of P(Gl$_x$-r-PDL$_y$) copolyesters

The thermal decomposition behavior of P(Gl$_x$-r-PDL$_y$) copolyesters was examined by TGA within the 20-600 ºC under an inert atmosphere. Their TGA traces and those recorded for the two parent homopolyesters (PGl and PPDL) as well as the respective derivative curves of all them are shown in Figures F4 of the Annex F. Onset and maximum rate decomposition temperatures and remaining weights estimated in these assays are listed in Table 9.2. Approximately the same thermal decomposition pattern was displayed by the copolyesters and the homopolyesters as it is evidenced by the similarity between their derivative curves. In fact, decomposition appears to proceed along two main steps in the 400-500 ºC range with $^{max}T_d$ values closely around those of PGl and PPDL. As it is commonly shared by most of aliphatic polyesters and as it should be largely expected from the high resistance to heat displayed by the parent polymacrolactones, the TGA data collected in this study ascertain the high thermal stability of P(Gl$_x$-r-PDL$_y$) copolyesters as well as their ability to decompose cleanly without hardly leaving residual product.

Table 9.2. Thermal properties of P(Gl$_x$-r-PDL$_y$) copolyesters.

Copolyester	TGA[a]			DSC[b]					
				1st heating		cooling		2nd heating	
	$^o T_d{}^a$ (°C)	$^{max}T_d$ (°C)	R_w (%)	T_m (°C)	ΔH_m (J·g^{-1})	T_c (°C)	ΔH_c (J·g^{-1})	T_m (°C)	ΔH_m (J·g^{-1})
PGI	349	419, 466	4	42	46	17	-31	27	31
P(Gl$_{82}$-r-PDL$_{18}$)	376	417, 466	2	54	55	38	-52	53	56
P(Gl$_{73}$-r-PDL$_{27}$)	387	420, 469	1	65	90	50	-62	66	82
P(Gl$_{48}$-r-PDL$_{52}$)	378	423, 470	1	74	120	57	-80	74	82
P(Gl$_{33}$-r-PDL$_{67}$)	374	431, 469	1	81	135	65	-97	80	92
P(Gl$_{13}$-r-PDL$_{87}$)	381	426, 470	1	90	135	74	-100	90	97
PPDL	396	427, 472	1	95	150	81	-126	95	135

[a]Onset for 5% weight loss ($^o T_d$) and maximum rate ($^{max}T_d$) thermal decomposition temperatures measured by TGA under inert atmosphere. R_w: weight (%) remaining after heating at 600 °C.
[b]Melting (T_m and ΔH_m) and crystallization (T_c and ΔH_c) temperatures and enthalpies measured by DSC.
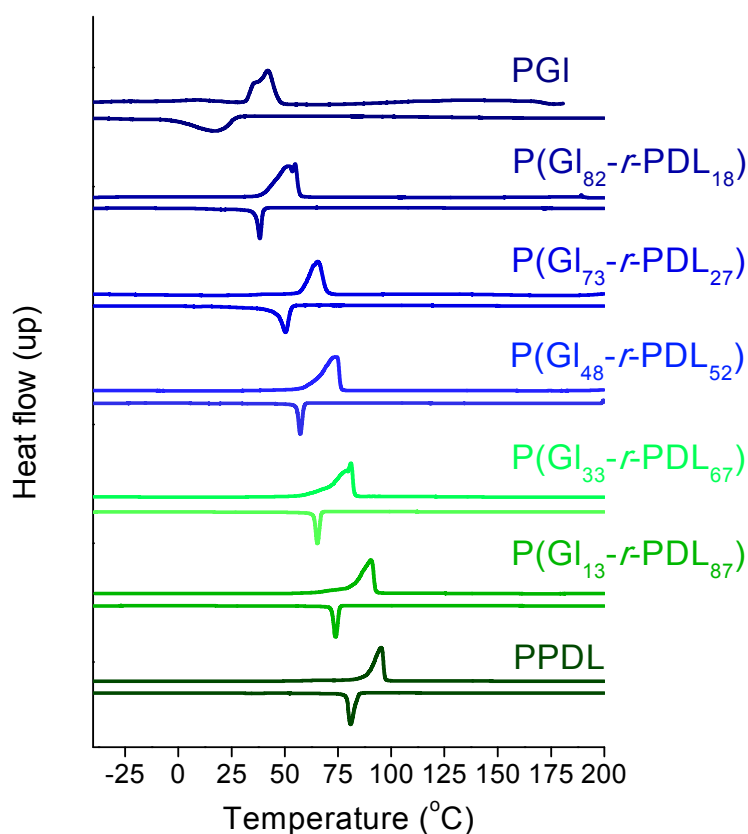
Figure 9.1 DSC traces of P(Gl$_x$-r-PDL$_y$) copolyesters recorded at the first heating and cooling in the -30-200 °C range.

The DSC analysis of the P(Gl$_x$-r-PDL$_y$) copolyesters was performed by recording heating-cooling-heating cycles over -30 °C and 200 °C. The first heating and cooling traces are shown in Figure 9.1 and those recorded at the second heating are

accessible in Figure F5 of the Annex F. The traces recorded for PGI and PPDL displayed melting peaks corresponding to T_m of 42 °C and 95 °C respectively, according to what is recurrently reported for these polymacrolactones. It was noticed however that the peak recorded for PGI was broader and had a much lower associated enthalpy than for PPDL. These features are indicative that PGI is made of more defective crystals and attain lower crystallinity, as it should be expected from the isomeric mixture present in this unsaturated polyester. P(GI$_x$-r-PDL$_y$) copolyesters were all crystalline and showed linearly decreasing melting temperatures as their content in GI increased over the whole composition range (Figure 9.2a). A similar trend was observed for the copolyesters melting temperatures recorded at the second heating with values very close to those registered in the first heating run in spite of that significant supercoolings (around 15-20 °C) were required for crystallization. It is also noteworthy that melting enthalpy displayed a steady increasing when going from PGI to PPDL (Figure 9.2b). Although the trend is by no means even, it indicates that the crystallinity of the copolyesters was not depressed when comonomers were mutually replaced. These results strongly suggest that GL and PDL units must be sharing the same crystal lattice, a prediction that will be supported by the X-diffraction study described below.
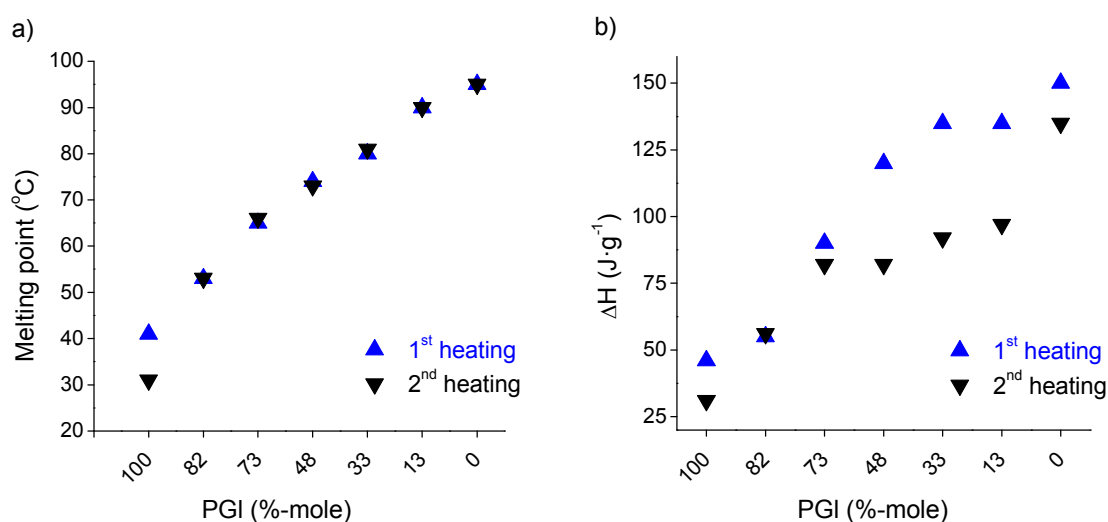
Figure 9.2. Melting temperatures (a) and enthalpies (b) of P(GI$_x$-r-PDL$_y$) copolyesters as a function of their content in PGI units.

9.2.3. XRD of P(Gl$_x$-*r*-PDL$_y$) copolyesters. Isomorphism

Aliphatic polyesters of A-B type tend to crystallize with chains in fully-extended conformation and side-by-side packed in a pseudo-rhombic crystal lattice containing two monomeric units in opposite orientation [26]. Specifically, the PPDL unit cell is described in the literature [27] as monoclinic (P2$_1$ space group) with dimensions: *a* = 0.749 nm, *b* = 0.5034 nm, *c* (chain axis) = 2,00 nm and α = 90.06°. The WAXS pattern of PPDL is characterized by two strong reflections at 0.41 nm and 0.37 nm arising from 110 and 200 interplanar distances, respectively, in addition to a weak reflection at 1.95 nm corresponding to the length of the repeating distance along the polymer chain. The crystal structure of globalide has not been determined yet but it has been suggested to be very close to that of PPDL since the dominating features of the powder diffraction patterns are shared by both polyesters [18].

In this work, the XRD study of P(Gl$_x$-*r*-PDL$_y$) copolyesters has been performed using synchrotron radiation on powder samples that were subjected to heating-cooling cycles within the 0-120 °C range. By this means the scattering produced in the wide and small angles regions (WAXS and SAXS) could be simultaneously recorded in real time. As an illustrative example, the evolution of the intensity profiles registered for P(Gl$_{82}$-*r*-PDL$_{18}$) as a function of temperature is shown in Figure 9.3, and all those obtained for the other copolyesters as well as for PPDL and PGl, are afforded in Figures F6 and F7 of the Annex F. The Bragg spacings measured at 0 °C (both before and after heating) and at 120 °C are collected in Table 9.3. The two sharp peaks observed in WAXS for PPDL at low temperature (110 and 200) are in full agreement with data previously reported for this polyester [27]. Both their disappearance at temperatures above 90 °C and their almost total recovery upon cooling at around 70-80 °C, are clear evidences of the reversible melting-crystallization transition characteristic of PPDL. The broad peak at 0.46 nm that appeared after melting is the characteristic scattering produced by polyesters in the disordered state.

Table 9.3 X-ray diffraction spacings (nm) for P(GI$_x$-r-PDL$_y$) copolyesters at different temperatures.

Copolyester	0 °C[a]		120 °C		0 °C[b]	
	SAXS	WAXS	SAXS	WAXS	SAXS	WAXS
PGI	17.4, 1.9	0.41, 0.37	-	0.46	21.6, 5.7, 1.9	0.41, 0.37
P(GI$_{82}$-r-PDL$_{18}$)	13.0, 6.5, 1.9	0.41, 0.37	-	0.46	20.0, 1.9	0.41, 0.37
P(GI$_{73}$-r-PDL$_{27}$)	13.0, 6.5, 1.9	0.41, 0.37	-	0.46	20.0, 1.9	0.41, 0.37
P(GI$_{48}$-r-PDL$_{52}$)	1.9	0.41, 0.37	-	0.46	1.9	
P(GI$_{33}$-r-PDL$_{67}$)	13.0, 6.5, 1.9	0.41, 0.37	-	0.46	20.0, 7.5, 1.9	0.41, 0.37
P(GI$_{13}$-r-PDL$_{87}$)	9.5, 4.7, 1.9	0.41, 0.37	-	0.46	20.0. 7.3, 1.9	0.41, 0.37
PPDL	1.9	0.41, 0.37	-	0.46		0.41, 0.37

[a]Data recorded from the original sample.
[b]Data recorded from the cooled sample after being heated at 120 °C.

The SAXS profiles of PPDL and PGI have in common the reflection at 1.9-2.0 nm indexed as 001 and corresponding to the repeat of the polyester chain in zigzag conformation with a backbone C-C and C-O bonds average projection length of ~0.125 nm. It seems that the small length shortening that could be expected for the GI unit (around 0.05 nm) due to the presence of the double bond cannot be distinguished in these diffractograms. Furthermore, it can be inferred from these results that the ~20% of *Z*-stereoisomers present in PGI, must have been segregated from the crystal lattice. Nevertheless the fact that the 001 peak becomes significantly broad for PGI, which is demonstrative of the fluctuation of its associated spacing, could be taken as due to the coexistence of homogeneous crystallites made of *E* and *Z* stereoisomers. A comparative plot of the 001 signals produced by every polyester suitably enlarged to show their differences in detail has been included in the Annex F (Figure F8). Other reflections appearing for both PPDL and PGI in the 5-20 nm range of the SAXS region must be related to crystallite size and they have found to be different not only for the two polyesters but also for samples of the same polyester with different thermal history. The precise understanding of these subtle reflections, which might arise both from copolyester crystallites with different PDL/GI composition or from crystallites made of different E/Z stereoisomers, is very challenging. A study in depth supported by further

experimentation, which is clearly out of the scope of this paper, would be required to attain a rational interpretation of the scattering associated to crystallite thickness.

The plots shown in Figure 9.3 for P(Gl$_{82}$-r-PDL$_{18}$) may be taken as representative of that is observed for the whole copolyester series. Main features revealed by these plots are the following: a) Characteristic reflections 110 and 200 with spacings at 0.41 nm and 0.37 nm respectively are dominating the WAXS profiles at low temperatures. These reflections disappeared upon heating just above the melting temperature of the polyester and the broad peak at 0.46 nm characteristic of amorphous material came out instead. After cooling, both reflections reappeared with lower intensity. b) The 1.9-2.0 nm reflection observed in SAXS (indexed as 001) showed the same response to heating as the 110 and 200 reflections with the difference that it was more hardly recovery after cooling. The intensity and breadth of this reflection was depending on the copolymer composition. c) A signal around 13 nm and its second order 6.5 nm were present in the profiles at low temperatures to vanish at melting. After cooling a new signal with spacing around 20 nm appeared.
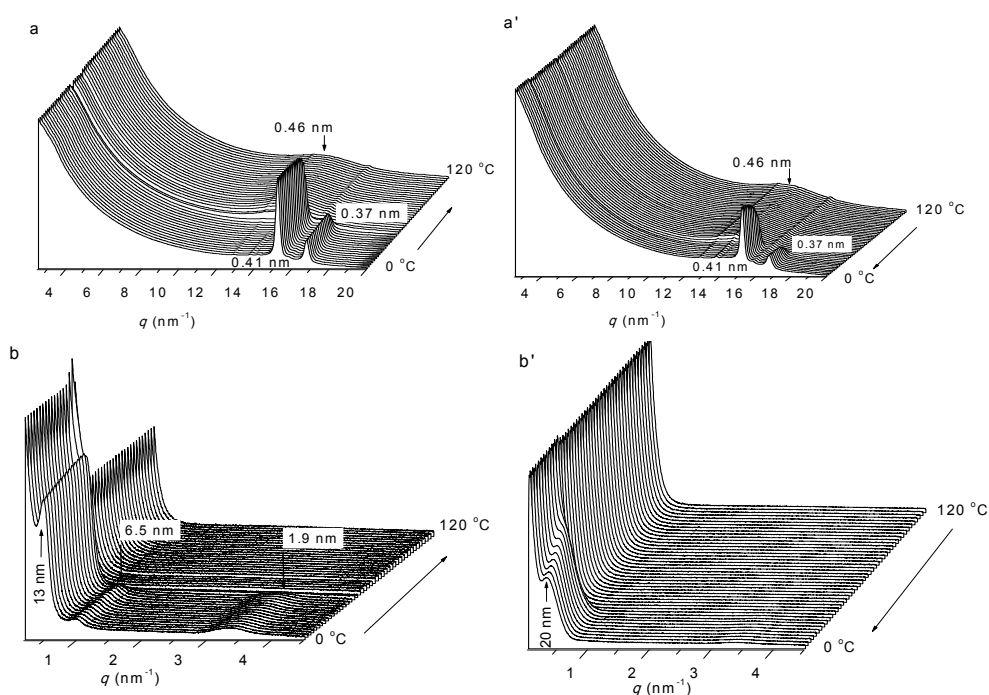
Figure 9.3 Evolution of the X-ray diffraction profiles recorded for P(Gl$_{82}$-r-PDL$_{18}$) at heating and cooling over the 0-120 °C range in the WAXS (a, a') and SAXS (b,b') regions.

The conclusions inferred from the XRD study is that P(Gl$_x$-r-PDL$_y$) copolyesters crystallize following the side-by-side chain packing arrangement commonly adopted by both PPDL and PGl, and that differences with homopolyesters are circumscribed to the relative azimuthal alignment of the chains. Such differences are probably due to some chain misalignment motivated by the uneven presence of the double bond throughout the lattice. The weakening or even full disappearance of the 001 reflection is reported as a clear evidence of cocrystallization of random copolyesters made of monomeric units of different length as it has been reported for the case of P(PDL-r-CL) [11]. Since the degree of azimuthal misalignment in these copolyesters is dependent on the PDL/Gl ratio, it does make sense that different crystallite thicknesses are observed for different copolymer compositions. These XRD results are in full agreement with DSC results and combination of both is taken as demonstrative of the occurrence of isomorphism in the crystallization of P(Gl$_x$-r-PDL$_y$) copolyesters.

9.2.4 Grafting of P(Gl$_x$-r-PDL$_y$) copolyesters with glutamic acid units: Synthesis of P[(Gl$_x$-r-PDL$_y$)-g-(LGlu)$_z$] copolymers

In order to make the P(Gl$_x$-r-PDL$_y$) susceptible to grafting, amino functionalities were inserted in the Gl units by thiol-ene click reaction with 2(Boc-amino)ethanethiol (BAET) followed by removal of the Boc group, as it is depicted in Scheme 9.1. This method has been proven before to be effective for the preparation of polyaminated PGl used as macroinitiator in its grafting with other amino acids by NCA ROP [21,28]. The evolution of the click reaction was followed by ^{1}H NMR (spectra are available in Figure F9) that allowed determining the coupling efficiency of BAET to the copolyester, which was found to be 90% and 50% for P[(Gl$_{13}$-r-PDL$_{87}$) and P[(Gl$_{48}$-r-PDL$_{52}$), respectively.

The amino-functionalized P(Gl$_x$-r-PDL$_y$) copolyesters were then grafted by ROP of the BLG-NCA initiated by the amino groups with an amino conversion close to 100%. The GPC analysis of the grafted copolymers provided unimodal chromatograms (Figure F10) that ascertained the achievement of the grafting reaction and the absence

of contaminant free homopolypeptide. After acidic treatment of P[(Gl$_x$-r-PDL$_y$)-g-(BLG)$_z$] with a TFA/HBr mixture, the COOH functionality of glutamic acid was readily regenerated to render P[(Gl$_x$-r-PDL$_y$)-g-(LGlu)$_z$] copolymers which were then duly characterized by NMR. The ^{1}H NMR spectra of P[(Gl$_{13}$-r-PDL$_{87}$)-g-(BLG)$_{10}$] and P[(Gl$_{13}$-r-PDL$_{87}$)-g-(LGA)$_{10}$] are shown in Figure 9.4 for illustrative purposes, and those registered from P[(Gl$_{48}$-r-PDL$_{52}$)-g-(BLG)$_2$] and P[(Gl$_{48}$-r-PDL$_{52}$)-g-(LGA)$_2$] are included in the Annex F as Figure F11. The area comparison of the 5.15 ppm signal arising from BLG-CH$_2$ with any of the signals characteristic of the copolyester (Figure 9.4a) demonstrated the success attained in the grafting reaction and allowed a precise estimation of the average length of the polypeptide chains grafted on the polyester. The total absence of aromatic signals in the spectra of the deprotected copolymers, which is indicated by the disappearance of the 5.15 ppm signal, was taken as demonstrative that COOH groups had been fully recovered (Figure 9.4b). Compositions, yields and average molecular weights of the grafted copolymers are collected in Table 9.4.

Table 9.4 Synthesis of P[(Gl$_x$-r-PDL$_y$)-g-(LGlu)$_z$] copolymers: Composition and molecular weight.

Copolymer[a]	Gl-BAET[b] (%)	Copolymer[c] Gl/PDL/Gl-LGlu	Side chain length[d] (LGlu units)	Yield[e] (%)	M_n[f] (g·mol^{-1})
P[(Gl$_{13}$-r-PDL$_{87}$)-g-(BLG)$_{10}$]	90	6/38/56	10	93	27,700
P[(Gl$_{48}$-r-PDL$_{52}$)-g-(BLG)$_2$]	50	24/26/49	2	85	16,700
P[(Gl$_{13}$-r-PDL$_{87}$)-g-(LGA)$_{10}$]	90	6/38/56	10	70	21,400
P[(Gl$_{48}$-r-PDL$_{52}$)-g-(LGA)$_2$]	50	24/26/49	2	74	15,100

[a]Subscripts for Gl (including both modified and unmodified) and PDL are their molar percentages in the copolymer. Subscripts for BLG and LGA represent the average number of such units in the grafting side chains.

[b]Molar percentage of amino-functionalized Gl units estimated by ^{1}H NMR Calculated by comparing peak areas that correspond to the double bond in PGl with the peak areas representative of methylene group adjacent to hydroxyl terminal group.

[c]Copolymer composition (%-mole) with explicit content in PDL and both modified and unmodified Gl units.

[d]Average number of L-Glu (either BLG or LGA) units in the side chains of the grafted copolyesters.

[e]Yield of the grafting reaction.

[f]Number-average molecular weight of the copolymer determined by ^{1}H NMR.
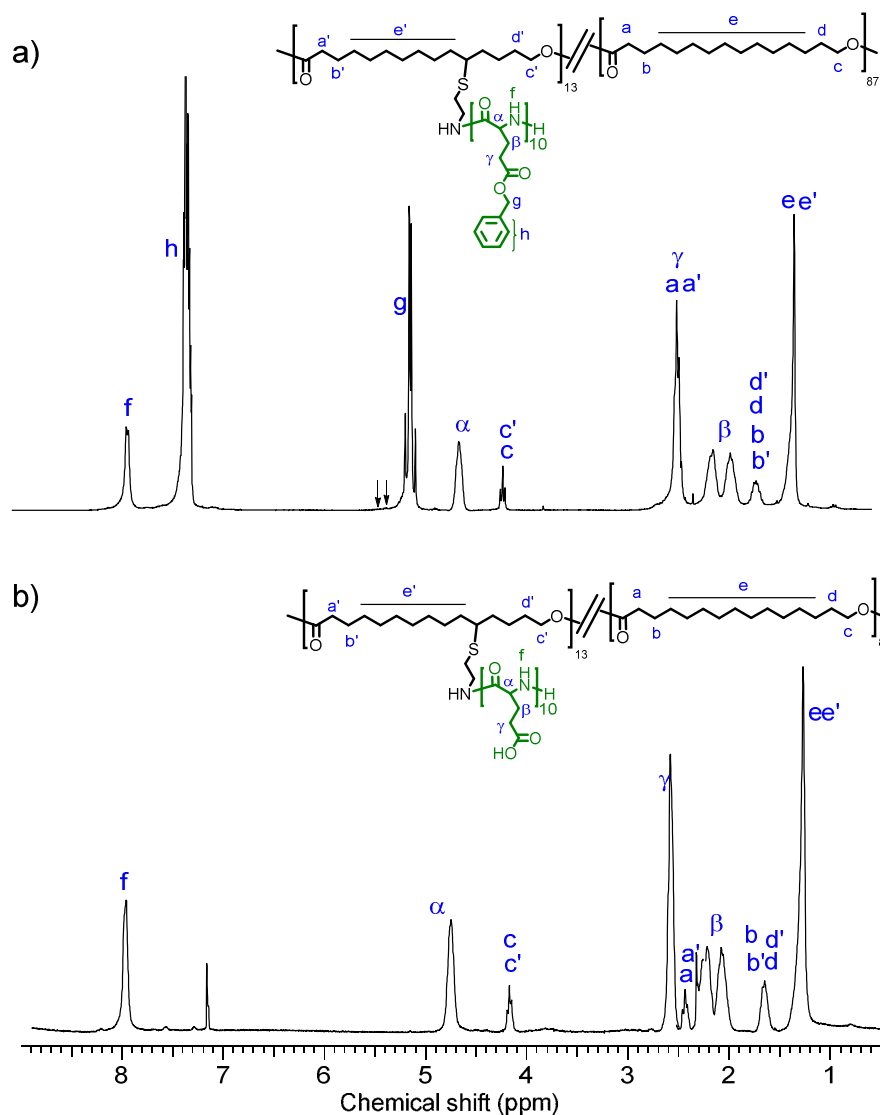
Figure 9.4. ^{1}H NMR spectra of P[(GI$_{13}$-r-PDL$_{87}$)-g-(BLG)$_{10}$] and P[(GI$_{13}$-r-PDL$_{87}$)-g-(LGA)$_{10}$] copolymers. Arrows point to signals arising from the CH=CH protons contained in the 1% of GI units present in these copolymers. Simplificar formula eliminando el residuo de GI1%

9.2.5. Thermal properties and solid-state structure of P[(GI$_x$-r-PDL$_y$)-g-(LGlu)$_z$] copolymers.

Thermal decomposition and transition temperatures of P[(GI$_x$-r-PDL$_y$)-g-(LGlu)$_z$] copolymers measured by TGA and DSC, respectively, are collected in Table 9.5. The TGA traces of the four grafted copolymers along with their respective derivative curves are displayed in Figure F12 of the Annex F. Comparison of TGA results with those obtained for the P(GI$_x$-r-PDL$_y$) copolyesters (Table 9.2) reveals a noticeable decrease

in thermal stability as a consequence of grafting. Furthermore, the decomposition processes became more complexes and the amount of residue left after heating at 600 ºC was considerable, in particular as far as the deprotected copolymers were concerned. These results are in line with those previously obtained for other amino acid-grafted polymacrolactones copolymers [21,28] and confirm the deleterious effect of the polypeptide on the thermal stability of the polyester.

The DSC traces recorded at heating and cooling for the four P[(Gl$_x$-r-PDL$_y$)-g-(LGlu)$_z$] together with those recorded for the PBLG$_{50}$ and PLGA$_{50}$ polypeptides are shown in Figure 9.5. Melting and crystallization temperatures and enthalpies measured by DSC are compared in Table 9.4. Although grafting made to decrease significantly the initial crystallinity of the P(Gl$_x$-r-PDL$_y$) copolyesters, melting and crystallization peaks associated to the presence of random Gl-PDL segments were still observed for

Table 9.5. Thermal properties of P[(Gl$_x$-r-PDL$_y$)-g-(LGlu)$_z$] copolymers.

Copolymer	TGA[a]				DCS[b]								
					first heating					cooling		second heating	
	$^o T_d$ ºC	$^{max}T_d$ ºC	R_w %		T_m ºC	ΔH J·g^{-1}	T_{LC}[c] ºC	ΔH J·g^{-1}		T_c ºC	ΔH J·g^{-1}	T_m ºC	ΔH J·g^{-1}
P[(Gl$_{13}$-r-PDL$_{87}$)-g-(BLG)$_{10}$]	235	230-280	18		52,76	4	115	2		34	-9	75	5
P[(Gl$_{48}$-r-PDL$_{52}$)-g-(BLG)$_2$]	220	290-320	12		68	21	-	-		43	-31	44	26
P[(Gl$_{13}$-r-PDL$_{87}$)-g-(LGA)$_{10}$]	285	310-450	42		80-95	9	-	-		58	-2	83	1
P[(Gl$_{48}$-r-PDL$_{52}$)-g-(LGA)$_2$]	215	270-400	29		72	18	-	-		48	-11	56	10

[a]Onset temperature for 5% of weight loss ($^o T_d$), maximum rate ($^{max}T_d$) decomposition temperature and remaining weight (R_w) after heating at 600 ºC.
[b]Glass transition (T_g), melting (T_m and ΔH_m) and crystallization (T_c and ΔH_c) temperatures and enthalpies measured by DSC.
[c]T_{LC} is the temperature for the structural transition undergone by the polypeptide hexagonal phase.

the four grafted copolymers. What it is particularly meaningful however is the presence of a broad endotherm spread over the 100-130 ºC range (centered about 115 ºC) on the first heating trace recorded from P[(Gl$_{13}$-r-PDL$_{87}$)-g-(BLG)$_{10}$]. Noticeably the DSC trace of PBLG$_{50}$ also showed an endothermal peak at 120 ºC whereas no heat exchanged at all was detected for PLGA$_{50}$. Such a peak is commonly interpreted in the

literature as due to the irreversible conformational transition taking place in the PBLG α-helices [29-31].
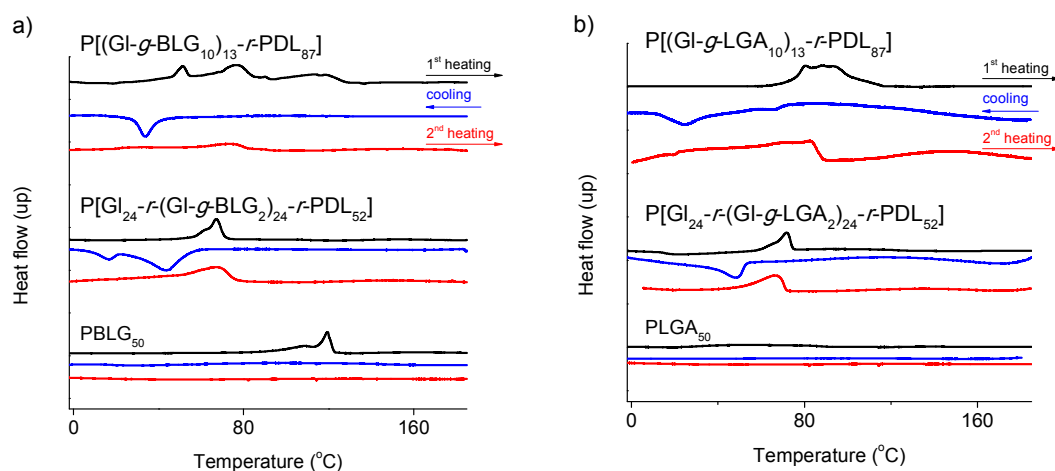
Figure 9.5. First heating and cooling DSC traces of P[(Gl$_x$-r-PDL$_y$)-g-(LGlu)$_z$] copolymers.

The 1800-1500 cm^{-1} region of the FTIR spectra recorded from P[(Gl$_x$-r-PDL$_y$)-g-(LGlu)$_z$] copolymers in the powder form are shown in Figure 9.6. The Amide I and Amide II bands appearing respectively at 1655 cm^{-1} and 1550 cm^{-1} on the spectra of both P[(Gl$_{13}$-r-PDL$_{87}$)-g-(BLG)$_{10}$] and PBLG$_{50}$ with strong intensity and the complete absence of absorption around 1650 cm^{-1} are firm indications of the existence of the polypeptide in α-helix conformation exclusively [32,33]. On the contrary, the spectra produced by P[(Gl$_{48}$-r-PDL$_{52}$)-g-(BLG)$_2$] shows a noticeable peak at 1630 cm^{-1} that reveals the presence of a considerable amount of β-form. The spectra of the unprotected copolymers showed broad amide bands more according with the polypeptide in a disordered state although the band at 1620 cm^{-1} observed in the spectrum of P[(Gl$_{48}$-r-PDL$_{52}$)-g-(LGA)$_2$] reveals the presence of β-form in this copolymer. The indications provided by the FTIR spectra of P[(Gl$_x$-r-PDL$_y$)-g-(LGlu)$_z$] are in good agreement with expectations, *i.e.* the preference for the α-helical conformation vs the β-sheet arrangement in polypeptides is favored by longer amino acid sequences but it becomes unstable in the presence of ionic charges [34,35]. The effect of temperature on the polypeptide conformation was examined for the P[(Gl$_{13}$-r-

PDL$_{87}$)-*g*-(BLG)$_{10}$] and P[(Gl$_{48}$-*r*-PDL$_{52}$)-*g*-(BLG)$_2$] copolymers in the 20-200 °C (spectra are reproduced in Figure F13 of Annex F). No absorption changes were apparent for neither of the two cases indicating that α-helix/β-sheet interconversion or disruption into the random coil state did not take place over such range of temperatures. This is in full agreement with the high stability of the two typical conformational forms of polypeptides, which are known to resist temperatures up to well above 200 °C [36,37].
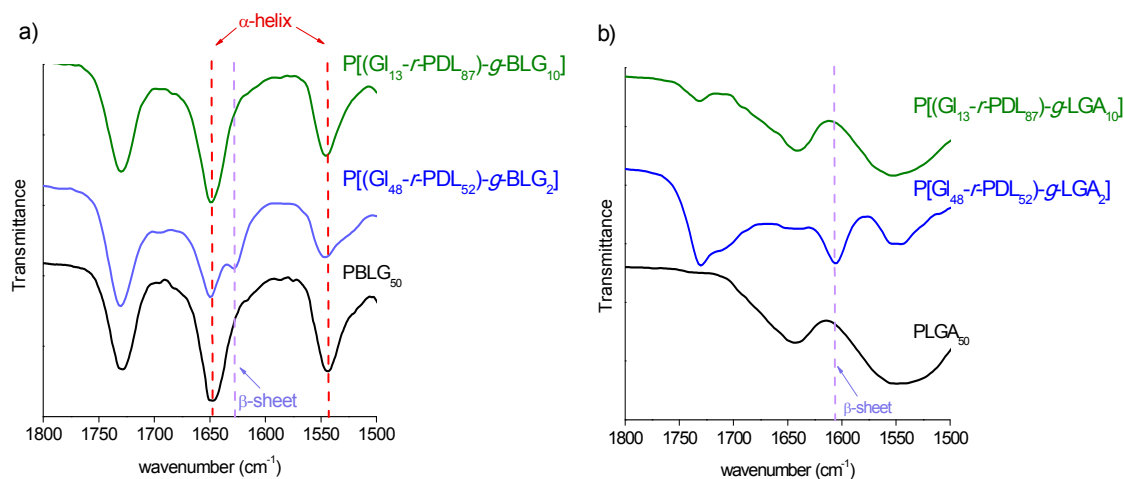
Figure 9.6. FTIR spectra of P[(Gl$_x$-*r*-PDL$_y$)-*g*-(LGlu)$_z$] copolymers.

WAXS and SAXS profiles of the P[(Gl$_{13}$-*r*-PDL$_{87}$)-*g*-(BLG)$_{10}$] copolymer recorded at real time over the 10-200 °C range are shown in Figure 9.7. The 0.41 and 0.37 nm peaks characteristic of the crystal structure adopted by P(Gl$_x$-*r*-PDL$_y$) copolyesters are present in the low temperature WAXS profiles registered at both heating and cooling. As expected, these peaks were absent at temperatures above melting/crystallization and therein replaced by the broad peak at 0.46 nm arising from the disordered state. Additionally a set of peaks corresponding to lattice spacings roughly related by the 1:√3:2 ratio, (*i.e.* 13.5, 0.75, 0,65 nm) was present in the SAXS. As it has been reported in several previous occasions [38-40], such diffraction pattern is indicative of the occurrence of two-dimensional hexagonal packing of the PBLG α-helices with a diameter of approximately 1.5 nm. A detailed inspection of the variation of such pattern with temperature revealed that the all three peaks were intensified at high temperatures

to practically disappear upon cooling below the temperature at which the polyester crystallized. This behavior is in agreement with both DSC and FTIR results commented above and it has been observed before for block copolymers made of PPDL and PBLG [21,38]. Such a behavior suggests that melting of the polyester phase favored the building of the polypeptide columnar phase. Results obtained in a similar analysis carried out on P[(Gl$_{48}$-r-PDL$_{52}$)-g-(BLG)$_2$] are available in Figure F14 of the Annex F. In this case, the low temperature profiles showed also the diffraction peaks characteristic of the crystallized polyester and their response to heating was also similar but they were not recovery after cooling. Moreover the diffraction peaks expected to arise from the columnar phase were only hardly detected at high temperature and they disappeared almost completely at low temperature. On the other hand the XRD analysis of the deprotected materials contained the 0.41 nm and 0.37 nm peaks as the only meaningful features. All other signals detected in these profiles were very weak and of difficult interpretation (Figure F15).
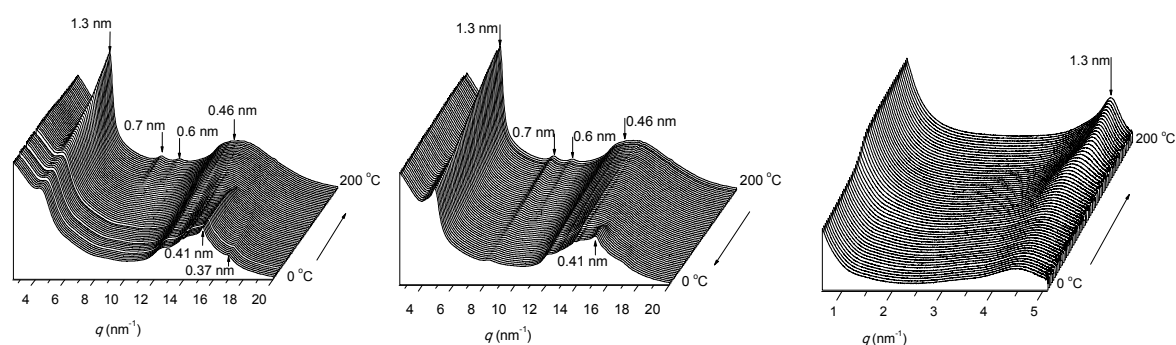
Figure 9.7. Evolution of the WAXS (heating and cooling) and SAXS (heating) profiles recorded from P[(Gl$_{13}$-r-PDL$_{87}$)-g-(BLG)$_{10}$] copolymer over the 0-200 ^{o}C range.

9.2.6. Self-assembly of P[(Gl$_x$-r-PDL$_y$)-g-(LGlu)$_z$] copolymers in aqueous media

The chemical form in which the amino acid units are found in the P[(Gl$_x$-r-PDL$_y$)-g-(LGlu)$_z$], *i.e.* with the carboxyl group free or in the ester form, decided the solubility properties of these copolyesters, and consequently determined the method that has to be used for promoting their self-assembly into nanoparticles. Thus the emulsion-

solvent evaporation method was applied to the non-water soluble P[(Gl$_{13}$-*r*-PDL$_{87}$)-*g*-(BLG)$_{10}$] copolymer to obtain nanoparticles of average diameter around 250 nm with moderate dispersity and displaying a zeta potential of -3.75 mV. The SEM analysis of these nanoparticles revealed that they have a round shape and are well delineate without show apparent aggregation (Figure 9.8).
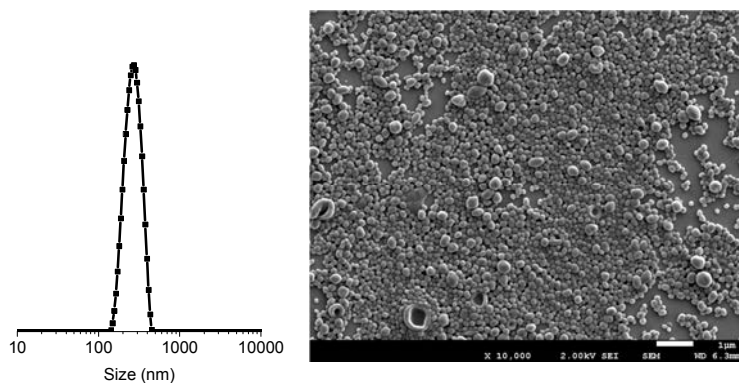
Figure. 9.8. DLS profile and SEM images of nanoparticles made of P[(Gl$_{13}$-*r*-PDL$_{87}$)-*g*-(BLG)$_{10}$] copolymer. Additional SEM images are available in Figure F16 of Annex F.

Deprotection of the COOH functionalities of P[(Gl$_{13}$-*r*-PDL$_{87}$)-*g*-(BLG)$_{10}$] led to the strongly amphiphilic and water-soluble P[(Gl$_{13}$-*r*-PDL$_{87}$)-*g*-(LGA)$_{10}$] copolymer. The emulsion-solvent evaporation method successfully used with the protected copolymer was not applicable after deprotection due to the non-solubility of the carboxylic copolymer in the usual volatile solvents required for preparing the organic solution. Conversely, when this copolymer was dissolved in water at concentrations above 0.5 mg·mL^{-1} it became spontaneously self-organized to form micelle-like objects as it was revealed by the DLS analysis. The critical micelle concentration (*cmc*) of P[(Gl$_{13}$-*r*-PDL$_{87}$)-*g*-(LGA)$_{10}$] measured by this technique was 0.15 mg·mL^{-1}. The micelle size increased with copolymer concentration with average diameter values ranging between 200 and 600 nm to become bimodal at 3.0 mg·mL^{-1} (Figure F17 of the Annex). The Z-potential of these micelles was around 34 mV with negative sign as it should be expected for nanoparticles containing carboxylate groups that are presumably located on the particle surface.

DOX is a well-known amphiphilic drug that is commonly used in cancer therapy. It contains an amino group attached to the sugar moiety that becomes positively charged at pH below 5 (Figure F18 in Annex F). DOX hydrochloride (DOX·HCl) has been used in several occasions to test the drug loading capacity of negatively charged nanoparticles made of carboxylic polymers able to interact electrostatically with the NH$_3^+$ group [41-46].   To assess the potential of P[(Gl$_{13}$-r-PDL$_{87}$)-g-(LGA)$_{10}$] as nanocarrier, it was mixed with DOX·HCl in water at different LGA/drug molar ratios (1:0.4, 1:0.15 and 1:0.07) and the resulting DOX-loaded micelles examined by DLS. The results found for a copolymer concentration of 1.25 mg·mL^{-1} and 3 mg·mL^{-1} a LGA/drug ratio of 1:0.4 are shown in Figure 9.9.
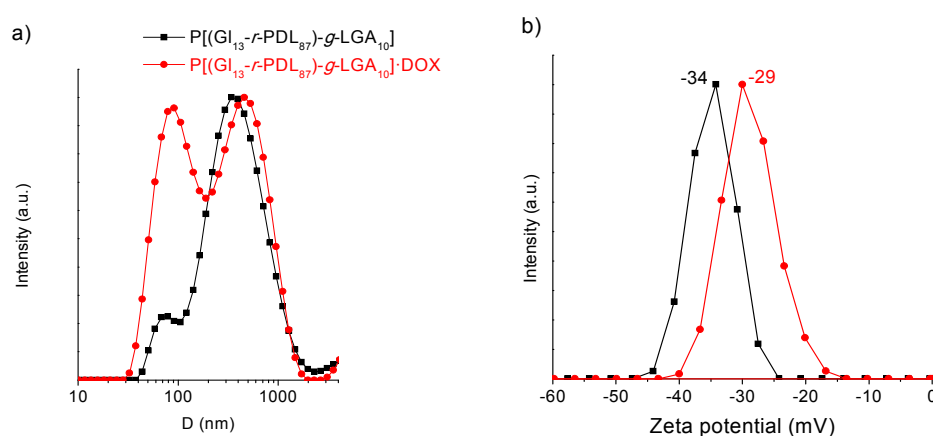
Figure 9.9. DLS profiles (a) and zeta potential (b) of the P[(Gl$_{13}$-r-PDL$_{87}$)-g-(LGA)$_{10}$] copolymer and the P[(Gl$_{13}$-r-PDL$_{87}$)-g-(LGA)$_{10}$] ·DOX conjugate.

The copolymer particles without DOX showed a practically monomodal distribution of sizes with an average diameter of 250 nm. The DLS of the DOX loaded particles revealed instead a bimodal distribution of sizes with average diameters of about 80 and 400 nm, respectively. As expected, the negative zeta potential of the particles decreased upon loading as a consequence of the partial neutralization of the copolymer negative charge that takes place by interaction with DOX.The suitability of P[(Gl$_{13}$-r-PDL$_{87}$)-g-(LGA)$_{10}$] for DOX loading was quantified by estimating the Drug-Loading-Eficiency (DLE) and Drug-Loading-Content (DLC) for the LGA/drug molar ratios tested in this study. The bar plot in Figure 9.10a shows the DLE and DLC

parameters values estimated for the three cases. Both parameters increased with the increasing amount of added DOX to attain values of 66% and 21% respectively for the LGA:drug ratio of 2.5, which was the lowest ratio assayed. This system was in fact the chosen one for evaluating the ability of P[(Gl$_{13}$-r-PDL$_{87}$)-g-(LGA)$_{10}$]·DOX to deliver the drug as well as to assess their response to pH changes. The DOX releasing profiles obtained upon incubation of this conjugate at pH 4.2 and 7.4 are compared in Figure 9.10b. In both cases, DOX was delivered following an asymptotic trace without burst that confirms that all the loaded DOX was chemically attached to the copolymer. The maximum amount of delivered DOX under neutral conditions was about 60% and it was attained after one day of incubation. On the other hand, more than 95% of DOX was released in 10 h when the loaded particles were incubated at pH 4.2. The observed differences must be attributed to the notable decrease in the ionization degree of the LGA moieties that is produced at acidic pH with the subsequent disruption of the copolymer-drug electrostatic interactions.
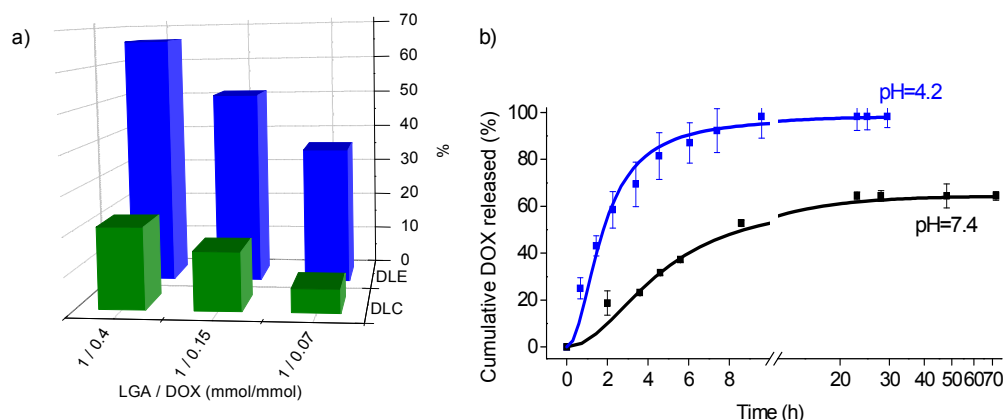
Figure 9.10. (a) DLE and DLC of P[(Gl$_{13}$-r-PDL$_{87}$)-g-(LGA)$_{10}$]·DOX at different LGA/DOX ratios. (b) Cumulative releasing profiles of DOX from the at the two indicated pHs. The data presented are means of ±SD (n=3).

9.3. Conclusions

Random copolymacrolactones made of globalide (Gl) and pentadecalactone (PDL) and covering the whole range of compositions were successfully prepared by enzymatic ROP. These copolyesters were crystalline for any composition and able to recrystallize from the melt. Their melting temperatures increased almost linearly with

the content in PDL units, and their crystallinity was fairly well maintained over the whole range of compositions. The combined WAXS-SAXS results showed that homopolyesters PGL and PPDL adopt the same pseudo-rhombic crystal lattice with identical lateral dimensions and differing only in the monomeric length, which is about 0.1 nm shorter in the former. The copolyesters were found to share the same crystal structure for any composition with tiny differences in the axial repeat. The outstanding conclusion drawn from this combined thermal-diffraction study is that PGl-*r*-PPDL cocrystallized with the two comonomeric units being isomorphically replaced within the crystal lattice, a property that has been found so far only for a few aliphatic copolyesters and never for copolymacrolactones.

Amino acid grafting of the PGl-*r*-PPDL copolyesters has been satisfactorily performed by ROP of BLG-NCA initiated by amino functions previously inserted in the Gl units. The benzyl protecting group could be then readily removed to produce strongly amphiphilic copolyesters bearing free carboxyl groups in the side chains. Both the amount of grafted Gl units as well as the average length of the grafting polyglutamate chains was precisely controlled, and copolymers displaying different water solubility could be therefore prepared. Neutral non-water soluble copolymers were able to self-assemble approximately spherical nanoparticles of 200-300 nm in average diameter. The water-soluble copolymers bearing polyglutamic side chains produced micelles that were able to load fair amounts of DOX drug with high capturing efficiency. Electrostatic ammonium-carboxylate interactions were responsible for the good loading capacity exhibited by the grafted copolymer, and also for the remarkable changes in the drug delivery profile displayed by the DOX loaded micelles when incubated in aqueous medium at different pH's.

9.4 References

[1]   C. Deng, J. Wu, R. Cheng, F. Meng, H.A. Klok, Z. Zhong, Functional polypeptide and hybrid materials: Precision synthesis via α-amino acid *N*-carboxyanhydride

polymerization and emerging biomedical applications, Prog. Polym. Sci. 39 (2014) 330–364.

[2]   L.A. Canalle, D.W.P.M. Löwik, J.C.M. van Hest, Polypeptide–polymer bioconjugates, Chem. Soc. Rev. 39 (2010) 329–353.

[3]   S. Dehn, R. Chapman, K.A. Jolliffe, S. Perrier, Synthetic strategies for the design of peptide/polymer conjugates, Polym. Rev. 51 (2011) 214–234.

[4]   A.C. Albertsson, I.K. Varma, Recent developments in ring opening polymerization of lactones for biomedical applications, Biomacromolecules 4 (2003) 1466–1486.

[5]   H.R. Kricheldorf, Polypeptides and 100 Years of Chemistry of α-amino acid *N*-carboxyanhydrides, Angew. Chemie Int. Ed. 45 (2006) 5752–5784.

[6]   J.A. Wilson, Z. Ates, R.L. Pflughaupt, A.P. Dove, A. Heise, Polymers from macrolactones: From pheromones to functional materials, Prog. Polym. Sci. 91 (2019) 29–50.

[7]   Kraft P, Bajgrowicz JA, Denis C, Frater G. Odds and trends: recent developments in the chemistry of odorants. Angew. Chem. Int. Ed. 2000;39:2980–3010

[8]   R. Todd, S. Tempelaar, G. Lo Re, S. Spinella, S.A. McCallum, R.A. Gross, J.-M. Raquez, P. Dubois, Poly(ω-pentadecalactone)-*b*-poly(L-lactide) block copolymers via organic-catalyzed ring opening polymerization and potential applications, ACS Macro Lett. 4 (2015) 408–411.

[9]   V. Ladelta, J.D. Kim, P. Bilalis, Y. Gnanou, N. Hadjichristidis, Block copolymers of macrolactones/small lactones by a "catalyst-switch" organocatalytic strategy. thermal properties and phase behavior, Macromolecules 51 (2018) 2428–2436.

[10]   C. Ulker, Y. Guvenilir, Enzymatic synthesis and characterization of biodegradable poly(ω-pentadecalactone-*co*-ε-caprolactone) copolymers, J. Renew. Mater. 6 (2018) 591–598.

[11]   G. Ceccorulli, M. Scandola, A. Kumar, B. Kalra, R.A. Gross, cocrystallization of random copolymers of ω-pentadecalactone and ε-caprolactone synthesized by lipase catalysis, Biomacromolecules 6 (2005) 902–907.

[12] M. Bouyahyi, M.P.F. Pepels, A. Heise, R. Duchateau, ω-Pentandecalactone polymerization and ω-pentadecalactone/ε-caprolactone copolymerization reactions using organic catalysts, Macromolecules 45 (2012) 3356–3366.

[13] Z. Jiang, H. Azim, R.A. Gross, M.L. Focarete, M. Scandola, Lipase-catalyzed copolymerization of ω-pentadecalactone with *p*-dioxanone and characterization of copolymer thermal and crystalline properties, Biomacromolecules 8 (2007) 2262–2269.

[14] P. Walther, S. Naumann, N -Heterocyclic Olefin-based (co)polymerization of a challenging monomer: homopolymerization of ω-pentadecalactone and its copolymers with γ-butyrolactone, δ-valerolactone, and ε-caprolactone, Macromolecules 50 (2017) 8406–8416.

[15] Y. Xiao, J. Pan, D. Wang, A. Heise, M. Lang, Chemo-enzymatic synthesis of poly(4-piperidine lactone-*b*-ω-pentadecalactone) block copolymers as biomaterials with antibacterial properties, Biomacromolecules 19 (2018) 2673–2681.

[16] B. Kalra, A. Kumar, R.A. Gross, M. Baiardo, M. Scandola, Chemoenzymatic synthesis of new brush copolymers comprising poly(ω-pentadecalactone) with unusual thermal and crystalline properties, Macromolecules 37 (2004) 1243–1250.

[17] J.A. Wilson, S.A. Hopkins, P.M. Wright, A.P. Dove, Synthesis and postpolymerization modification of one-pot pentadecalactone block-like copolymers, Biomacromolecules 16 (2015) 3191–3200.

[18] I. van der Meulen, M. de Geus, H. Antheunis, R. Deumens, E.A.J. Joosten, C.E. Koning, A. Heise, Polymers from functional macrolactones as potential biomaterials: enzymatic ring opening polymerization, biodegradation, and biocompatibility, Biomacromolecules 9 (2008) 3404–3410.

[19] Z. Ates, A. Heise, Functional films from unsaturated poly(macrolactones) by thiol–ene cross-linking and functionalisation, Polym. Chem. 5 (2014) 2936.

[20] F.C.S. de Oliveira, D. Olvera, M.J. Sawkins, S.-A. Cryan, S.D. Kimmins, T.E. da Silva, D.J. Kelly, G.P. Duffy, C. Kearney, A. Heise, Direct UV-triggered thiol–ene cross-linking of electrospun polyester fibers from unsaturated

poly(macrolactone)s and their drug loading by solvent swelling, Biomacromolecules 18 (2017) 4292–4298.

[21] E. Tinajero Díaz, A. Martínez de Ilarduya, B. Cavanagh, A. Heise, S. Muñoz-Guerra, Poly(amino acid)-grafted polymacrolactones. Synthesis, self-assembling and ionic properties, React. Func. Polym. (2019) (submitted).

[22] M. Letizia Focarete, M. Scandola, A. Kumar, R. a Gross, Physical characterization of poly(ω-pentadecalactone) synthesized by lipase-catalyzed ring-opening polymerization, J. Polym. Sci. Part B Polym. Phys. 39 (2001) 1721–1729.

[23] A.E. Polloni, V. Chiaradia, E.M. Figura, J.P. De Paoli, D. de Oliveira, J.V. de Oliveira, P.H.H. de Araujo, C. Sayer, Polyesters from macrolactones using commercial Lipase NS 88011 and Novozym 435 as biocatalysts, Appl. Biochem. Biotechnol. 184 (2018) 659–672.

[24] Z. Ates, F. Audouin, A. Harrington, B. O'Connor, A. Heise, Functional brush-decorated poly(globalide) films by ARGET-ATRP for bioconjugation, Macromol. Biosci. 14 (2014) 1600–1608.

[25] M.T. Hunley, N. Sari, K.L. Beers, Microstructure analysis and model discrimination of enzyme-catalyzed copolyesters, ACS Macro Lett. 2 (2013) 375–379.

[26] H. Tadokoro, Structure of crystalline polymers, Wiley, 1979.

[27] M. Gazzano, V. Malta, M.L. Focarete, M. Scandola, R. a Gross, Crystal structure of poly(ω-pentadecalactone), J. Polym. Sci. Part B Polym. Phys. 41 (2003) 1009–1013.

[28] E. Tinajero-Díaz, A. Martínez de Ilarduya, S. Muñoz-Guerra, Block and graft copolymers made of 16-membered macrolactones and L-alanine: A comparative study, Macrol. Chem. Phys. (2019) (submitted).

[29] G. Rong, M. Deng, C. Deng, Z. Tang, L. Piao, X. Chen, X. Jing, Synthesis of poly(ε-caprolactone)-b-poly(γ-benzyl-L-glutamic acid) block copolymer using amino organic calcium catalyst, Biomacromolecules 4 (2003) 1800–1804.

[30] M. Schappacher, A. Soum, S.M. Guillaume, Synthesis of polyester−polypeptide

diblock and triblock copolymers using amino poly(ε-caprolactone) macroinitiators, Biomacromolecules 7 (2006) 1373–1379.

[31] J. Watanabe, I. Uematsu, Anomalous properties of poly(γ-benzyl-L-glutamate) film composed of unusual 7/2 helices, Polymer 25 (1984) 1711–1717.

[32] J. Babin, J. Rodriguez-Hernandez, S. Lecommandoux, H.-A. Klok, M.-F. Achard, Self-assembled nanostructures from peptide–synthetic hybrid block copolymers: complex, stimuli-responsive rod–coil architectures, Faraday Discuss. 128 (2005) 179–192.

[33] P. Papadopoulos, G. Floudas, H.-A. Klok, I. Schnell, T. Pakula, Self-assembly and dynamics of Poly(γ-benzyl-L-glutamate) peptides, Biomacromolecules 5 (2004) 81–91.

[34] H. Lu, J. Wang, Y. Bai, J.W. Lang, S. Liu, Y. Lin, J. Cheng, Ionic polypeptides with unusual helical stability, Nat. Commun. 2 (2011) 206.

[35] E.R. Blout, A. Asadourian, Polypeptides. V. The Infrared spectra of polypeptides derived from γ-benzyl-L-glutamate, J. Am. Chem. Soc. 78 (1956) 955–961.

[36] H.-A. Klok, J.F. Langenwalter, S. Lecommandoux, Self-Assembly of peptide-based diblock oligomers, Macromolecules 33 (2000) 7819–7826.

[37] S. Lecommandoux, M. Achard, J.F. Langenwalter, H. Klok, Self-assembly of rod−coil diblock oligomers based on α-helical peptides, Macromolecules 34 (2001) 9100–9111.

[38] E. Tinajero-Díaz, A. Martínez de Ilarduya, S. Muñoz-Guerra, Synthesis and properties of diblock copolymers of ω-pentadecalactone and α-amino acids, Eur. Polym. J. 116 (2019) 169–179.

[39] A. Minich, A.P. Nowak, T.J. Deming, D.J. Pochan, Rod–rod and rod–coil self-assembly and phase behavior of polypeptide diblock copolymers, Polymer 45 (2004) 1951–1957.

[40] S. Caillol, S. Lecommandoux, A.-F. Mingotaud, M. Schappacher, A. Soum, N. Bryson, R. Meyrueix, Synthesis and self-assembly properties of peptide−polylactide block copolymers, Macromolecules 36 (2003) 1118–1124.

[41]   M. Li, W. Song, Z. Tang, S. Lv, L. Lin, H. Sun, Q. Li, Y. Yang, H. Hong, X. Chen, Nanoscaled poly(L-glutamic acid)/doxorubicin-amphiphile complex as pH-responsive drug delivery system for effective treatment of nonsmall cell lung cancer, ACS Appl. Mater. Interfaces. 5 (2013) 1781–1792.

[42]   Y. Cheng, S. Yu, X. Zhen, X. Wang, W. Wu, X. Jiang, Alginic acid nanoparticles prepared through counterion complexation method as a drug delivery system, ACS Appl. Mater. Interfaces. 4 (2012) 5325–5332.

[43]   Y. Du, W. Chen, M. Zheng, F. Meng, Z. Zhong, pH-Sensitive degradable chimaeric polymersomes for the intracellular release of doxorubicin hydrochloride, Biomaterials 33 (2012) 7291–7299.

[44]   N. V. Nukolova, H.S. Oberoi, S.M. Cohen, A. V. Kabanov, T.K. Bronich, Folate-decorated nanogels for targeted therapy of ovarian cancer, Biomaterials 32 (2011) 5417–5426.

[45]   W.-C. Huang, W.-H. Chiang, Y.-F. Huang, S.-C. Lin, Z.-F. Shih, C.-S. Chern, C.-S. Chiang, H.-C. Chiu, Nano-scaled pH-responsive polymeric vesicles for intracellular release of doxorubicin, J. Drug Target. 19 (2011) 944–953.

[46]   B. Manocha, A. Margaritis, Controlled release of doxorubicin from doxorubicin/γ-polyglutamic acid ionic complex, J. Nanomater. 2010 (2010) 1–9.

Chapter 10. PEGlylated nanoparticles of poly(ethylene glycol-globalide) block copolymers grafted with L-phenylalanine

Abstract

Triblock/grafted poly(ether-ester-peptide) copolymers made or PEG, poly(globablide) and poly(L-phenylalanine) were synthesized by sequential ROP starting from diaminated PEG as first initiator. The aromatic functionality of L-phenylalanine inserted on the globalide units was utilized to impart the amphiphilicity required to drive their self-assembly in water and to provide aromaticity of potential value for the efficient loading of aromatic drugs. Depending of the method used for preparation, nanoparticles possessing diameters between 25 and 600 nm were obtained by self-assembling in aqueous medium.

10.1 Introduction

Success of polymeric nanocarriers is due to their physicochemical features such as nanoscopic size, surface charge, enhanced solubility of poorly soluble drugs, high encapsulation efficiency, target specific delivery, and improved therapeutic efficacy [1]. The colloidal nanocarriers are however cleared from the systemic circulation as a result of opsonization and subsequent uptake by the reticuloendothelial system (RES) [2]. A promising strategy to make nanocarriers less susceptible to recognition by RES, is coating with poly(ethylene glycol) (PEG) which avoids their interactions with components of bloodstream, imparting "stealth" properties.

On the other hand, the modification of the core is as important as modifying the surface of the nanocarriers. Some drugs have affinity to certain functional groups present on the core, thus improving the encapsulation of them [3–6]. When PEG comes to poly(α-amino acids), it is also highly biocompatible, non-toxic, and economic with versatile functional groups such as hydroxyl, carboxyl, amino, thiol or aromatic groups. Such a variety of functional groups is of great benefit to modify the chemical structure of the core for drug conjugation [7,8]. In this paper we wish to report the preparation of novel nanocarriers in where both the surface and the core were designed by marrying poly(ethylene glycol) to poly(globalide) and poly(L-phenylalanine) to yield an amphiphilic copolymer able to self-assemble in aqueous milieu forming nanoobjects with diameters between 20 and 600 nm.

10.2 Results and discussion

10.2.1 Synthesis of P(Gl-*g*-Phe$_z$)$_x$-*b*-(PEG$_{56}$)-*b*-P(Gl-*g*-Phe$_z$)$_x$ copolymers.

The first stage in the preparation of these block/graft copolymers was devoted to the synthesis of the amino-functionalized P(Gl-NH$_2$)$_x$-*b*-PEG$_{56}$-*b*-P(Gl-NH$_2$)$_x$ triblock copolymers to be used as macroinitiators for the grafting reaction. These copolymers were obtained according to the synthetic route depicted in Figure G2 and results are shown in Table G1. The enzymatic ring-opening polymerization (eROP) of globalide

initiated by bisamino-ended PEG (M_n~2600 g·mol^{-1}) provided two copolymers, namely

PGl$_{15}$-*b*-PEG$_{56}$-*b*-PGl$_{15}$ and PGl$_{70}$-*b*-PEG$_{56}$-*b*-PGl$_{70}$, differing in the length of the

polyglobalide blocks Then, the application of thiol-ene click chemistry using 2-

(Bocamino)ethanethiol (BAET) as coupling reactant and AIBN as thermoinitiator

allowed inserting amino-protected groups onto the poly(globalide) blocks with a

coupling efficiency between 50% and 90% as revealed by ^{1}H NMR (Figure G3 of the

Annex G). The regeneration of the NH$_2$ groups was readily achieved by treatment of

the P(Gl$_{15}$-BAET)$_y$-*b*-PEG$_{56}$-*b*-P(Gl$_{15}$-BAET)$_y$ with TFA t for 2 h. The P(Gl$_{15}$NH$_2$)$_y$-*b*-

PEG$_{56}$-*b*-P(Gl$_{15}$-NH$_2$)$_y$ copolymers with y values of 15 and 70, respectively, were thus

obtained with a yield close to 100%. The NMR spectrum of the copolymer with y = 15 is

shown in Figure G4 of the Annex G.
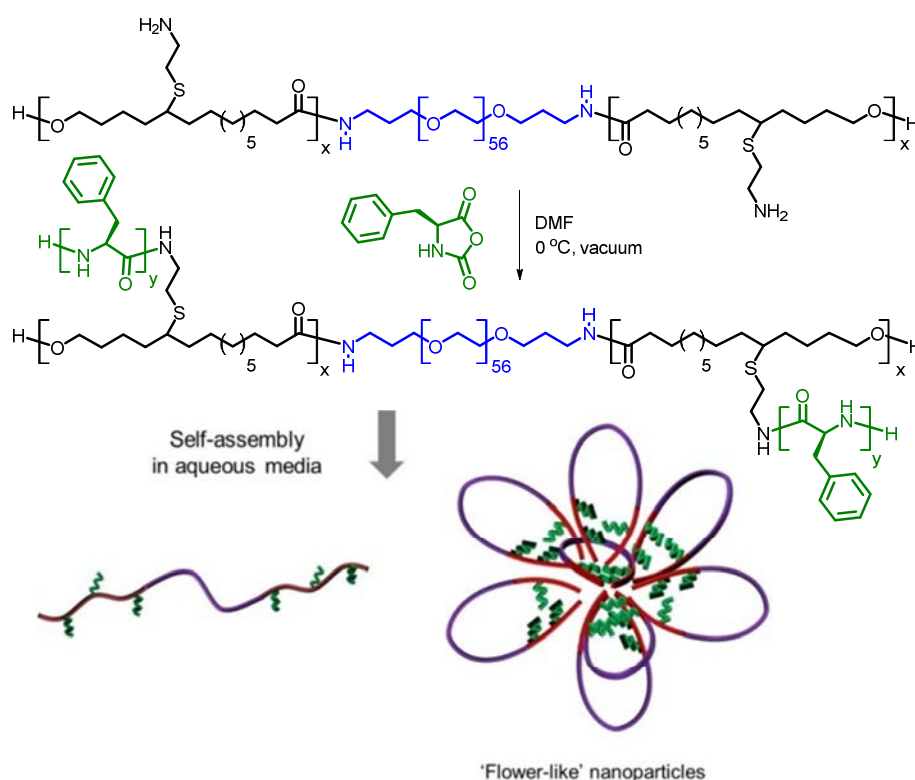
Scheme 10.1. Synthesis of P(Gl$_x$-*g*-Phe$_y$)-*b*-PEG$_{56}$-*b*-P(Gl$_x$-*g*-Phe$_y$) copolymers and a likely self-assembly behavior in water.

The ROP of NCA is normally initiated by primary amines in such a way that the

initiator remains attached to the terminated polymer chain [11,12]. As it is depicted in

Scheme 10.1, poly(L-phenylalanine) chains were grafted onto the polyglobalide blocks

by ROP of L-phenylalanine *N*-carboxyanhydride (Phe-NCA) using the amino functionalized copolymer. The success of the copolymerization was confirmed by SEC as well as by ^{1}H NMR and FTIR spectroscopies. Comparison of the SEC peaks of the P(Gl$_{15}$-NH$_2$)-*b*-PEG$_{56}$-*b*-P(Gl$_{15}$-NH$_2$) triblock copolymer and the P(Gl-*g*-Phe$_4$)$_{15}$-*b*-PEG$_{56}$-*b*-P(Gl-*g*-Phe$_4$)$_{15}$ block/graft copolymer confirmed an increase of the molar mass upon grafting according to what should be expected from the amount of amino acid attached to the copolymer (see Figure G5 of the Annex G). Yields, M_n, and Đ of the synthesized block/graft copolymers are collected in Table 10.1.

Table 10.1. Results for the synthesis of amphiphilic P(Gl$_x$-*g*-Phe$_y$)-*b*-PEG$_{56}$-*b*-P(Gl$_x$-*g*-Phe$_y$) copolymers

Polymer	Yield (%)	$M_n{}^a$ (g·mol^{-1})	$M_n{}^b$ (g·mol^{-1})	Đ^b
P(Gl$_{15}$-*g*-Phe$_2$)-*b*-PEG$_{56}$-*b*-P(Gl$_{15}$-*g*- Phe$_2$)	70	13,500	16,500	1.8
P(Gl$_{15}$-*g*-Phe$_4$)-*b*-PEG$_{56}$-*b*-P(Gl$_{15}$-*g*-Phe$_4$)	80	13,800	21,000	1.9
P(Gl$_{70}$-*g*-Phe$_8$)-*b*-PEG$_{56}$-*b*-P(Gl$_{70}$-*g*-Phe$_8$)	84	45,160	22,600	4.6

^{b}Determined by ^{1}H NMR end-group analysis.
^{b}Determined by GPC using PMMA as standards.

NMR spectroscopy was used to elucidate the chemical structure of the block/graft copolymers. Figure 1 displays the ^{1}H NMR (CDCl$_3$/TFA) spectrum of a representative polymer, i.e. P(Gl$_{15}$-*g*-Phe$_4$)-*b*-PEG$_{56}$-*b*-P(Gl$_{15}$-*g*-Phe$_4$). The alpha and aromatic hydrogens characteristic of the phenylalanine units are identified at 4.6 ppm and 7.2 ppm, respectively along with signals arising from EG (peak a) and globalide (peaks c,d,f) units. Furthermore, a new signal at 3.4 ppm arising from the amide bond formed in the ROP of Phe NCA confirmed the success of the grafting reaction. The number of grafted Phe units was assessed comparing the integration ratio of the macroinitiator (C$\underline{H}_2$NHCO, peak h) to the α-protons from Phe (C$\underline{H}$, peak α). ^{1}H NMR spectra of the P(Gl$_{15}$-*g*-Phe$_2$)-*b*-PEG$_{56}$-*b*-P(Gl$_{15}$-*g*-Phe$_2$) and P(Gl$_{70}$-*g*-Phe$_8$)-*b*-PEG$_{56}$-*b*-P(Gl$_{70}$-*g*-Phe$_8$) copolymers are shown in Figure G6 of the Annex G.
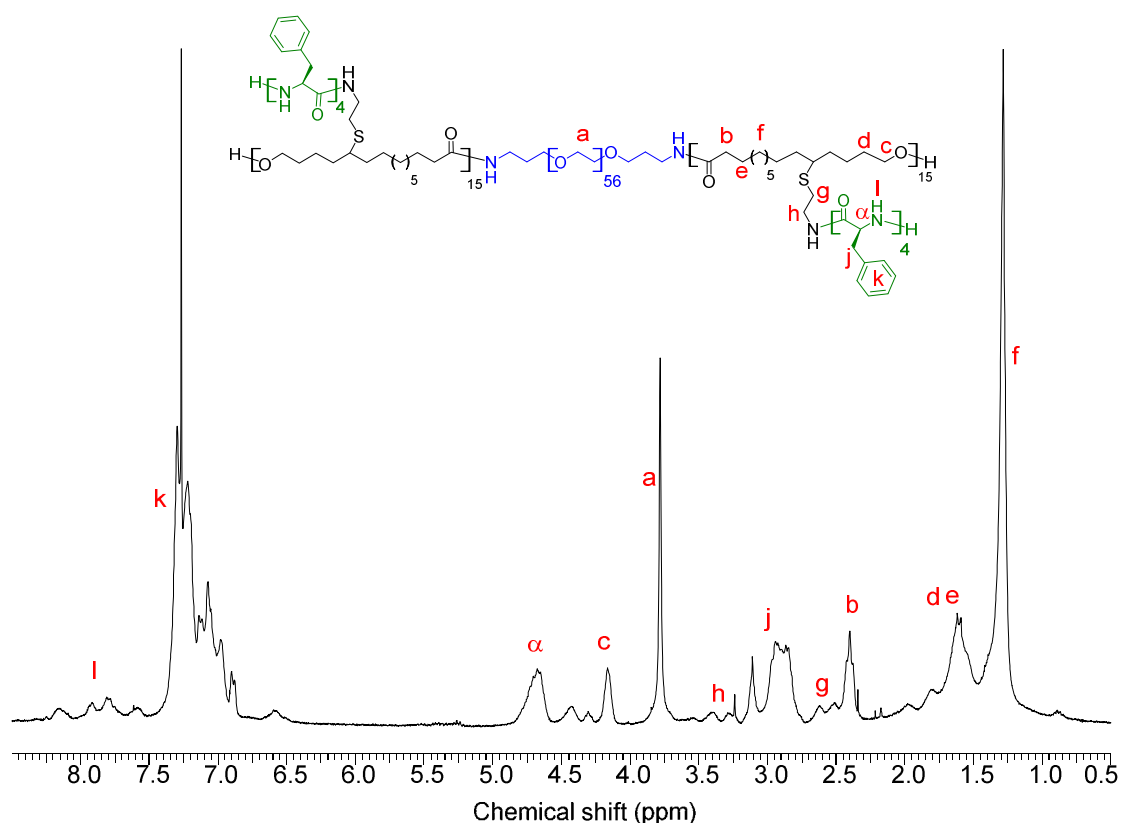
Figure 10.1 ^{1}H-NMR (CDCl$_3$/TFA) spectrum of the P(Gl$_{15}$-*g*-Phe$_4$)-*b*-PEG$_{56}$-*b*-P(Gl$_{15}$-*g*-Phe$_4$) copolymer.

10.2.2 Structure of the graft/block copolymers in the solid state

The thermal stability of the three P(Gl$_x$-*g*-Phe$_y$)-*b*-PEG$_{56}$-*b*-P(Gl$_x$-*g*-Phe$_y$) copolymers was measured by TGA (Figure G7 of the Annex G). They did not lose appreciable weight until around heated at the proximities of 200 ºC and bulk decomposition was found to take place around 300 ºC. The DSC analysis of the copolymers was performed to check the occurrence of thermal transitions. No sign of heat exchange was detected on the DSC traces recorded from the copolymers (Figure G8 of the Annex G) in spite that polyglobalide is a semicrystalline polyester with a T_m around 50 ºC. In the grafted copolymers the PGl segments were unable to crystallize because the severe alteration of their chemical structure produced by grafting. The PEG block was also in the disordered state, a fact more difficult to explain unless than the topological constrain exerted by the P(Gl-*g*-Phe) block is taken into consideration.

Poly(L-phenyl alanine) (PPhe) is a polypeptide that displays a scarce tendency to crystallize, a property that is reflected in the DSC traces recorded from the $P(Gl_x$-g-$Phe_y)$-b-PEG_{56}-b-$P(Gl_x$-g-$Phe_y)$ copolymers. Nevertheless, it could be expected that PPhe side chains are arranged in some of the conformations characteristic of polypeptides. Information on the secondary structure of PPhe adopted in these copolymers was obtained by FTIR spectroscopy. The Amide I + II region of these spectra (Figure 10.2) shows two peaks at 1630 cm^{-1} and 1680 cm^{-1}, respectively. indicative of the presence of β-sheet structure, more probably in the antiparallel arrangement [14,15].
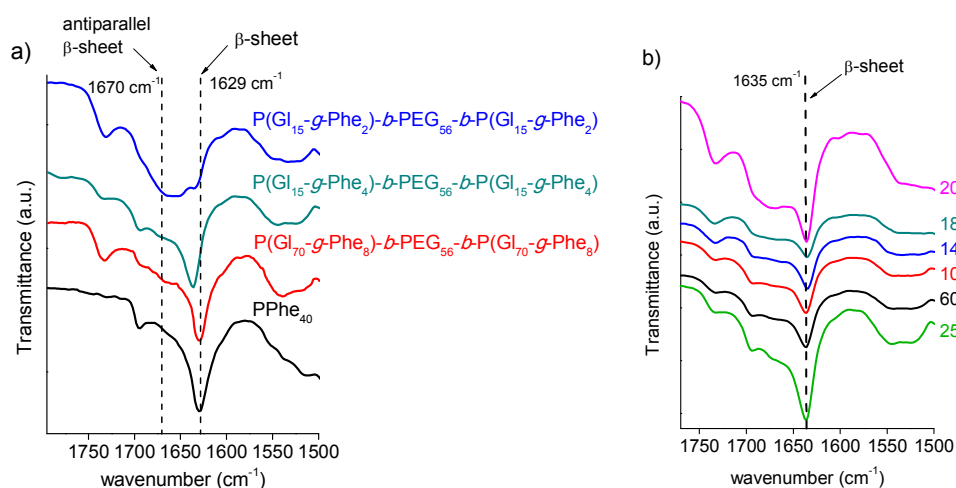
Figure 10.2. (a) FTIR spectra of the $P(Gl_x$-g-$Phe_y)$-b-PEG_{56}-b-$P(Gl_x$-g-$Phe_y)$ copolymers in the 1500-1800 cm^{-1}region. (b) Spectra of $P(Gl_{15}$-g-$Phe_4)$-b-PEG_{56}-$P(Gl_{15}$-g-$Phe_4)$ copolymer recorded at different temperatures.

As expected, the intensity of these peaks was observed to increase with the content in Phe in the copolymers. On the other hand, the effect of heating on the Amide I band was insignificant according to the thermal stability of the sheet structure which is known to remain unaltered up to temperatures well above 200 ºC.

To get insight into a possible ordered organization existing in the copolymers at either molecular or supramolecular level, a real-time X-ray diffraction study was carried out on samples subjected to variable temperature using synchrotron radiation. Both wide and small angle scattering were simultaneously recorded at either heating or cooling within the 10-200 ºC temperature range. The evolution followed by the

scattering profile of a pristine sample of P(Gl$_{15}$-g-Phe$_4$)-b-PEG$_{56}$-b-P(Gl$_{15}$-g-Phe$_4$) with temperature changes is displayed in Figure 10.3. Reflections in the SAXS region (Figure 3a) corresponding to the spacing d=3.8 nm that increased up to 5.3 nm with temperature could be attributed to the presence of a lamellar biphasic structure [14]. Some reflections in the WAXS profiles (Figure 10.3b) are indicative that the copolymer is arranged in the β-sheet form. The reflection at d=0.46 nm could be made to correspond to the separation of between adjacent peptide chains organized into β-strands. SAXS and WAXS cooling profiles are available in Figure G9 of the Annex G).
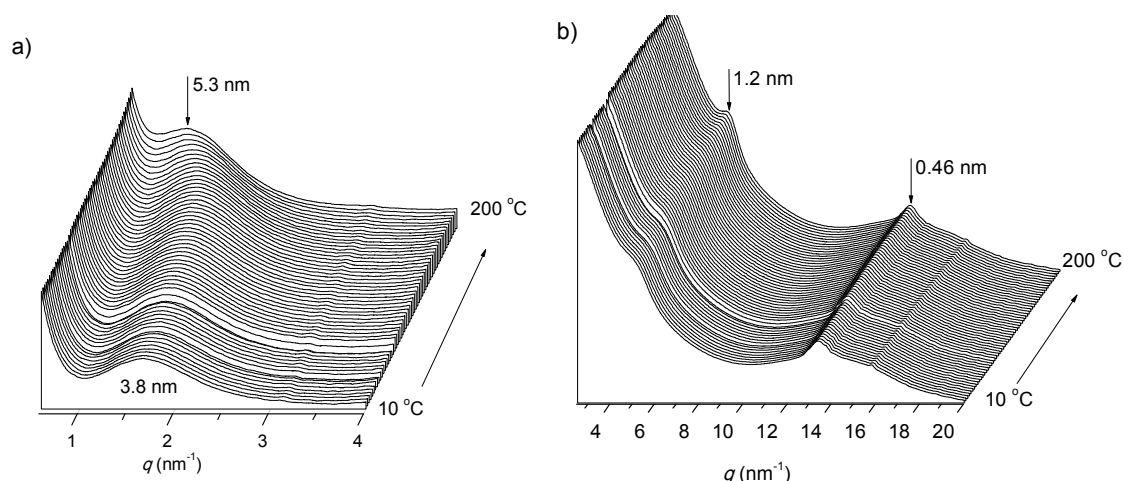
Figure 10.3. Evolution of the X-ray diffraction profiles of P(Gl$_{15}$-g-Phe$_4$)-b-PEG$_{56}$-P(Gl$_{15}$-g-Phe$_4$) recorded at heating over the 10-200 °C range: (a) SAXS and (b) WAXS.

10.2.3 Self-assembly in aqueous media

Spherical NPs were prepared by the emulsion-solvent evaporation method previously used by us for other related systems. Particles with diameters between 220 nm and 600 nm, as measured by DLS were thus obtained. Scanning electronic microscopy (SEM) revealed the almost spherical morphology of these particles, as shown in Figure 4a for the P(Gl$_{15}$-g-Phe$_4$)-b-PEG$_{56}$-b-P(Gl$_{15}$-g-Phe$_4$) copolymer. Such nanoparticles were found to be stable up to three weeks of storing as measured by DLS (see Figure G1 of the Annex G). Similarly, NPs of P(Gl$_{70}$-g-Phe$_8$)-b-PEG$_{56}$-b-P(Gl$_{70}$-g-Phe$_{8'}$) exhibiting similar well-spherical morphologies could be also prepared. SEM images of these particles are available in Figures G11-G13 of Annex G.

Since the copolymers are DMSO-soluble, the nanoprecipitation method using this solvent was also used to drive the self-assembly of the P(Gl$_x$-g-Phe$_y$)-b-PEG$_{56}$-b-P(Gl$_x$-g-Phe$_{y'}$) copolymers.

Table 10.2. Characterization of nanoparticles derived of the P(Gl$_x$-g-Phe$_y$)-b-PEG$_{56}$-b-P(Gl$_x$-g-Phe$_y$) copolymers

Copolymer	Method	D (nm)	PDI
P(Gl$_{15}$-g-Phe$_2$)-b-PEG$_{56}$-b-P(Gl$_{15}$-g-Phe$_2$)	nanoprecipitation	108	0.19
	emulsion-solvent evaporation	160/820	0.44
P(Gl$_{15}$-g-Phe$_4$)-b-PEG$_{56}$-b-P(Gl$_{15}$-g-Phe$_4$)	nanoprecipitation	20/190	0.50
	emulsion-solvent evaporation	620	0.05
	nanoprecipitation	25/190	0.40
P(Gl$_{70}$-g-Phe$_8$)-b-PEG$_{56}$-b-P(Gl$_{70}$-g-Phe$_8$)	emulsion-solvent evaporation	220	0.17

DLS analysis was performed after removing DMSO by dialysis. By this method, the three copolymers self-assembled in NPs with diameters between 20 nm and 190 nm (DLS profiles are accessible in Figure G10 of the Annex G). Table 2 collects the obtained results. TEM was used to probe the morphology displayed by the NPs made of P(Gl$_{70}$-g-Phe$_8$)-b-PEG$_{56}$-b-P(Gl$_{70}$-g-Phe$_8$) after self-assembly (Figure 10.4b). Despite no apparent differences observed in the morphology of the NPs, the diameter decreased noticeably when self-assembly was induced by nanoprecipitation.
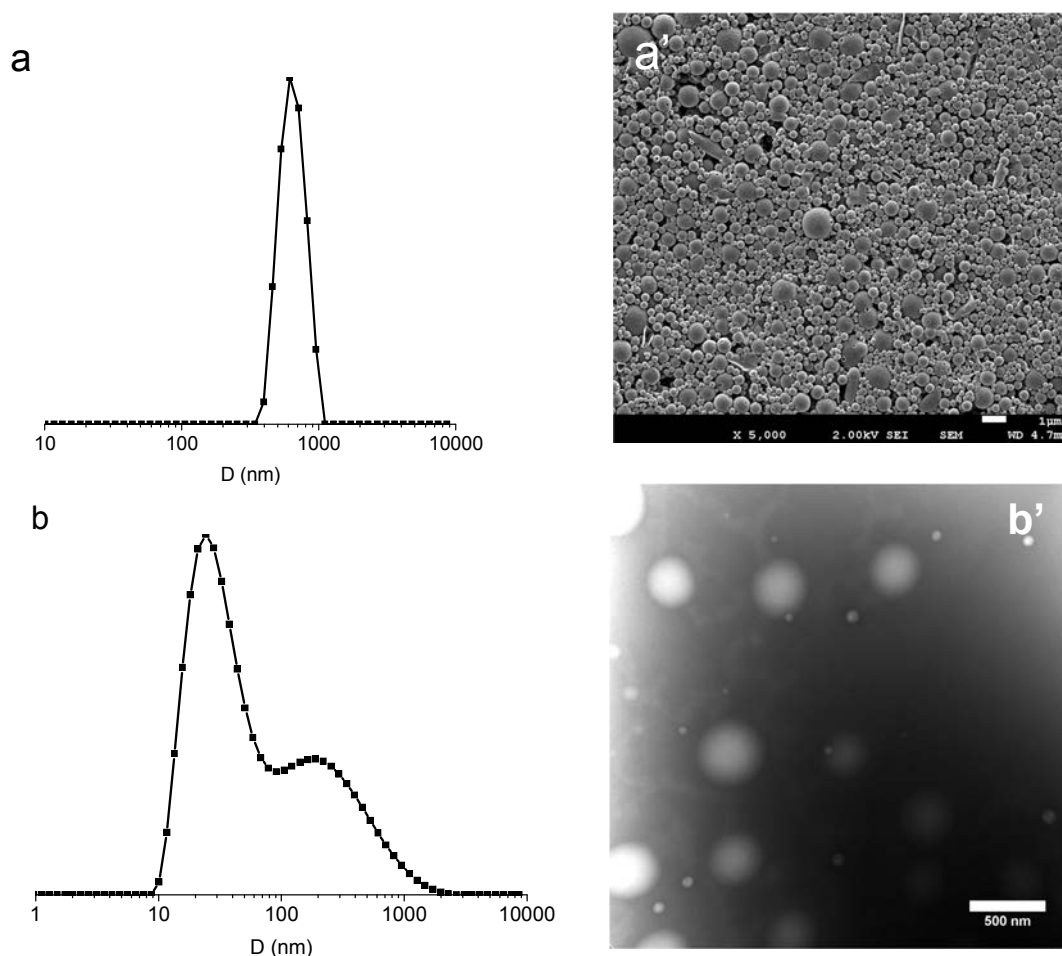
Figure 10.4. (a, a') NPs prepared by emulsion-solvent evaporation from the P(Gl$_{15}$-*g*-Phe$_4$)-*b*-PEG$_{56}$-P(Gl$_{15}$-*g*-Phe$_4$) copolymer, and (b, b') and NPs prepared by nanoprecipitation from the P(Gl$_{70}$-*g*-Phe$_8$)-*b*-PEG$_{56}$-P(Gl$_{70}$-*g*-Phe$_8$) copolymer.

10.3 Conclusions

A versatile and facile route for building PEGlylated nanoparticles based on fully biobased building blocks has been developed. The amino functionalized poly(ether-ester) macroinitiator was able to initiate the ROP of NCA and to afford amphiphilic-hybrid copolymers with controlled branches lengths. Self-assembly of the copolymers in water afforded nanoparticle with sizes roughly adjustable by selecting the method used for assembling. Since the surface of the nanostructures is "PEGylated" and the core is composed of aromatic-functional groups, these materials are highly promising as drug nanocarriers.

10.4 References

[1]   Z. Hussain, S. Khan, M. Imran, M. Sohail, S.W.A. Shah, M. de Matas, PEGylation: a promising strategy to overcome challenges to cancer-targeted nanomedicines: a review of challenges to clinical transition and promising resolution, Drug Deliv. Transl. Res. 9 (2019) 721–734.

[2]   D. Owensii, N. Peppas, Opsonization, biodistribution, and pharmacokinetics of polymeric nanoparticles, Int. J. Pharm. 307 (2006) 93–102.

[3]   G. Kwon, M. Naito, M. Yokoyama, T. Okano, Y. Sakurai, K. Kataoka, Block copolymer micelles for drug delivery: Loading and release of doxorubicin, J. Control. Release. 48 (1997) 195–201.

[4]   A. Matsushima, T. Fujita, T. Nose, Y. Shimohigashi, Edge-to-face CH/π interaction between ligand Phe-phenyl and receptor aromatic group in the thrombin receptor activation, J. Biochem. 128 (2000) 225–232.

[5]   K.M. Makwana, R. Mahalakshmi, Implications of aromatic-aromatic interactions: From protein structures to peptide models, Protein Sci. 24 (2015) 1920–1933.

[6]   S. Fleming, R. V. Ulijn, Design of nanostructures based on aromatic peptide amphiphiles, Chem. Soc. Rev. 43 (2014) 8150–8177.

[7]   Y. Bae, K. Kataoka, Intelligent polymeric micelles from functional poly(ethylene glycol)-poly(amino acid) block copolymers, Adv. Drug Deliv. Rev. 61 (2009) 768–784.

[8]   S. Lv, M. Li, Z. Tang, W. Song, H. Sun, H. Liu, X. Chen, Doxorubicin-loaded amphiphilic polypeptide-based nanoparticles as an efficient drug delivery system for cancer therapy, Acta Biomater. 9 (2013) 9330–9342.

[9]   G.J.M. Habraken, M. Peeters, C.H.J.T. Dietz, C.E. Koning, A. Heise, How controlled and versatile is *N*-carboxy anhydride (NCA) polymerization at 0 °C? Effect of temperature on homo-, block- and graft (co)polymerization, Polym. Chem. 1 (2010) 514.

[10]   W.H. Daly, D. Poché, The preparation of N-carboxyanhydrides of α-amino acids using bis(trichloromethyl)carbonate, Tetrahedron Lett. 29 (1988) 5859–5862.

[11]   H.R. Kricheldorf, Polypeptides and 100 Years of Chemistry of α-Amino acid *N*-carboxyanhydrides, Angew. Chemie Int. Ed. 45 (2006) 5752–5784.

[12]   N. Hadjichristidis, H. Iatrou, M. Pitsikalis, G. Sakellariou, Synthesis of well-defined polypeptide-based materials via the ring-opening polymerization of α-amino acid *N*-carboxyanhydrides, Chem. Rev. 109 (2009) 5528–5578.

[13]   Z. Ates, P.D. Thornton, A. Heise, Side-chain functionalisation of unsaturated polyesters from ring-opening polymerisation of macrolactones by thiol–ene click chemistry, Polym. Chem. 2 (2011) 309–312.

[14]   C. Diaferia, F.A. Mercurio, C. Giannini, T. Sibillano, G. Morelli, M. Leone, A. Accardo, Self-assembly of PEGylated tetra-phenylalanine derivatives: structural insights from solution and solid state studies, Sci. Rep. 6 (2016) 26638.

[15]   V. Castelletto, I.W. Hamley, Self assembly of a model amphiphilic phenylalanine peptide/polyethylene glycol block copolymer in aqueous solution, Biophys. Chem. 141 (2009) 169–174.

General conclusions

I.   ROP of macrolactones has normally been carried out with alcohols as initiators whereas the use of amines has been under-estimated and not tested before. In this Thesis, the efficacy of amino-ended compounds for initiating the ROP of ω-pentadecalactone has been demonstrated. Furthermore, the use of an amino initiator carrying a second functionality susceptible of post-polymerization modification to create additional amino groups has been shown to be an excellent approach to design copolymers exhibiting complex architectures and controlled compositions.

II.   The synthesis of hybrid poly(ester-peptide) copolymers has over-exploited the use of medium-ring size lactones such as ε-caprolactone or L-lactide. Combination of macrolactones (PGl or PDL) with glutamic acid and lysine for the synthesis of poly(ester-peptide) copolymers as it has been carried out in this Thesis generated biphasic materials with the two phases organized in ordered arrangements. The poly(ester-peptide) copolymers with the amino acids conveniently protected were able to self-assemble in nanoparticles in spite of their poor amphiphilic character. Water-soluble copolymers were obtained by deprotection of the amino acid residues, which were able to self-assemble in water to form 100-200 nm nanoparticles. The peripheral location of the either positive or negative charged segments made these nanoparticles particularly suitable for anchoring charged molecules by ionic coupling.

III.   Macrolactones with inherent functionalities are interesting monomers to design complex polymeric architectures. The double bond present in the globalide backbone afforded the possibility to perform post-polymerization reactions entailing the introduction of amino functionalities suitable for triggering NCA polymerizations. Graft copolymers were prepared from Gl and glutamic acid and lysine using this approach. The P[Gl$_{20}$-g-(LGA)$_z$] and P[Gl$_{20}$-g-(LL)$_z$] copolymers

were found to exhibit a great potential as hosts for doxorubicin and DNA, respectively.

IV. The amino-functionalized macroinitiators $PPDL_{10}-NH_2$ and $P(Gl_8-co-(Gl_{12}-NH_2)$ were proven to initiate the polymerization of Ala-NCA to render diblock and graft poly(macrolactone-alanine) copolymers. A conformational mixture of α-helical and β-sheet forms was adopted by the polyalanine counterpart in both types of copolymers. The diblock copolymers formed nanoparticles with diameters between 300 and 350 nm while only large aggregates from $P[Gl_{20}-g-(Ala)_z]$ copolymer were obtained instead.

V. Copolymerization of macrolactones (Gl or PDL) mediated by Novozyme 435 in solution afforded PGl-*r*-PPDL copolyesters covering the whole range of compositions. Interestingly, the copolymers were found to adopt the same crystal structure for any composition. It seems that the two monomeric units are isomorphicallly replaced within the crystal lattice.

VI. Gl served as excellent comonomer to introduce functionalities in their copolymers making them susceptible to undergo post-polymerization reactions. Amino groups were introduced in PGl-*r*-PPDL copolyesters through the Gl moieties, which were then used to initiate the BLG-NCA polymerization. After the removal of Bn groups, hybrid copolymers bearing COOH functional groups were formed with the capacity of entrapping DOX·HCl and to release it at a pH-controlled rate.

VII. PEGlylation is a well-recognized method of minimizing opsonization of polymeric nanoparticles while running in the blood flow. $P(Gl-g-Phe_z)_y-b-PEG_{56}-b-P(Gl-g-Phe_z)_y$ copolymers were prepared by using diamino-ended PEG as initiator for ROP of Gl and subsequent grafting of the amino-functionalized Gl units by ROP of Phe NCA. Well shaped nanoparticles with a core integrated by Gl-(Phe_z) segments and the PEG block located on the surface were made by self-assembling of these copolymers. The presence of the L-phenylalanine on

nanoparticle core will improve their affinity for aromatic drugs enhancing therefore

the entrapping efficiency as nanocarrier.

Acknowledgements

The realization of this Thesis would not have succeeded without fine people, and I would like to express my thankfulness to all them:

I want to thank Prof. Dr. Sebastián Muñoz Guerra for giving me the chance to work in his research group. My thankfulness to him is not only for shared me his huge wisdom but also for his greatly valuable help.

I wish to thank Dr. Antxon Martínez for his guidance during my entire stay in the doctorate school, and mainly for shared me his knowledge.

I also wish to express my gratitude to Prof. Andreas Heise for gave me the chance to do research in his laboratory in RCSI.

I greatly thank to all my labmates of both Barcelona and Dublin, I always intended that being with me were easy, and being with all of you definitely was!

Mere words would not explain the unconditional support that Pilar gave me in spite of the distance. My deepest gratitude is to her.

About the author

Ernesto Tinajero-Díaz was born in Zacatecas (México) on June 27, 1987. He received the Chemical Engineer degree at the Universidad Autónoma de Zacatecas, (México) in 2009. In 2008 he was awarded with a grant by the Academia Mexicana de Ciencias to perform an internship in the Centro de Graduados e Investigación en Química in Baja California Norte (México). Afterwards, he was awarded with a CONACyT grant, to be specialized in polymer chemistry at the Universidad de Guadalajara (México), holding the Master´s Chemistry Degree in 2013. The CONACyT support was then continued to allow him coming to Spain to make his PhD in polymer chemistry at the Universitat Politécnica de Catalunya (Barcelona) under the supervision of Prof. Dr. Sebastián Muñoz Guerra and Dr. Antxon Martínez de Ilarduya. Within this period, he was awarded with an international grant by "La Caixa Bank, Spain" to carry out an internship in the Royal College of Surgeons in Ireland under the guidance of Prof. Dr. Andreas Heise, in Dublin (Ireland). His actual interests are focused on the design of advanced-polymeric structures based on hybrid systems made of polypeptides and synthetic polymers with potential applications in the biomedical field.

Scientific production derived of this thesis

Scientific papers

1. E. Tinajero-Díaz, A. Martínez-de Ilarduya, S. Muñoz-Guerra, M.-V. De-Paz, E. Galbis, Metal-free catalyzed ring-opening polymerization and block copolymerization of ω-pentadecalactone using amino-ended initiators, Eur. Polym. J. 108 (**2018**) 380–389.

2. E. Tinajero-Díaz, A. Martínez de Ilarduya, S. Muñoz-Guerra, Synthesis and properties of diblock copolymers of ω-pentadecalactone and α-amino acids, Eur. Polym. J. 116 (**2019**) 169–179.

3. E. Tinajero Díaz, A. Martínez de Ilarduya, B. Cavanagh, A. Heise, S. Muñoz-Guerra, Poly(amino acid)-grafted polymacrolactones. Synthesis, self-assembling and ionic properties, React. Func. Polym. (**2019**) (under revision).

4. E. Tinajero-Díaz, A. Martínez de Ilarduya, S. Muñoz-Guerra, pH-Responsive diblock copolymers made of ω-pentadecalactone and ionically charged α-amino acids, Eur. Polym. J. (**2019**) (under revision).

5. E. Tinajero-Díaz, A. Martínez de Ilarduya, S. Muñoz-Guerra, Block and graft copolymers made of 16-membered macrolactones and L-alanine: A comparative study, Macrol. Chem. Phys. (**2019**) (submitted)

6. E. Tinajero-Díaz, A. Martínez de Ilarduya, Lourdes Urpí, S. Muñoz-Guerra, Isomorphic pentadecalactone-globalide random copolyesters grafted with L-glutamic acid. Synthesis and nanocarrier properties, (2019) (submitted).

7. E. Tinajero-Díaz, A. Martínez de Ilarduya, S. Muñoz-Guerra, PEGylated nanoparticles made of poly(globalide) and poly(L-phenylalanine) as building blocks, (2019) (in preparation).

Congress contributions

1. E. Tinajero-Díaz, A. Martínez-de Ilarduya, C. Lavilla, S. Muñoz-Guerra, Ring opening polymerization of macrolactones using amines as initiators, "XIV Reunión del Grupo Especializado de Polimeros GEP 2016 (RESEQ, RSEF)" Burgos, Spain (**2016**).

2. E. Tinajero-Díaz, A. Martínez-de Ilarduya, S. Muñoz-Guerra, Amphiphilic block copolymers obtained by enzymatic ring-opening polymerization of ω-pentadecalactone initiated by peg-bis-amines, "IX Congreso de Jóvenes Investigadores en Polímeros" Tarragona, Spain (2017).

3. Ernesto Tinajero-Díaz, Antxon Martínez de Ilarduya, Andreas Heise, Sebastián Muñoz-Guerra, Poly(ω-pentadecalactone)-*b*-poly(peptide) block copolymers for biomedical applications, "8th World Congress on Biopolymers &Bioplastics" Berlin, Germany (**2018**).

4. E. Tinajero-Díaz, A. Martínez-de Ilarduya, S. Muñoz-Guerra, Synthesis of amphiphilic-graft copolymers derived of globalide and α-amino acids, XIV Reunión del Grupo Especializado de Polimeros GEP 2018 (RESEQ, RSEF)" Punta Umbría, Spain (**2018**).

5. Ernesto Tinajero-Díaz, Antxon Martínez de Ilarduya, Andreas Heise, Sebastián Muñoz-Guerra, Novel nanoparticles made of polyester-peptide copolymers, "NanoBio&Med 2018 International Conference" Barcelona, Spain (**2018**).

6. E. Tinajero-Díaz, A. Martínez-de Ilarduya, S. Muñoz-Guerra, Poly(ether-ester-peptide) triblock copolymers: synthesis and self-assembly behaviour, "X Congreso de Jóvenes Investigadores en Polímeros" Burgos, Spain (**2019**).
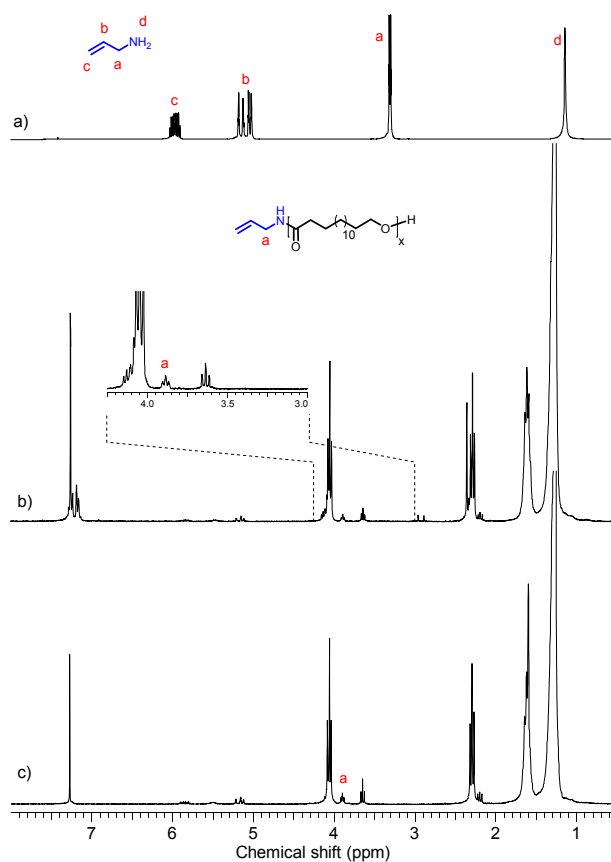
Figure A1. ^{1}H NMR spectra of: a) Allylamine, b) AllA-PPDL before purification, and c) AllA-PPDL after purification (Table 1, entry 8).
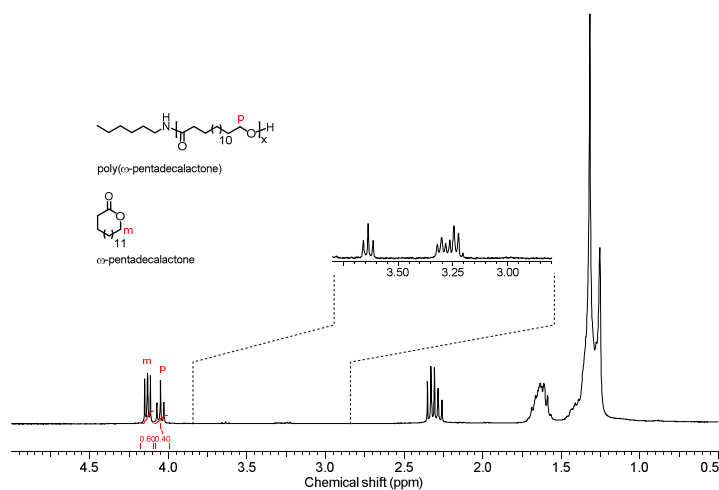
Figure A2. ^{1}H NMR spectrum of PPDL initiated by hexylamine before purification (Table 1, entry 2).
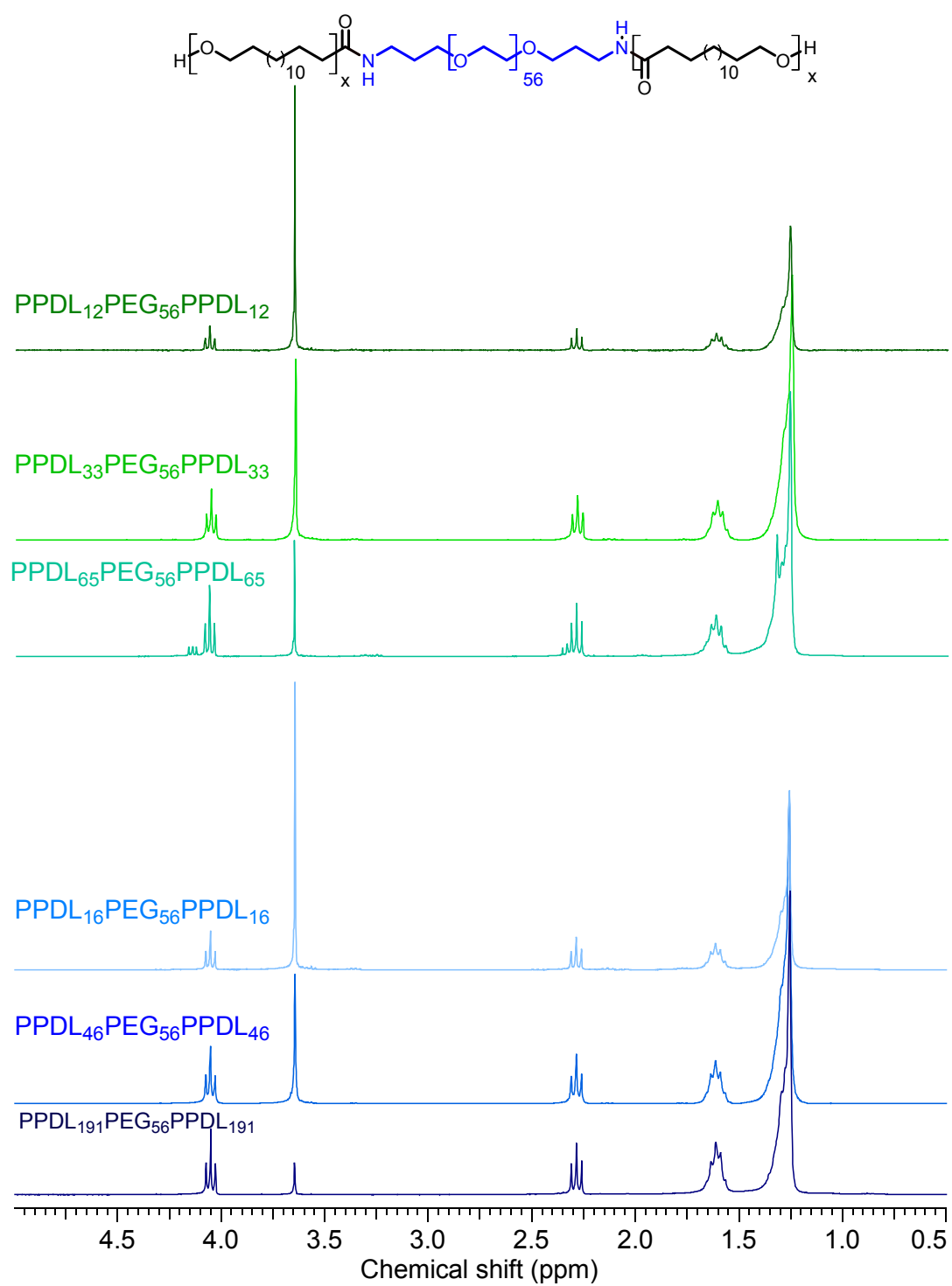
Figure A3. ^{1}H-NMR spectra of the $PPDL_xPEG_{56}PPDL_x$ triblock copolymers.
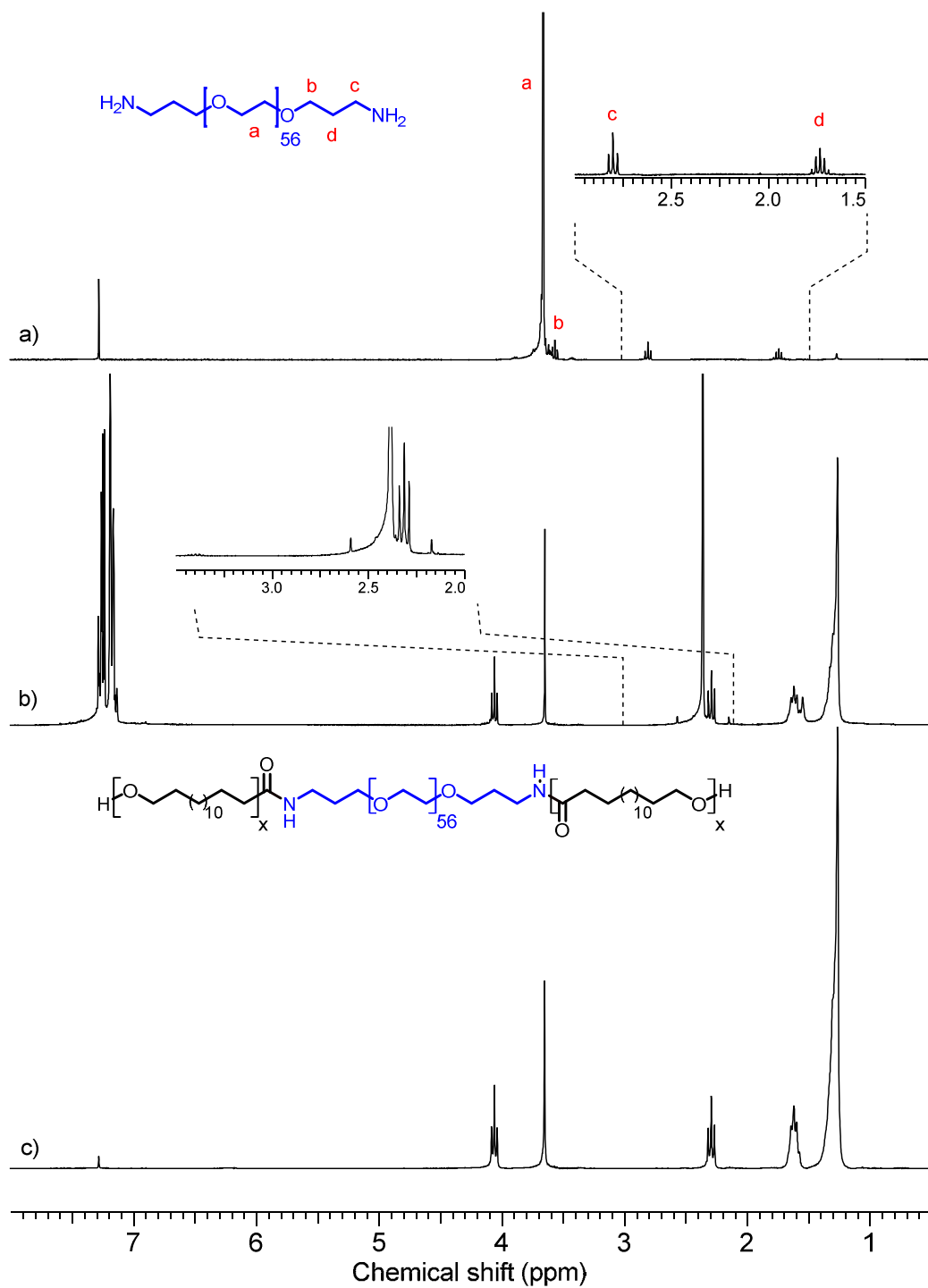
Figure A4. ^{1}H NMR spectra of a) A-PEG56-A, b) copolymer PPDL$_{46}$PEG$_{56}$PPDL$_{46}$ before purification, and c) copolymer PPDL$_{46}$PEG$_{56}$PPDL$_{46}$ after purification.
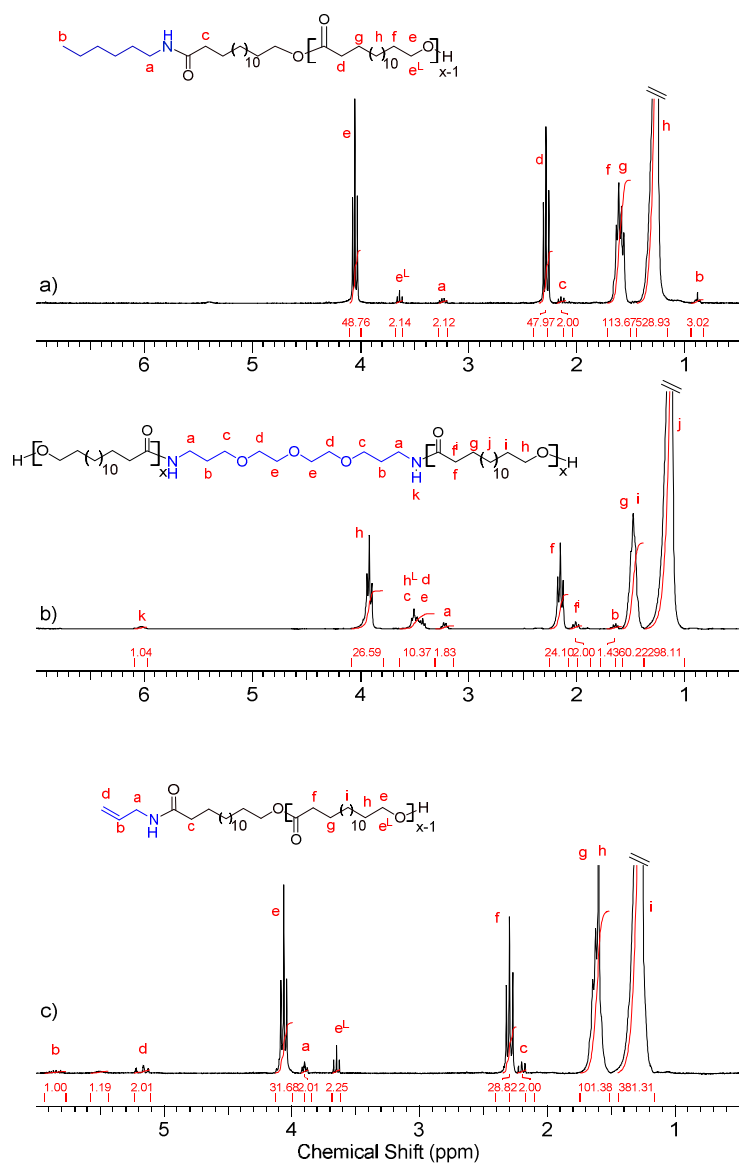
Figure A5. ^{1}H NMR spectra of: a) HA-PPDL, b) PPDL-DEG-PPDL, c) AllA-PPDL.
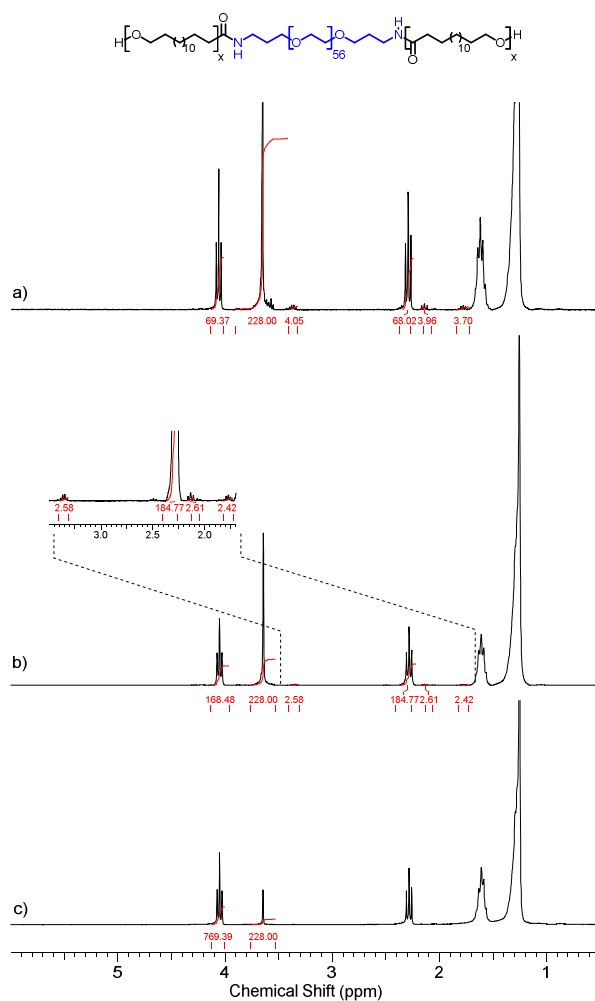
Figure A6. ^{1}H NMR spectra of the triblock copolymers displaying the end-group analysis of: a) PPDL$_{16}$PEG$_{56}$PPDL$_{16}$, b) PPDL$_{46}$PEG$_{56}$PPDL$_{46,}$ and c) PPDL$_{191}$PEG$_{56}$PPDL$_{191}$.
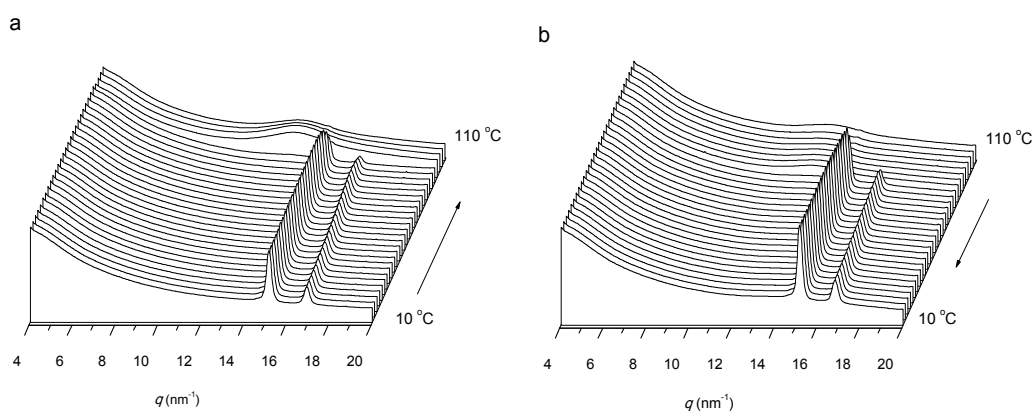
Figure A7. WAXS profiles of PPDL$_{191}$PEG$_{56}$PPDL$_{191}$ triblock copolymer (a) at heating, and (b) at cooling
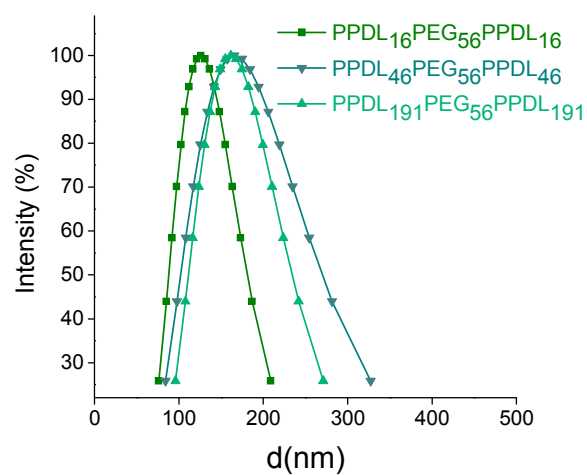
Figure A8. Size distribution profiles of nanoparticles.
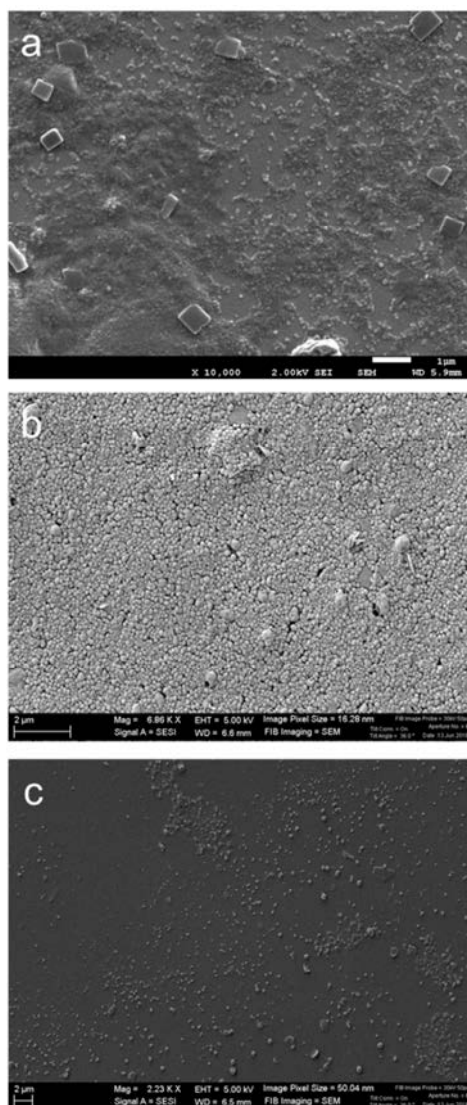
Figure A9. SEM images of nanoparticles made from PPDL$_{16}$PEG$_{56}$PPDL$_{16}$ (a), PPDL$_{46}$PEG$_{56}$PPDL$_{46}$ (b) and PPDL$_{191}$PEG$_{56}$PPDL$_{191}$(c) triblock copolymers.
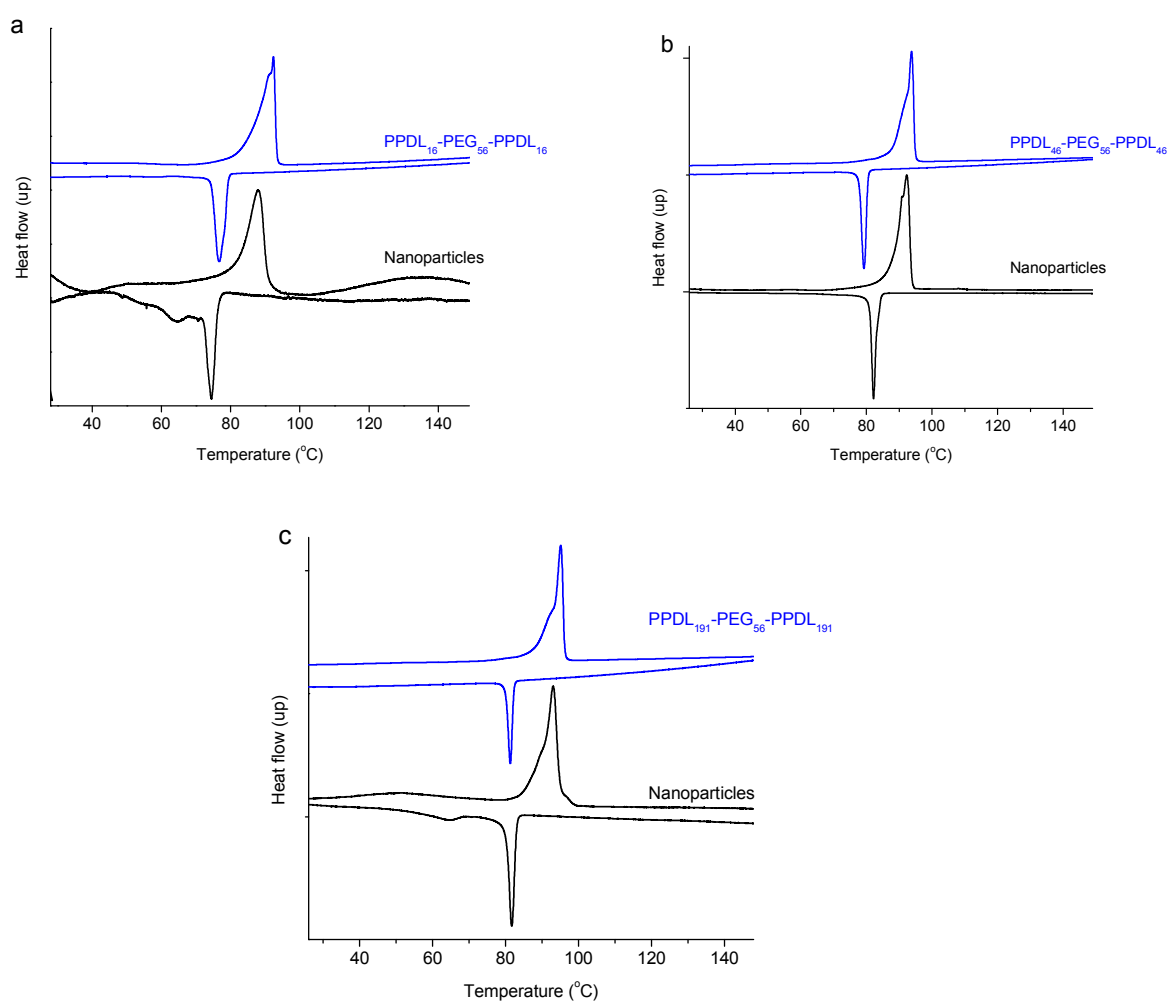
Figure A10. Compared DSC traces for PPDL$_x$PEG$_{56}$PPDL$_x$ triblock copolymers in bulk and as nanoparticles.

Table A1. Melting temperatures and enthalpies of PPDL$_x$PEG$_{56}$PPDL$_x$ triblock copolymers in bulk and as nanoparticles.

Copolymer	In bulk		NPs	
	T_m ºC	ΔH_m J·g^{-1}	T_m ºC	ΔH_m J·g^{-1}
PPDL$_{16}$PEG$_{56}$PPDL$_{16}$	92	122	88	8
PPDL$_{46}$PEG$_{56}$PPDL$_{46}$	94	132	92	109
PPDL$_{191}$PEG$_{56}$PPDL$_{191}$	95	180	93	46

Calculations based on ^{1}HNMR data for molecular weight determinations

^{1}H NMR spectroscopy was used to determine polymer number-average molecular weights (M_n).

Firstly, the M_n of the macroinitiator was assessed according the ^{1}HNMR spectrum shown in Figure S1A. To calculate the number of repeating units (x) in the PPDL-NH_2, the peak area of protons a ($CONHCH_2$, δ 3.28) and protons b (CH_2OH, δ 4.12) signals were compared as followed

$$x = \frac{(31.35 + 2.06)/2}{2/2} = 16.7 \sim 15$$

The $PPDL_{15}$-b-$PBLG_{30}$ copolymer is taken as representative for M_n copolymer determination. The ^{1}HNMR spectrum is displayed in Figure S1B. By comparing the area of signal a (δ 3.51) and signal b (δ 4.52), the degree of polymerization y of the PBLG block was obtained according to the equation:

$$y = \frac{34.65/1}{4/4} = 34.65 \sim 30$$

With the respective values of x and y for the PPDL and PBLG blocks, the M_n of the block copolymer $PPDL_{15}$-b-$PBLG_{30}$ was estimated:

$$M_n = [(240*15) + (132) + (219*30)] \text{ g·mol}^{-1}$$

$$M_n = 10,300 \text{ g·mol}^{-1}$$
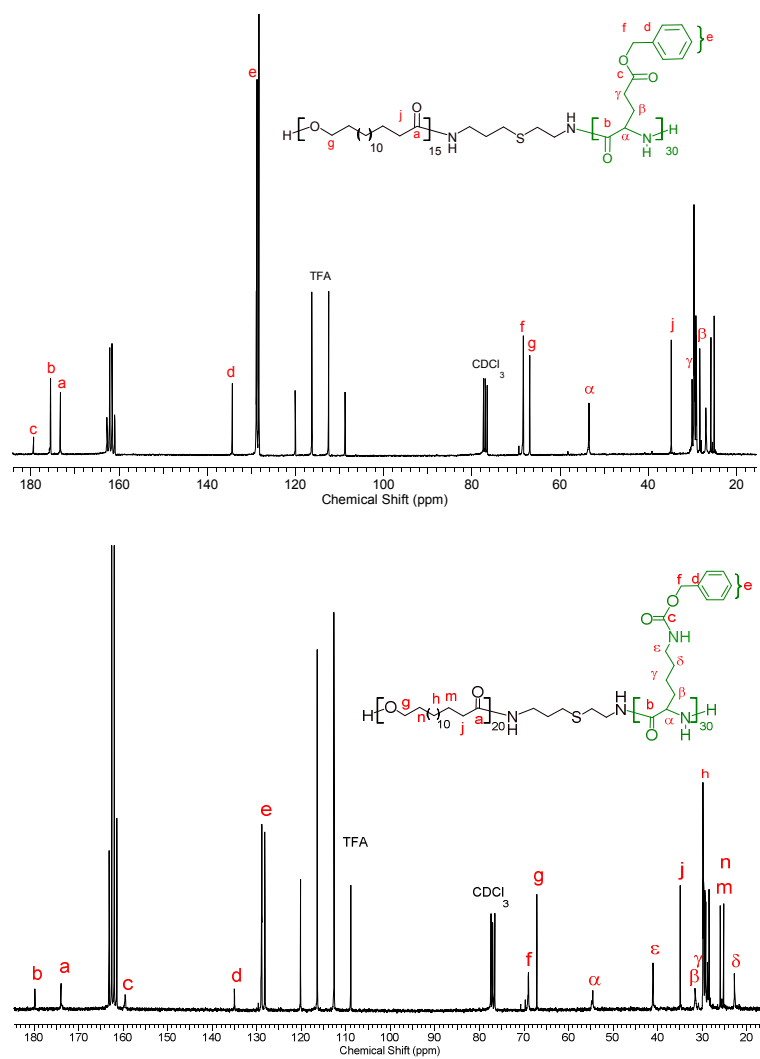
Figure B1. ^{13}C NMR of representative PPDL$_x$-*b*-pPAA$_y$ copolymers.
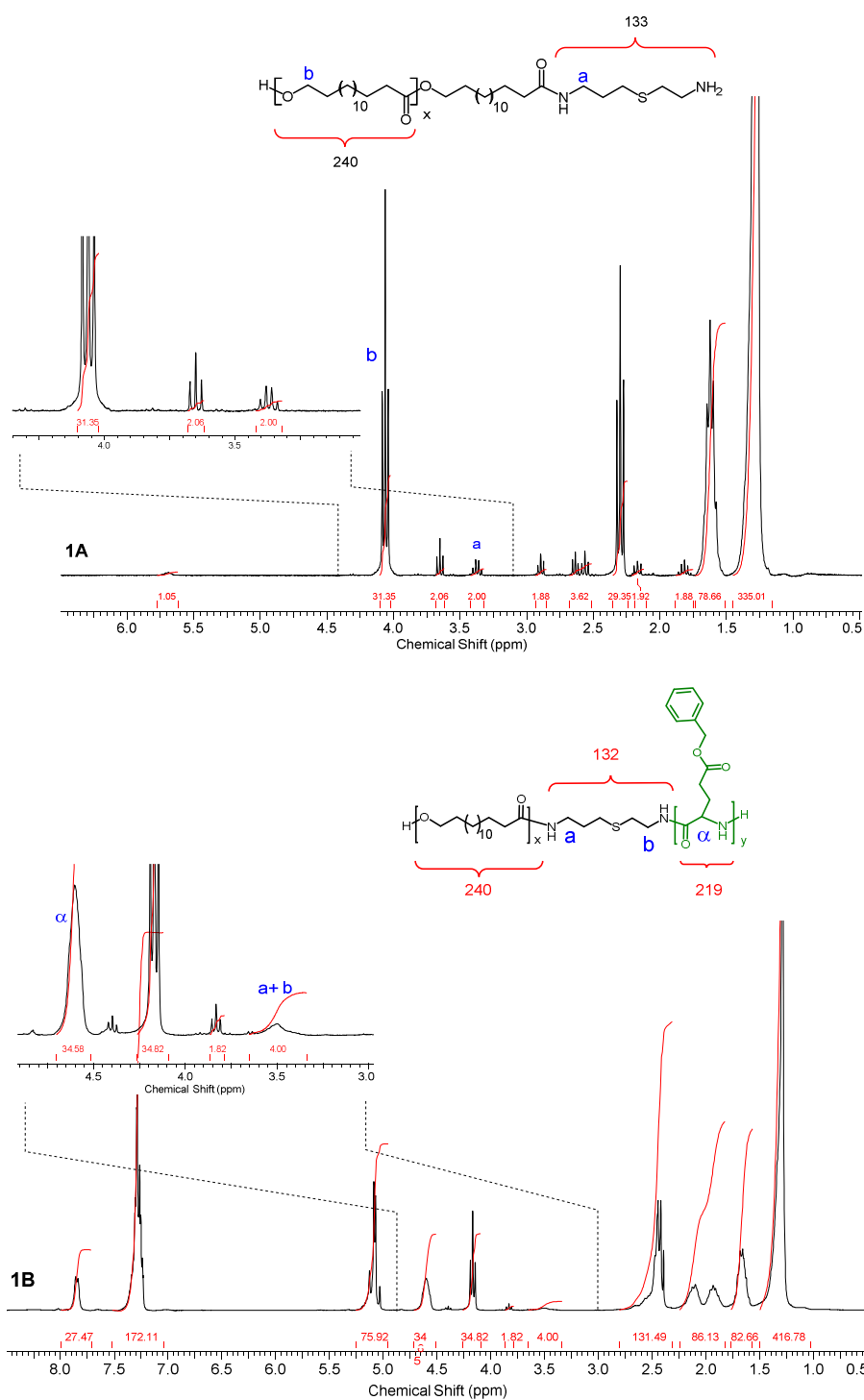
Figure B2. ^{1}H MNR spectra used for calculation of PPDL$_x$-b-pPAA$_y$ copolymer compositions.
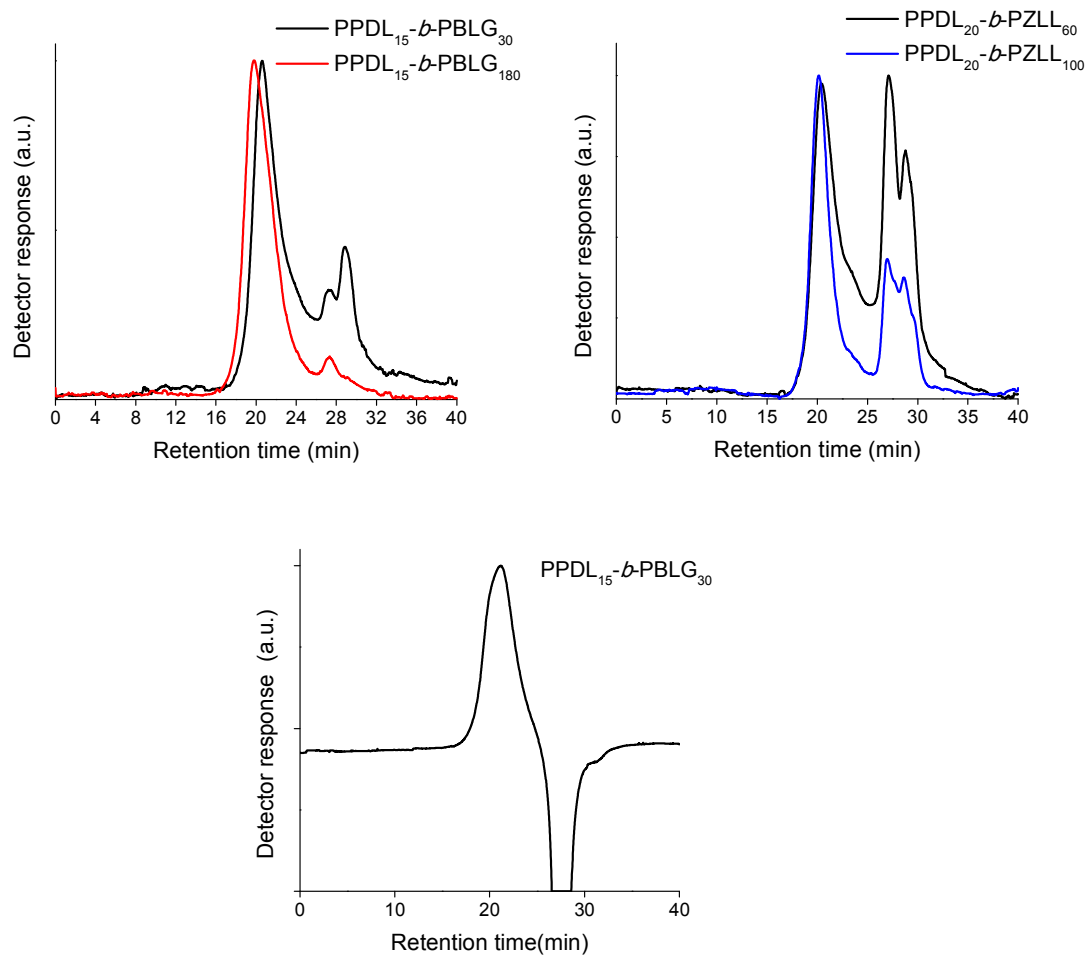
Figure B3. Top: GPC chromatograms of representative PPDL$_x$-*b*-pPAA$_y$ copolymers. Bottom: GPC chromatogram from the PPDL$_{15}$-*b*-pPBLG$_{30}$ sample injected in neat HFIP to evidence the salt effect.
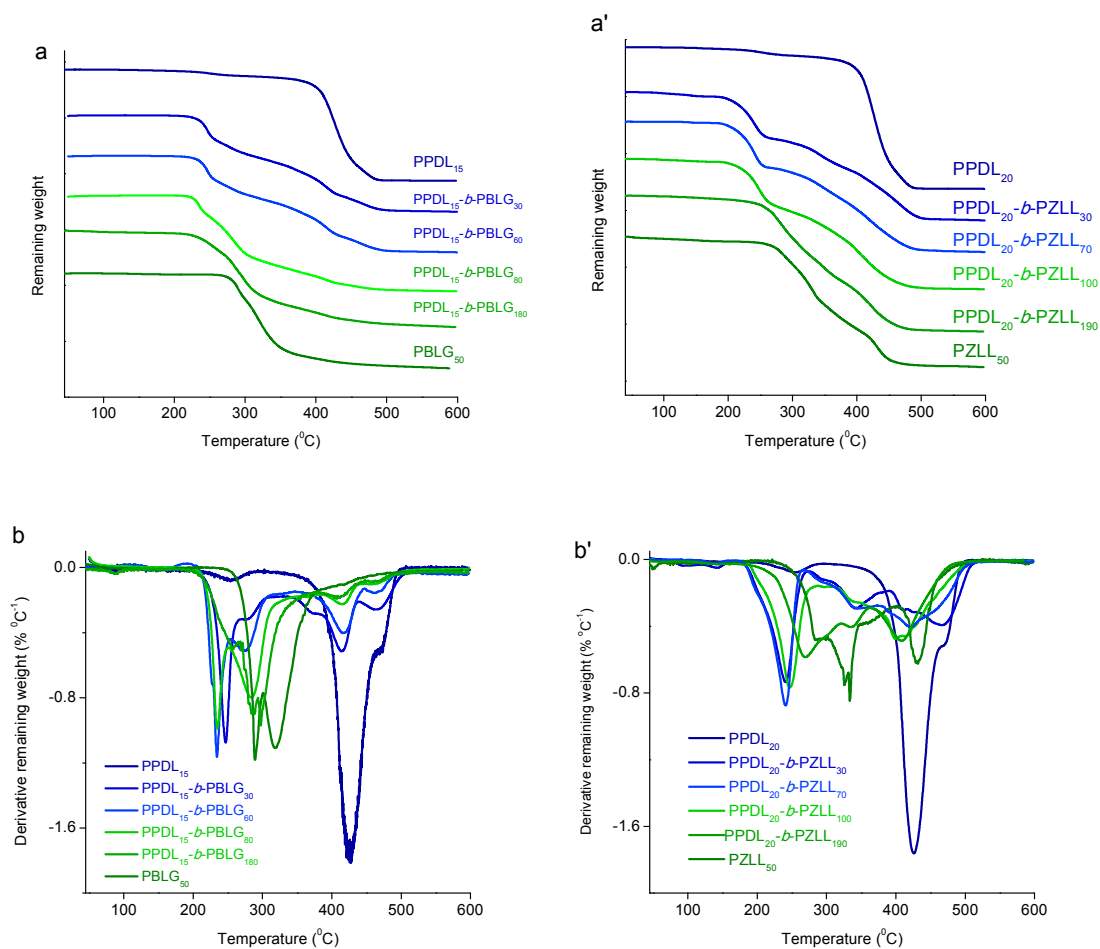
Figure B4. TGA plots of PPDL$_x$-b-PBLG$_y$ (a) and PPDL$_x$-b-PZLL$_y$ (b) copolymers and their respective derivative curves (b and b').
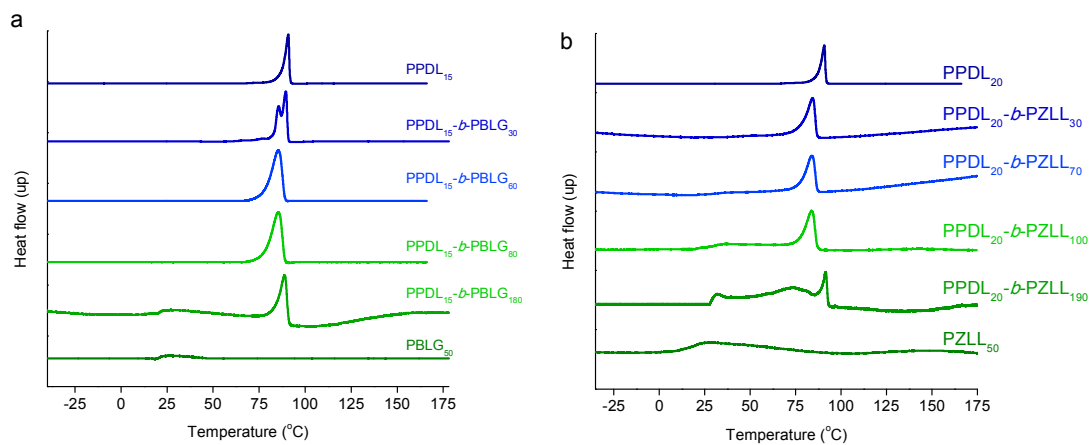
Figure B5. Second heating DSC traces of PPDL$_x$-b-pPAA$_y$ copolymers. a) PPDL$_x$-b-PBLG$_y$; b) PPDL$_x$-b-PZLL$_y$.
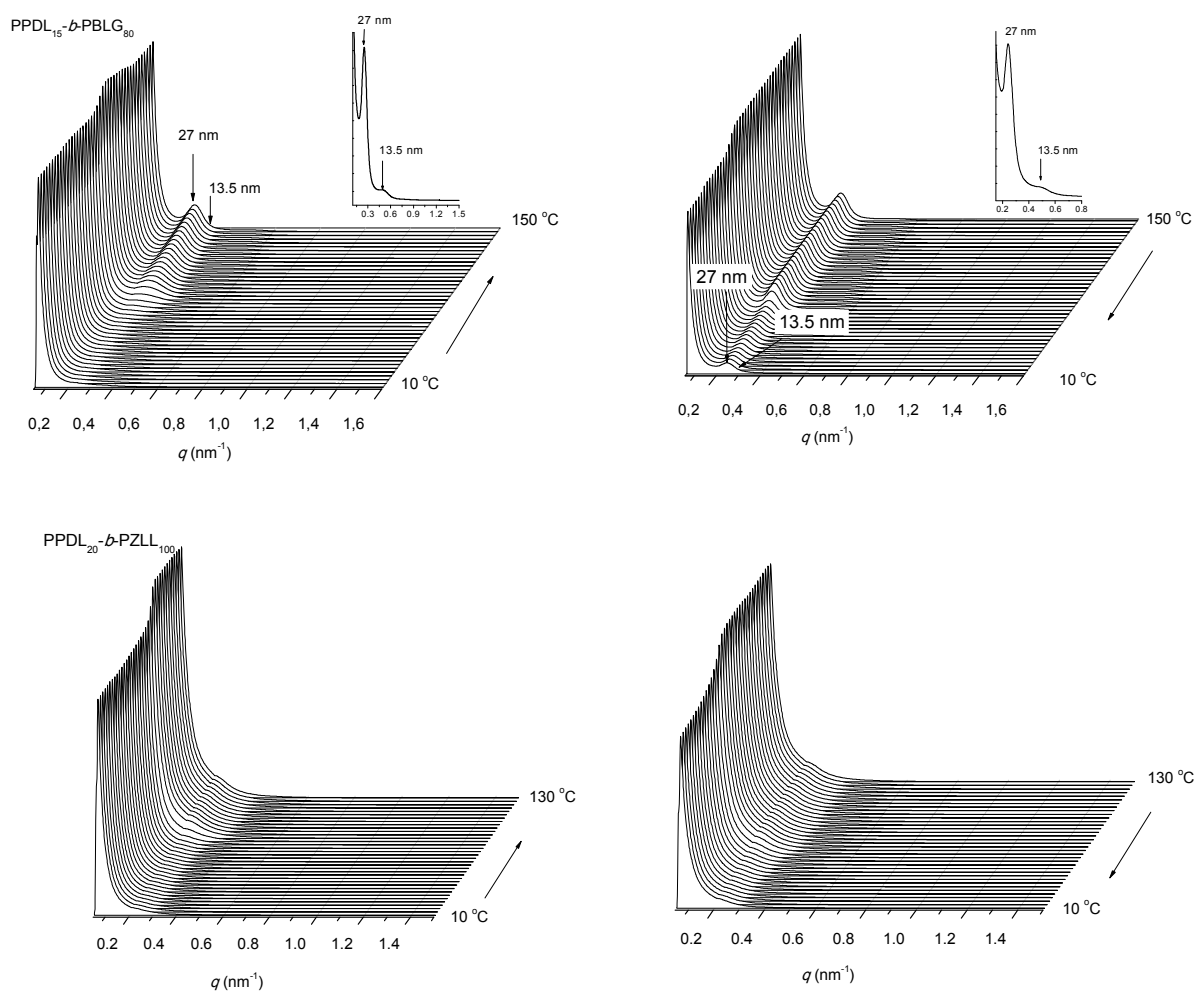
Figure B6. SAXS profiles of the indicated copolymers at both heating and cooling.
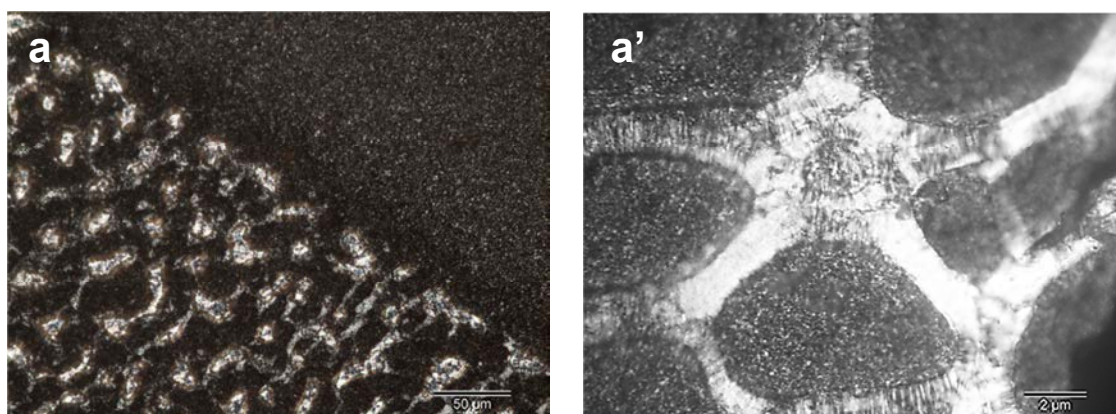
Figure B7. Polarizing optical micrographs of the PPDL$_{15}$-*b*-PBLG$_{80}$ copolymer taken at room temperature from a film casted from chloroform (a) and from a film solidified from the melt (a').
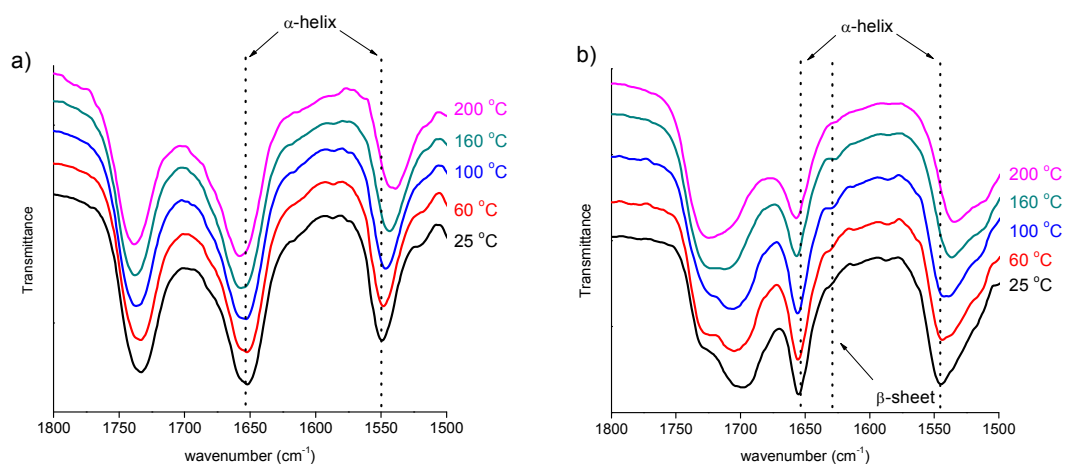
Figure B8. FTIR spectra recorded at different temperatures highlighting the amide I and II bands region: a) PPDL$_{15}$-*b*-PBLG$_{80}$ and b) PPDL$_{20}$-*b*-PZLL$_{100}$.
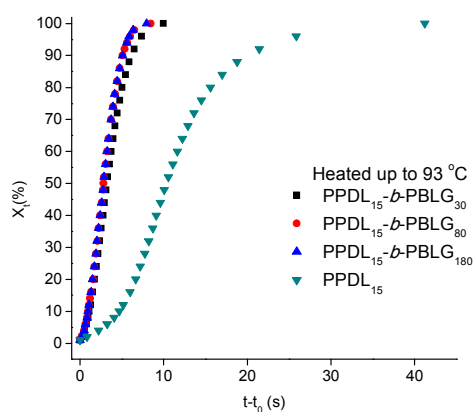
Figure B9. Relative crystallinity *vs* crystallization time for the isothermal crystallization of the indicated copolymers previously heated at 93 $^{\circ}$C.
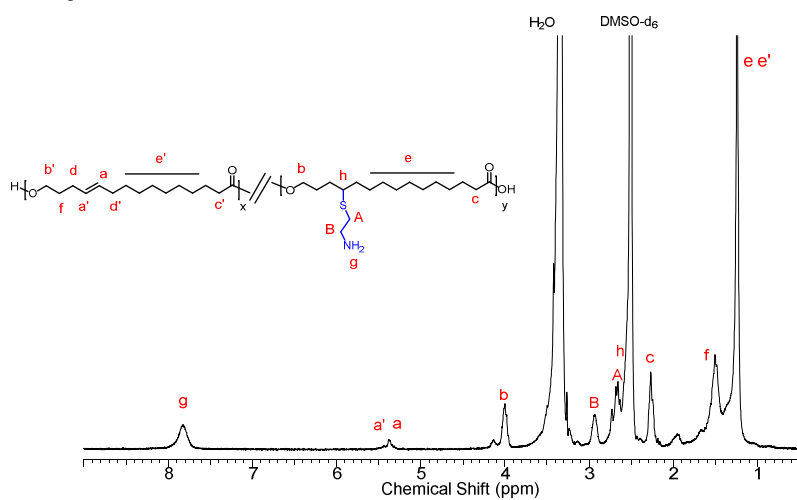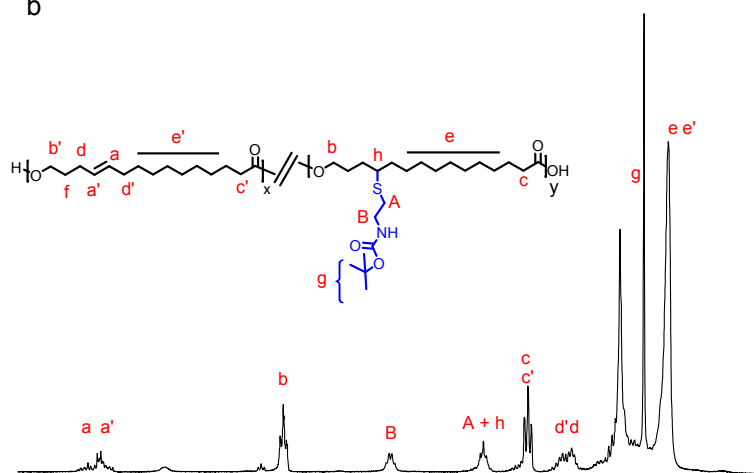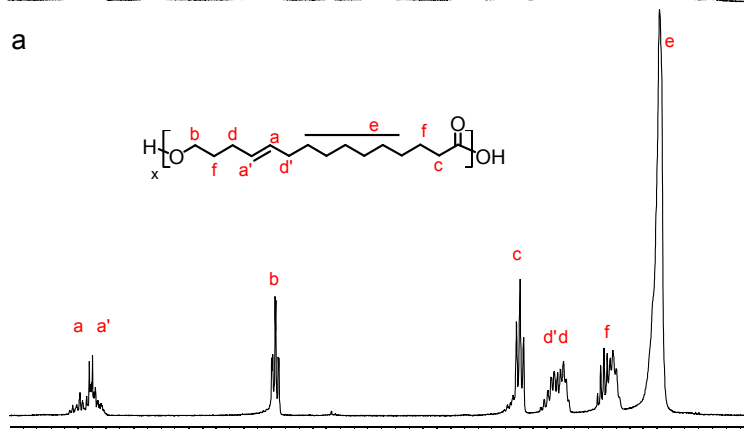
Figure. C1. ^{1}H-NMR (CDCl$_3$) spectra of: (a) polyglobalide, (b) poly[Gl$_8$-*co*-(Gl-AET)$_{12}$], and (c) poly[Gl$_8$-*co*-(GlNH$_2$)$_{12}$] (DMSO-$_{d6}$).
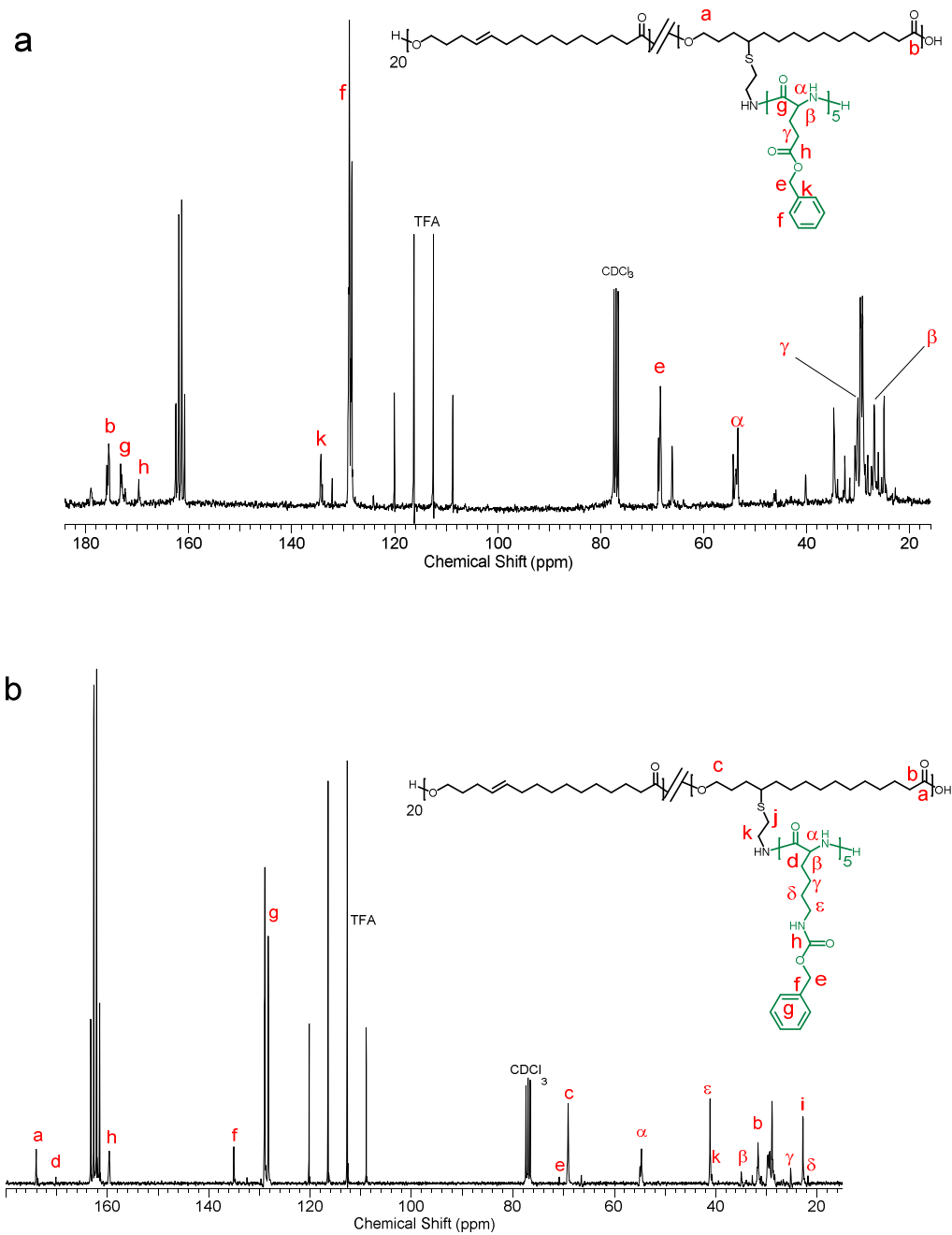
Figure C2. ^{13}C NMR (CDCl$_3$/TFA) spectra of a) poly[Gl20-*graft*-(BLG)5] and b) poly[Gl20-*graft*-(ZLL)5] copolymers.
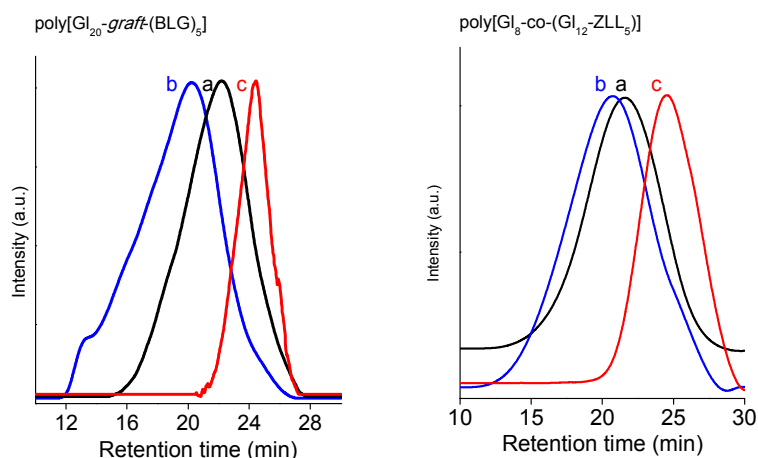
Figure C3. GPC traces of poly[Gl$_{20}$-*graft*-(AA)$_z$] copolymers and precursors: BLG-grafted (left) and ZLL-grafted (right). a: poly[Gl$_8$-*co*-(AA-NH$_2$)$_{12}$], b: poly[Gl$_{20}$-*graft*-(BLG or ZLL)$_5$], c: poly[Gl$_{20}$-*graft*-(LGA or LL)$_5$].
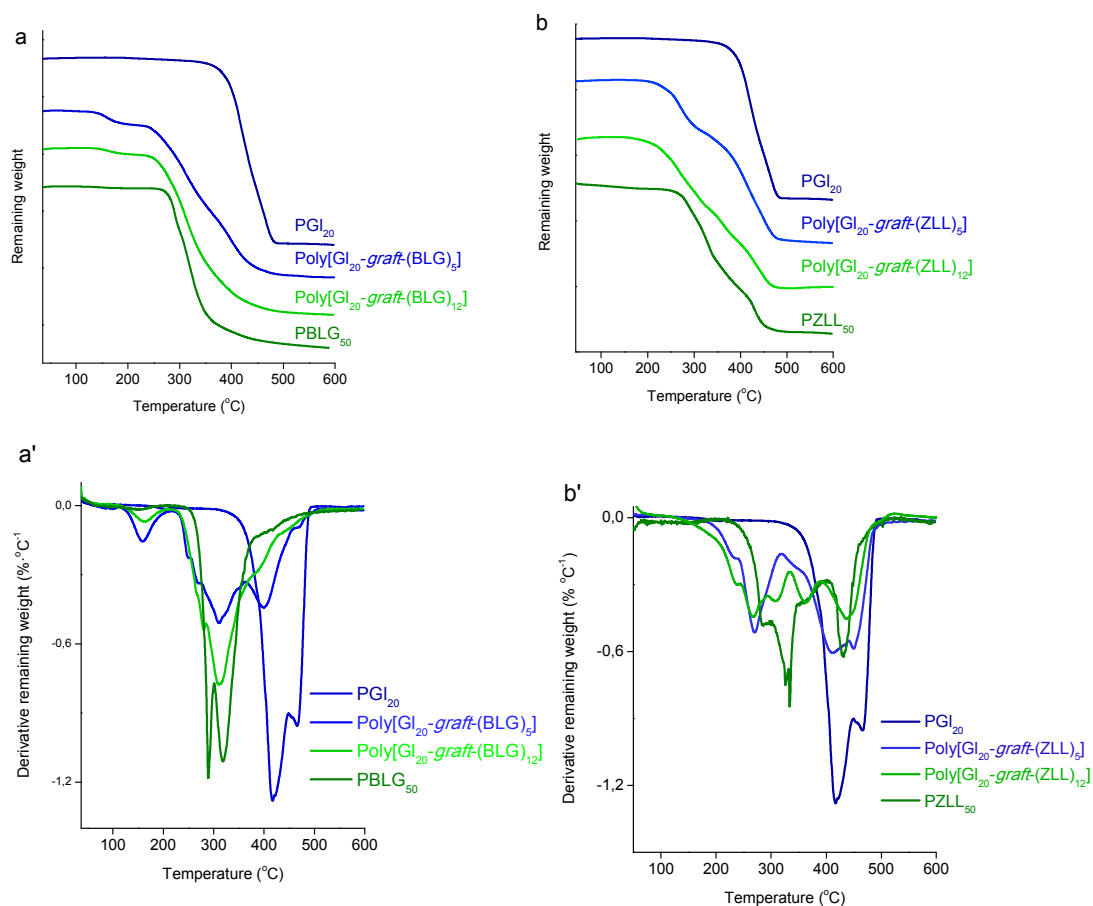
Figure C4. TGA traces (a,b) registered for protected poly[Gl$_{20}$-*graft*-(AA)$_z$] copolymers and their respective derivative curves (a',b').
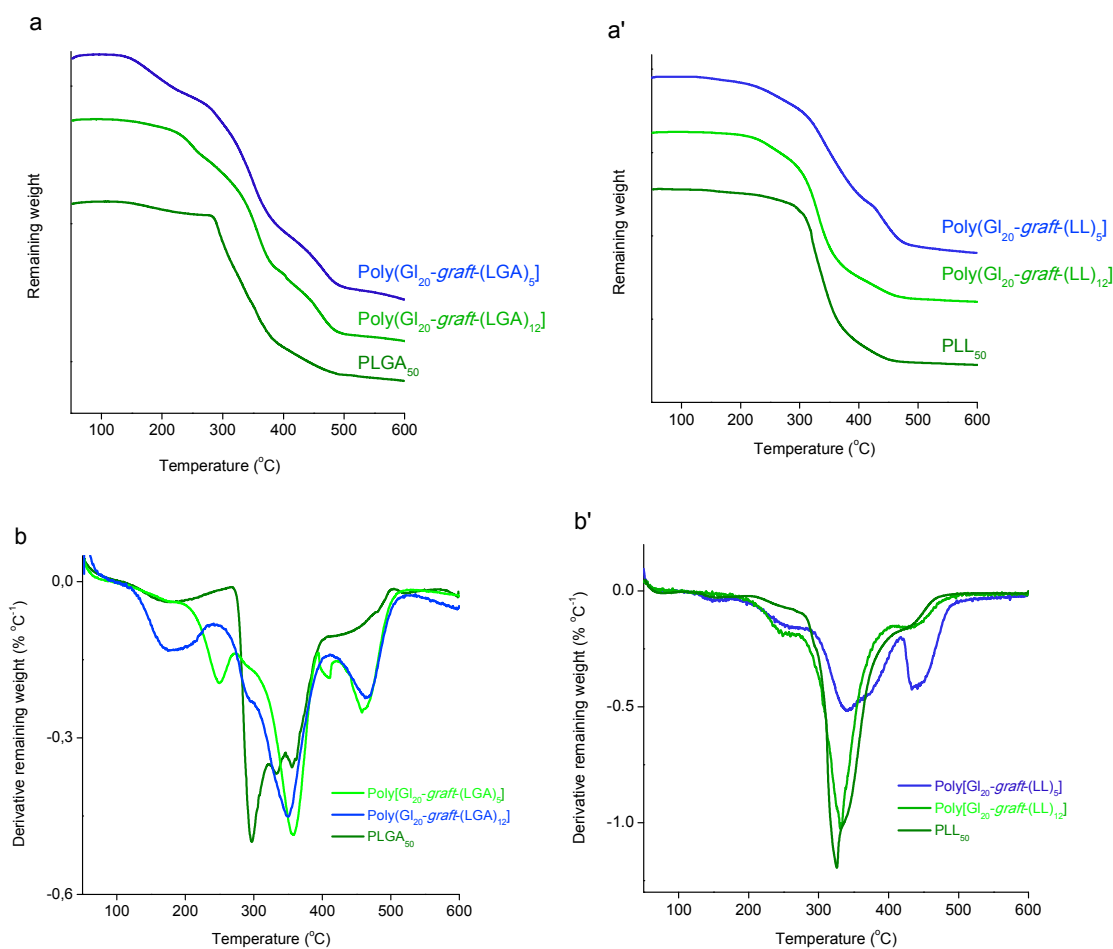
Figure C5. TGA traces (a,b) registered for deprotected poly[Gl$_{20}$-*graft*-(AA)$_z$] copolymers and their respective derivative curves (a',b').
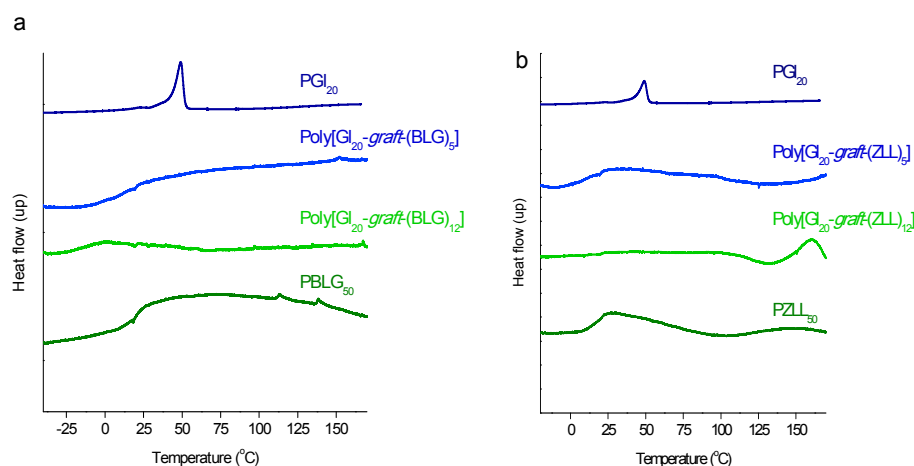
Figure C6. DSC curves (2nd heating) of protected poly[Gl$_{20}$-*graft*-(pAA)$_z$] copolymers and their parent homopolymers.
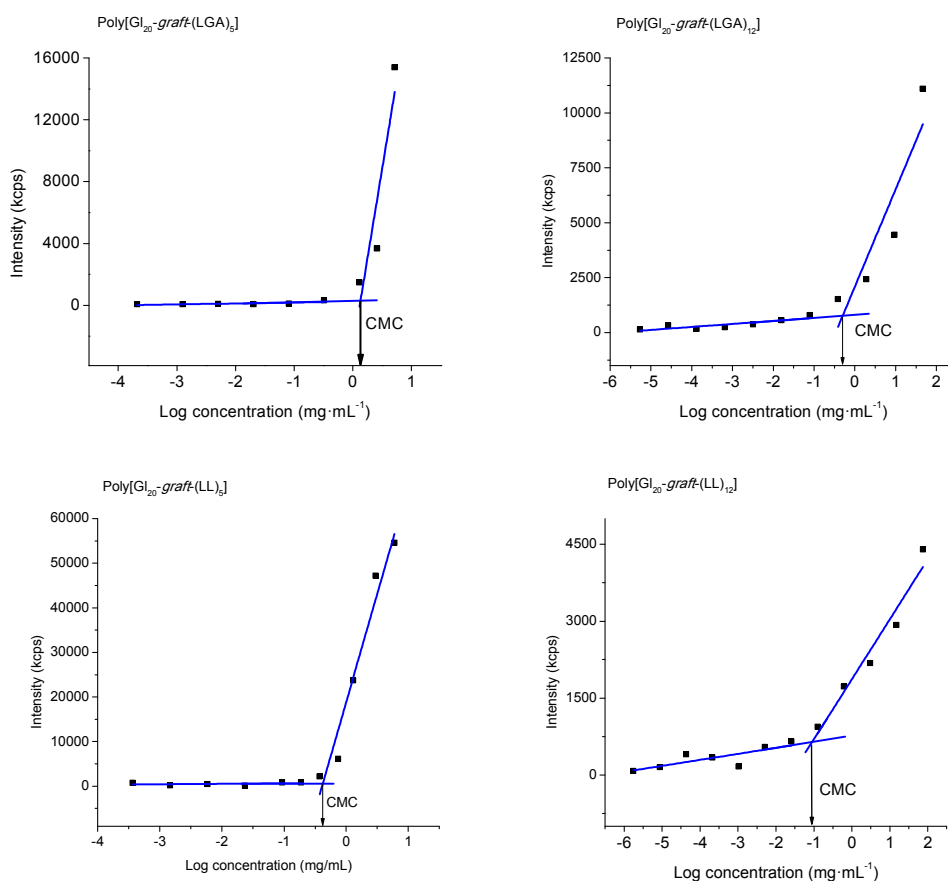
Fig. C7. Scattered light intensity *vs.* concentration for deprotected poly[Gl$_{20}$-*graft*-(AA)$_z$] copolymers. The CMC is taken as the point of intersection of the two straight lines.
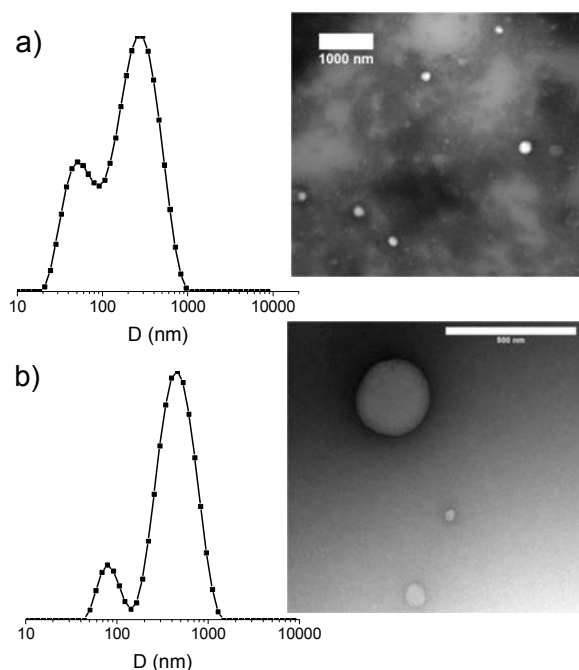
Figure C8. Size distribution profiles and TEM micrographs of nanoparticles made of: a) Poly[Gl$_{20}$-*graft*-(LGA$_5$)] and b) Poly[Gl$_{20}$-*graft*-(LL$_{12}$)] by using the nanoprecipitation method.
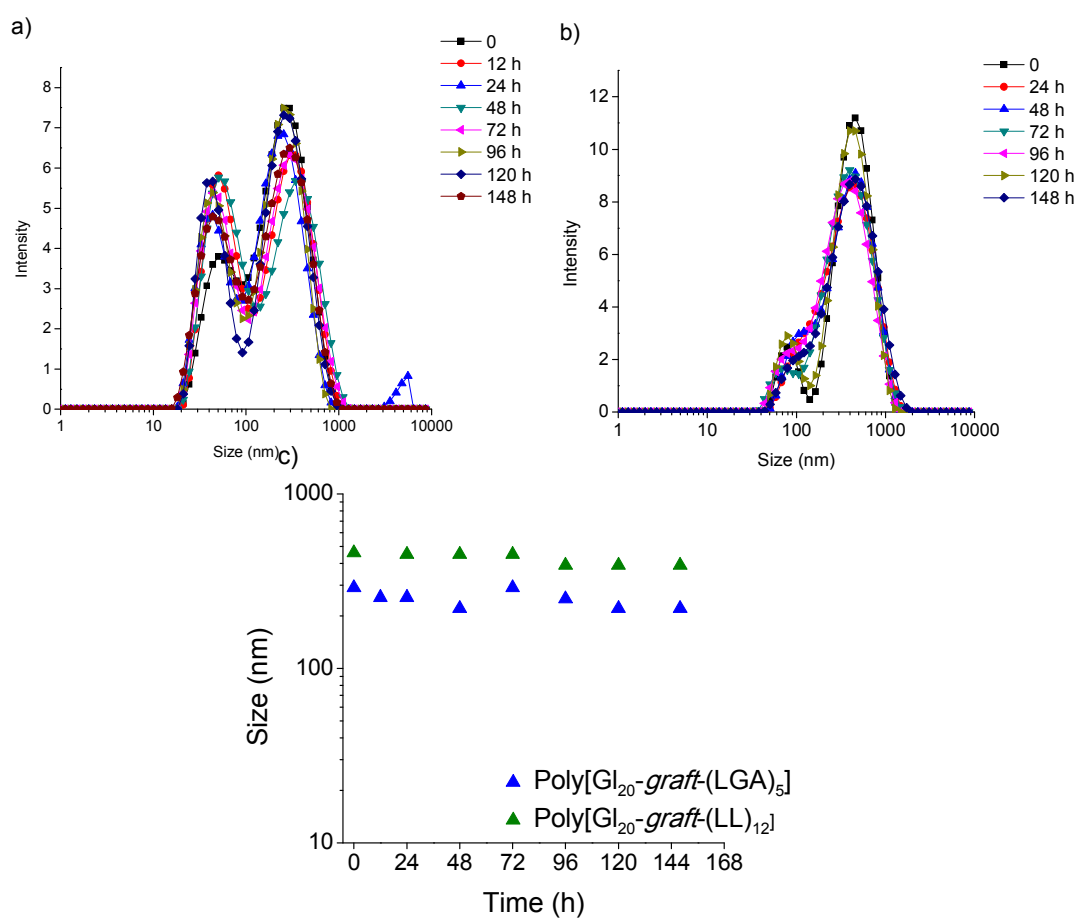
Figure C9. Size distribution profiles of nanoparticles measured along incubation time in water: a) Poly[Gl$_{20}$-*graft*-(LGA)$_5$] and b) poly[Gl$_{20}$-*graft*-(LL)$_{12}$]. c) Plot of diameters against incubation time.
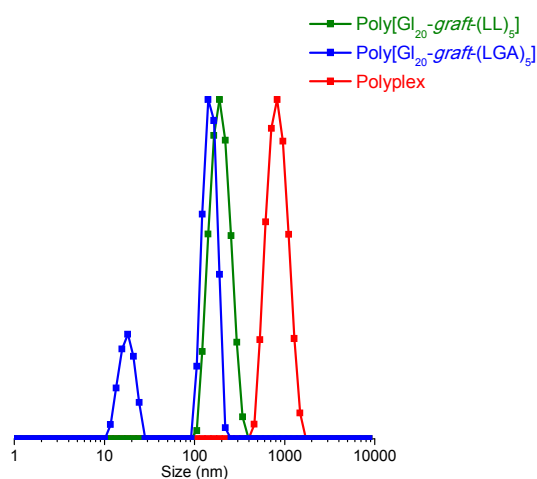
Figure C10. DLS profile of the poly[Gl$_{20}$-*graft*-(LGA)$_5$] + poly[Gl$_{20}$-*graft*-(LL)$_{12}$]. polyplex formed upon addition of the former to the latter.
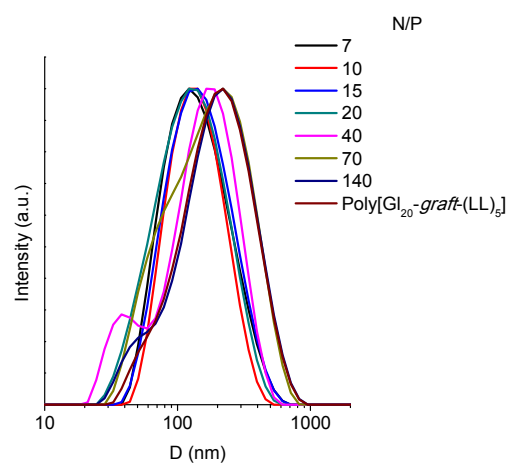
Figure C11. DLS profiles of polyplexes formed from poly[Gl$_{20}$-*graft*-(LL)$_5$] and *st*DNA.
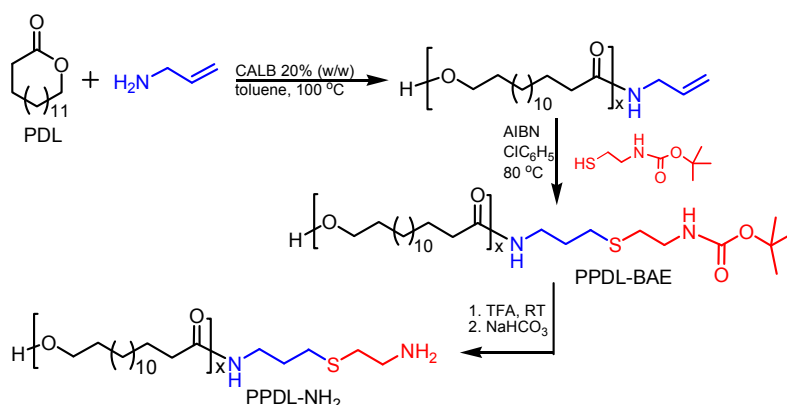
Scheme D1. Synthetic pathway leading to tPPDL-NH$_2$ macroinitiator .

a)
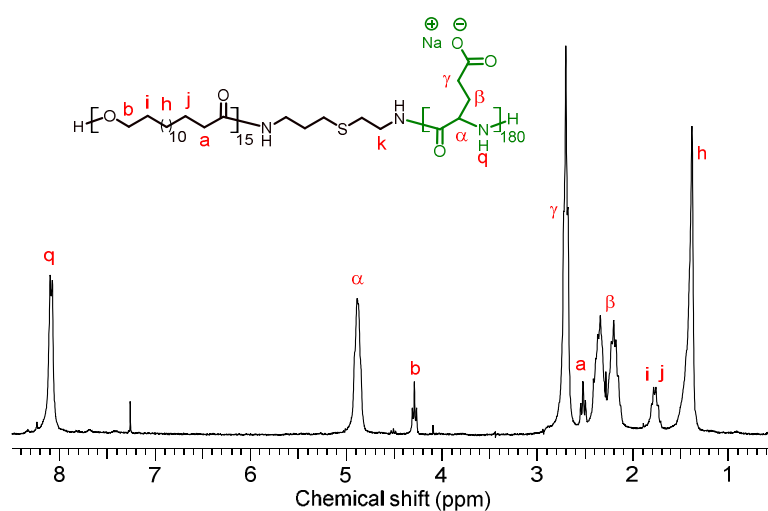
b)
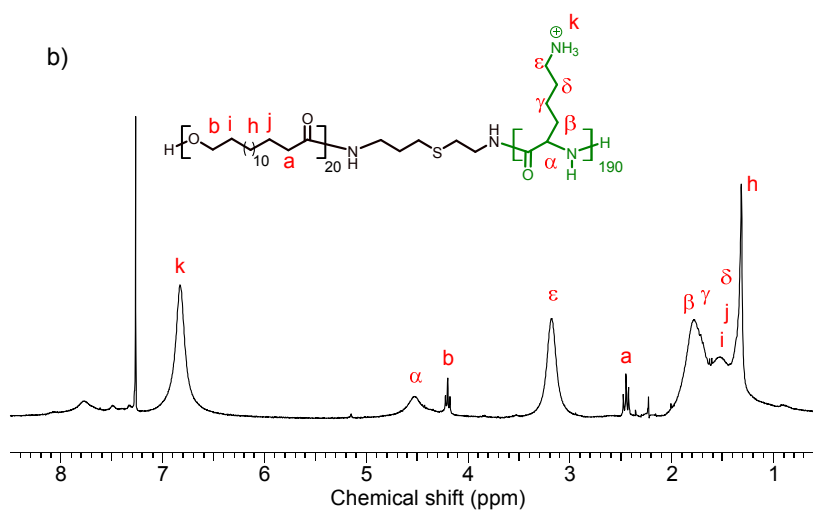
Figure D1. ^{1}H NMR (CDCl$_3$/TFA) spectra of PPDL$_x$-b-PAA$_y$ diblock copolymers: (a) PPDL$_{15}$-b-PLGA$_{180}$, and (b) PPDL$_{20}$-b-PLL$_{190}$
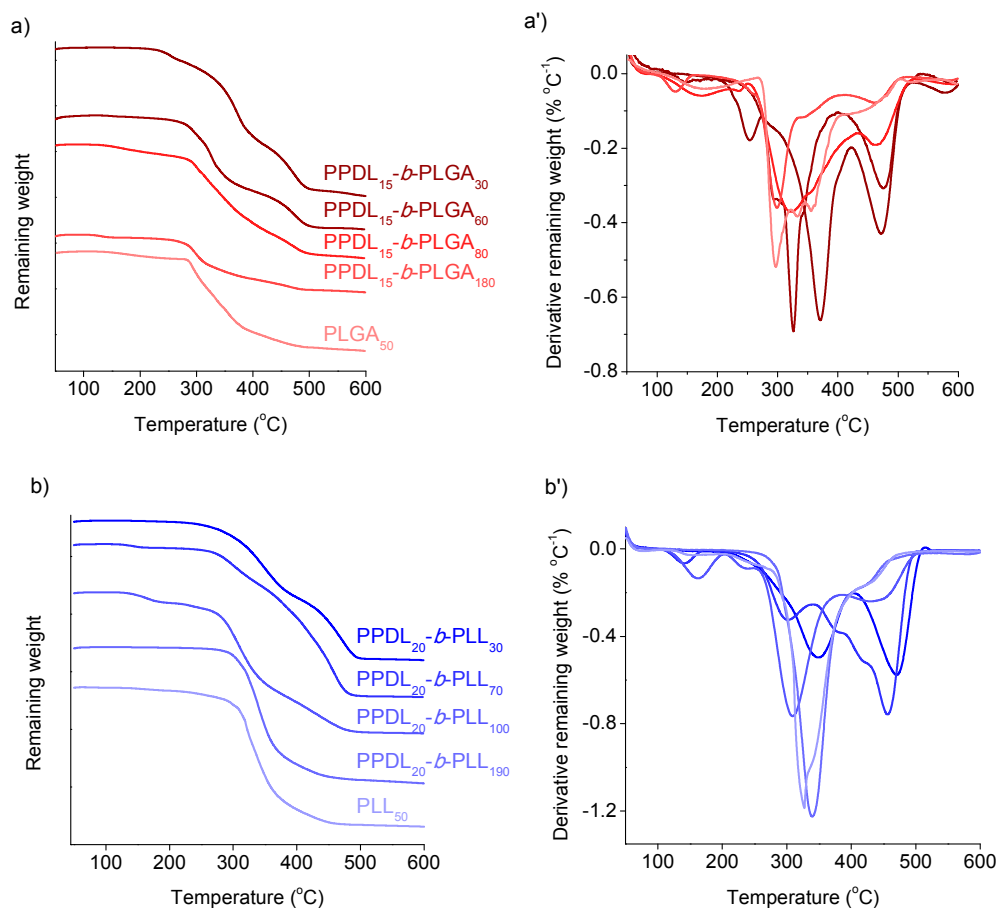
Figure D2. TGA traces (a, b) and derivative curves (a',b') of the PPDL$_x$-b-PAA$_y$ diblock copolymers.
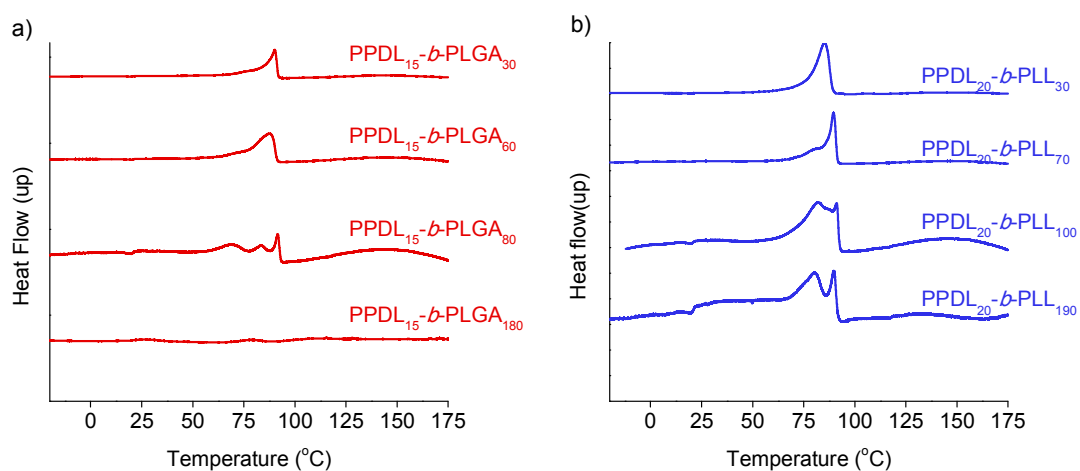
Figure D3. DSC curves (second heating) of the PPDL$_x$-b-PAA$_y$ diblock copolymers.
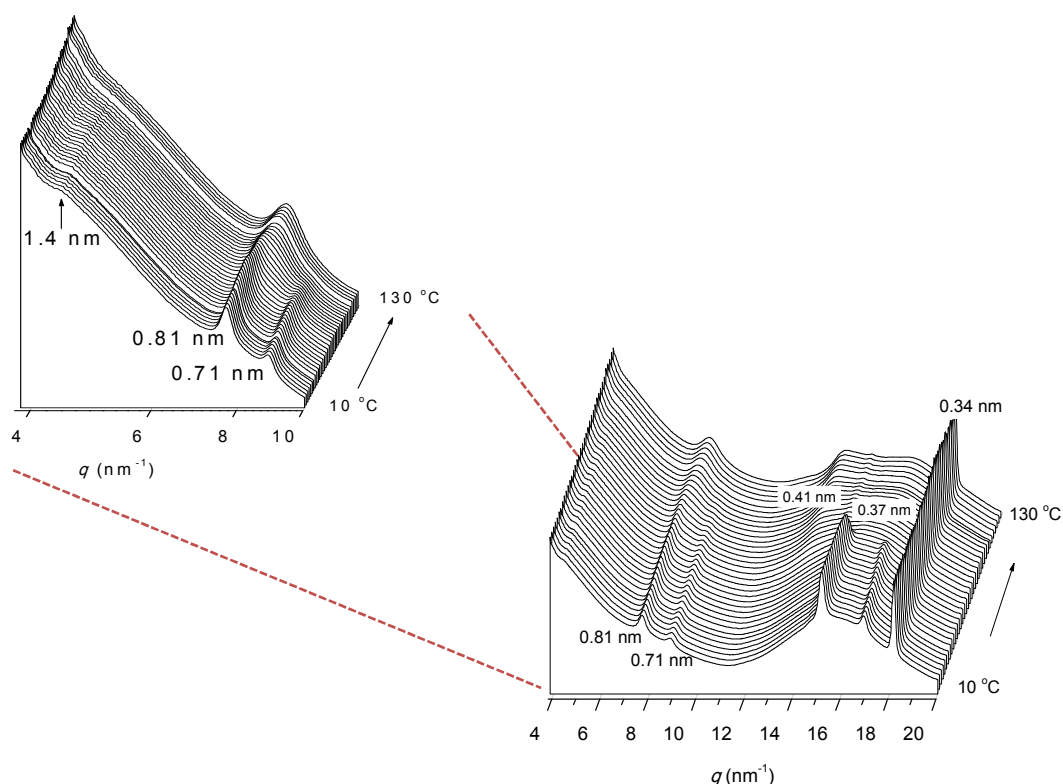
Figure D4. Enlarged region of the PPDL$_{20}$-*b*-PLL$_{100}$ diblock copolymer XRD profiles evidencing the presence of the 1.4 nm reflection.
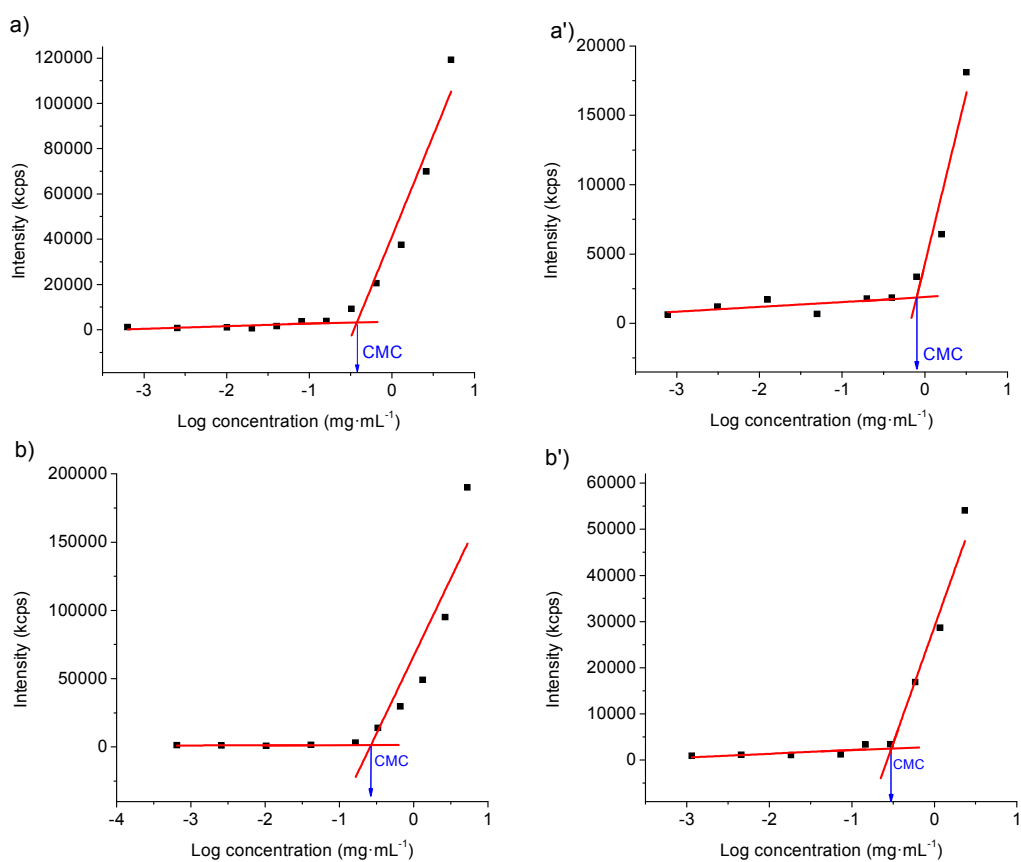
Figure D5. Critical micelle concentration of the PPDL$_{x}$-*b*-PAA$_{y}$ copolymers: (a) PPDL$_{15}$-*b*-PLGA$_{80}$ and (a') PPDL$_{15}$-*b*-PLGA$_{180}$ and (b) PPDL$_{20}$-*b*-PLL$_{100}$ and (b') PPDL$_{20}$-*b*-PLL$_{190}$.
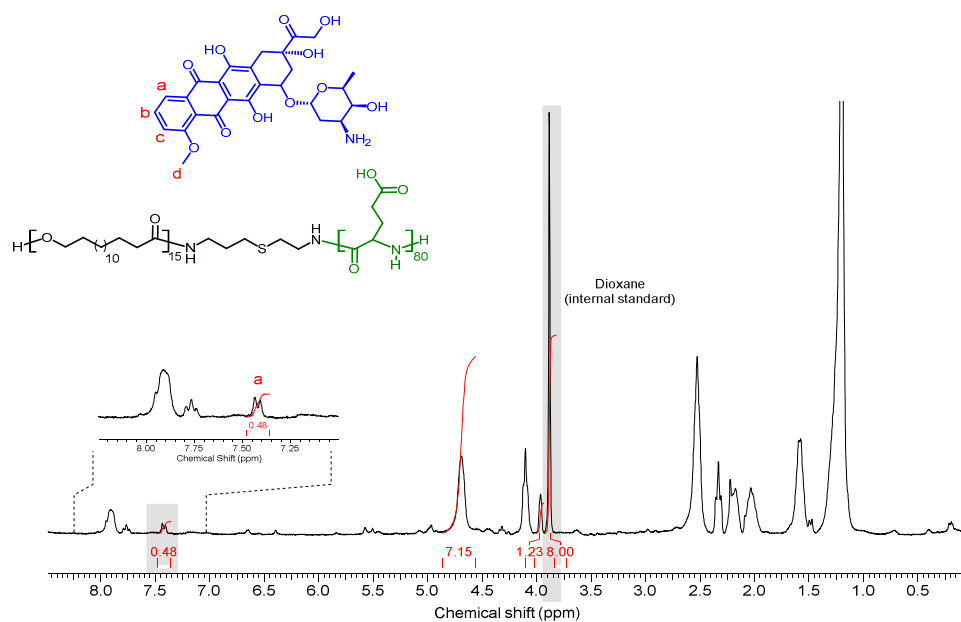
Figure D6. ^{1}H NMR spectrum (TFA-d) of the (PPDL$_{15}$-*b*-PLGA$_{80}$)+DOX conjugate containing dioxane as internal standard.
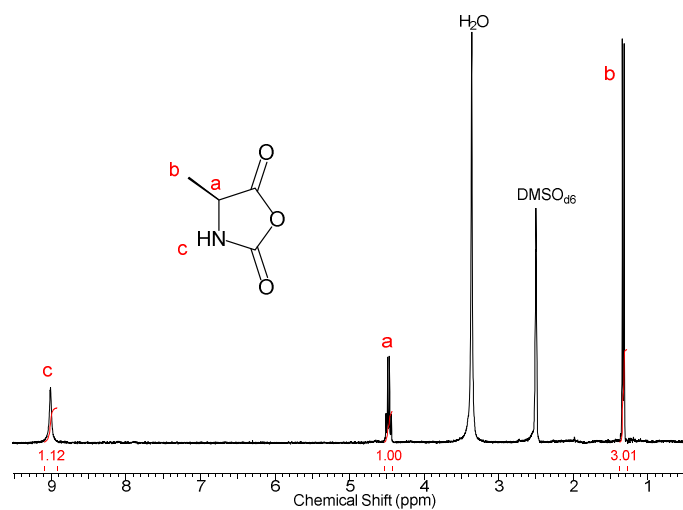
Figure E1. ^{1}H NMR (DMSO-d_6) spectrum of Ala-NCA.
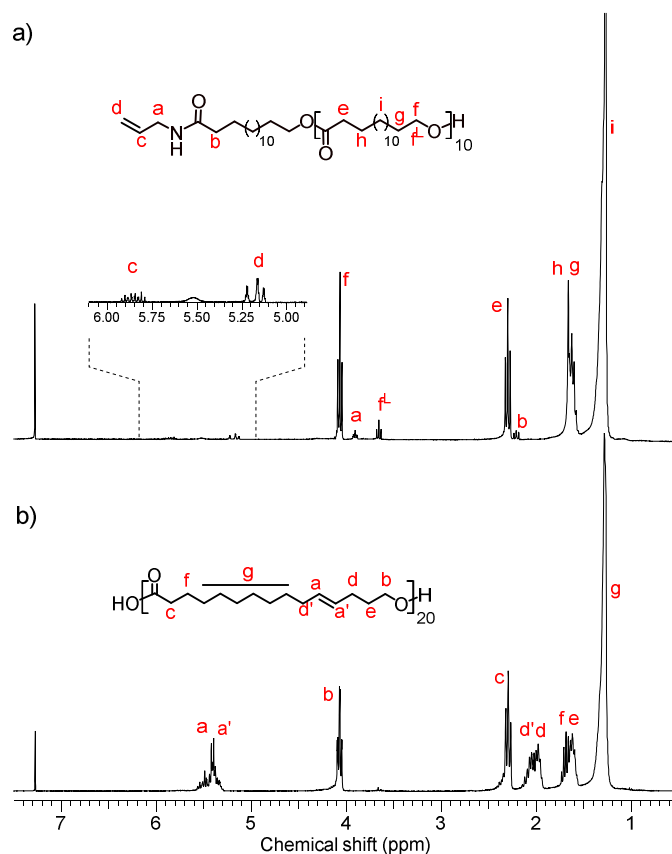
Figure E2. ^{1}H NMR (CDCl$_3$) spectra of PPDL$_{10}$ (a) and PGl$_{20}$ (b).
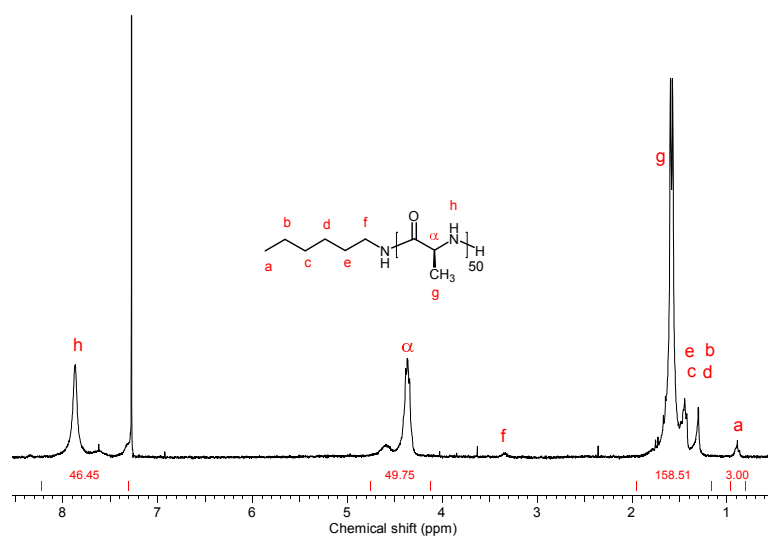
Figure E3. ^{1}H NMR (CDCl$_3$/TFA) of PAla$_{50}$.
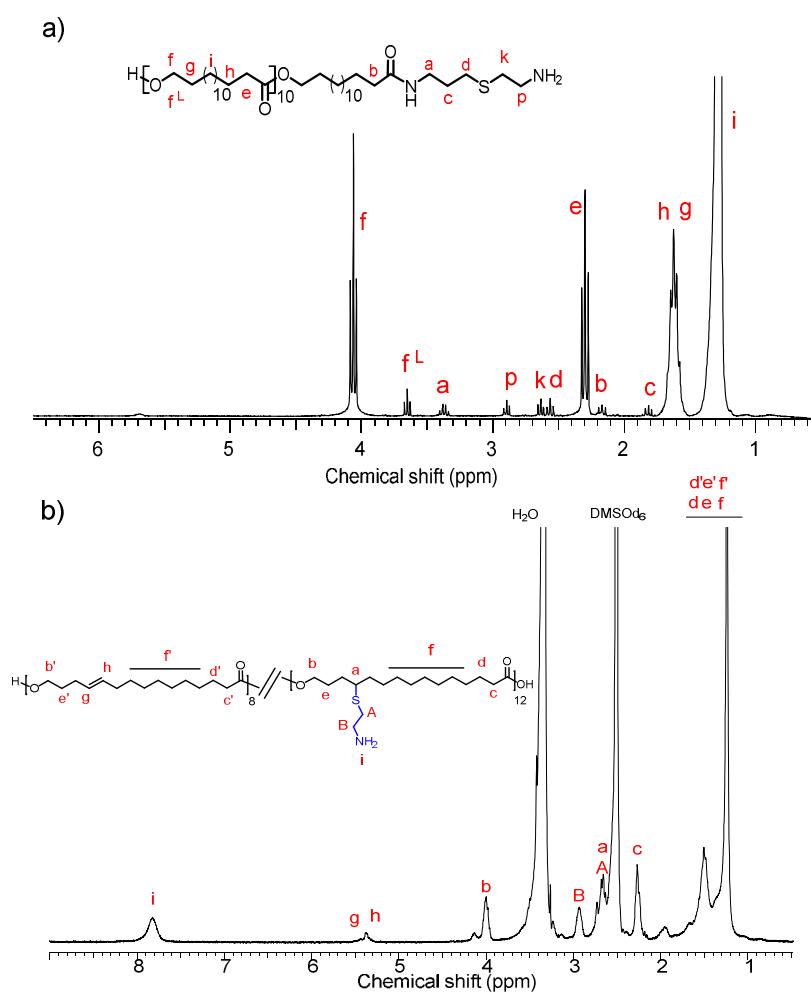
Figure E4. ^{1}H NMR spectra of the PPDL$_{10}$NH$_2$ (CDCl$_3$) and P[Gl$_8$-*co*-(GlNH$_2$)$_{12}$] (DMSO-*d*$_6$) macroinitiators.
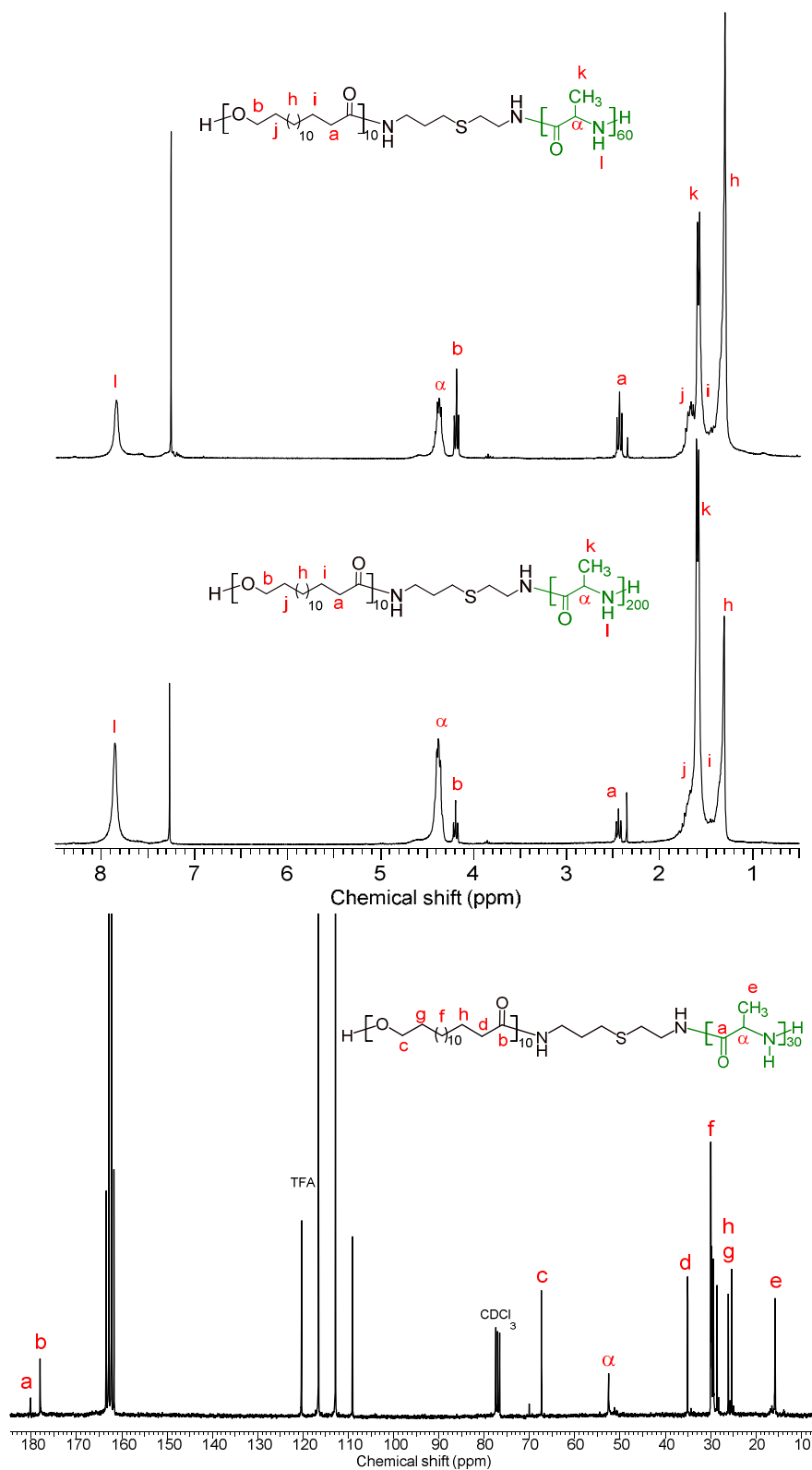
Figure E5. ^1H and ^{13}C NMR (CDCl$_3$/TFA) spectra of the indicated PPDL$_{10}$-*b*-PAla$_y$ diblock copolymers.
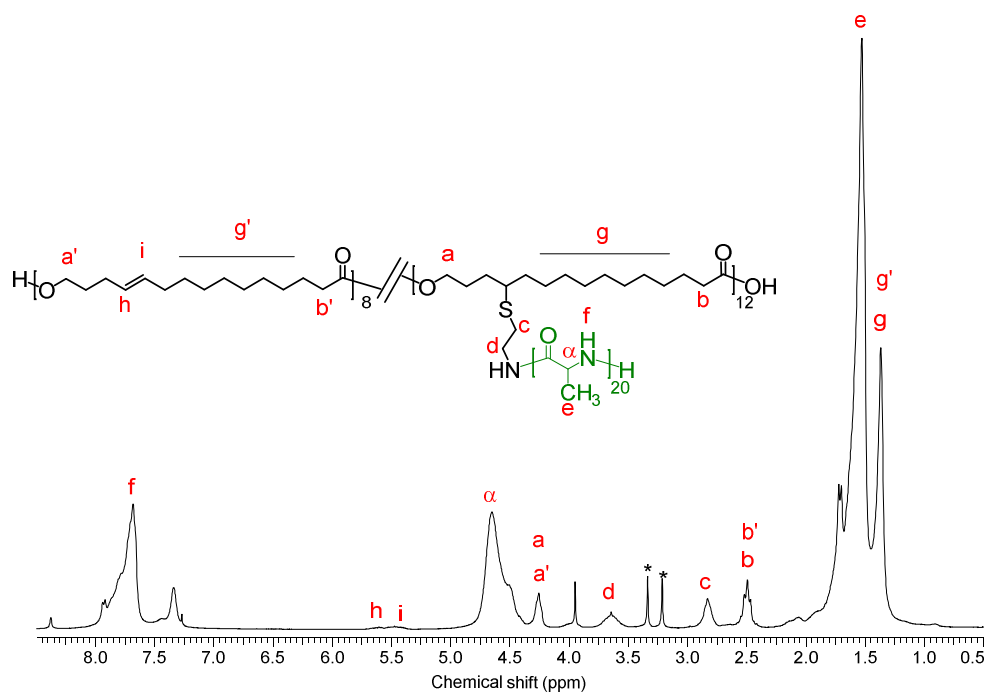
Figure E6. ^{1}H NMR (CDCl$_3$/TFA) spectrum of P[Gl$_{20}$-g-(Ala)$_{20}$] graft copolymer. *DMF.
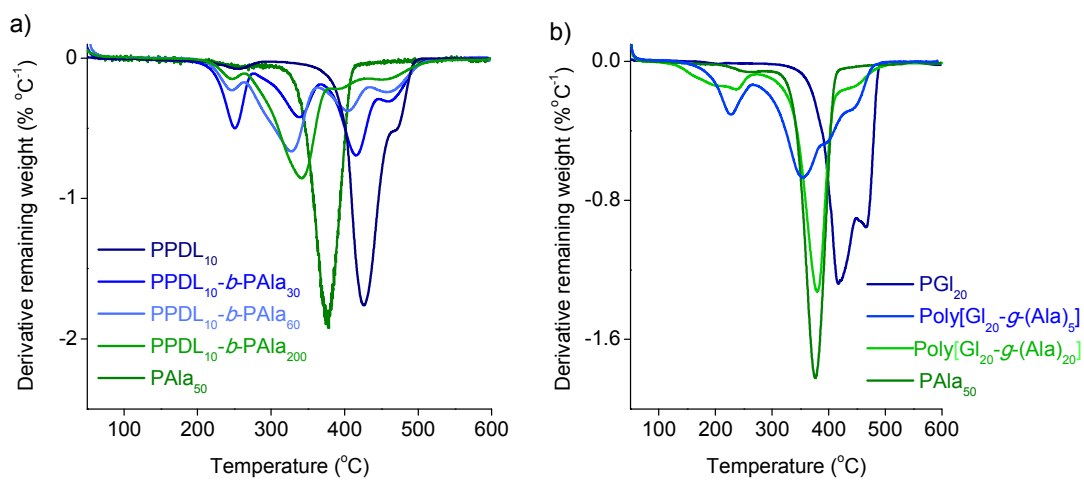
Figure E7. Derivative curves of the TGA traces registered for analysis of the PPDL$_{10}$-b-PAla$_y$ diblock (a) and P[Gl$_{20}$-g-(Ala)$_z$] (b) graft copolymers.
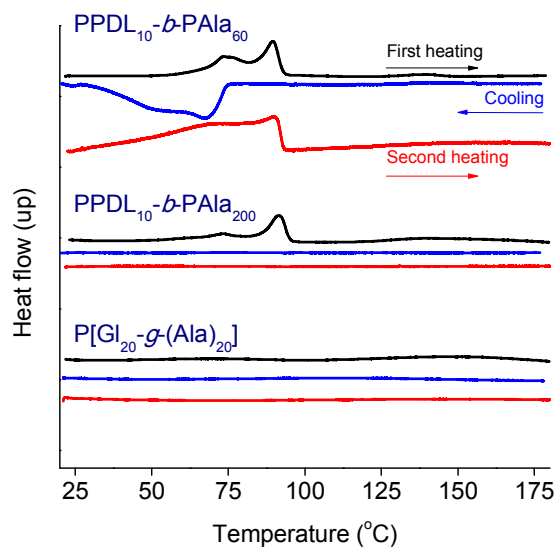
Figure E8. DSC curves of PPDL$_{10}$-b-PAla$_{60}$ and PPDL$_{10}$-b-PAla$_{200}$ diblock and P[Gl$_{20}$-g-(Ala)$_{20}$] graft copolymers.
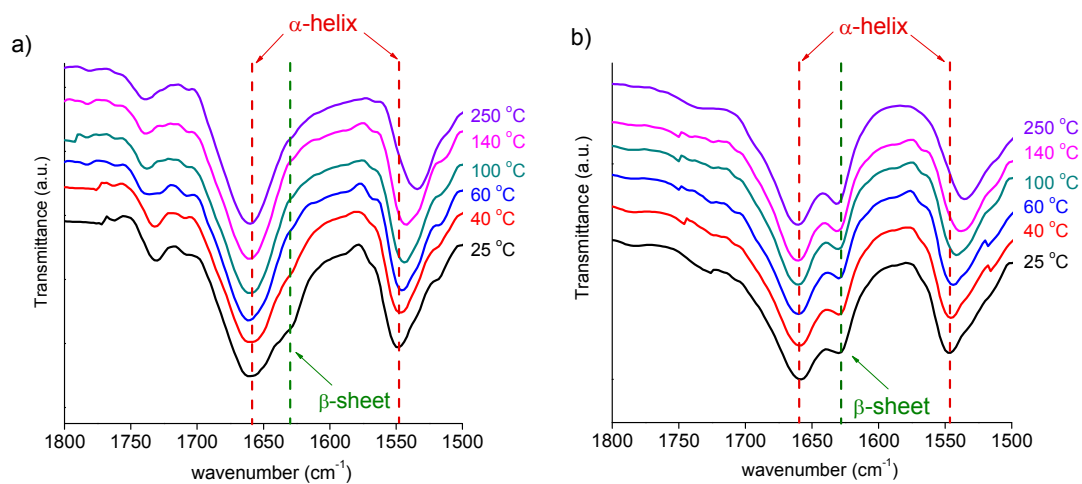
Figure E9. FTIR 1800-1500 cm^{-1} spectral region displaying the Amide I and Amide II bands recorded at heating over the 25-250 °C range of temperatures. a) PPDL$_{10}$-b-PAla$_{200}$ and b) P[Gl$_{20}$-g-(Ala)$_{20}$] copolymers.
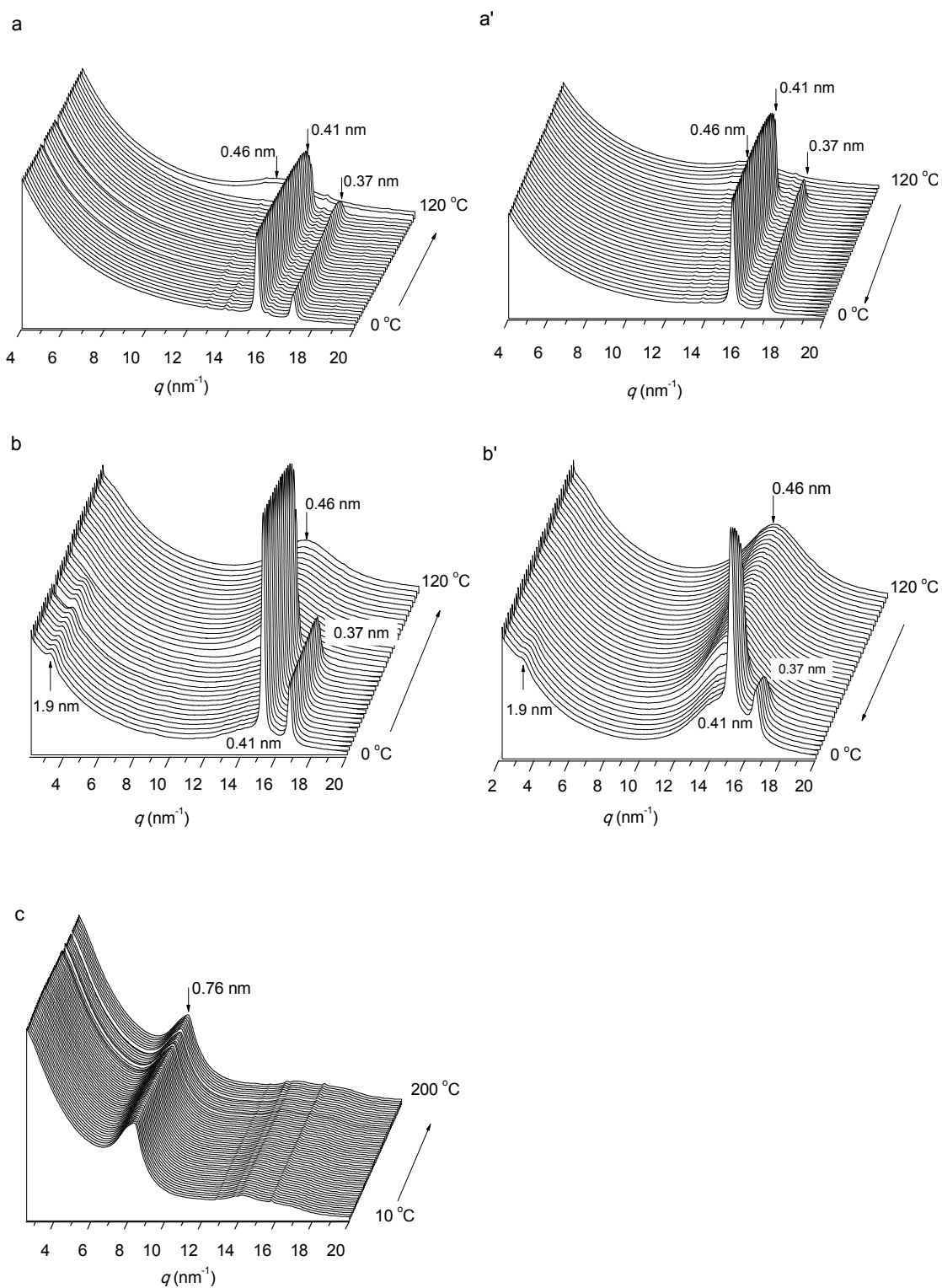
Figure E10. WAXS profiles at cooling and heating of PDL$_{10}$ (a, a'), PGl$_{20}$ (b, b') and PAla$_{50}$ (c).
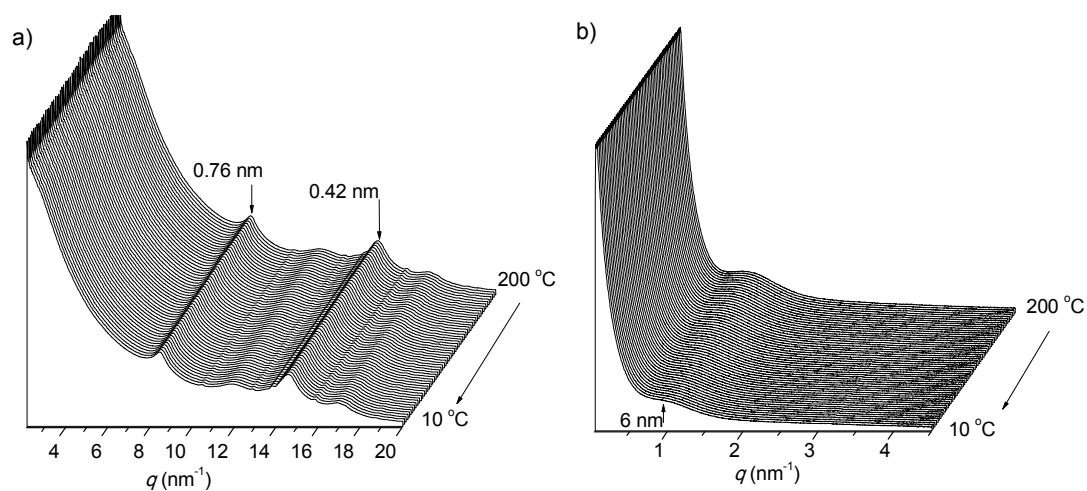
Figure E11. WAXS (a) and SAXS (b) profiles of P[Gl$_{20}$-*g*-(Ala)$_{20}$] graft copolymer registered at cooling.
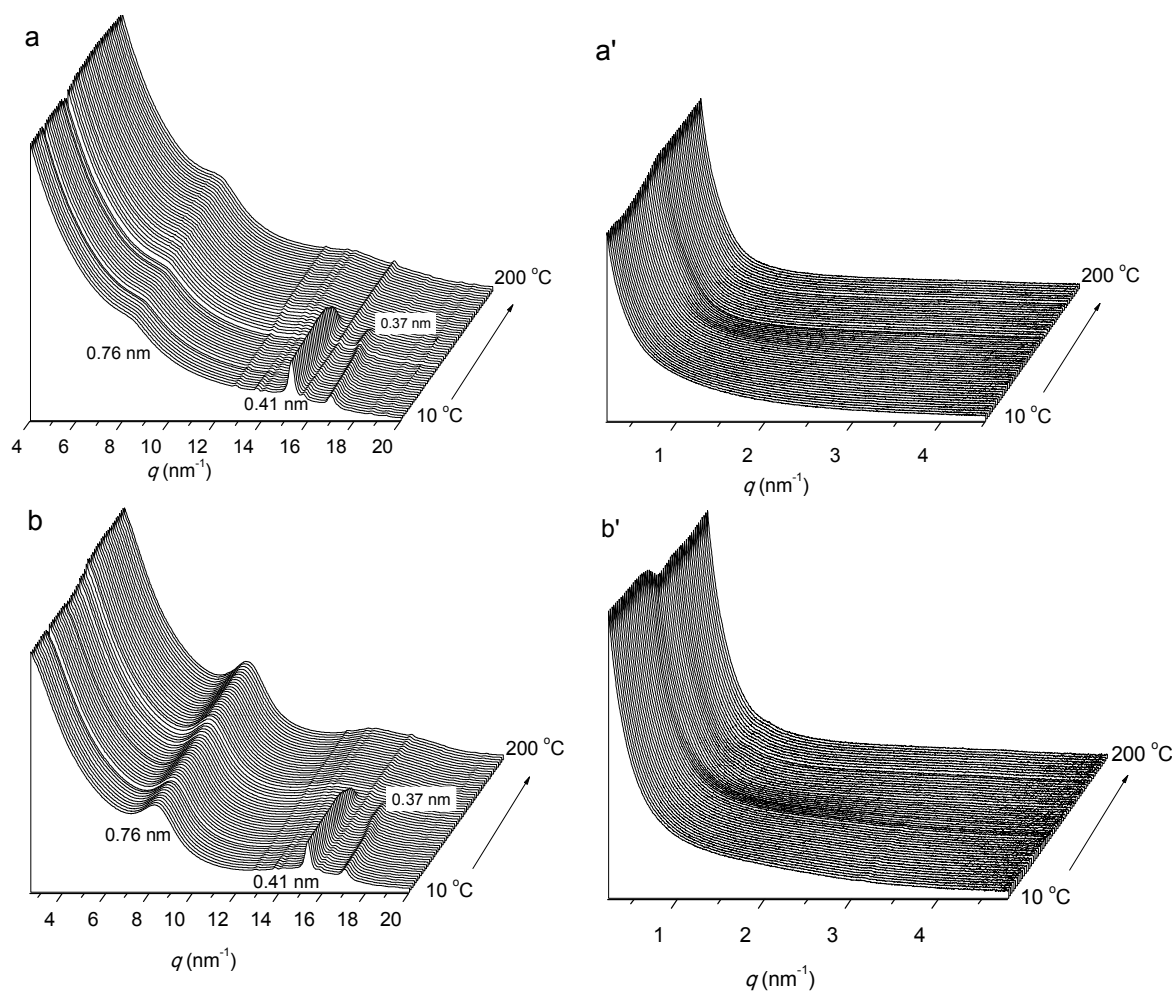
Figure E12. WAXS and SAXS profiles registered at heating from PPDL$_{10}$-*b*-PAla$_{60}$ (a, a') and PPDL$_{10}$-*b*-PAla$_{200}$ (b, b') block copolymers.
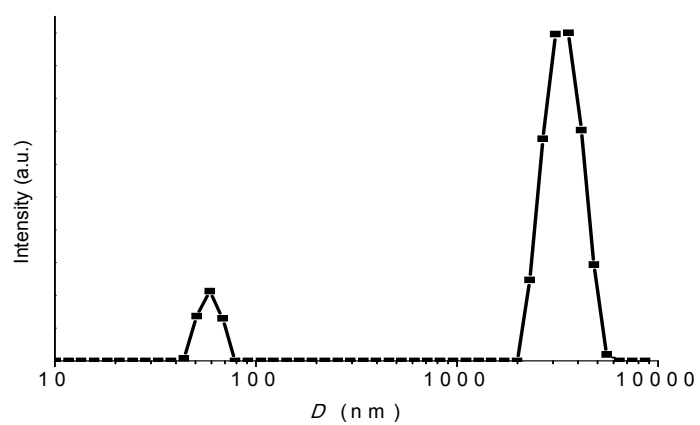
Figure E13. DLS profile of particles prepared from P[Gl₂₀-*g*-(Ala)₅] graft copolymer.
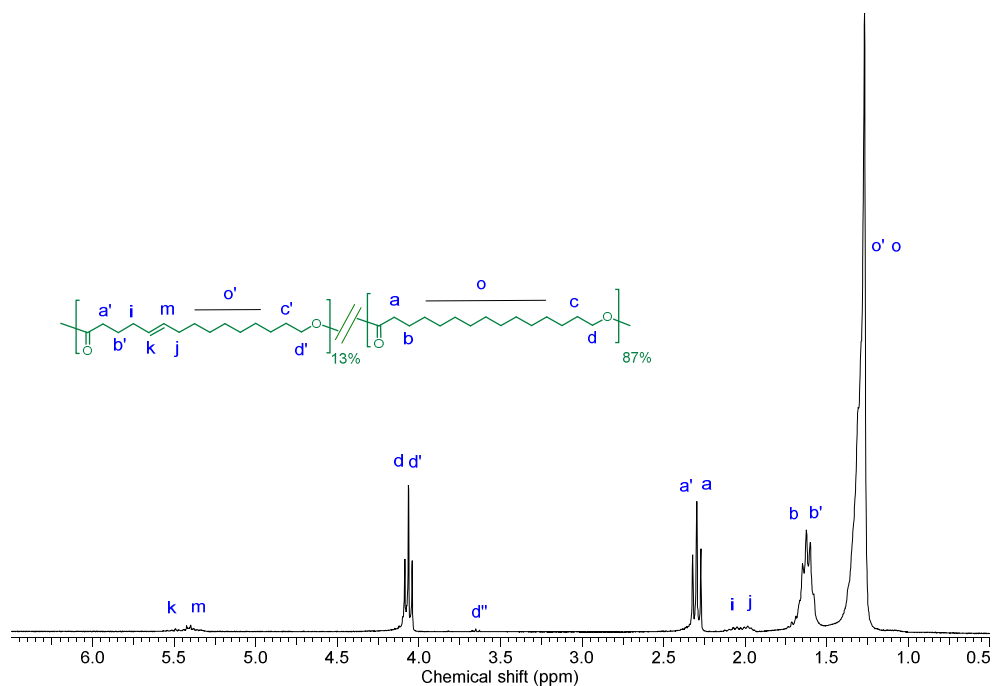
Figure F1. ^{1}H NMR (CDCl$_3$) of the P(GI$_{13}$-r-PDL$_{87}$) copolyester.
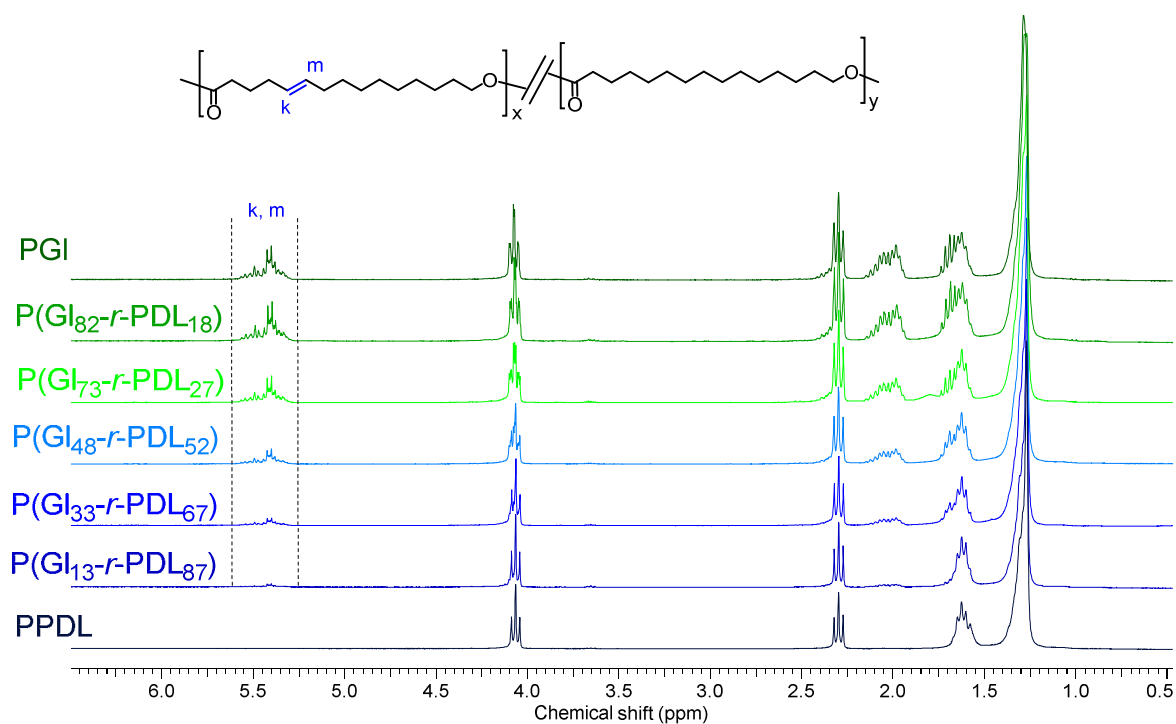
Figure F2. ^{1}H NMR (CDCl$_3$) of the P(GI$_x$-r-PDL$_y$) copolyesters

Figure F3. ^{13}C-NMR spectra of GI and PGI highlighting the peaks of the different isomers.
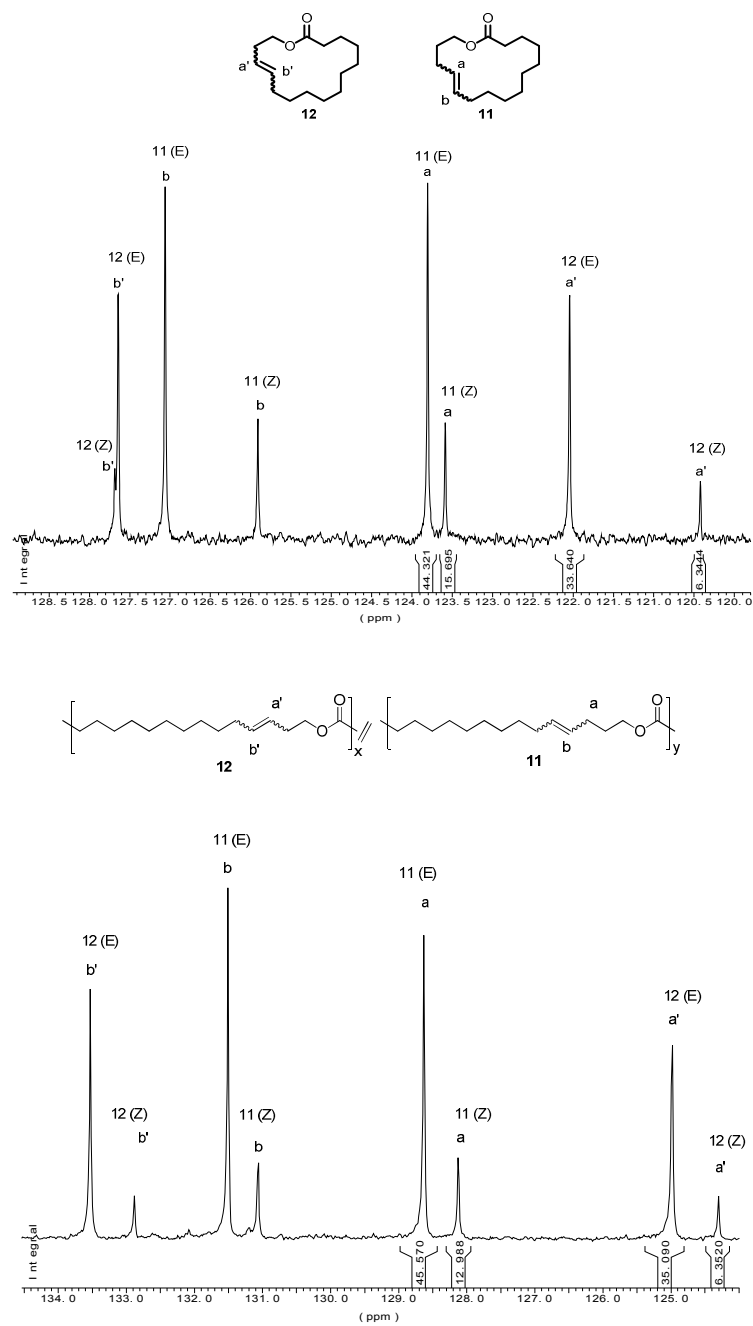
Sample	% mol-mass isomers			
	11-pentadecen-15-olide		12-pentadecen-15-olide	
	E	Z	E	Z
GI	44.3	15.7	33.6	6.3
PGI	45.6	13.0	35.1	6,3
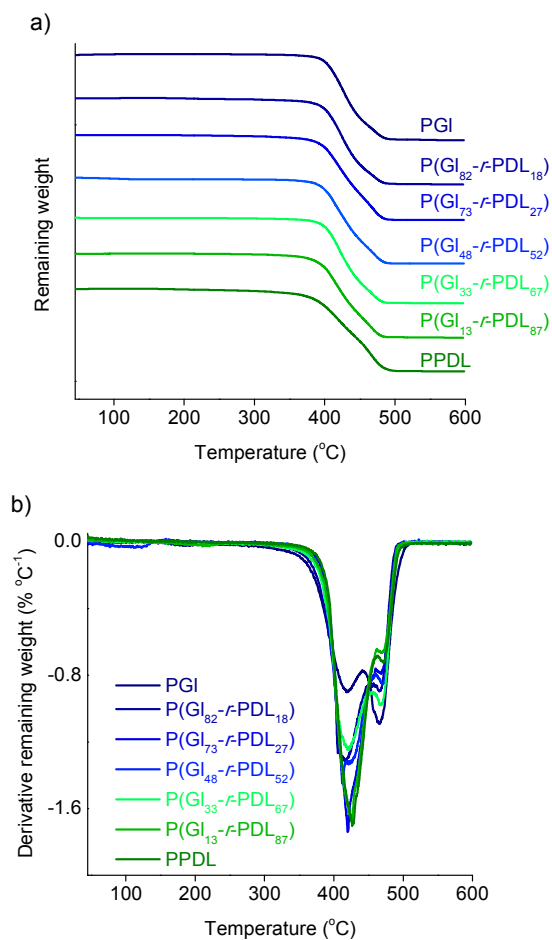
Figure F4. TGA traces (a) and derivative curves (b) of the P(GI$_x$-r-PDL$_y$) copolyesters.
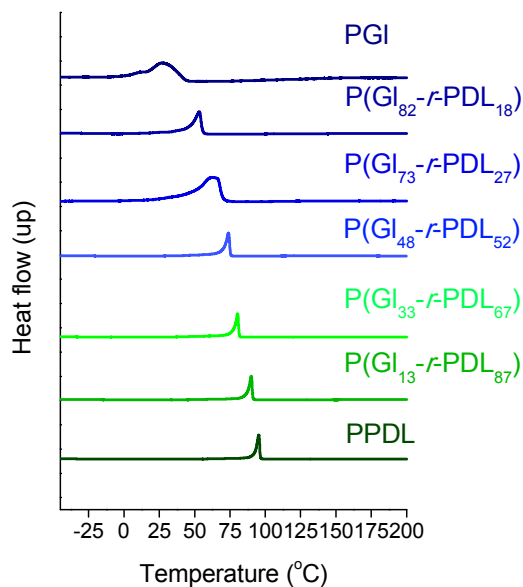
Figure F5. DSC traces of P(GI$_x$-r-PDL$_y$) copolyesters recorded at the second heating in the -30-200 ºC range.
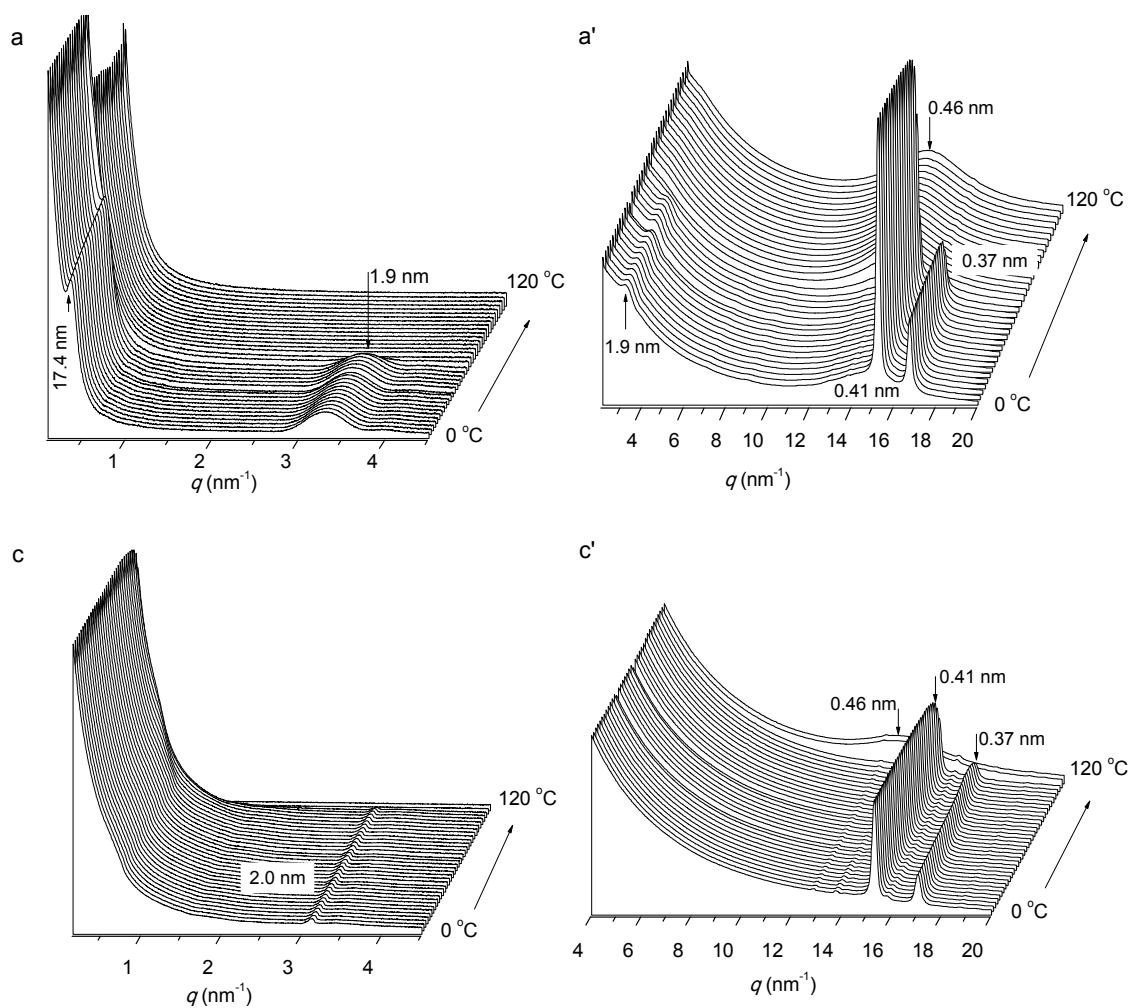
Figure F6. Evolution of the X-ray diffraction (SAXS and WAXS) profiles recorded at heating over the 0-120 °C range of poly(globalide) (a, a') and poly(ω-pentadecalactone) (PPDL) (c,c').
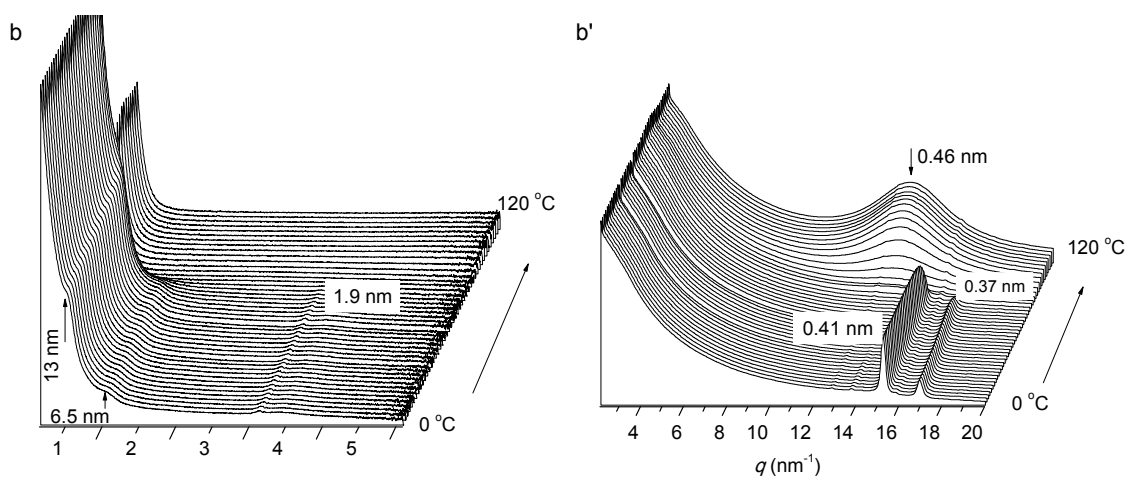
Figure F7. Evolution of the X-ray diffraction (SAXS and WAXS) profiles recorded at heating over the 0-120 °C range of the P(Gl$_{33}$-r-PDL$_{67}$) (b, b').
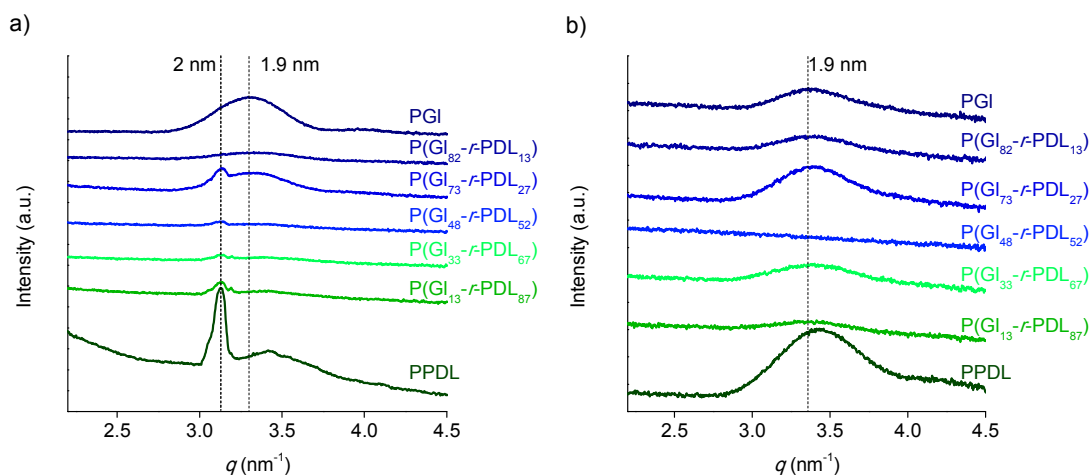
Figure F8. SAXS profiles highlighting the signal at 1.9-2.0 nm arising from the axial repeat of the crystal structure of P(Gl$_x$-r-PDL$_y$) copolyesters: a) recorded at 0 $^\circ$C and b) recorded at 0 $^\circ$C after heating at 120 ºC.
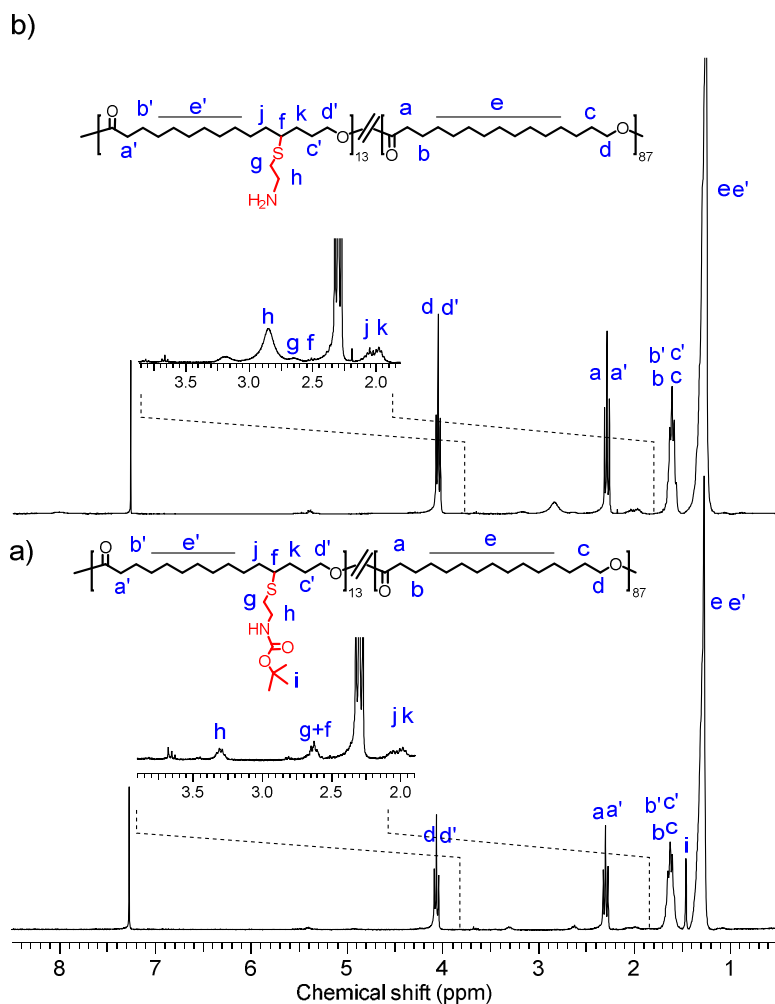
Figure F9. ^{1}H NMR (CDCl$_3$) spectra of the P[(Gl-BAET)$_{13}$-r-PDL$_{87}$] (a), and P[(Gl-NH$_2$)$_{13}$-r-PDL$_{87}$].
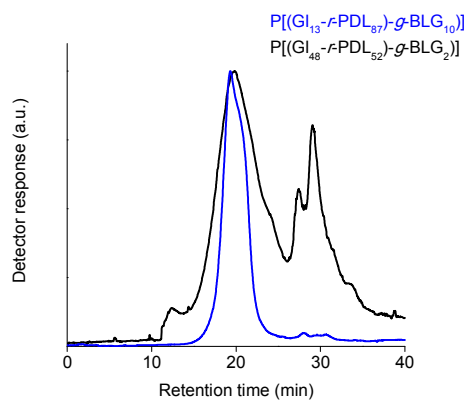
Figure F10. GPC curves of the P[(Gl$_x$-r-PDL$_y$)-g-(LGlu)$_z$] copolymers. Peaks observed at elution times longer than 25 min are due to salts present in the running solvent.
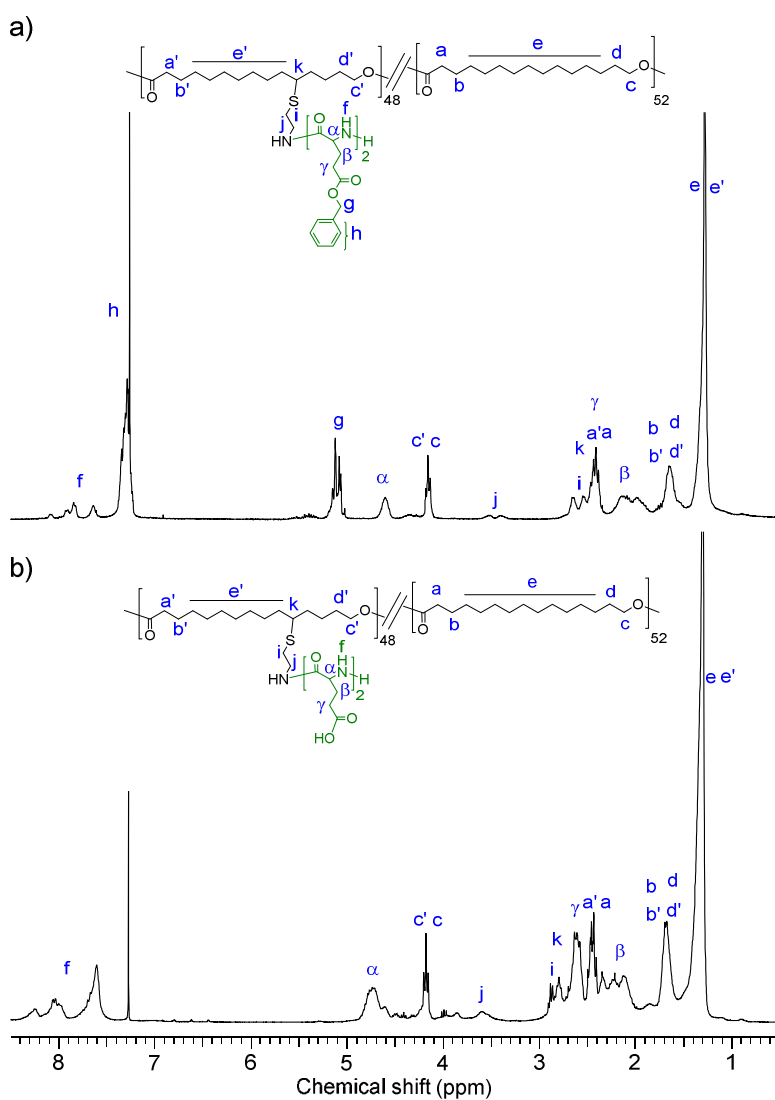
Figure F11. ^{1}H NMR (CDCl$_3$/TFA) spectra of the P[(Gl$_{48}$-r-PDL$_{52}$)-g-(BLG)$_2$] (a), and P[(Gl$_{48}$-r-PDL$_{52}$)-g-(LGA)$_2$].
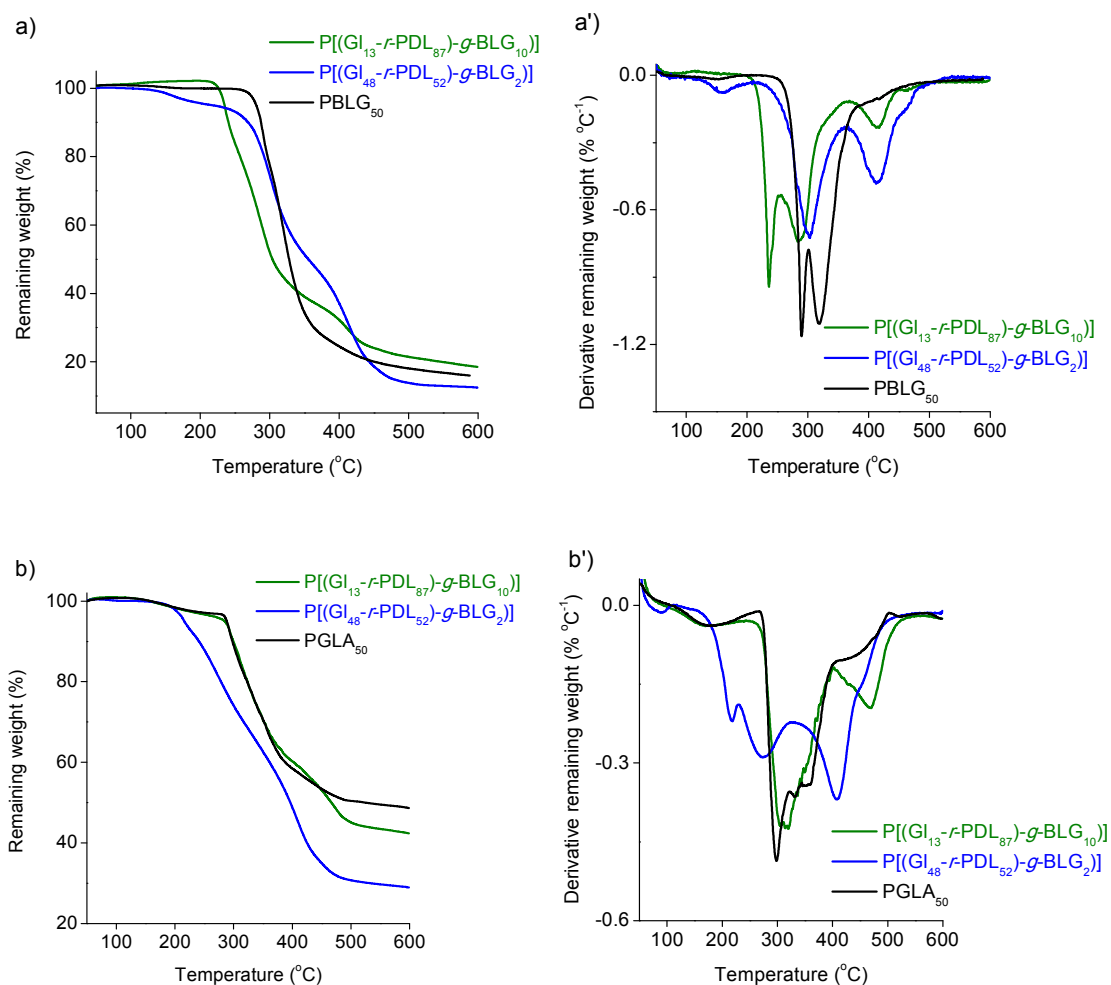
Figure F12. TGA traces (a, a') and derivative curves (b, b') of the P[(Gl$_x$-*r*-PDL$_y$)-*g*-(BLG)$_z$] and P[(Gl$_x$-*r*-PDL$_y$)-*g*-(LGA)$_z$] copolymers.
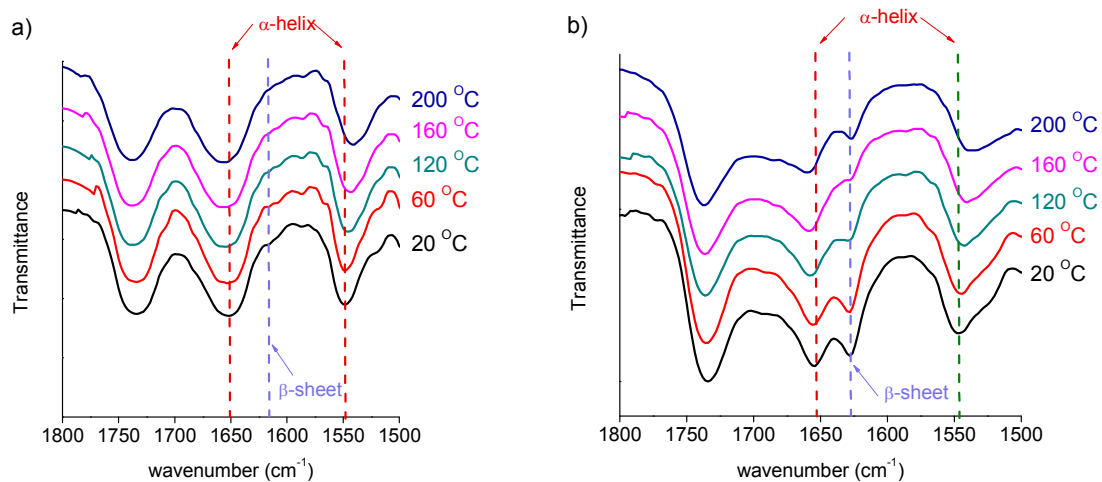
Figure F13. FTIR spectra highlighting the Amide 1800-1500 cm^{-1} region at different temperatures of: (a) P[(Gl$_{13}$-*r*-PDL$_{87}$)-*g*-(BLG)$_{10}$] and (b) P[(Gl$_{48}$-*r*-PDL$_{52}$)-*g*-(BLG)$_2$] copolymers.
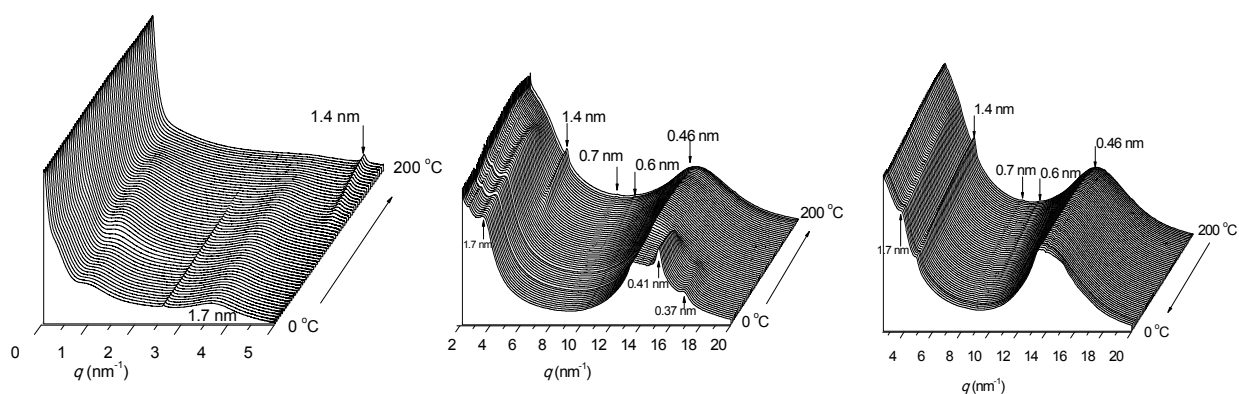
Figure F14. Evolution of the X-ray diffraction (WAXS and SAXS) profiles of the P[(GI$_{48}$-*r*-PDL$_{52}$)-*g*-(BLG)$_2$] graft-copolymer recorded at heating and cooling over the 10-120 ^{o}C range.
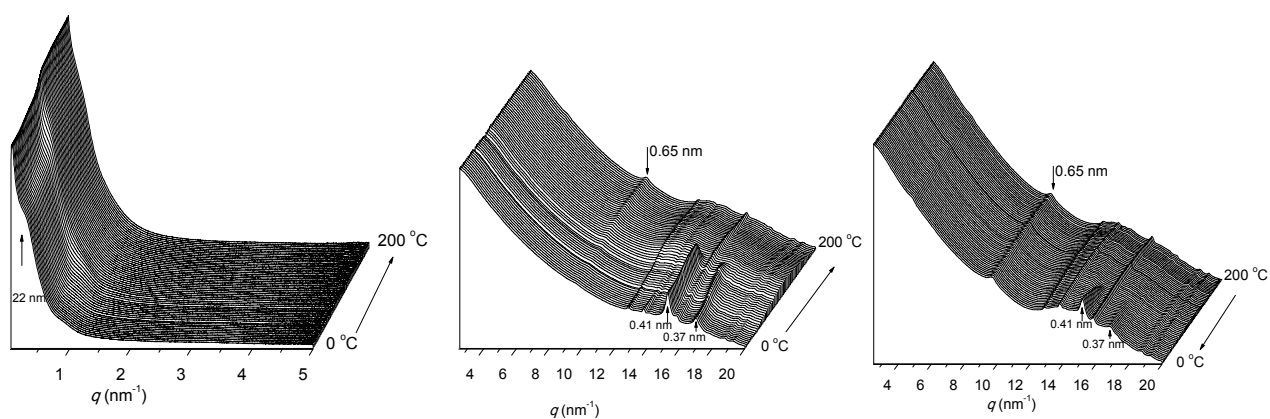
Figure F15. Evolution of the X-ray diffraction (SAXS and WAXS) profiles of the P[(GI$_{48}$-*r*-PDL$_{52}$)-*g*-(LGA)$_2$] graft-copolymer recorded at heating and cooling over the 0-200 ^{o}C range.
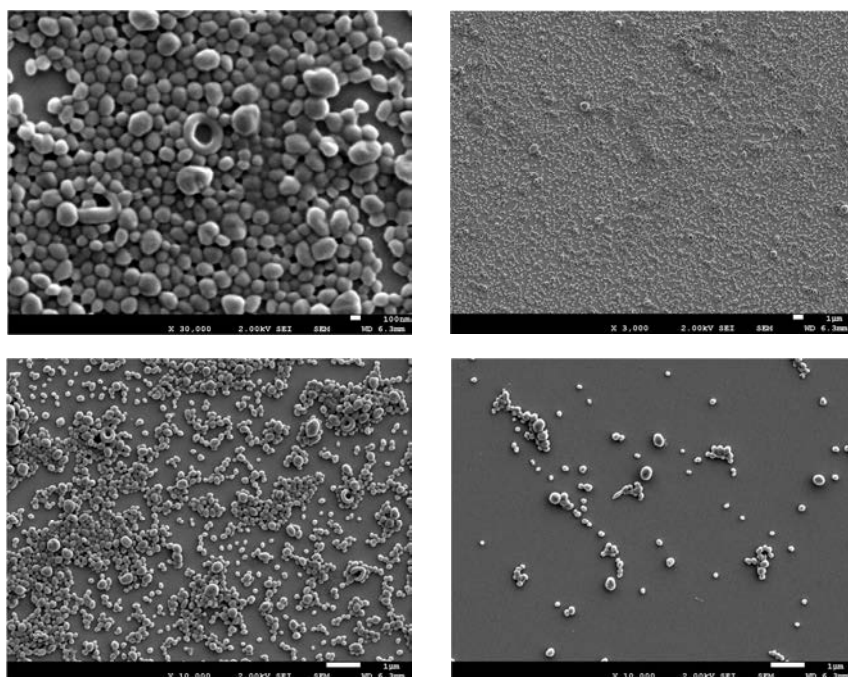
Figure F16. SEM images of nanoparticles made of P[(GI$_{13}$-*r*-PDL$_{87}$)-*g*-(BLG)$_{10}$] copolymer.
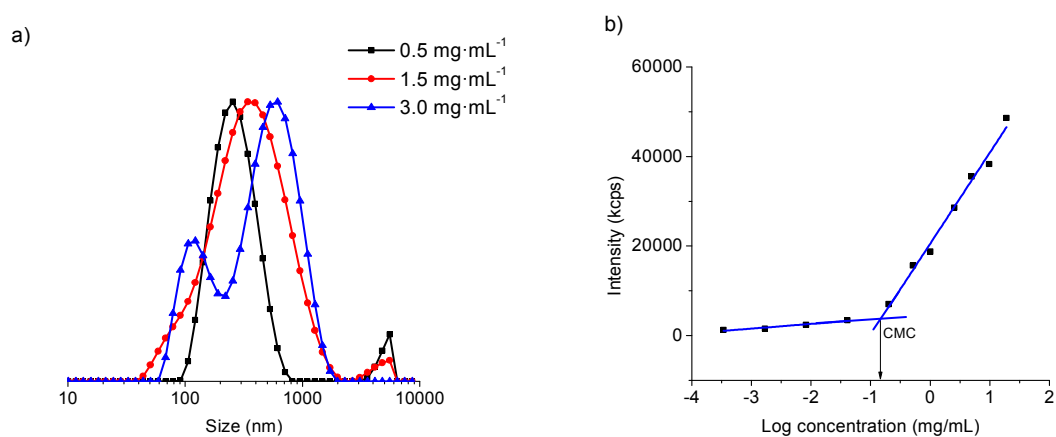
Figure F17. DLS profiles (a), and critical micelle concentration (b) of micelles-like objects derived of the P[(GI$_{13}$-*r*-PDL$_{87}$)-*g*-(LGA)$_{10}$] copolymer.
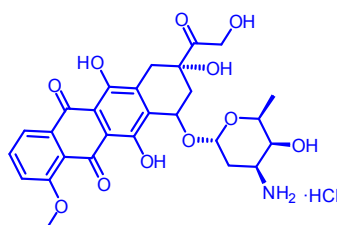
Figure F18. DOX·HCl is an amphiphilic drug containing a protonable amino group in the sugar moiety.
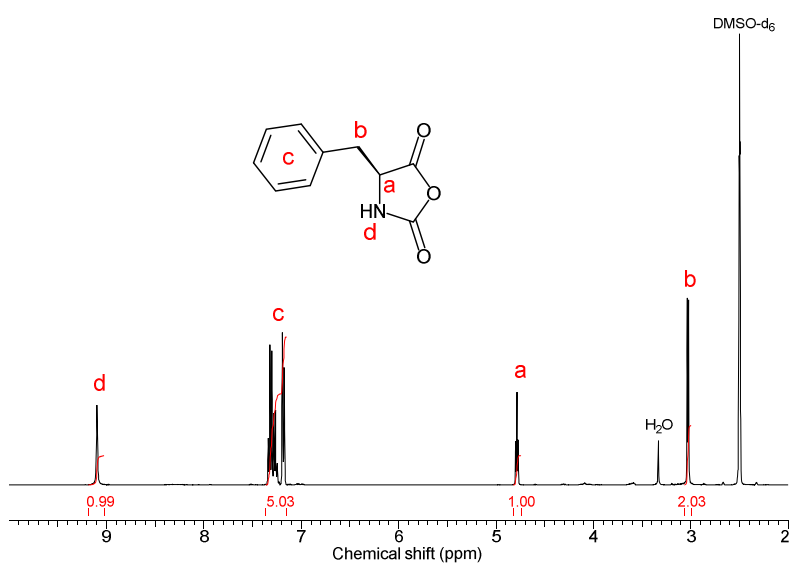
Figure G1. ^{1}H-NMR (DMSO-$_{d6}$) spectrum of the L-phenylalanine N-carboxyanhydride (Phe-NCA).

(PGl$_x$-NH$_2$)-b-(PEG$_{56}$)-b-(PGl$_x$-NH$_2$)
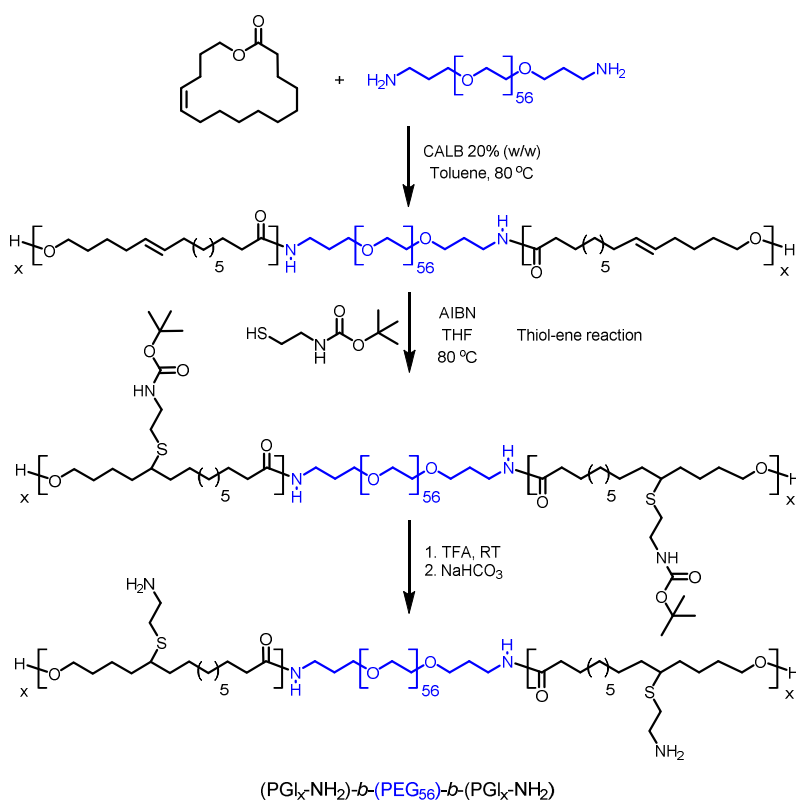
Fig. G2. Synthesis of the (PGl$_x$-NH$_2$)-PEG$_{56}$-(PGl$_x$-NH$_2$) macroinitiator.

Table G1. Results for the synthesis of (PGI)$_y$-*b*-PEG$_{56}$-*b*-(PGI)$_y$ triblock copolymers

Polymer	Feed molar ratio NH$_2$/GI	Yield (%)	Molar[a] compositon PEG/PGI	M_n[a] (g·mol^{-1})	Thiol-ene Coupling effiency[b] (%)
PGI$_{15}$-*b*-PEG$_{56}$-*b*-PGI$_{15}$	1/40	90	62/38	10800	96
(PGI)$_{70}$-*b*-PEG$_{56}$-*b*-PGI$_{70}$	1/150	89	28/72	36850	65

[a]Copolymer composition (%-mole)
[b]Calculated from ^{1}H-NMR.
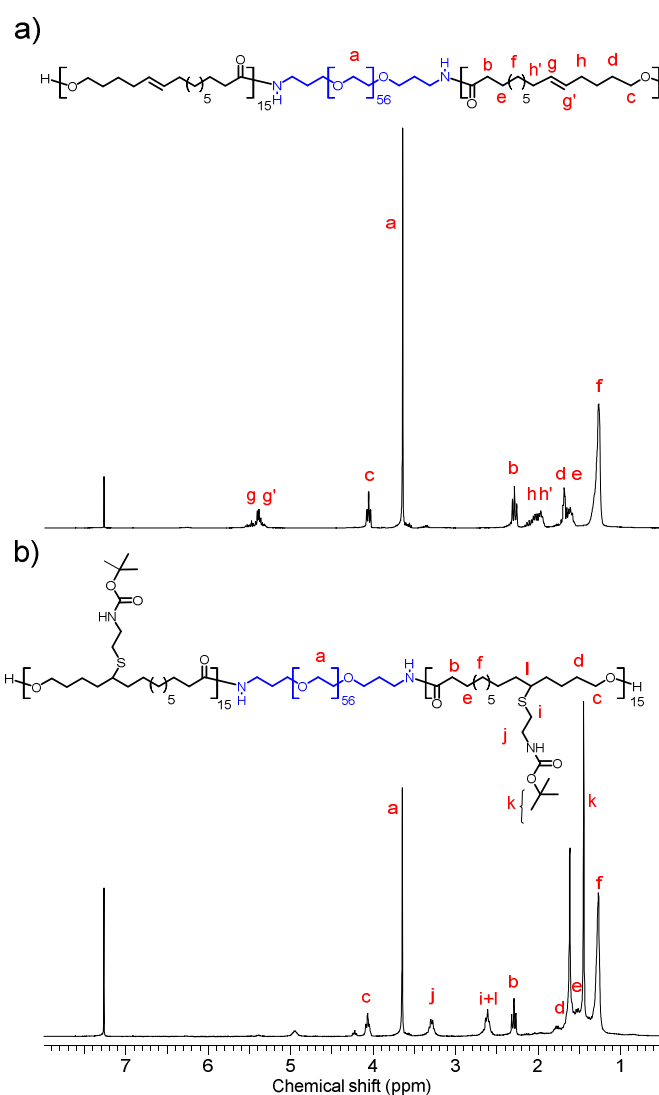
Figure G3. ^{1}H-NMR (CDCl$_3$) spectra of: a) PGI$_{15}$-*b*-PEG$_{56}$-*b*-PGI$_{15}$ and b) (PGI-BAE)$_{15}$-*b*-PEG$_{56}$-*b*-(PGI-BAE)$_{15}$.

Figure G4. ^{1}H-NMR (DMSO-$_{d6}$) spectrum of the (PGl$_x$-NH$_2$)-*b*-(PEG$_{56}$)-*b*-(PGl$_x$-NH$_2$) macroinitiator. *Traces of acetone.

Figure G5. SEC traces of (a) P(Gl$_{15}$-*g*-Phe$_4$)-*b*-PEG$_{56}$-*b*-P(Gl$_{15}$-*g*-Phe$_4$) and (b) P(Gl$_{70}$-*g*-Phe$_8$)-*b*-PEG$_{56}$-*b*-P(Gl$_{70}$-*g*-Phe$_8$) copolymer.
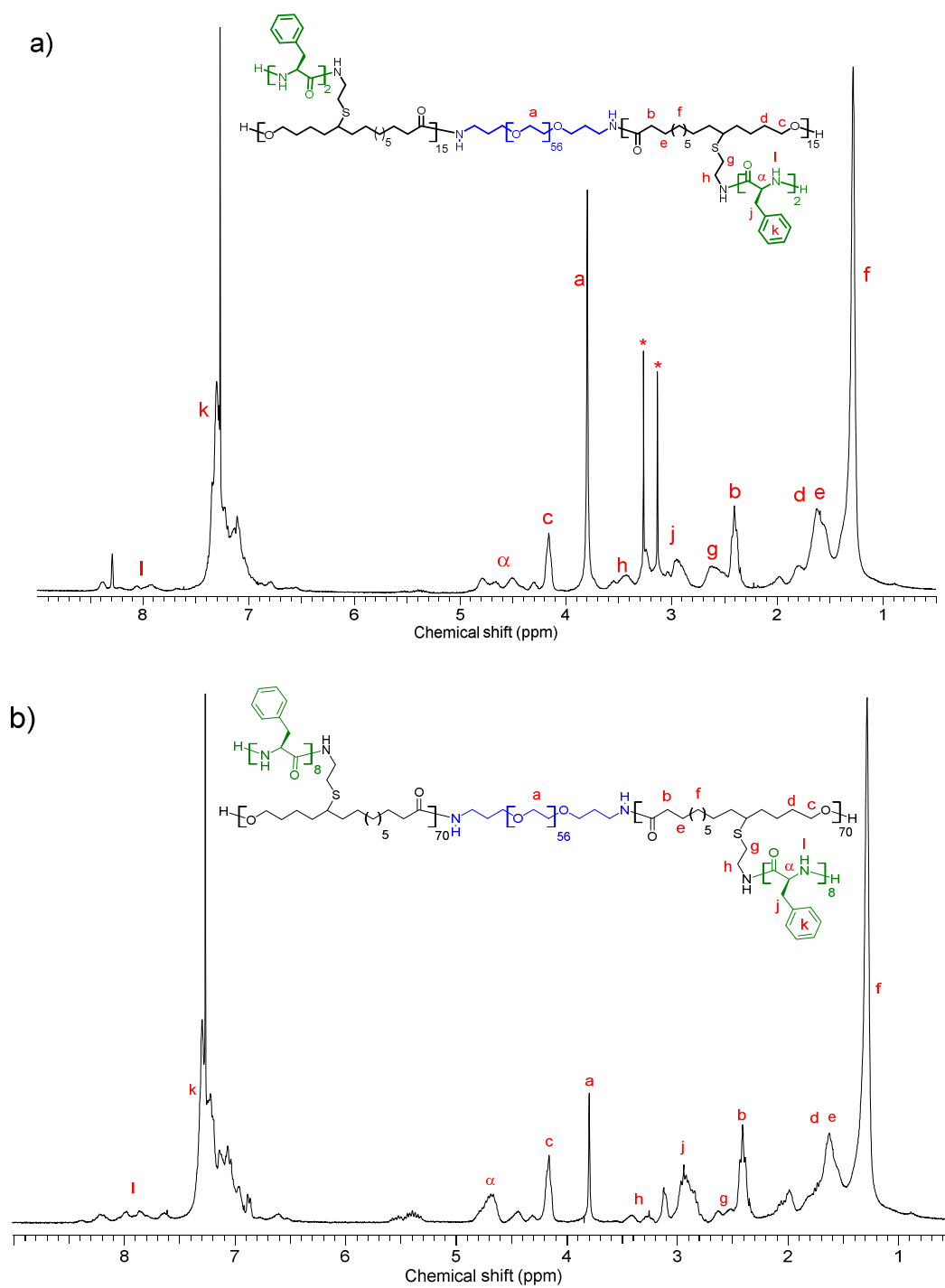
Figure G6. ^{1}H-NMR (CDCl$_3$/TFA) spectra of: (a) P(Gl$_{15}$-*g*-Phe$_2$)-*b*-PEG$_{56}$-*b*-P(Gl$_{15}$-*g*-Phe$_2$) and (b) P(Gl$_{70}$-*g*-Phe$_8$)-*b*-PEG$_{56}$-*b*-P(Gl$_{70}$-*g*-Phe$_8$) copolymer. *Traces of solvent.
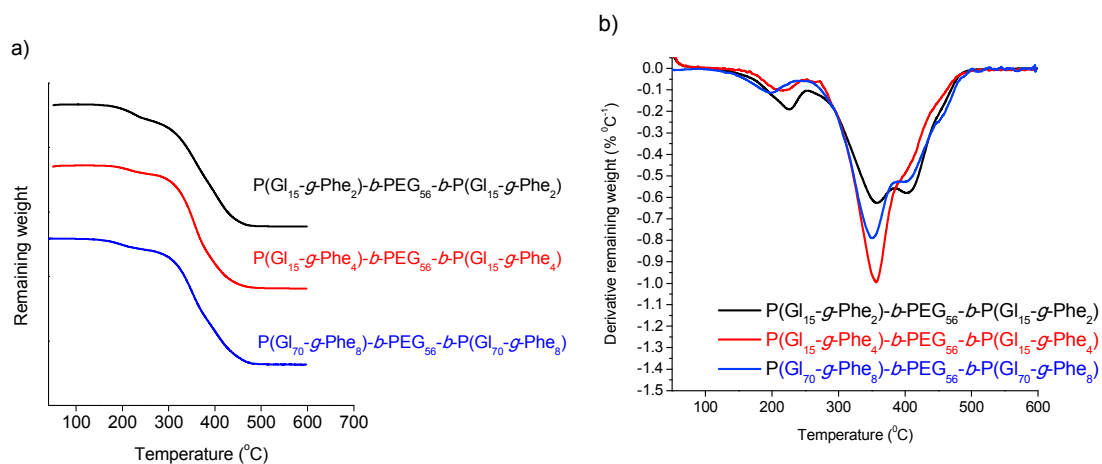
Figure G7. (a) TGA traces and (b) derivative curves of the $(PGI_x\text{-}g\text{-}Phe_y)\text{-}b\text{-}PEG_{56}\text{-}b\text{-}(PGI_x\text{-}g\text{-}Phe_y)$ copolymers.
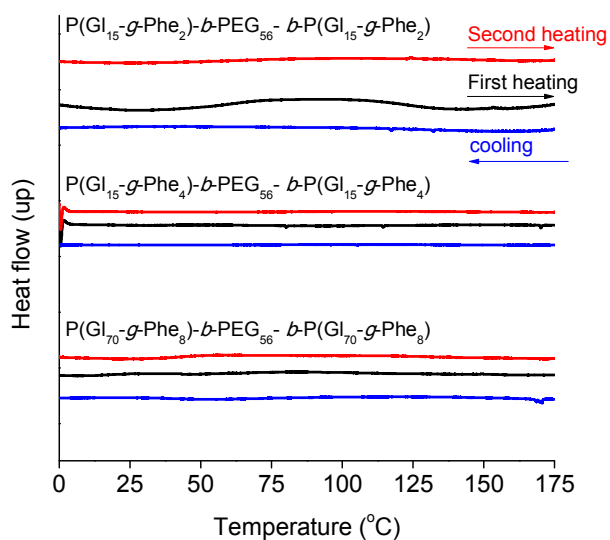
Figure G8. DCS curves of the $(PGI_x\text{-}g\text{-}Phe_y)\text{-}b\text{-}PEG_{56}\text{-}b\text{-}(PGI_x\text{-}g\text{-}Phe_y)$ copolymers.
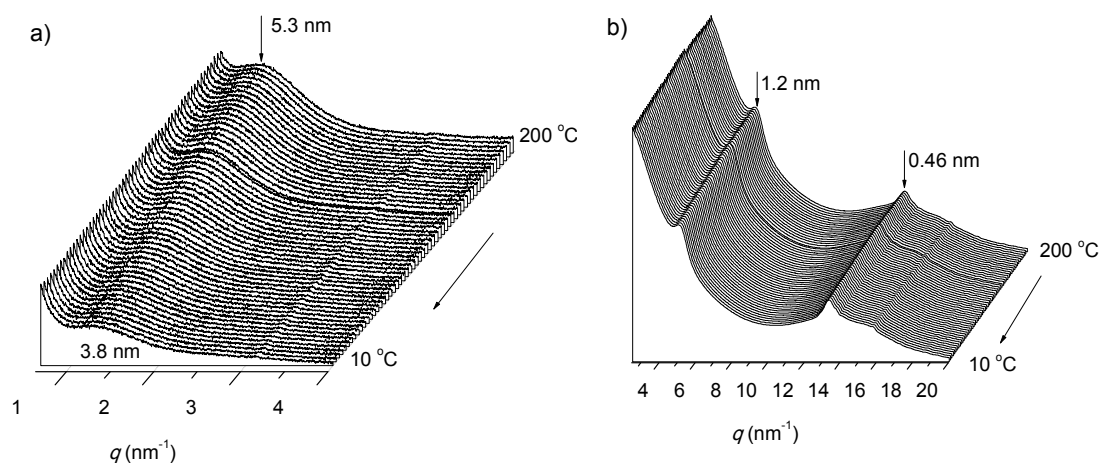
Figure G9. Evolution of the X-ray diffraction profiles of P(Gl$_{15}$-*g*-Phe$_4$)-*b*-PEG$_{56}$-P(Gl$_{15}$-*g*-Phe$_4$) recorded at cooling over the 10-200 °C range: (a) SAXS and (b) WAXS.
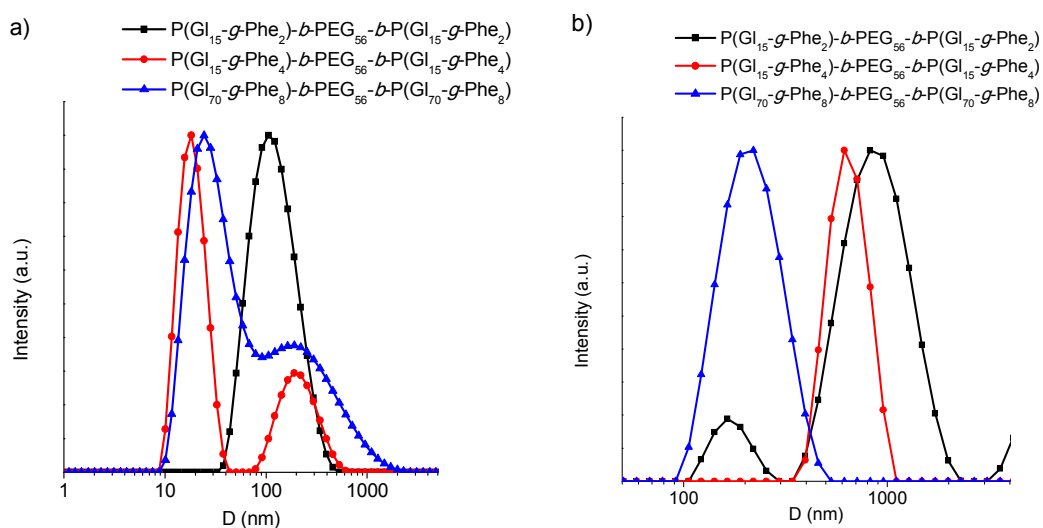
Figure G10. DLS profiles of nanoparticles prepared by (a) nanoprecipitation and (b) emulsion-solvent evaporation.
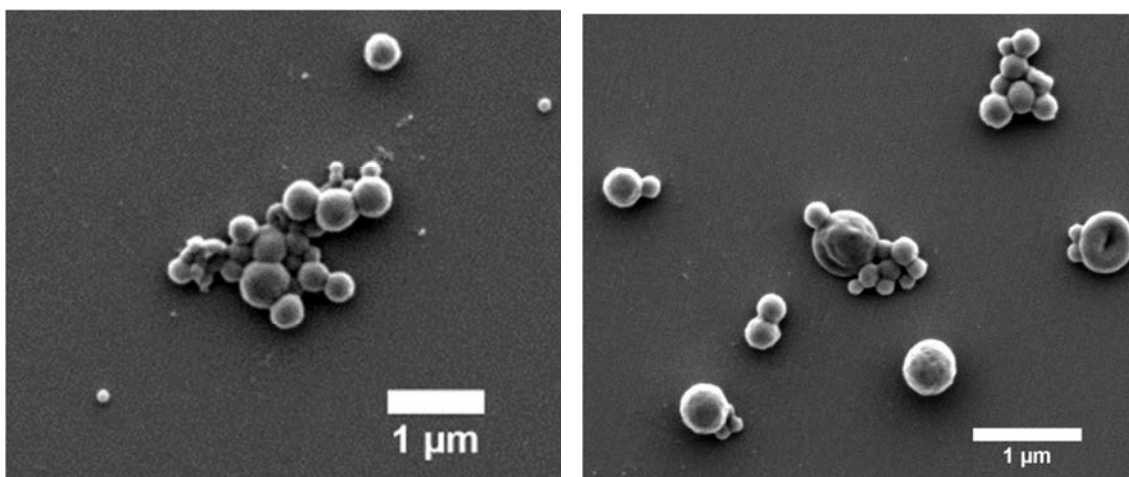
Figure G11. SEM images of nanoparticles derived of the $P(Gl_{70}$-g-$Phe_8)$-b-PEG_{56}-b-$P(Gl_{70}$-g-$Phe_{8'})$ copolymer. NPs were prepared by the emulsion-solvent evaporation method.
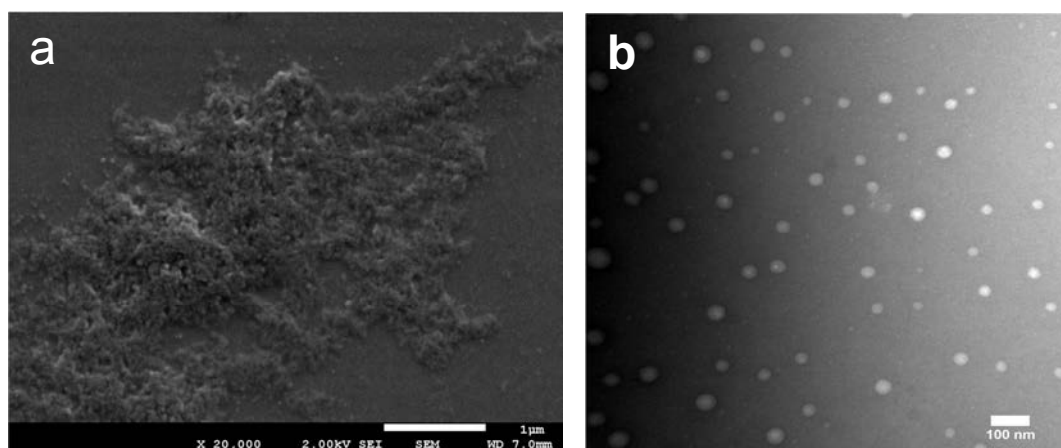
Figure G12. (a) SEM and (b) TEM images of nanoparticles made of $P(Gl_{70}$-g-$Phe_8)$-b-PEG_{56}-$P(Gl_{70}$-g-$Phe_8)$. NPs were prepared by the nanoprecipitation.
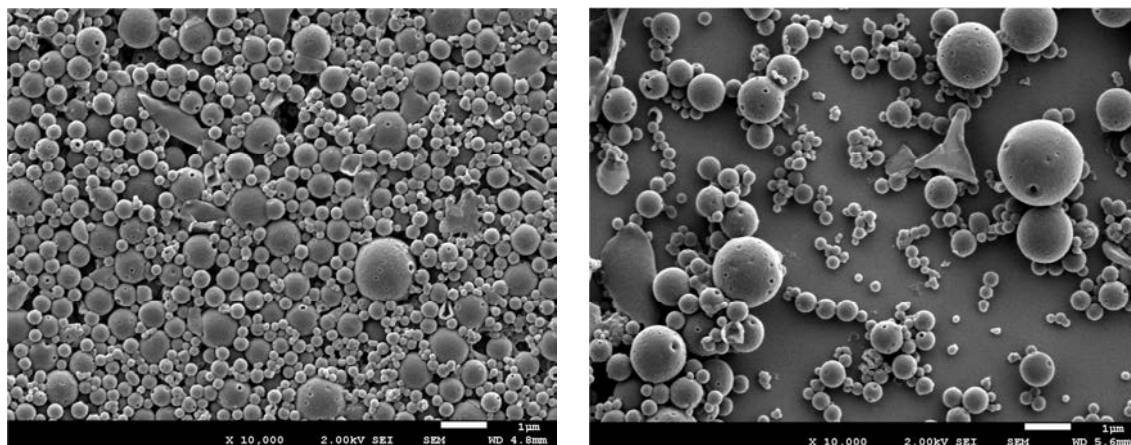
Figure G13. SEM images of nanoparticles derived of the P(Gl$_{15}$-*g*-Phe$_4$)-*b*-PEG$_{56}$-*b*-P(Gl$_{15}$-*g*-Phe$_4$) copolymer. NPs were prepared by the emulsion-solvent evaporation method.

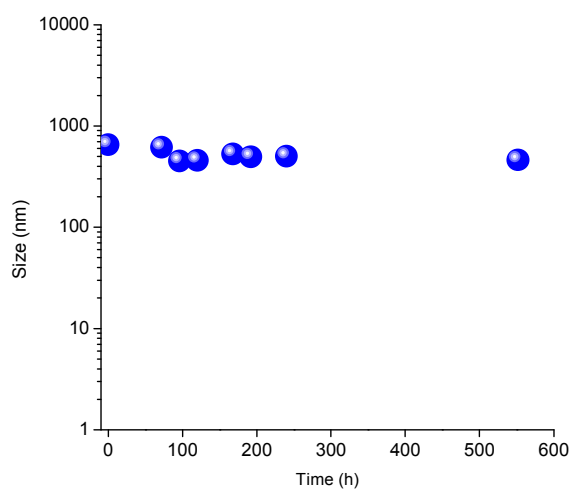**Figure G14.** Size measurements by DLS over the time to evaluate the stability of the nanoparticles derived of the P(Gl$_{15}$-*g*-Phe$_4$)-*b*-PEG$_{56}$-P(Gl$_{15}$-*g*-Phe$_4$) copolymer.